FACULTY OF SCIENCE
UNIVERSITY OF COPENHAGEN, DENMARK

PhD Thesis

THE ELECTRICAL AND DYNAMICAL PROPERTIES OF BIOMEMBRANES

By Lars D. Mogaard

Academic advisor: Thomas Heimburg

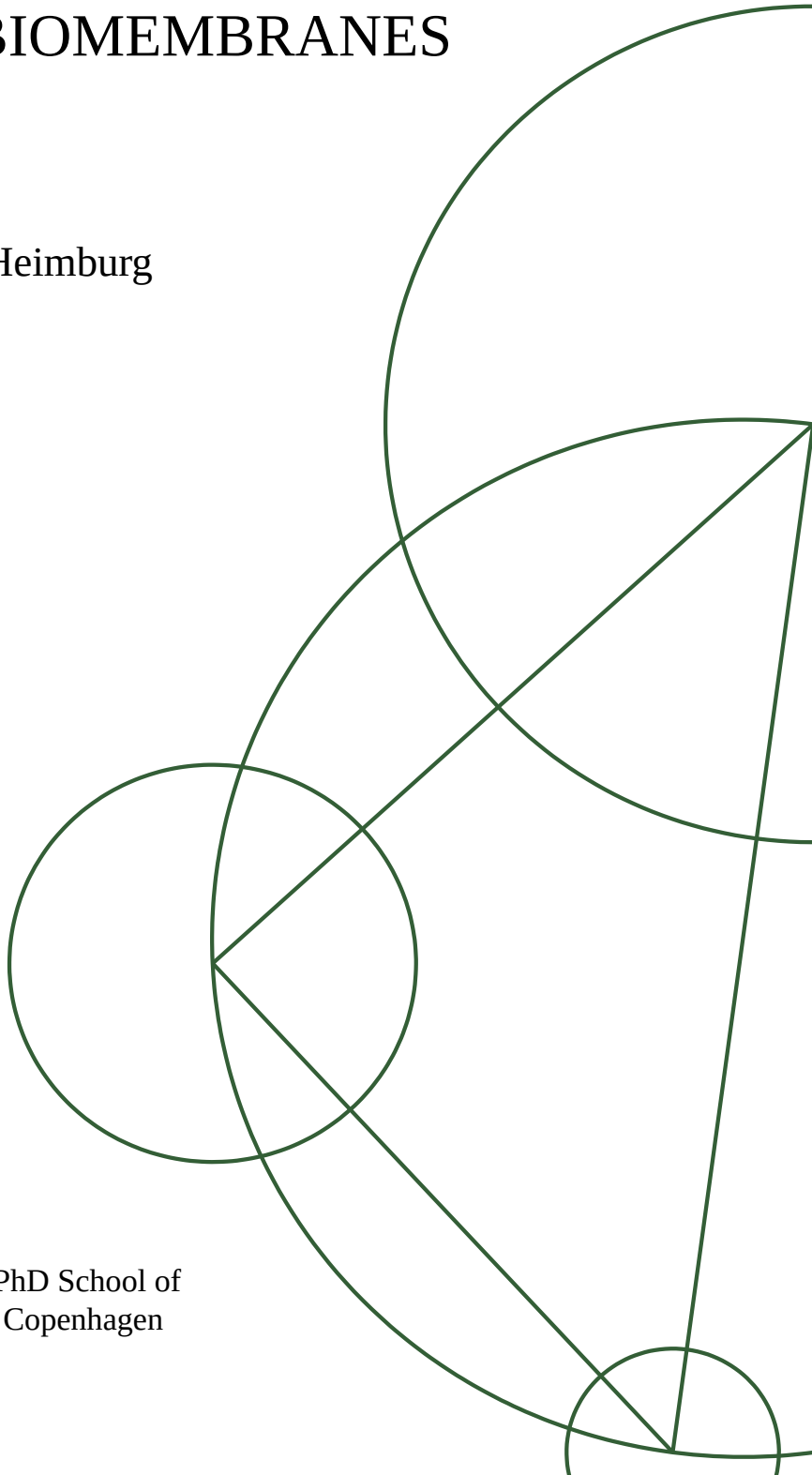

This thesis has been submitted to the PhD School of
The Faculty of Science, University of Copenhagen

Submitted: 17 Dec 2014

Your theory is crazy, but it's not crazy enough to be true.

- Niels Bohr

Acknowledgments

I would like to thank my collaborates: Foremost my advisor Prof. Thomas Heimburg who has been a great source of inspiration and has both challenged me and given me the freedom to pursue my own answers. Prof. Andrew D. Jackson for inspiring discussions and insight. Karis Zecchi, whom I have work closely with and has acted as a great sanity control. Dr. Alfredo Gonzalez-Perez for our long and tough fight with the experiments. Dr. Rima Budvytyte and Prof. Edgar Villagran Vargas for their great experimental knowhow and vigilance. Dr. Mathias Garden for including me in his ambitious and extraordinary work. Prof. Patrica Bassereau for hosting me and welcoming me into her group in Paris. To Prof. David Lacoste for interesting and inspiring discussions.

I would like to thank old and new fellow students for sharing the journey together. One never forgets the bonds formed when one has shared trenches. I also want to give extra thanks to the people that have helped me making my thesis readable, Ila, Karis, Alfredo and Rima, thanks.

I thank my family for their support and patience. You have always believed in me and have given me the virtue of not giving up and giving it my all. Virtues to which i owe all accomplishments. Thank you. I will finally thank Ilaria for being by my side through it all. Thank you for the support, the help, for cheering me on when things got tough and keeping me balanced (as much as possible). You being there have meant the world to me, thanks.

Note on used software

All Monte Carlo simulations have be written in `FORTRAN` using Intel's fortran compiler (`ifort`). Data analysis and plots have be made with `Matlab`. Analytical calculation and numerical solving of PDE's and ODE's have been done in `Mathematica`. Experimental data acquisition has been done in `LabChart`. For figures adobe `CS5`, `PovRay` and `Blender` have been used.

Abstract

Biological membranes in living organisms play the fundamental role of acting as *boundaries* and facilitate *compartmentalization*. From a structural perspective they are essentially constituted by an amphiphilic lipid membrane in which sugars, peptides and proteins are incorporated. These quasi-2-dimensional layers are literally vital for the cell, as membranes work as catalysts for some of the main chemical reactions involved in cell survival and homeostasis and govern all communication between a cell and its surroundings. The focus of the work presented in this thesis is to understand how the physical properties of lipid membranes relate to the behavior and functional properties of biological membranes, with special attention to the role of biological membranes in nerve signal propagation.

We start by exploring the properties of *polar* lipid membranes in order to tackle the problem of the coupling between the membrane and the electrical field within a universal thermodynamic framework. Within this framework, known electrical phenomena associated with lipid membranes such as offset voltage, electrostriction, piezoelectricity and flexoelectricity can be captured and viewed as special cases of a more general treatment. This purely thermodynamical treatment only describes the *equilibrium* properties of the membrane, however biological processes are of course dynamical in nature. A clear understanding of the *dynamical* behavior of lipid membranes is therefore essential when we aim at unraveling the functional behavior of membranes in biological systems. In order to do so we apply linear response theory and non-equilibrium thermodynamics to lipid membranes and propose a new approach: we investigate the relaxation behavior of lipid membranes in the vicinity of their lipid melting transition, taking into account the coupling between thermodynamical fluctuations and the available heat reservoir. The next step is to combine the knowledge on lipid membranes subjected to an electrical field with the knowledge on their relaxation behavior and use our understanding to attempt to re-evaluate the results of common electrophysiological methods such as "jump experiments" and impedance spectroscopy performed on lipid membranes. By doing so we observe that a number of non-linear phenomena previously thought to be associated with the presence of proteins embedded in the membrane can just as well be produced by a 'pure' lipid membrane.

As mentioned before, ultimately we aim at deepen the understanding of physical properties of lipid membranes in connection with the role of membranes in nerve signal propagation, in general and within the framework of the relatively recently proposed Soliton Model. The Soliton Model is at present the main alternative to the Hodgkin-Huxley model, the latter is currently the only widely accepted theoretical explanation of nerve signal propagation but fails at capturing several phenomena associated with nerve signals. In order to do so, first of all we focus on the implications of the relaxation properties of lipid membranes for the propagation of solitons in the membrane. By including relaxation effects in the theory of solitons propagation we find not only that soliton solutions are possible, but also that they are fully characterized by the thermodynamical and fluid-dynamical properties of the membrane. At last, we experimentally test the predictions of the soliton model regarding signal propagation in nerves. Our ex-

perimental observations validate the main predictions of the soliton model, that are not captured by other theoretical frameworks. More specifically, we observe that nerve signal propagating in the same axon penetrate upon collision and that nerve signals, beyond the commonly appreciated electrical component, exhibit a mechanical component, which is in-phase with the electrical one, thus dismissing the possibility of it being *caused by* the propagating electrical signal.

Dansk resume

Biologiske membraner i levende organismer har den grundlæggende rolle, at de definerer grænser og muliggører opdeling af celler. Fra et strukturelt synspunkt er de en amfifil lipidmembran, hvori sukkermolekyler, peptider og proteiner er inkorporeret. Disse kvasi-2-dimensionelle lag er afgørende for cellen, da membraner virker både som katalysatorer for vigtige kemiske reaktioner, der er involveret i celle overlevelse og homeostase, og regulerer al kommunikation mellem en celle og dens omgivelser. Fokus for arbejdet præsenteret i denne afhandling er at forstå, hvordan de fysiske egenskaber af lipidmembraner er forbundet med biologiske membraners adfærd og funktionelle egenskaber. Vi lægger særlig vægt på den rolle, som biologiske membraner spiller i nerve signaludbredelse.

Vi starter med at udforske egenskaberne af polære lipidmembraner vha. en termodynamisk fremgangsmåde, for at forstå koblingen mellem membranen og elektriske felter. Vha. denne termodynamiske fremgangsmåde ses det, at kendte elektriske fænomener associeret med lipidmembraner, som offsetspænding, electrostriction, piezoelektricitet og flexoelektricitet er specialtilfælde af en mere generel beskrivelse. Termodynamik beskriver udelukkende ligevægts egenskaber af membranen, men biologiske processer er naturligvis dynamiske i naturen. En klar forståelse af den dynamiske adfærd af lipidmembraner er derfor vigtig, når vi sigter mod at udrede den funktionelle adfærd af membraner i biologiske systemer. For at gøre dette anvender vi lineær respons teori og ikke-ligevægts termodynamik, og vi foreslår en ny beskrivelse af den dynamiske adfærd af membraner. Vi undersøger, hvordan relaksations adfærden af lipidmembraner tæt på deres faseovergang er koblet med dets tilgængelige varmereservoir. Det næste skridt er at kombinere vores viden om hvordan lipidmembraner er koblet til elektriskfelter med vores viden om deres dynamiske adfærd. Ved at kombinere disse, forsøger vi at reevaluere resultaterne af typiske elektrofysiologiske metoder såsom "jump eksperimenter" og impedans spektroskopi udført på lipidmembraner. Vi bemærker, at en række ikke-lineære elektriske fænomener tidligere forbundet med tilstedeværelsen af membranproteiner kan forkomme i en "ren" lipidmembran.

Som nævnt før, sigter vi i sidste ende mod at uddybe forståelsen af de fysiske egenskaber af lipidmembraner for at forstå rollen af membraner i nervesignalers udbredelse, i almindelighed og i den nyligt fremlagte Soliton model. Soliton modellen er i øjeblikket det vigtigste alternativ til Hodgkin-Huxley modellen, hvor sidstnævnte i øjeblikket er den bredt accepterede model, som dog ikke formår at forklare flere fænomener forbundet med nervesignaler. For at gøre dette, har vi først og fremmest fokusere på konsekvenserne af de dynamiske egenskaber af lipidmembraner på udbredelsen af solitoner i membraner. Ved at inkludere membranens relaksations adfærd i Soliton modellen, finder vi ikke kun at soliton løsninger er mulige, men også at de fuldt ud er karakteriseret af de termodynamiske og fluid-dynamiske egenskaber af membranen. Foruden dette har vi eksperimentelt testet forudsigelser af Soliton modellen vedrørende signaludbredelse i nerver. Vores eksperimentelle observationer validerer de testede forudsigelser af Soliton modellen, forudsigelser som ikke er inkluderet i Hodgkin-Huxley modellen. Vi har, mere specifikt, set at nerve signaler i et axon går igennem hinanden ved sammenstød og at nerve signaler, ud over det almindeligt elektrisk signal, har et mekanisk signal, som er i fase med det elektriske.

Dermed vi kan afvise, at det mekaniske signal følger efter det elektrisk signal, som tidligere antaget.

Publications

The work presented in this thesis has led to the following publications:

- Mosgaard, L. D., A. D. Jackson, and T. Heimburg. 2012. Low-frequency sound propagation in lipid membranes. Adv. Planar Lipid Bilayers Liposomes 16:51 – 74.
- Mosgaard, L. D., and T. Heimburg. 2013. Lipid ion channels and the role of proteins. Acc. Chem. Res. 46:2966 – 2976.
- Mosgaard, L. D., A. D. Jackson, and T. Heimburg. 2013. Fluctuations of systems in finite heat reservoirs with applications to phase transitions in lipid membranes. J. Chem. Phys. 125101:1 – 8.
- Gonzalez-Perez, A., R. Budvytyte, L. D. Mosgaard, S. Nissen, and T. Heimburg. 2014. Penetration of action potentials during collision in the median and lateral giant axons of invertebrates. Phys. Rev. X 4:031047.
- Heimburg, T., A. Blicher, L. D. Mosgaard and K. Zecchi. 2014. Electromechanical properties of biomembranes and nerves. J. Phys.: Conf. Ser. 558:012018.
- Mosgaard, L. D., K. A. Zecchi and T. Heimburg. 2014. Electrical properties of polar membranes. arXiv: 1411.6883$v1$.

The publications can be found, in the above order, in the Appendix B.

Contents

Preface

The main motivation behind the work presented in this thesis is the ambition to describe the physical macroscopic properties of biological membranes and unravel especially how these properties connect to the propagation of nerve signals. Biological membranes are fascinating structures which have features that are vital to life on all scales, from nanometers (protein activity) to centimeters (nerve signals). Research on these structures conventionally focuses on the nanometer scale and the large scale properties have often been marginalized. However, with the introduction of the Soliton model for the propagation of nerve signals and its success in describing a number of previously unexplained aspects of nerve propagation, the importance of the macroscopic properties of membranes has been emphasized. It is this model and its foundation in the macroscopic properties of biological membranes that has been the central motivation throughout this thesis.

Chapter 1

Introduction

The primary role of biological membranes is to define boundaries and enable compartmentation, a basic requirement for the existence of life. Membranes surround living cells as well as many of their inner components. It is these semi permeable structures that enable up-concentration of molecules and also generate gradients, fueling the activity of the cell. Biology is a vastly complicated field whose radius of action spans from chemical signal pathways, on intercellular and extracellular level, to macroscopic signaling as the propagation of nerve signaling and the behavior of life. Membranes and their function are central in understanding the impact of the environment on the cell and in unraveling complex behavior as in the case of nerve signal propagation. Studying properties of these structures is therefore vital for understanding cells as the unit of life, at a single cell level as well as organism level.

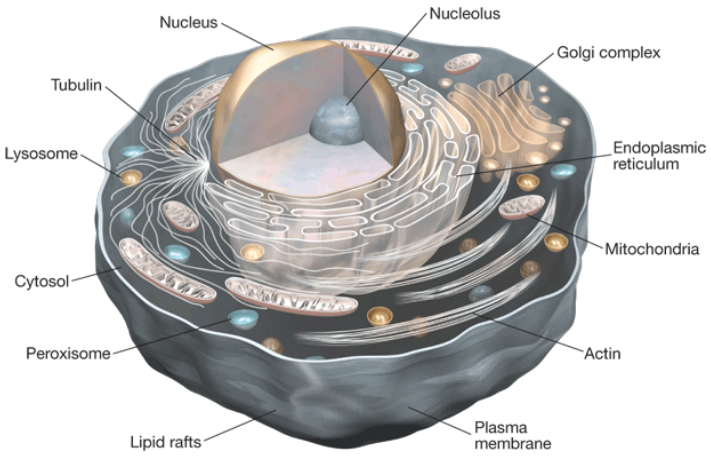

Figure 1.1: *A illustration of a mammalian cell, showing the outer membrane and the inner organelles. Taken from [1].*

1.1 Lipid membranes

Overton [2] in 1899 suggested that cells are surrounded by a "fatty oil". In 1925 Gorter and Grendel [3] extended this, by finding that cells "are covered by a layer of fatty substances that is two molecules thick". It became clear in 1935, from experiments conducted by Danielli and Harvey [4], that the fatty layer is constituted of both lipids and proteins. These discoveries lead to years of speculation about the organization of these fatty layers. In 1972 Singer and Nicolson [5] proposed the Fluid Mosaic model. The Fluid Mosaic model describes the structure of the fatty layer as a homogeneous bilayer of lipids ("a two-dimensional oriented viscous solution" [5]), wherein proteins and other macro-molecules can be anchored or immersed due to mainly hydrophobic interactions, see Fig. (1.1), *left*, for visualization. The idea of the Fluid Mosaic model was extended in 1984 by Mouritsen and Bloom [6] in the Mattress model. In the Mattress model the bilayer is viewed as a pseudo 2-dimensional heterogeneous solution, where mismatching between the hydrophobic regions of the lipids and the proteins induces inhomogeneities in the bilayer, see Fig. (1.1), *right*.

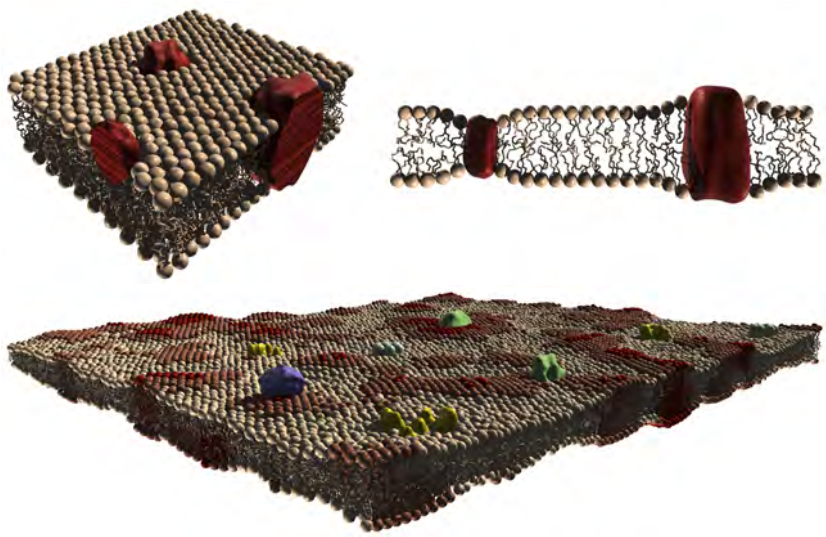

Figure 1.2: *Patches of membrane in accordance with;* ***left****, the Fluid Mosaic model,* ***right****, the Mattress model.* ***Bottom****, modern veiw of the membrane, where the membrane is considered to be a highly heterogeneous and dynamic structure. The illustration has been provided by Andreas Blicher.*

Both models describes the membrane as a dynamic structure. Already before the introduction of the Mattress model it became evident that the mechanical and fluid dynamical properties of natural occurring membranes are crucial for cellular activity and several biological functions [7]. In the efforts of understanding these properties, it became apparent that membranes can be found in a number of smectic phases and that the phase transitions between these, are often close to physiological conditions. These phases, the transitions and their mechanical and dynamical implications for the physical properties of membranes have been the focus of both intense experimental and theoretical studies.

The lipid composition of biological membranes can vary a lot, depending for example on the tissue type and the growth conditions. It has been shown that when *E. coli* is grown at different temperatures the lipid composition of its membrane is altered so that the membrane show similar physical properties across different growth conditions [8]. Similar lipid composition changes have also been observed for trouts. Specifically, changes in lipid composition of liver tissue of trouts raised at different temperatures [9]. It has further been observed that lipid composition changes take place in deep-sea bacteria grown at different pressure [10]. All these experimental findings indicate that the physical properties of biological membranes are tightly controlled, further underlining the importance of these properties for the functionality of the membrane and therefore biology.

1.1.1 Introduction to Lipids

A variety of lipids is found in biological membranes, these can be divided up into sterols (e.g. cholsterol), sphingolipids and phospholipids. In cell membranes the majority of lipids are phospholipids, these have, as the majority of all lipids in membranes, a polar and non-polar region making them amphiphilic molecules.

The non-polar region is, in phospholipids, composed of two hydrocarbon chains typically containing 16 or 18 carbons molecules [11]. The length can though vary from 12 to 22 molecules and the chain can be either saturated, unsaturated (containing double bonds) or one of each, which is the most common. The hydrocarbon chains are linked through ester bonds to adjacent carbons of a glycerol backbone. The last carbon in the glycerol backbone is, in the case of a phospholipid, linked to a negatively charged phosphate group via another ester bond. The head group is attached to this phosphate group, making up the polar region of the lipids. The head group can be a number of different biological compounds such as choline, ethanolamine, serine and glycerol. Both serine and glycerol head groups will result in a net negative charge of the polar region, whereas with choline and ethanolamine the region will be zwitterionic, all at neutral pH. Zwitterionic head groups carries no net charge but present spatially separated charges which render the head group very polar. Zwitterionic lipids commonly display a large dipole moment pointing towards their tail, amounting to a monolayer surface potential of $300 - 500\ mV$ [12, 13]. Additionally, in the majority of biological membranes about $10 - 20\%$ of the lipids are charged and this percentage can go up to 40% in the case of mitochondrial membranes [14]. It is known that charged lipids are often asymmetrically distributed between the two leaflets of the membrane, the inner leaflet carrying more charges [15, 16]. This asymmetry means that biological membranes can be polarized structures (see section 2.3).

The naming convention for phospholipids is based on the lipid chains and on the head group. For example, two palmitic acids linked to a choline group is called dipalmitoylphosphatidylcholine (DPPC). DPPC is depicted in Fig. (1.1.1) **(a)**.

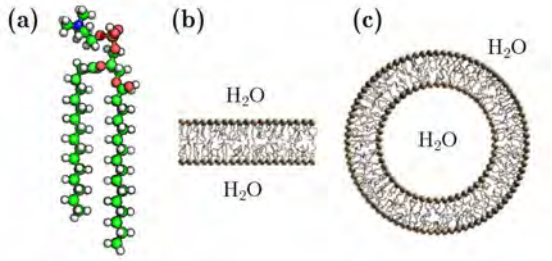

Figure 1.3: ***A**: Illustration of a 1,2-dipalmitoylphosphatidylcholine (DPPC) lipid.* ***B**: A patch of a bilayer.* ***C**: Unilamellar vesicle. The illustration has been provided by Andreas Blicher*

Due to the amphiphilic nature of the majority of lipids, when mixed with a polar solvent (e.g. water), they will self-organize to minimize unfavorable polar-nonpolar interactions. This self-organization will result in the formation of macroscopic structures, such as micelles, planar bilayers (see Fig. (1.1.1) **B**) or vesicles (see Fig. (1.1.1) **C**). In general other non-lamellar structures can be formed, but they are rarely observed in excess water. Vesicles in particular are interesting in the context of biological membranes. These energetically favorable bilayer structures are identical in structure to native biological membranes - thus represents a valuable model system for studying physical properties of biological membranes. Throughout this thesis large unilamellar vesicles of DPPC will commonly be used as a general model system for biological membranes.

1.1.2 Membrane Phases

Lipid bilayers can be found in a number of smectic phases[1] varying with lipid composition. Common for these phases is that they are neither crystalline nor fluid, they share properties from both classes.

Lipid bilayers are considered to have four smectic phases. The customarily designated procedure for the lipid bilayer phase is the following: To describe the long-range ordering an upper-case letter is used; L for one-dimensional lamellar, and P for two-dimensional oblique. A lower-case subscript is used to describe the short-range ordering of the lipid chains; α disordered (fluid); β ordered - not tilted with respect to the normal of the bilayer; β', ordered - tilted (gel) [17]. The four phases are presented below in the generalized sequence of thermotropic transitions [18]:

- L_c (L_β): Crystalline phase, in which the lipids are ordered in three dimensions.
- $L_{\beta'}$: Crystalline molecular order. Chains are mostly "all-trans" [2] ordered and tilted. Lipids are in this phase is packed in a distorted quasihexagonal lattice. This phase is often called the solid phase or simply the gel phase.
- $P_{\beta'}$: So called "ripple" phase. The membrane is partially solid, partially fluid organized in a periodic structure in the plane of the lamellae. The

[1] By a phase is meant a state of a medium that share physical properties.
[2] Spatial orientation of the two chains.

lipid chains are tilted but packed in a regular hexagonal lattice. This phase forms prior to chain melting.

- L_α: Lipid chains are disordered. Order of lattice is lost. This phase is often called the liquid-disordered phase or simply the fluid phase.

The main lipid melting transition between $L_{\beta'}$ and L_α is the most biologically relevant, whereas the ripple phase will be ignored. The ripple phase has been shown to be easily abolished by the presence of various biomolecules in the membrane, and is rarely seen in biological membranes [19]. The topology of the gel and fluid phases is illustrated in Fig. (1.4).

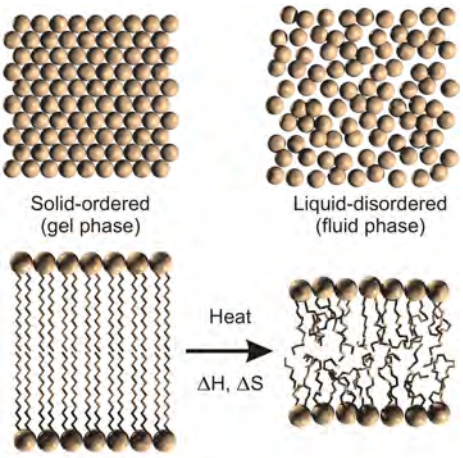

Figure 1.4: ***Top**, illustrates the lateral ordering of the gel phase (**left**) and the fluid phase (**right**). The **bottom** depicts the ordering of the lipid chains. The illustration is provided by Andreas Blicher.*

1.1.3 Membrane Phase Transition

A *phase transition* is defined as a transformation from one phase of a system to another, e.g. ice to water. Depending on the nature of the transition, a system undergoing a phase transition can display a number of extraordinary properties, such as drastic changes in the susceptibilities and in the relaxation behavior of the system.

The lipid melting transition has been found to take place just under the physiological growth temperature in naturally occurring membranes, see Fig. (1.1.3)[3]. As previously mentioned, organisms have been found to adjust their lipid composition so that their membranes conserve their physical properties at different growth condition, this includes the lipid melting transition. Organisms shift their membranes lipid melting transition point to conserve the relation between the transition and their growth conditions (i.e. the relation between transition temperature and growth temperature), even under extreme conditions [8].

[3]A similar behavior has be shown to be true for the lipid melting transition in the lipid membrane from rat brain, not shown.

The close coupling between the lipid melting transition and growth conditions indicates the importance of the transition for the function of biological membranes and therefore biology in general. This has motivated extensive research of the nature of the main lipid melting transition between the gel- and fluid-phase [17, 20, 21].

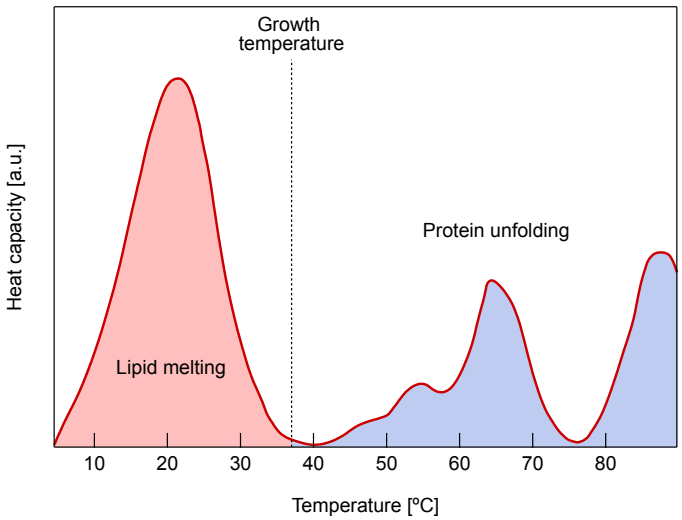

Figure 1.5: *The calorimetric profile of a intact* E. coli *membrane. The red shaded region is associated to the lipid transition, whereas the blue region is associated to protein unfolding. Notice that the lipid transition is immediately below the growth temperature. The figure is adopted from [8].*

The lipid melting transition[4] is a exothermic transition occurring over a narrow but finite temperature range, which is driven by the entropy gain of collective melting of lipid chains. The exothermic transition is easily monitored by differential scanning calorimetry (DSC), where the heat capacity show a spike of finite extend during the transition. The transition associated heat capacity is referred to as the excess heat capacity. During the transition a number of other susceptibilities likewise display spikes, e.g. the compressibility and lateral compressibility. The topography of the membrane during the lipid melting transition is dominated by the formation of domains of various sizes and compositions, though phase separation is not observed[5]. The domains are stabilized by the interplay between configuration entropy and interfacial associated free energy. The fluctuations of these cooperative domains display very slow relaxation times in the transition region [22, 23], see chapter 3.

The main lipid melting transition is found consistently close to physiological conditions and represent a potentially powerful means for biology to respond to environmental changes and to regulate behavior of the membrane, which plays a central role in a vast number of biological functions.

[4] A systematic classification of the lipid melting transition is difficult, however it has been described as a weak first order transition [7, 20].

[5] This observation is at odds with a true first order phase transition, which display complete phase separation that renders interface phenomenas unimportant.

1.2 Nerve models

For larger organisms like humans, fast and long-range signaling is essential for the organism to respond to the environment or to act coherently. This signaling is done through the nervous system which allow the brain, in the span of few milliseconds, to send and receive signals to and from the entire organism. Understanding how signals propagate through the nervous system is vital for understanding the phenomenon itself but represents also the first step towards understanding the brain and has, therefore, been the subject of vast research and a crucial point of interest in the history of medicine.

There is two types of models that aim at explaining the propagation of nerve signals. The first is the textbook electrical model of the propagation of nerve signal of Hodgkin and Huxley [24][6]. The second type proposes that the propagation of nerve signals is facilitated by solitons (electro-mechanical waves) and has been proposed by Heimburg and Jackson [26].

1.2.1 Hodgkin & Huxley Model

In 1791 Luigi Galvani discovered that he could get the legs of dead frogs to move by stimulating the spine electrically. This finding, paved the way for a description of nerve signaling as being electrical in nature. In 1952 Hodgkin and Huxley [24] presented a mathematical model for the initiation and propagation of nerve pulses in giant squid axons. Their effort was originally only intended as an empirical description of the experimentally found transient voltage change of a nerve signal (or action potential) by Cole and Curtis [27]. Their description however gained widespread acceptance throughout the neural field, resulting in them receiving the Nobel prize in medicine in 1963 for their work.

The giant squid axon was early on found to have a significantly higher potassium concentration inside the nerve compared to outside and a higher sodium concentration outside than inside. These concentration differences give rise to a voltage difference (through the Nernst potential) over the nerve membrane, assuming that a selective permeability is present. Hodgkin and Huxley [24] assumed that the cell membrane acts like a barrier, in which trans-membrane ion channels are embedded. These ion channels are assumed to be voltage gated and specific in their conduction of ions – either conducting sodium or potassium. In their purely electrical view, the membrane is considered impermeable to ions and is assumed to be equivalent in function to a capacitor with constant capacitance. This is schematically depicted in Fig. (1.2.1) **A**.

Hodgkin and Huxley proposed the concept that a local depolarization will lower the potential difference over the membrane causing a local flux of ions through the channels. This will result in further depolarization of the membrane which in turn will cause additional channels to conduct ions, hereby creating a cascade effect through which the nerve signal is propagated. The beauty of their model is that the axon membrane can be depicted as a rather simple basic electrical circuit unit. The equivalent circuit can be seen in Fig. (1.2.1) **B**. Though the basic equivalent circuit seem quite straightforward, the detailed

[6] Extensions of this model have been made to describe specific nerves type but these are all based on the framework of Hodgkin and Huxley, i.e. [25].

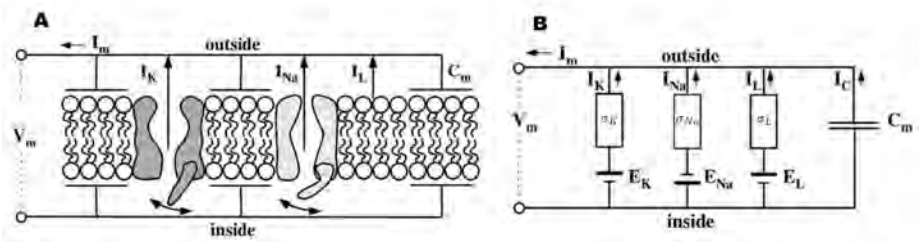

Figure 1.6: ***A**: Illustration of the axon membrane in view of the Hodgkin-Huxley model.* ***B**: The equivalent electrical circuit of the membrane, where the ion channels are replaced with resistors and the membrane acts as a capacitor. The figure has been adopted from [8]*

dynamics of the ion channels is rather complicated. The ion channels have a complex time and voltage dependence which have to be empirically fitted for any system under consideration.

Hodgkin and Huxley proposed the following differential equation (cable equation) for describing the propagation of the voltage pulse in a nerve (giant squid axon),

$$\frac{a}{2R_i}\frac{\partial^2 V}{\partial x^2} = C_m \frac{\partial V}{\partial t} + \sigma_K(V - E_K) + \sigma_{Na}(V - E_{Na}) + \sigma_L(V - E_L), \quad (1.1)$$

where V is the voltage, which is a function of time and position, R_i is the resistivity along the interior of the nerve, C_m is the capacitance of the membrane and a is the radius of the axon. Here the geometry of the axon has been assumed to be a perfect cylinder. E_K and E_{Na} are the respective *resting* potentials associated with potassium and sodium, with E_L being the leak potential. σ_K, σ_{Na} are conductance of potassium and sodium respectively, and σ_L is the leak conductance, all being complicated functions of voltage and time.

As pointed out by Hodgkin and Huxley, their model is an empirical model specifically made for the action potential in giant squid axon [24]. No explanation is provided for the time- and voltage-dependence of the involved ion-channel proteins on which the model is based. This mean that in principle these dependencies have to be measured for any new nerve system. The empirical nature of the model strongly limits its predictive power. The general predictions that can be made by the Hodgkin and Huxley model and akin models are that the nerve signal is generated by a tightly regulated ionic currents through the membrane of the axon and that any disruptance of these currents will affect the nerve signal.

The assumptions made by Hodgkin and Huxley imply that the lipid membrane is a constant structure with no drastic changes in geometry or any other physical property. These assumption seem in conflict with the dynamic nature of lipid membrane, especially in the vicinity of the lipid melting transition. Experimental findings even indicates the occurrence of a phase transition during the nerve pulse [28, 29]. Furthermore, the very complex and selective gating of the ion channels can in itself be questioned. Tasaki *et al.* [30] showed that the axon of a giant squid can still accommodate propagation of nerve pulses with no

monovalent cations in the exterior solution (e.g. Na, K). Further, new studies of the conduction of pure lipid membrane have shown voltages gating along with a number of behavioral traits previously associated to proteins [31–33]. In the literature these contradicting observations have been attributed to secondary selectivity of the ion channels, which seems somewhat of an unsatisfactory explanation, or have simply been ignored.

In the equivalent circuit terminology, the ion channels are viewed as resistors through which ion (charges) flow. This is a strictly dissipative process independent of flow direction. The HH-model describes the action potential as being produced mainly by ion flows, making the propagation of nerve signals a stringently dissipative process. Hill *et al.* [34] published in 1958 a review on the heat production of a nerve pulse, showing that during a nerve pulse heat is first release and then entirely reabsorbed, following the profile of the electrical pulse within experimental errors. This fundamental finding has later been confirmed in great detail for nerves pulses originating from a number of different myelinated [35] and non-myelinated [36,37] nerves. The re-absorption of the produced heat strictly classifies the nerve pulse as an adiabatic process (see Fig. (1.2.1), *B*), which is very much at odds with the dissipative nature of the HH-model.

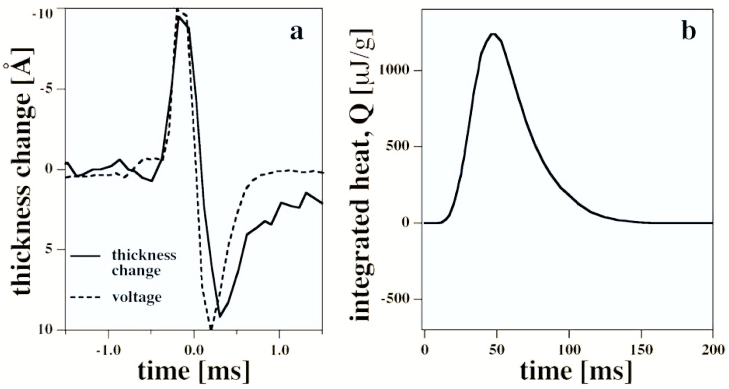

Figure 1.7: *During the nerve pulse the thickness and the heat of the nerve axon changes.* ***A****: Shows that thickness change scales with the electrical nerve pulse. Experiment was conducted on giant squid axons. The figure has been adopted from [38].* ***B****: Shows the integral of the heat released during a nerve pulse, showing no net production of heat. Experiments were conducted on non-myelinated fibers of the pike olfactory nerve. The figure has been adopted from [36].*

The Hodgkin-Huxley model solely describes the electrical aspect of a nerve pulse. It have been shown that the electrical pulse is coupled with a swelling of the membrane [36,38,39] (see Fig. (1.2.1), **A**). The adiabatic nature of the nerve pulse combined with the mechanical changes and the physical size of the pulse, indicates that the nerves pulses could be a type of *sound wave*. This deduction lead to the proposal of the Soliton model by Heimburg and Jackson in 2005 [26].

1.2.2 Soliton Model

In a series of recent publications Heimburg and Jackson have proposed an alternative thermodynamical model for the propagation of nerve pulses [26, 40]. In this model nerve signals are described as a class of localized sound waves known as solitons. Solitons are self-reinforced waves that propagate with constant velocity without attenuating[7]. This description address a number of poorly understood experimental observation, the adiabatic nature of nerve pulses, the electrical and mechanical nature of the nerve signal and the effect of anesthetics. Observations that are hard to reconcile with models which are based on the framework of electrical circuits.

Heimburg and Jackson [26] relaying their theory on thermodynamics and hydrodynamics proposed that nerve signals are localized electro-mechanical density waves (solitons). For the existence of solitary waves both non-linearity and dispersion have to be present. For the Soliton model the non-linearity is in the speed of sound which is a function of lateral density and dispersion is the frequency dependency of the speed of sound. In the vicinity of the lipid melting transition the lipid membrane meet both of these requirements, see Fig. (1.2.2).

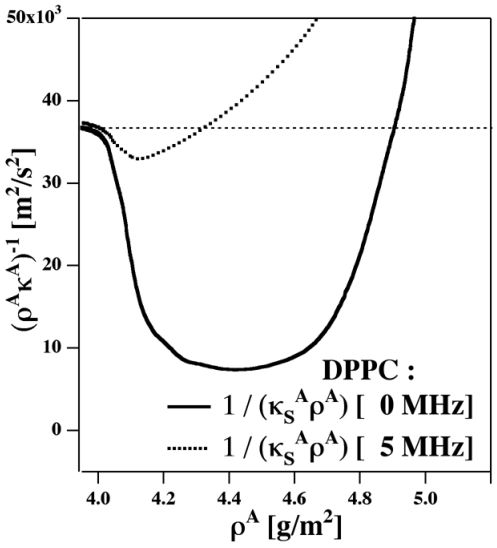

Figure 1.8: *The speed of sound as a function of lateral density, for large unilamellar vesicles of DPPC at* $T = 318.15\ K$. *The speed of sound is shown for the theoretical low frequency limit (*$0\ Hz$*) and for* $5\ MHz$, *from ultra-sonic experiments. [26].*

The Soliton model is based on the equation of sound. Using that the nerve axon is a long approximately homogeneous cylinder we can restrict ourself to consider the 1-dimensional equation of sound,

$$\frac{\partial^2}{\partial t^2}\Delta\rho^A = \frac{\partial}{\partial x}\left(c^2\frac{\partial}{\partial x}\Delta\rho^A\right), \tag{1.2}$$

[7] Recently experiments have verified the existence of lateral density solitons in quasi 2-dimensional sheets [41].

where $\Delta\rho^A(x,t) = \rho^A(x,t) - \rho_0^A$[8] is the change in lateral density of the nerve membrane and c is the speed of sound. As illustrated in Fig. (1.2.2), the speed of sound in plane of the lipid membrane is a non-linear function of density and a function of frequency in the vicinity of the lipid melting transition. To capture the non-linear dependency on lateral density, Heimburg and Jackson expand the speed of sound squared into a power series to second order

$$c^2(\Delta\rho^A) = c_0^2 + p\Delta\rho^A + q(\Delta\rho^A)^2 + \dots, \tag{1.3}$$

where c_0 is the phase velocity in the fluid phase, far from the transition. $p < 0$ and $q > 0$ are the taylor expansion coefficients which are determined from the density dependent speed of sound of membrane[9].

Having no detailed data on the frequency dependence of the speed of sound at low frequencies, Heimburg and Jackson chose the dispersion term to take the simplest possible form $(-h\frac{\partial^4}{\partial x^4}\Delta\rho^A)$, resulting in the final formulation of the Soliton model

$$\frac{\partial^2}{\partial t^2}\Delta\rho^A = \frac{\partial}{\partial x}\left(\left(c_0^2 + p\Delta\rho^A + q(\Delta\rho^A)^2\right)\frac{\partial}{\partial x}\Delta\rho^A\right) - h\frac{\partial^4}{\partial x^4}\Delta\rho^A, \tag{1.4}$$

where $h > 0$ is the dispersion constant which sets the width of the pulse (see chapter 5). By considering the low-amplitude periodic solution of Eq. (1.4), $\Delta\rho^A(x,t) = \Delta\rho_0^A \exp(i\omega(t - x/c_0))$ using that $c(\rho^A) \approx c_0$ we see the nature of the assumed dispersion term,

$$c^2(\omega) = c_0^2 + hk^2 \approx c_0^2 + h\frac{\omega^2}{c_0^2}. \tag{1.5}$$

We see that the dispersion constant acts as the taylor expansion coefficient of the second order term of the frequency dependent speed of sound, around $\omega = 0$. The sign of the frequency is of no importance since it is only represents a phase shift, meaning that the speed of sound must be an even function of frequency. By this argument the chosen dispersion term truly poses the simplest meaningful choice, as the lowest order, non-trivial, expansion of the speed of sounds frequency dependence.

Assuming that the general solution to Eq. (1.4) propagates with a constant velocity ($z = x - vt$, where $v \leq c_0$), is localized and vanishes for $|z| \to \infty$, it can be solved analytically [42]:

$$\Delta\rho^A(z) = \frac{p}{q}\frac{1 - \left(\frac{v^2 - v_{min}^2}{c_0^2 - v_{min}^2}\right)}{1 + \left(1 + 2\sqrt{\frac{v^2 - v_{min}^2}{c_0^2 - v_{min}^2}}\cosh\left(\frac{c_0}{h}z\sqrt{1 - \frac{v^2}{c_0^2}}\right)\right)}, \tag{1.6}$$

where $v_{min} = \sqrt{c_0^2 - \frac{p^2}{6q}}$ is the minimum group velocity. This type of localized solution is referred to as solitary wave or simply soliton and is the namesake

[8] ρ_0^A is the lateral density of the membrane in the fluid phase and is used as the zero point for the lateral density.

[9] For LUV of DPPC at $T = 318.15\ K$ the parameters takes the values $\rho_0^A = 4.035 \cdot 10^{-}3\ g/m^2$, $c_0 = 176.6\ m/s$, and the expansion coefficients: $p = -16.6 \cdot c_0^2/\rho_0^A$ and $q = 79.5 \cdot c_0^2/(\rho_0^A)^2$.

of the model. From Eq. (1.6) it can be seen that the solution is symmetric around the peak, and that the width of the soliton scales with the dispersion constant. Heimburg and Jackson chose $h = 2\ m^4/s^2$, based on the physical length (distance) of measured nerve pulses. Using this value, the Soliton model predicts a minimum velocity of solitons in DPPC membranes to be $v_{min} \approx 0.65 \cdot c_0 = 115\ m/s$ – a number which is very close to the pulse velocity measured in myelinated nerves. The minimum velocity corresponds to the maximum amplitude or density change of $\Delta\rho^A_{max}/\rho^A_0 \approx 0.21$. Soliton profiles for a number of different propagation velocities are presented in Fig. (1.2.2).

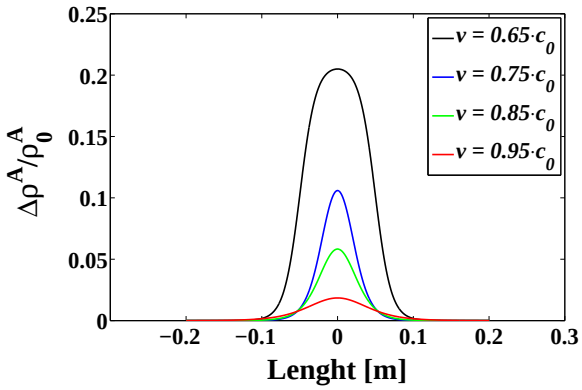

Figure 1.9: *Soliton profiles for LUV of DPPC calculated for velocities between the lower limit* $v = 0.65 \cdot c_0$ *and* $v = 0.95 \cdot c_0$.

Lautrup *et al.* [42] have shown that the Soliton model is stable over ranges of physical relevance (several meters) with respect to noise and heterogeneities in the membrane – which is essential for a model that attempts to describe a biological system. They further showed that the soliton can be produced (excited) by arbitrary localized non-solitonic excitation, meaning that any perturbation of a sufficient amplitude should be able initialize a soliton, and hereby a nerve pulse.

The soliton is locally pushing the lipid membrane into its lipid melting transition as it propagates. As we will see in the next chapter (2.2) the state of the membrane is coupled to thickness, charge density, etc. and that these change drastically during the transition. This means that during the propagation the soliton will display a number of secondary effect such as geometric changes and changes in electrical properties. Beyond the fact that biological membrane often are polarized, one has to consider that nerves present a voltage drop across the membrane such that the membrane acts like a charged capacitor. A change in thickness will therefore produced an electrical signal [43]. The propagation of the soliton will result in changes in thickness of the membrane and also have an electrical component, both observed during the propagation of nerve signals. The most important feature of the Soliton model is its ability to predict the reversible heat changes in phase with the action potential. It should however be emphasized that the present form of the Soliton model only describes nerve pulses in myelinated nerves where all propagation is kept in 1-dimension.

The essential feature of the membrane that makes propagation of solitons possible, is the existence and the vicinity of the lipid melting transition to the physiological conditions. Any change to the membrane system which acts upon the melting transition will therefore influence the propagation of a nerve signal. Among these are anesthetics which are known to lower the lipid melting temperature significantly. Based on this Heimburg and Jackson made a number of prediction about the nature of anesthetics [40]. Predictions that answer questions previously unanswered in anesthesiology.

The Soliton model still has unanswered details, some of which will be addressed here: The electromechanical coupling and properties of membranes which link the mechanical nature of the soliton to the electrical component of the nerve signal and the nature of dispersion in membranes. However, unlike the Hodgkin and Huxley model the Soliton model provides testable predictions, and some of these will also be addressed experimentally in the present thesis.

Chapter 2

Thermodynamical description of lipid membranes

We will in this chapter brush-up thermodynamics, introduce the reader to a thermodynamical description of lipid membranes around the main lipid melting transition and show how we can include electrostatics in this description.

2.1 Introduction to thermodynamics

Problems in the field of biology are often tackled with a bottom-up approach and from single molecules properties the sophisticated behavior of biological systems is believed to emerge. The membranes surrounding cells are mesoscopic layers covering areas of several 100 μm^2 and contain a number of molecules of the order of 10^{10}. Given the size and complexity of biological membranes, throughout this thesis we will take the other approach, top-down. We will understand the physical and biological features of membranes using a thermodynamical approach where membranes are described in terms of the set of molecules that they are composed of and their ensemble properties. Thermodynamic is used throughout the thesis and we will introduce the first two thermodynamical laws and key thermodynamical relations in the following section.

First law of thermodynamics which is a conservation law, stating that the changes in the internal energy (U) is given by sum of the change in heat (Q) and the work (W) done by/of the system,

$$\mathrm{d}U = \delta Q + \delta W. \tag{2.1}$$

The change in internal energy is a perfect differential (denoted by d), where the change in heat and work are not (denoted by δ). The change in internal energy is a state function and only depends on the start and end point, therefore $\mathrm{d}U$ is a perfect differential, whereas the change in heat and work dependent on the path, e.g. on how they change. Thermodynamics was developed to fully describe the equilibrium state of a system through a state function. To describe

the system we need to describe both the change in heat and work. We will first consider thermodynamical work: We assume that any equilibrium state can be reached through processes going only through equilibrium states. This assumption is equivalent to assuming that any equilibrium state can be reached through reversible processes. Using this assumption we consider work done on/by the system by a infinitesimal and reversible change. In thermodynamics textbooks the thermodynamical work is exemplified by the mechanical work ($\delta W = -p\mathrm{d}v$) needed to change a volume (v) against a pressure (p). In general the work term in the internal energy (Eq. (2.1)) is the sum of reversible infinitesimal work contributions,

$$\delta W = -p\mathrm{d}v - \pi\mathrm{d}A + \sum_i \mu_i \mathrm{d}n_i + \ldots, \tag{2.2}$$

where A is area and π is lateral pressure, these constitute the mechanical work needed to change the area. The third term is the work done to change the number of particles, where μ_i is the chemical potential and n_i is the number of particles of species i. We will see in the next section (2.3) that in the presences of an electrical field an additional term is added to add the work done by the electrical field.

The second law of thermodynamics states,

$$\mathrm{d}S = \mathrm{d}S_r + \mathrm{d}S_i \geq \frac{\delta Q}{T}, \tag{2.3}$$

where $\mathrm{d}S$ is the change in entropy. The change in entropy can be split up in two parts $\mathrm{d}S_r$ being the reversible part and $\mathrm{d}S_i$ being the irreversible part. Irreversible processes are the spontaneous processes (like heat conduction or diffusion) that seek to equilibrate the system, these processes will always produce entropy ($\mathrm{d}S_i \geq 0$) whereas the reversible term can both be positive and negative. In other words, the reversible term of the entropy is due strictly to exchange with the outside, and the irreversible term is due strictly to processes inside the system [1] [46]. For a reversible process the state of the system is the same before and after the process, so that

$$\oint \frac{\delta Q}{T} = 0 \Rightarrow \mathrm{d}S_r = \frac{\delta Q}{T}. \tag{2.4}$$

From Eq. (2.4) we see that the reversible change in entropy is a perfect differential [2], and a thermodynamical state function. From Eq. (2.4) the heat can be written as the change in entropy due to reversible processes. Having defined the change in heat and the work done on the system we can rewrite the internal energy (Eq. (2.1)), as

$$\mathrm{d}U = T\mathrm{d}S_r - p\mathrm{d}v - \pi\mathrm{d}A + \sum_i \mu_i \mathrm{d}n_i + \ldots \tag{2.5}$$

[1] In modern thermodynamics the concept of irreversible processes is artificial since it strictly dependents on the choice of system, which mean that with an appropriate choice of system one can describe reversible processes as irreversible and vise a versa. For a discussions on this [44–46].

[2] We will not in this thesis discuss the differentiability of the irreversible part of the entropy, which would dependent on detailed interpretation of the system.

Again, using the assumption that any equilibrium state can be achieved through reversible processes we can drop the reversible notation on the entropy and write the internal energy as,

$$\mathrm{d}U = T\mathrm{d}S - p\mathrm{d}v - \pi\mathrm{d}A + \sum_i \mu_i \mathrm{d}n_i + \dots \ . \tag{2.6}$$

Each term in Eq. (2.6) is constituted by what is referred to as "conjugated variables", the one variable being extensive (additive with system size) and the other being intensive (independent on system size). Using these properties we see that the internal energy (Eq. (2.6)) is a homogeneous first order function, so for any λ, we have

$$U(\lambda S, \lambda v, \lambda A, \dots) = \lambda U(S, v, A, \dots). \tag{2.7}$$

Differentiating with respect to λ, we can show

$$U = TS - pv - \pi A + \sum_i \mu_i n_i + \dots \ , \tag{2.8}$$

from which one can show that each product on the right hand side also is a state function [47]. For the sake of simplicity of notation we in the following omit all work terms but the pv term. From Eq. (2.8) we can then construct a new set of useful state functions,

$$F \equiv U - TS \qquad \text{Helmholtz free energy} \tag{2.9}$$
$$H \equiv U - vp \qquad \text{Enthalpy} \tag{2.10}$$
$$G \equiv H - TS \qquad \text{Gibbs free energy} \tag{2.11}$$

The construction of these new state functions is done through Legendre transformations. By preforming a Legendre transformation we change the natural coordinate system of the state function, as it can be illustrated by considering the differential of Eq. (2.10) and Eq. (2.11) as follows

$$\mathrm{d}H = \mathrm{d}U - \mathrm{d}(pv) = T\mathrm{d}S + v\mathrm{d}p, \tag{2.12}$$
$$\mathrm{d}G = \mathrm{d}H - \mathrm{d}(TS) = -S\mathrm{d}T + v\mathrm{d}p. \tag{2.13}$$

The internal energy is a function of entropy, volume, etc. (these being the independent variables), whereas, the enthalpy is a function of pressure instead of volume, and the Gibbs free energy is now a function of temperature instead of entropy, and pressure instead of volume. Any constructed state function represents an allowed Legendre transform for which the choice of independent variables is free. This enables a thermodynamical description of any system, independent of its constrains, with an appropriate state function. As an example, throughout this thesis, an appropriately modified Gibbs free energy is used to describe the equilibrium state of the lipid membrane given constraint of constant temperature and pressure.

2.2 Thermodynamics of lipid melting transition

Biological cell membranes are known to display a lipid melting transition close to physiological conditions. As mentioned in the introduction (2.2) this vicinity, and biologys effort to conserve this vicinity have motivated the belief that the melting transition is vital to the functioning of the membrane. We will throughout this thesis focus on the material property implications of this transition and its implications for our understanding of biological functions.

We consider the lipid melting transition as a two state phase transition where each lipid in the membrane can be found in a gel-state ($L_{\beta'}$) or a fluid-state (L_α)[3]. We will further assume that changes outside the transition region are small (negligible). The transition temperature or melting temperate (T_m) is defined as the temperature where the two states are equally likely:

$$\frac{P_{fluid}(T_m)}{P_{gel}(T_m)} = \exp\left(-\frac{\Delta G}{RT_m}\right) = 1 \tag{2.14}$$

where $\Delta G = G_{fluid} - G_{gel}$ is the difference in Gibbs free energy between the two states. From Eq. (2.14) and using Eq. (2.11)

$$\Delta G = \Delta H - T_m \Delta S = 0 \Leftrightarrow T_m = \frac{\Delta H}{\Delta S}. \tag{2.15}$$

The difference in enthalpy (ΔH) and entropy (ΔS) between the two states can be found experimentally for a given membrane using Differential Scanning Calorimetry (DSC), which measures the heat capacity at constant pressure. The heat capacity at constant pressure is defined as

$$c_p \equiv \left(\frac{\partial Q}{\partial T}\right)_p = T\left(\frac{\partial S}{\partial T}\right)_p = \left(\frac{\partial H}{\partial T}\right)_p, \tag{2.16}$$

using Eq. (2.11) under constrains of constant pressure. Integrating over the heat capacity signal from the transition we find ΔH (see Fig. (2.1), **right**) and integrating over the heat capacity divided with the temperate we find ΔS. For pure Large Unilamallar Vesicles (LUV) of DPPC one finds $\Delta H \approx 39\ kJ/mol$, $\Delta S = 124.14\ J/mol \cdot K$ and $T_m = 314.15\ K$ [8]. We are interested in the lipid melting transition and its associated thermodynamical implications. Changes associated to the transition are referred to as excess quantities often denote with a Δ, e.g. ΔH and ΔS are respectively the excess enthalpy and the excess entropy.

The lipid melting transition is known to be affected by changes in other parameters than temperature, these can be changes in pH, ions [48–50], pressure, lateral pressure [51], electrical fields [52], lipid composition, presence of proteins and peptides [53] and various chemicals (among the most interesting are anesthetics, neurotransmitters, cooling and heating agents like menthol and capsaicin [31,54]). Using the assumption that changes outside the transition are small, the difference in free energy between the two states takes the form

$$\Delta G = \Delta H_0 - T\Delta S_0 + \delta p \Delta v + \delta\pi \Delta A + \dots, \tag{2.17}$$

[3] See section 2.2 for definition of lipid states.

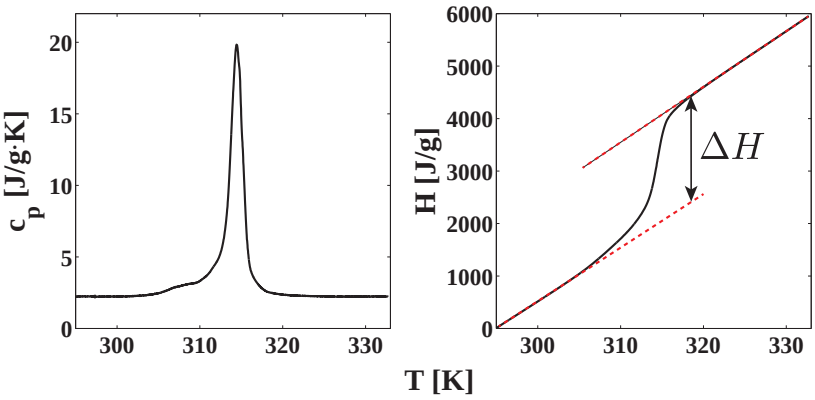

Figure 2.1: ***Left**: Heat capacity of DPPC large unilamellar vesicle [26]. **Right**: Enthalpy of DPPC large unilamellar vesicle. The jump in the enthalpy is the lipid melting transition which have a excess enthalpy ΔH.*

where the subscript 0 indicate the melting enthalpy and melting entropy values measured using DSC and the additional terms represent changes in free energy due to changes (δ) in regard to the DSC conditions. From Eq. (2.17) it is sufficient to know the difference in the state variables between the two states, to calculate the difference in free energy, e.g. the change between the two states in volume, area or thickness. The volume change is $\sim 4\%$, the area change is $\sim 25\%$ and the thickness change is $\sim -16\%$ going from the gel to the fluid state (see values in appendix A.1) [51,55]. It has additionally been shown throughout the transition region, both for pure lipid membrane and biological membranes, that the change in volume is proportional to the change in enthalpy

$$\Delta v(T) = \gamma_v \Delta H(T), \tag{2.18}$$

where the proportionality constant of LUVs of DPPC is $\gamma_v = 8.599 \cdot 10^{-10}\ m^3/J$ [51, 55]. Additionally, Molacular Dynamics (MD) simulations have shown that this relation holds beyond the transition region [56]. Heimburg [51] proposed that a similar proportionality relation should hold between change in enthalpy and change of area

$$\Delta A(T) = \gamma_A \Delta H(T), \tag{2.19}$$

where the proportionality constant for LUV of DPPC is $\gamma_A = 8.93 \cdot 10^{-1}\ m^2/J$ [51]. This prediction has been justified indirectly by lipid monolayer experiments [57] and by elasticity experiments [58]. The proportionality coupling stated in Eq. (2.18) and Eq. (2.19) holds not only for average quantities, also for all higher moments (statistical), so that their respective susceptibilities[4] are proportional

[4]Thermodynamical susceptibilities are quantities describing a extensive variables dependent on its conjugated variable, e.g. heat capacity, compressibilities.

(see appendix A.2),

$$\Delta\kappa_T^v = \frac{\gamma_v^2 T}{v}\Delta c_p \tag{2.20}$$

$$\Delta\kappa_T^A = \frac{\gamma_A^2 T}{A}\Delta c_p \tag{2.21}$$

where $\Delta\kappa_T^v$ is the excess volume compressibility, and $\Delta\kappa_T^A$ is the excess area compressibility[5]. The coupling between the geometry of the membrane and its excess enthalpy drastically reduce the complication of the lipid membrane melting transition. From this, using an experimentally found heat capacity we can predict the mechanical behavior of the membrane.

The lipid melting transition is a cooperative transition. This means that lipids do not change state independently, but that several lipids changes state simultaneously in a cooperative fashion. The cooperativity of the transition can be visualized by the presence of macroscopic domains (gel domains in a fluid phase or visa versa), in which the lipids will fluctuation together, see Fig. (2.2). The melting transition should though be considered subcritical with finite correlation lengths.

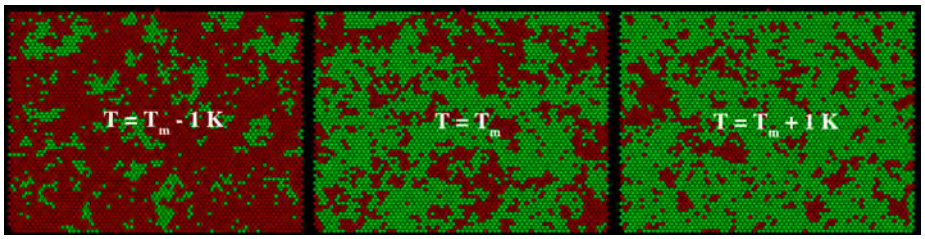

Figure 2.2: *Simulated snapshots of lipid membrane at different stages through the lipid melting transition. Red indicates lipid gel state and green is for lipid in fluid state. The simulation have been carried out as described in [59].*

We will for simplicity model the transition as a two-state transition governed by a van't Hoff law. We will write the equilibrium constant between the gel and fluid states as,

$$K(T) = \exp\left(-n\frac{\Delta G}{RT}\right), \tag{2.22}$$

where n is the cooperative unite size which describes the number of lipids that change state cooperatively. For LUVs of DPPC the cooperative size is $n_{DPPC} \approx 170$ whereas biological membranes are less cooperative $n_{bio} \approx 40$, see Fig. (2.3). From the equilibrium constant (Eq. (2.22)) we can calculate the fluid fraction, the fraction of the lipids in the system that are in the fluid state,

$$f_{fluid} = \mathrm{P}_{fluid} = \frac{K(T)}{1 + K(T)}, \tag{2.23}$$

[5]The volume compressibility is defined as $\kappa_T^v = -\frac{1}{v}\left(\frac{\partial v}{\partial p}\right)_T$. The area compressibility is defined in a similar fashion.

from which the average extensive properties can be found (e.g. $\Delta H(T) = f_{fluid} \cdot \Delta H_0$). From Eq. (2.23) and Eq. (2.16) we can calculate the excess heat capacity

$$\Delta c_p = \frac{K(T)}{(1+K(T))^2} \frac{\Delta H_0^2}{RT^2} n \tag{2.24}$$

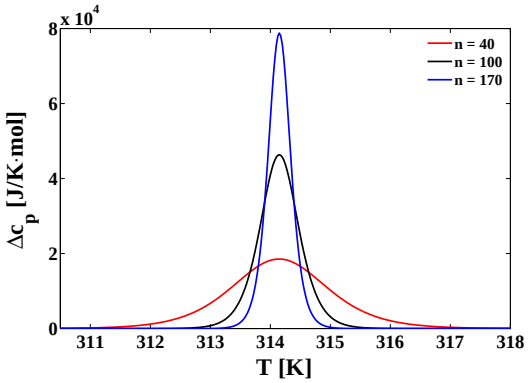

Figure 2.3: *The excess heat capacity for different cooperative unit sizes using van't Hoff law. Values for melting enthalpy and entropy are from LUV of DPPC.*

The van't Hoff law approach is a simplification of the transition and for more accurate and thorough investigation other tools, e.g. Monte Carlo simulations, can be used [22, 59–61]. However for simple predictions we will use van't Hoff law to approximate the behavior of the lipid melting transition.

2.3 Including electrical fields

Biological membranes are often subject to an applied voltage and it is therefore essential to understand how an applied voltage influences the membrane. This will be the topic of the following section. [6]

The voltage drop across biological membranes is attributed to Nernst potentials. The Nernst potential is generated by the interior and the exterior of the membrane having different ion concentrations. For instance, the concentration of potassium is about 400 mM inside and only 20 mM outside the giant squid axon. If one assume that the membrane is selectively permeable to potassium, an electrical gradient will build up due to the chemical gradient. Biological membranes are commonly subject to a voltage of around 100 mV. The non-conducting nature of the hydrophobic core of the membrane results in biological membranes acting like a charged capacitor. The membrane being pseudo 2-dimentional allows for approximating the membrane as a homogenous planar capacitor ($C_m = \varepsilon A/d$). We assume that only the component of the electrical fields or polarization orthogonal to the membrane are contributing. We hereby simplify the electrical considerations to a 1-dimensional problem so that vector notation can be dropped. We will use these simplifying approximation

[6] The development presented below has been done in collaboration with Karis A. Zecchi.

throughout this thesis.

The applied voltage (ψ) across the membrane is facilitated by a respective up and down concentration of either positive or negative ions in the electrolytic solution on the two sides of the membrane, effectively acting like charges on the capacitor, see Fig. (2.4). The electrolytic solution surrounding the membrane acts as conductors and hereby the "plates" of the capacitor.

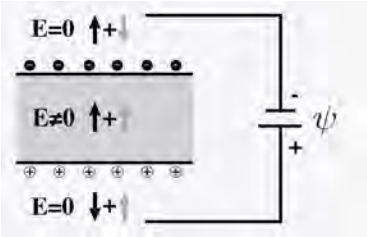

Figure 2.4: *A charge capacitor displays an internal field different from zero, while the field outside the capacitor is zero. Black arrows indicated field from positive charges and gray indicates field from negative charges.*

The charges on a charged capacitor generate a compressing force on the capacitor. For ordinary capacitors, the capacitor plates are mechanically locked and the dimensions of the capacitor are constant, which has also often been assumed for the membrane (e.g. Hodgkin and Huxley model). However, lipid membranes are deformable structures and the compressive force can therefore change the dimensions of the membrane, changing both area and thickness, see Fig. (2.5). Generally one can therefore not assume the capacitance of the membrane to be constant, since the capacitance increases upon a decrease in membrane thickness. This effect is known as "electrostriction" and have recently been described by Heimburg [43]. As we discussed in the previous section, the force needed to deform the membrane is intimately connected to the lipid melting transition. In the transition region the compressibilities of the membrane drastically increases, meaning that little force is needed to deform the membrane. In the vicinity of the lipid melting transition the membrane should therefore be considered as a non-linear capacitor (a voltage dependent capacitor)[7].

As we mentioned previously, not only are biological membranes often charged but they are often also polar structures. This means that membranes can be polarized in the absence of an applied electrical field[8]. The potentially polar nature of membranes can originate from the often found asymmetric distribution of charged lipids [15, 16] or other molecules on the two sides of the membrane, resulting in a net polarization of the membrane. Due to the large dipole moment of lipids (including non-charged species) [12, 13] any asymmetry between the two layers of the membrane can also result in a substantial net polarization orthogonal to the membrane surface. The asymmetry can be of both chemical

[7] The non-linear capacitive properties of lipid membranes is extensively discussed in chapter 4.

[8] Throughout this thesis applied field (or applied voltage) refers to a electrical field which is controllable from outside the membrane. Meaning that a field generated by a Nernst potential and applied by electrodes are both considered applied.

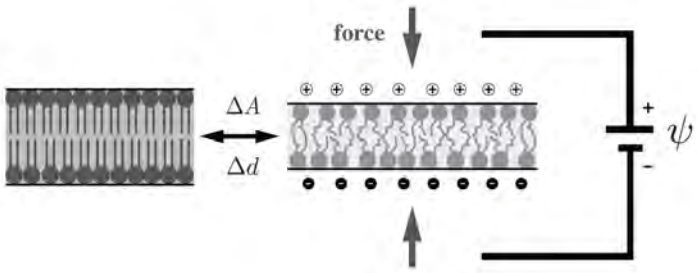

Figure 2.5: *Illustration of the electrostriction effect. The compressive force generated by the applied voltage (ψ) deforms the membrane to a state with larger area and lower thickness.*

or geometrical nature. Flexoelectricity is an example of geometric asymmetry generating polarization in lipid membrane [13, 62] (see 2.3.2). This polarization of the membrane will be referred to as "offset polarization" or "spontaneous polarization". A spontaneous polarized membrane will, in the absence of an applied electrical potential or field, be charged such that the electrical field inside and outside the membrane is zero, see Fig. (2.6) (left). To discharge a spontaneously polarized membrane a potential difference of $\psi = -\psi_0$ has to be applied, see Fig. (2.6) (right). We will refer to ψ_0 as the "spontaneous membrane potential", "offset potential" or "voltage offset". The offset potential (ψ_0) is the voltage which would have needed to be applied to the non-polarized membrane to generate the spontaneous polarization (P_0).

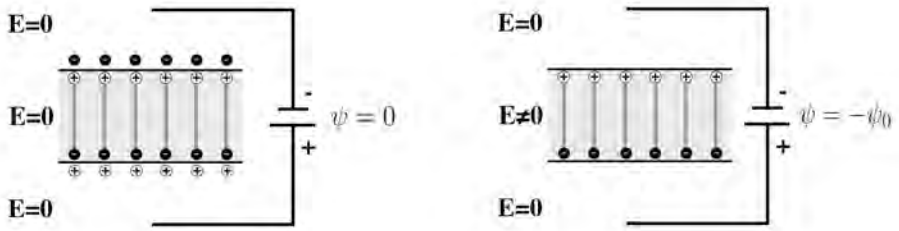

Figure 2.6: *Illustration of polarization by chemical asymmetry.* ***Left****: A spontaneously polarized membrane is charged in the absence of an applied field, to cancel the electrical field both inside and outside the membrane.* ***Right****: To discharge a membrane with a spontaneous polarization a potential of $\psi = -\psi_0$ has to be applied.*

In the next section we will carry out a careful theoretical treatment of both the capacitive and polarization effect of lipid membranes in a thermodynamical framework. We will see that capacitance, polarization, flexoelectricity, and piezoelectricity are all aspects of the same electrostatic description. Will apply our generalized electrostatic description to understand the effect of applied electrical fields on the membrane and on its lipid melting transition.

2.3.1 Framework

A dielectric material in an electric field will arrange itself so as to minimize the free energy of the system. In ordinary dielectric materials this means inducing dipoles to counteract the applied field. For more sophisticated dielectric materials, mechanical changes can be observed as a response to an applied electric field (e.g. piezoelectric crystals). To deal with these effects, authors like Frank proposed to treat an applied electric field within a thermodynamical framework [63]. He included the energetic contribution of an electric field by considering the electrical work done on a fluid during any infinitesimal and reversible change. The internal energy including the electrical work term takes the form

$$\mathrm{d}U = T\mathrm{d}S - p\mathrm{d}v + E\mathrm{d}(vD), \tag{2.25}$$

where the last term is the electrical work done on the fluid, E is the electrical field and vD is the electrical displacement in a volume v. Frank assumed a plate capacitor geometry and that the dielectric fluid was isotropic allowing for dropping the vector notation for the electrical displacement (D)[9] and the electrical field, since all but the component perpendicular to the flat surface is non-zero. We, following Frank's approach, assume a plate capacitor geometry and isotropy for the lipid membrane.

Choosing the pressure (p), temperature (T) and applied electric field (E) as independent variables we can write the appropriate Gibbs free energy,

$$\mathrm{d}G = -S\mathrm{d}T + v\mathrm{d}p - (vD)\mathrm{d}E + ... \tag{2.26}$$

The electrical contribution to the free energy due to an applied electric field comes from the third term, which we will refer to as the electrical enthalpy (H^{el}). The electric displacement is, from electrostatics, given by

$$D = \varepsilon_0 E + P_{tot}, \tag{2.27}$$

where ε_0 is the vacuum permittivity and P_{tot} is the total polarization. Most materials have zero polarization at zero electric field, and polarization only happens due to electrically induced dipoles. For a linear dielectric material the electrically induced polarization is given by $P_{\text{induced}} = \varepsilon_0 \chi_{el} E$, χ_{el} being the electric susceptibility. We are interested in extending our considerations to a dielectric material which can have an intrinsic polarization, a spontaneous polarization, of the form

$$P_{tot} = \varepsilon_0 \chi_{el} E + P_0. \tag{2.28}$$

The spontaneous polarization or offset polarization (P_0) considered is due to an asymmetry in the lipid bilayer, of either geometrical or chemical nature. Considering both the polarization offset and the electrically induced polarization in the membrane, the electric displacement takes the form

$$D = \varepsilon E + P_0, \tag{2.29}$$

[9] Frank originally only considered the polarization effect on the fluid but we will here consider the full electric displacement since we do not have a fixed capacitor surrounding the membrane. The membrane itself acts as the mechanical separation between the capacitor plates (i.e. the surrounding electrolytic solution) and as the dielectric material.

where ε is the dielectric constant ($\varepsilon = \varepsilon_0(1 + \chi_{el})$). The electrical enthalpy is from Eq. (2.29) given by

$$H^{el} = -\int_0^E (vD)\mathrm{d}E' = -\frac{\varepsilon v}{2}E^2 - vP_0E, \tag{2.30}$$

where we have assumed the volume of the lipid membrane (v) and the offset polarization to be constant. Assuming that the dielectric properties of the medium are homogeneous over the thickness (d), we can use $Ed = \psi$ (ψ being the electrical potential difference, or the applied voltage) to rewrite the electrical enthalpy,

$$H^{el} = -\frac{\varepsilon}{2}\frac{A}{d}\psi^2 - AP_0\psi \tag{2.31}$$

Alternatively, we can express the offset polarization as the voltage offset (ψ_0). The voltage offset is give by the voltage at which a membrane would have $D = P_0$ assuming only electrically induced polarization

$$\psi_0 = \frac{P_0 d}{\varepsilon} \tag{2.32}$$

We recognize the pre-factor in Eq. (2.31) as the capacitance of a planar capacitor ($C = \varepsilon A/d$). Using this and Eq. (2.32) we write an alternative form of Eq. (2.31),

$$H^{el} = -\frac{C}{2}\left(\psi^2 + 2\psi_0\psi\right) \tag{2.33}$$

For both Eq. (2.31) and Eq. (2.32) the electrical enthalpy is zero for no applied potential or field.

Note that choosing ψ_0 or P_0 involve different assumptions, since ψ_0 is geometry dependent and P_0 is not. The choice throughout this thesis will depend on the experimental conditions assumed.

Influence of applied potential on the state of the lipid membrane

Assuming that the lipids can only exist in a ground state (gel) and an excited state (fluid), the difference in enthalpy (Eq. (2.31)) due to an applied voltage between the two states can be written as

$$\Delta H^{el} = H^{el}_{fluid} - H^{el}_{gel} = -\frac{\Delta C}{2}\psi^2 - \Delta A P_0 \psi. \tag{2.34}$$

We have here assumed that the offset polarization is independent of the state of the membrane. Note that Eq. (2.34) is a generalization of the electrical contribution to the melting enthalpy described by Heimburg [43].

We see that the difference in electrical enthalpy (Eq. (2.34)) can favor the gel or the fluid state of the membrane depending on the sign of the change in capacitance and on the polarization offset. For DPPC[10] the capacitance in the fluid state is ~ 1.5 times greater then in the gel and the differences in capacitance is positive. We can assume similar differences for other lipid species.

[10] For DPPC the area is $\sim 25\%$ larger and the thickness $\sim 16\%$ thinner in the fluid state compared to the gel, see appendix A.1.

We have assumed the dielectric constant to be independent of the state of the membrane. From the difference in the electrical enthalpy (Eq. (2.34)) between the gel and the fluid state of lipid membranes we can calculate the effect of an applied electric field on the lipid melting temperature using Eq. (2.15), as shown in Fig. (2.7).

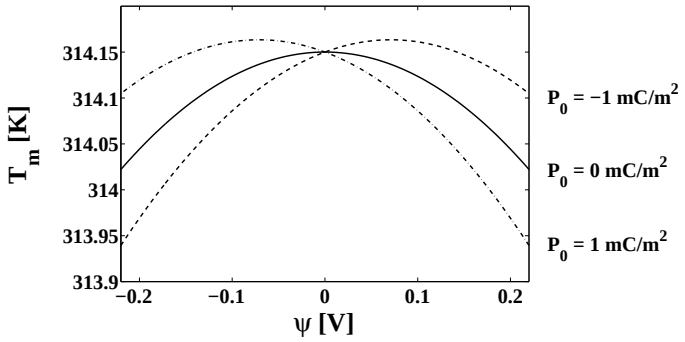

Figure 2.7: *The lipid melting temperature as a function of applied voltage for different offset polarizations. Value used are from LUV of DPPC, where* $\Delta C \approx 656\ J/(mol \cdot V^2)$ *for* $\varepsilon = 4 \cdot \varepsilon_0$.

We use the lipid melting temperature as a proxy for the state of the membrane and see from Fig. (2.7) that an applied voltage can influence the state of the membrane both towards the gel and fluid state depending on the applied voltage and the offset polarization.

Loosening the assumption of the polarization offset being independent of the state of the membrane, we get the general expression for the difference in electrical enthalpy,

$$\Delta H^{el} = -\frac{\Delta C}{2}\psi^2 - \Delta(AP_0)\psi. \tag{2.35}$$

We see in Fig. (2.8) that we allowing the polarization offset to be dependent on the state of the membrane can have great influence on the coupling between the applied voltage and the state of the lipid membrane.

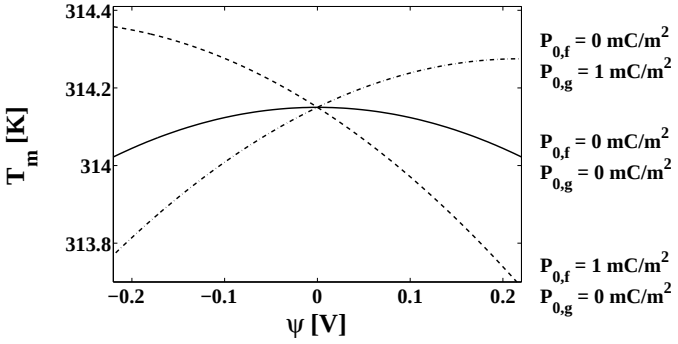

Figure 2.8: *The lipid melting temperature as a function of applied voltage assuming the offset polarization is different in the two lipid states. Value used are from LUV of DPPC, where* $\Delta C \approx 656\ J/(mol \cdot V^2)$ *for* $\varepsilon = 4 \cdot \varepsilon_0$.

2.3.2 Polarization effect

Above we introduced the appropriate general thermodynamical framework to describe electrostatics in membranes. We will here show how this framework relates to known electrostatic properties of membranes, covering electrostriction, capacitive susceptibility, piezoelectricity and flexoelectricity, and how these can be generalized.

Electrostriction

The charges on the two sides of a charged capacitor attract one another exerting a compressive force on the capacitor. We can from Eq. (2.33) calculate the electrostrictive force on the capacitor (membrane). The compressive force ($\mathcal{F}$) acting on the membrane is given by,

$$\mathcal{F} = \frac{\partial H}{\partial d} = \frac{\partial H^{el}}{\partial d} + const. \tag{2.36}$$

$$= -\frac{1}{2}\left(\frac{\partial C}{\partial d}\right)\psi^2 - \left(\frac{\partial (C\psi_0)}{\partial d}\right)\psi + const. \tag{2.37}$$

Assuming that $A \approx const.$, $\psi_0 \approx 0$ and $\psi = const.$ we recover the electrostriction force as given in the literature, e.g. [43],

$$\Delta\mathcal{F}(\psi) = \frac{1}{2}\frac{C}{d}\psi^2. \tag{2.38}$$

Allowing for a constant but non-zero offset voltage the electrostrictive force get an offset,

$$\Delta\mathcal{F}(\psi) = \frac{1}{2}\frac{C}{d}\left(\psi^2 + 2\psi_0\psi\right). \tag{2.39}$$

The electrostrictive force is a quadratic function of the applied voltage and can, for polar capacitors, display an additional linear term. Note, that for a polar capacitor the compression force exerted on the capacitor can be negative. Considering only small change in thickness ($\Delta d << d$) and constant area, the

change in capacitance can be approximated as $\Delta C \approx -C/d\Delta d$. We can likewise linearize the electrostrictive force to be proportional to the change in thickness (ordinary spring). Doing this we see that the change in capacitance can be approximated as being proportional to the electrostrictive force,

$$\Delta C \propto \left(\psi^2 + 2\psi_0\psi\right), \tag{2.40}$$

where the proportionality constant depends on the elastic properties of the membrane. Note that the assumptions leading to Eq. (2.40) are not satisfied in the vicinity of the lipid melting transition.

Electrostriction in pure lipid membranes and biological membranes has been investigated by various authors [64, 65]. Alvarez and Latorre [64] investigated the voltage dependence of the capacitance in both symmetric and asymmetric black lipid membrane, see Fig. (2.3.2). They found the same functional dependence as in Eq. (2.40) with an offset voltage of respectively 47 mV and 116 mV for two different salt concentrations, for an asymmetric membrane with zwitterionic lipids one side and charge lipids on the other. They found no offset voltage for the symmetric membrane. In their findings, we observe that the quadrating dependence of the capacitance of the two asymmetric membranes is conserved and only the offset is affected by changing the salt concentration, indicating a salt dependence of the offset voltage.

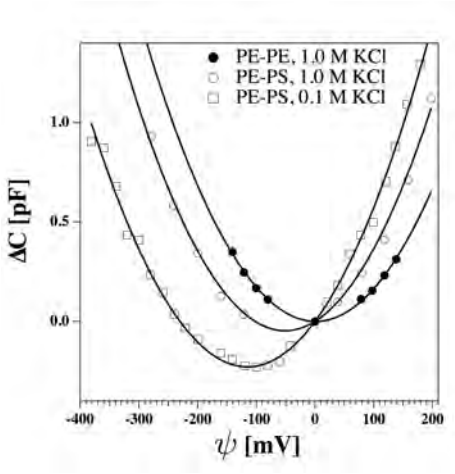

Figure 2.9: *The change in capacitance as a function of applied voltage in a black lipid membrane.* ***Solid cycles****: Two symmetric layers of zwitterionic lipids constitutes the membrane in* 1 *M KCl.* ***Open cycles****: Asymmetric membrane, one layer of zwitterionic lipids, and one of charged lipids in* 1 *M KCl.* ***Open squares****: Assymetric membrane as for* ***open cycles*** *in* 0.1 *M KCl. The membrane capacitance at* $\psi = 0$ *is approximately* 300 pF*. Adapted from [64].*

The change in capacitance observed by Alvarez and Latorre [64] is only about $\sim 0.5\%$ of the membrane capacitance for an applied voltage of 300 mV. Ferrell et al. [65] observed in biological membranes an offset of about 70 mV and a change in capacitance of $\sim 0.5\%$ due to an applied 200 mV. Both of these experiments are carried out outside the transition region. The dependence on

the elastic properties of the membrane in Eq. (2.40) indicates that we can expect large voltage dependence of the capacitance in the vicinity of the lipid melting transition. The non-linear behavior of the membrane capacitance in the vicinity of the lipid melting transition is the topic section 4.2.

Dependencies of the charges on the capacitor

When measuring the electrical properties of a capacitor, a common approach is to perturb the capacitor and measure the change in charges (q), by measuring the current ($I = \mathrm{d}q/\mathrm{d}t$)[11]. Here the perturbation is applied through changes in the applied voltage (ψ), the area (A) and curvature (c)[12]

$$\mathrm{d}q = \left(\frac{\partial q}{\partial \psi}\right)_{A,c} + \left(\frac{\partial q}{\partial A}\right)_{\psi,c} + \left(\frac{\partial q}{\partial c}\right)_{\psi,A}. \tag{2.41}$$

This corresponds to a experiment where the applied voltage, area and curvature can be controlled. From Gauss law and using the pseudo 2-dimensional nature of the lipid membrane the charge on the membrane is given by,

$$q = A \cdot D = A\left(\varepsilon E + P_0\right) = \varepsilon \frac{A}{d}\left(\psi + \psi_0\right) = C_m\left(\psi + \psi_0\right). \tag{2.42}$$

Inserting Eq. (2.42) in Eq. (2.41) we get the expression for the change in charge on the membrane,

$$\begin{aligned}\mathrm{d}q = &\left[\left(\psi + \psi_0\right)\left(\frac{\partial C_m}{\partial \psi}\right)_{A,c} + C_m + C_m\left(\frac{\partial \psi_0}{\partial \psi}\right)_{A,c}\right]\mathrm{d}\psi \\ &+ \left[\left(\psi + \psi_0\right)\left(\frac{\partial C_m}{\partial A}\right)_{\psi,c} + C_m\left(\frac{\partial \psi_0}{\partial A}\right)_{\psi,c}\right]\mathrm{d}A \\ &+ \left[\left(\psi + \psi_0\right)\left(\frac{\partial C_m}{\partial c}\right)_{\psi,A} + C_m\left(\frac{\partial \psi_0}{\partial c}\right)_{\psi,A}\right]\mathrm{d}c\end{aligned} \tag{2.43}$$

We can construct a similar expression for any choice of controlled variables, e.g. instead of controlling the area we could control the lateral pressure (π).

Capacitive susceptibility

The first term in Eq. (2.43) describe the change in charge on the membrane capacitor upon a changes in applied voltage. Assuming the area and the curvature are constant and taking the partial derivative in regard to the applied voltage we get the differential capacitance or, as defined by Heimburg [43], the capacitive susceptibility ($\hat{C}_m \equiv \partial q/\partial \psi$),

$$\hat{C}_m = \left(\psi + \psi_0\right)\left(\frac{\partial C_m}{\partial \psi}\right)_{A,c} + C_m + C_m\left(\frac{\partial \psi_0}{\partial \psi}\right)_{A,c}. \tag{2.44}$$

[11] This will be explored in chapter 4.

[12] The curvature $c = 2/R$, where R is the principle radii of curvature. We assume spherical geometric.

Assuming the offset voltage is zero and constant, we recover the expression for the capacitive susceptibility given by Heimburg [43],

$$\hat{C}_m = C_m + \psi \left(\frac{\partial C_m}{\partial \psi} \right)_{A,c}. \tag{2.45}$$

Direct piezoelectric effect

The second term in Eq. (2.43) describe the change in charge on the membrane capacitor upon a change in area. Considering no applied voltage and curvature this corresponds to a variant of the classical direct piezoelectrical effect

$$\mathrm{d}q = \left[\psi_0 \left(\frac{\partial C_m}{\partial A} \right)_{\psi,c} + C_m \left(\frac{\partial \psi_0}{\partial A} \right)_{\psi,c} \right] \mathrm{d}A, \tag{2.46}$$

where a mechanical change generates a electrical response. Considering small change in area such that Eq. (2.44) can be linearized and assuming $\psi_0(\Delta A = 0) = 0$ we recover the piezoelectric formulation of Petrov [66],

$$q(\Delta A) \approx C_m \left(\frac{\partial \psi_0}{\partial A} \right)_{\psi,c} \Delta A \quad \text{or} \quad \psi_0(\Delta A) \approx \left(\frac{\partial \psi_0}{\partial A} \right)_{\psi,c} \Delta A. \tag{2.47}$$

Petrov writes $(\partial \psi_0 / \partial A)_{\psi,c}$ as $e_s/(\varepsilon A_0)$ where e_s is a constant which is estimated to be $e_s \sim \varepsilon_0$ and A_0 is the area before perturbation. Note that Eq. (2.47) is a special case of the general Eq. (2.46).

Inverse piezoelectric effect

The elastic free energy density[13] of a lateral compression (g^A) is given by,

$$g^A = \frac{1}{2} K_T^A \left(\frac{\Delta A}{A_0} \right)^2, \tag{2.48}$$

where K_T^A is the isothermal lateral compression modulus and A_0 is the area before compression. Including the electrical enthalpy contribution to the free energy density we get,

$$g^A = \frac{1}{2} K_T^A \left(\frac{\Delta A}{A_0} \right)^2 - \frac{1}{2} \frac{C_m}{A_0} \left(\psi^2 + 2\psi_0 \psi \right). \tag{2.49}$$

Equilibrium will be established so that $\partial g^A / \partial A = 0$. Assuming constant lateral compression modulus and constant applied voltage the change in area that satisfy this is given by

$$\Delta A(\psi) = A_0 \left(\frac{C_m}{K_T^A} \left(\frac{\partial \psi_0}{\partial A} \right)_{\psi,c} \psi + \frac{1}{K_T^A} \left(\frac{\partial C_m}{\partial A} \right)_{\psi,c} \left(\psi^2 + 2\psi_0 \psi \right) \right) \tag{2.50}$$

This expression describes the inverse piezoelectric effect, e.g. the mechanical response on a change in the applied voltage, of a polar lipid membrane.

[13] The free energy is recovered from the free energy density by integrating over the surface of the membrane.

Direct flexoelectric effect

The last term in Eq. (2.43) describe the change in charge on the membrane capacitor upon curving or flexing the membrane. Considering constant applied voltage and constant area this corresponds to the direct flexoelectric effect

$$\mathrm{d}q = \left[(\psi + \psi_0) \left(\frac{\partial C_m}{\partial c} \right)_{\psi,A} + C_m \left(\frac{\partial \psi_0}{\partial c} \right)_{\psi,A} \right] \mathrm{d}c, \tag{2.51}$$

where, like in the case off the piezoelectric effect, a mechanical change (curvature) generates an electrical response. Assuming the membrane capacitance is independent of the curvature and that $(\partial\psi_0/\partial c)_{\psi,A} = const.$ we recover a flexoelectric description equivalent to that of Petrov [62] whom pioneered the field,

$$q(c) \approx C_m \left(\frac{\partial \psi_0}{\partial c} \right)_{\psi,A} c \quad \text{or} \quad \psi_0(c) \approx \left(\frac{\partial \psi_0}{\partial c} \right)_{\psi,A} c. \tag{2.52}$$

Petrov introduced a flexoelectric coefficient (f) which in this special case Eq. (2.52) is give by $f = \varepsilon(\partial\psi_0/\partial c)_{\psi,A}$. Petrov and collaborators have conducted extensive work experimentally finding $f \sim 10^{-18}\ C$, which corresponds to $(\partial\psi_0/\partial c)_{\psi,A} \sim 3 \cdot 10^{-8}\ V \cdot m$ assuming $\varepsilon = 4 \cdot \varepsilon_0$ [13].

Inverse flexoelectric effect

In a similar fashion as in Eq. (2.49), we can write the elastic free energy density of bending (g^B), assuming no spontaneous curvature, as

$$g^B = \frac{1}{2} K_B c^2 - -\frac{1}{2} \frac{C_m}{A_0} \left(\psi^2 + 2\psi_0 \psi \right), \tag{2.53}$$

where K_B is the bending modulus and we have included the electrical contribution. Again, equilibrium is established so that $\partial g^B/\partial A = 0$. Assuming that the capacitance and the bending modulus are independent of curvature and constant applied voltage, we find the voltage dependence of the membrane curvature as

$$c(\psi) = \frac{1}{K_B} \frac{C_m}{A_0} \left(\frac{\partial \psi_0}{\partial c} \right)_{\psi,A} \psi. \tag{2.54}$$

This is known as the inverse flexoelectric effect, e.g. curvature induced by an applied voltage. We see that we have recovered an expression for the inverse flexoelectric effect equivalent to the one given by Petrov [13].

2.4 Discussion of thermodynamic approach

Nerve membranes are known to be both polar structures and to be subject to an applied field (Nernst potential). To understand the properties of these structures it is vital to understand how polarization influences the system and how both polarization and electrical field couples to the membrane. To this end we have provided a general thermodynamical framework for treatment of polarization effects on the properties of lipid membranes. The framework unifies and generalizes a multitude of known electrical material properties, including piezoelectric and flexoelectric properties, offset potentials and non-linear capacitance. Additionally the thermodynamical framework allows for a detailed treatment of the coupling between electrical field and the membrane state.

In the case of a non-polar membrane applying an electric field will charge the membrane which in turn will lead to a compression of the lipid membrane, the so-called electrostriction. This compression will shift the state of the lipid membrane towards its thinnest state, the fluid state. This has been shown by Heimburg in [43], who calculated a quadratic decrease of the melting temperature as a function of voltage. However, when dealing with a membrane with an offset polarization, an applied field can result in a discharging of the membrane (see Fig. (2.6)) and hereby a reduced compression of the membrane. This leads to the possibility of an applied field shifting the state of the lipid membrane towards its thicker state, the gel state. The offset polarization, both for constant offset polarization and lipid state dependent offset polarization, introduces a linear dependence on voltage of the free energy of the membrane, which is illustrated by the linear shift in the lipid melting temperature in Fig. (2.7) and Fig. (2.8). Antonov *et al.* [52] showed in their experimental investigation of the effect of an applied voltage on the lipid melting temperature that the melting temperature approximately followed a linear dependence of voltage. Results that can be understood as the membrane investigated by Antonov *et al.* [52] being polar. Likewise, for permeability studies of pure lipid membranes, an offset voltage in the current voltage relationship is observed, notably in membrane formed at the tip of glass pipettes [31]. The offset voltage can be explained by the membrane being polar, likely due to curvature [32], see 4.3 for details. We saw in 2.3.2, that chemically asymmetric membranes displaye an offset voltage and that a similar offset was observed in biological membranes, both of which can be explained by the polar nature of the membrane.

The offset polarization of membranes can originate from various polarization asymmetries between the two lipid leaflets, both chemical and geometrical asymmetries. For biological membranes, polarization asymmetries can originate from any constituting element of the membrane, not only asymmetries in lipid composition. An obvious example could be the presence of membrane proteins which can result in the membrane showing a net polarization. We can also speculate that other membrane adhesive molecules with large dipoles can be used to create an asymmetric membrane, fluorophores could be an example. Depending on the nature of the offset polarization, the system can display i.e. piezoelectric properties, an area dependence of the polarization offset[14]. Even electro-mechanical

[14] Note that also electrostriction couples the area of the membrane to voltage.

response of a lipid membrane can been recorded upon addition of "chemicals", as calcium [67]. The details of the polarization offset depends not only on its origin but also on external conditions as salt concentration [64], pH and the presence of divalent ions.

2.4.1 Electrolyte solution

In our treatment (2.3.2) the electrolyte solution surrounding the membrane is considered as perfect conductor. This view is an oversimplification and the electrolytic surroundings can have strong effects on the membrane. To fully capture the effect of electrical fields on the lipid melting transition we need to understand the effect of the electrolyte on the membrane and the electrical behavior of the total system, electrolyte and membrane. Ions can interact with the membrane hereby changing polarization properties of the membrane and they can affect lipid-lipid interactions, and ion gradients across the membrane leads to the generation electrical potentials (Nernst potential).

Monolayer experiments have shown that surface polarization of charge lipid monolayers change significantly with changing concentration of NaCl or pH [12], and we can expect divalent ions to have an even stronger effect. The ion concentration on the two sides of biological membranes is different and in experiments on artificial membranes different ion concentrations on the two sides can easily be achieved. For asymmetric ion concentrations, one need to consider that changing the ion concentration affect the polarization of each leaflet of the membrane, beyond the effect of Nernst potential.

Beyond changing the polarization of the lipids, ions also affect the lipid-lipid interaction as illustrated by the experimental evidence that the ionic solutions, especially divalent cations ions and hydrogen ions, can drastically affect the state of the lipid membrane [48, 50, 68–71]. The magnitude and nature of the effect of ions on the lipid melting transition depends strongly on the lipids, for especially charged lipid species the effect is large, but also on the ions. Both "diffusive" shielding of lipid group electrostatic interactions and also "binding" or association has been observed [72]. For charged lipids changing the concentration of monovalent cations 0.1 M to 0.5 M at physiological pH result in a decrease in the lipid melting temperature of more the then 5 K [48]. For DPPC (zitterionic lipid) a change from no salt to 1 M decreases the melting temperature of about 1.5 K [73]. For divalent ions the effect is much stronger. For charge lipids, an increase in the melting temperature of more then 10 K, due to the addition of one divalent ion per two lipids ($\sim$ 1 mM) at physiological monovalent ion concentration, have been reported. Likewise, a lowering of the pH result in drastic increase in the melting temperature [48]. For non-charged lipids the effect of divalent ions and pH much smaller than for charged lipids but still significant at physiological concentrations.

All effects of ions on the membrane, both on polarization and the state, depends on ion concentration, independently on the underlying interaction mechanism, diffusive shielding or binding. The charged nature of the ions means that they are compliant to electrical fields, including applied electrical fields. This can result in a local down or up concentration of respectively anion and cations

near an interface (membrane) depending on the local electrical field. Following calculations done by Ambjörnsson *et al.* [74] we can calculate the change in concentration of anion and cations (monovalent), due to an applied electrical field, close to a flat membrane using the Debye-Hückel approximation[15]. This calculation is naive, as it does not takes into account the advanced electrostatic effects close to the membrane, but it serves to illustrate the electrical effect on the ion concentration close to the membrane, see Fig. (2.10).

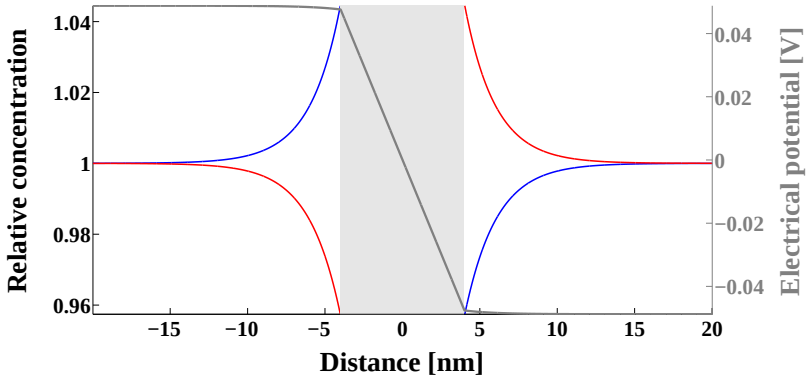

Figure 2.10: *The change in concentration of anions (red) and cations (blue) relative to bulk close to a flat membrane (light gray box) due to an applied electrical potential ($\psi = 0.1\ V$). The electrical potential is shown in gray, left y-axis. The Debye length used for the electrolyte solutions (monovalent ions, 100 mM) is $\kappa^{-1} = 1\ nm$ and dielectric constants are $\varepsilon_{electrolyte} = 80 \cdot \varepsilon_0$ and $\varepsilon_{membrane} = 4 \cdot \varepsilon_0$. The electrodes are assumed to be far alway ($L \to \infty$) and the membrane thickness is $d = 4\ nm$.*

In the naive example illustrated in Fig. (2.10) we see that going from an applied electrical potential of 0.1 V to no applied potential changes the ion concentration experienced by the membrane by $\sim 5\%$. We see from this example that an applied electric potentials effectively can act as a regulator of the ion-membrane interaction, and hereby affect the state and the polarization of the membrane. Traüble [70] showed that for electrically asymmetric lipid membranes changes on one side, like the absorption of divalent ions, can change the local electrical field on the other side, effectively leading to electrical signaling across the a globally neutral membrane.

One can imagine that in the case of nerve membranes, which are highly asymmetric and have very different ion concentrations on the two sides (including divalent ions), a depolarization, which effectively is a redistribution of the ions, can lead to significant changes in both the polarization and the state of the membrane and even an asymmetric release of ions absorbed on the membrane surface. A thorough treatment of the ion-membrane interactions is therefore necessary for understanding the electrical properties of cells and especially nerves and their action potential.

[15] The Debye-Hückel approximation is valid under the conditions that the electrical energy is small compared to the thermal energy, which is viable when considering high salt concentration or low electrical fields.

2.4.2 Electro-mechanical coupling

Based on the framework we presented for polarization effects in lipid membrane and taking into account the possible effects of the electrolytic solution we see that membranes can display a significant electro-mechanical coupling. Not only can an applied electrical field affect the state of the membrane and hereby its thickness and area but a state change of the membrane can lead to significant electrical signal from the membrane. From Eq. (2.43) we see that the change in the charge on the membrane depends on the area of the membrane as

$$\mathrm{d}q = \left[(\psi + \psi_0) \left(\frac{\partial C_m}{\partial A} \right)_{\psi,c} + C_m \left(\frac{\partial \psi_0}{\partial A} \right)_{\psi,c} \right] \mathrm{d}A. \tag{2.55}$$

Here we assume that the applied voltage and curvature is constant. Considering a nerve membrane which is both polar and subjected to an "applied" voltage of around 100 mV we can expect substantial piezoelectrical response to a change in area. The Soliton model proposed that the nerve signal is a lateral density soliton propagating in the cylindrical nerve membrane. The soliton locally pushes the membrane from its native fluid state in to the gel state. Considering this the soliton will produce a biphased electrical current response with amplitudes around 80 $\mu A/cm^2$ assuming no offset polarization [8]. Including polarization effects we can then expect a significant increase in the electrical response. Interestingly this yields results not far from the electrical current signal calculated by Hodgkin and Huxley model for the squid giant axon [75]. A common method for stimulating a nerve signal (see chapter 6) is to apply an electrical pulse to the membrane, both voltage and current stimulation is possible. Interestingly the inverse piezoelectrical effect means that an electrical change has a mechanical response, allowing for a coupling between electrical stimulation and the excitation of a soliton.

The electrical properties of the membrane is the topic of chapter 4, where we will explore the electrical implications of the polar and non-constant nature of membranes.

Chapter 3

Response behavior of lipid membranes

In the previous chapter (2) we introduced and further developed the thermodynamics description of the lipid melting transition, with which we can find equilibrium properties of the lipid membrane in the vicinity of its transition. The beauty of a thermodynamical description is its ability to describe vastly complex systems by relative few macroscopic variables (temperature, volume, pressure, etc.). However, classical thermodynamics only describes the equilibrium and contains a priori no insight on the dynamics of the system around equilibrium. With the development made over the last century by non-equilibrium thermodynamics, predictions regarding the dynamic behavior of thermodynamical systems can be made [45][1].

In this chapter we will first describe the dynamics of a thermodynamic system close to equilibrium, formally known as linear response theory. We will do this by considering the response of a system subject to perturbations. In describing the response we are introduced to dynamical susceptibilities which act as transfer functions. In the second part of the chapter we will discuss the nature of dynamical susceptibilities and specifically we will discuss the appropriate transfer function for the relaxation behavior of the lipid membrane in the vicinity of the lipid melting transition.

3.1 Response theory

To illustrate the response of a thermodynamical system to perturbations we choose to consider a system subject to temperature perturbations. Thermodynamically, changes in temperature are coupled to changes in the dependent thermodynamical variables. Here we consider the enthalpy of the system as the only dependent variable,

$$\mathrm{d}H = \left(\frac{\partial H}{\partial T}\right)_{p,\,\ldots} \mathrm{d}T = c_p(T)\mathrm{d}T. \tag{3.1}$$

[1] Other authors whom have contributed greatly are Einstein, Callen, Green, Prigogine, Jarzynskis, Crooks.

Considering small changes in temperature, such that the system is kept close-to-equilibrium, a linear relation between the perturbation (change in temperature) and response (change in enthalpy) can be assumed. Using this assumption and writing the change in temperature as a rate ($\dot{T}(t) = \partial T(t)/\partial t$),

$$\Delta H(t) = \int_{-\infty}^{t} c_p(t-t')\dot{T}(t')\mathrm{d}t'. \tag{3.2}$$

In Eq. (3.2) the heat capacity has been written as a transfer function. The transfer function depends on the time difference rather then the absolute time so that Eq. (3.2) assumes the form of a convolution. The time difference dependence of the transfer function originates from the consideration that if changes happen faster than the transfer rate (or relaxation rate), the energy transferred during the change will only be partial. We write the transfer function (dynamic heat capacity) as

$$c_p(t-t') = c_{p,0} + \Delta c_p \left(1 - \Psi_{c_p}(t-t')\right), \tag{3.3}$$

where Δc_p is the equilibrium excess heat capacity and Ψ_{c_p} is the relaxation function which describes the dynamical properties of the transfer function. The relaxation function is a decaying function such that as the system approaches equilibrium the relaxation function approaches zero ($0 \geq \Psi_{c_p} \geq 1$). Last, $c_{p,0}$ is the part of the dynamic heat capacity which relaxes much faster than the perturbation under consideration. For the lipid membrane this would be the relaxation of the lipid chains. We can using Eq. (3.3) write Eq. (3.2) as

$$\Delta H(t) = \int_{-\infty}^{t} \left(c_{p,0} + \Delta c_p \left(1 - \Psi_{c_p}(t-t')\right)\right) \dot{T}(t')\mathrm{d}t'. \tag{3.4}$$

$\Delta H(t)$ is the dynamic change in enthalpy as a response to a imposed dynamic change (perturbation) in temperature. From the response function (Eq. (3.4)) we can calculate the response of the system to a perturbation[2].

Perturbations

In perturbation experiments mainly two types of perturbations are used to probe the relaxation behavior of a system, jump and sinusoidal perturbations. In our example, jump perturbations are preformed by changing the temperature from an initial value to a target value in an "instantaneous" jump, such that

$$\dot{T}(t) = \Delta T \delta(t), \tag{3.5}$$

where ΔT is the magnitude of the temperature perturbation and $\delta(t)$ is the Dirac delta[3] which represent the rate ($[1/s]$). Eq. (3.5) leads to the common form of the response,

$$\Delta H(t)_{jump} = \left(c_{p,0} + \Delta c_p \left(1 - \Psi_{c_p}(t)\right)\right) \Delta T. \tag{3.6}$$

This perturbation approach has a number of issues: performing the jump as a step and measuring reliably the response over course of the relaxation is experimentally difficult and non-linear response behavior can occur, for which the

[2] From the fluctuation-dissipation theorem [76, 77] the perturbation considered above can be both spontaneous fluctuations of the system or externally imposed.

[3] We assumed the jump to be a perfect step at $t = 0$.

relaxation is not governed by linear response theory. This led Manfred Eigen to develop the sinusoidal perturbation technique circumventing the bulk of issues of jump techniques and for which he received the Nobel prize in chemistry [78]. Sinusoidal perturbation is performed by perturbing the system in a sinusoidal fashion,

$$T(t) = \Delta T \exp(i\omega t), \tag{3.7}$$

such that Eq. (3.4) takes the form

$$\Delta H(\omega)_{sin} = \left(c_{p,0} + \Delta c_p \int_0^\infty \exp(-i\omega t) \dot{\Psi}_{c_p}(t)\, \mathrm{d}t \right) T(\omega). \tag{3.8}$$

where ω is the angular frequency of the perturbation and $T(\omega)$ is the Fourier transform of $T(t)$. Derivation is carried out in the appendix in Mosgaard *et al.* [79].

We see that the response to both jump and sinusoidal perturbations can be calculated knowing the transfer function. The nature of the thermodynamical transfer functions or dynamic susceptibilities is the focus of the next section.

3.2 Dynamic susceptibilities

We introduced thermodynamical susceptibilities in chapter 2. The thermodynamical susceptibilities are quantities describing the dependence of an extensive variables on their conjugated intensive variables. The enthalpy dependence on temperature is expressed by the heat capacity at constant pressure. The heat capacity describes the new enthalpy at equilibrium after a change in temperature from a prior equilibrium state. Hence, with knowledge of the heat capacity we know the equilibrium enthalpy after a change in temperature. The generalized or dynamic susceptibilities generalizes this concept, to hold also out of equilibrium (though close), such that we know the trajectory of the enthalpy between the two equilibrium states through the dynamic heat capacity. From non-equilibrium thermodynamics we can describe the dynamics of fluctuations in enthalpy and hereby the dynamics of the dynamic heat capacity.

Einstein [44] inspired with his 1910 paper authors like Onsager [45] to develop linear non-equilibrium or close to equilibrium thermodynamics which deals with the nature of irreversible processes. Following Einstein, we consider the entropy (which is a state function) around equilibrium,

$$S - S_0 = \frac{1}{2} \sum_{ij} \left(\frac{\partial^2 S}{\partial \xi_i \xi_j} \right)_0 \xi_i \xi_j + O(\xi^3), \tag{3.9}$$

where the subscript 0 indicates equilibrium values, and ξ is the change from equilibrium of an extensive thermodynamical variable. Note that this change from equilibrium will be referred to as a perturbation. We assume that we are close to equilibrium so that we can drop higher order terms and all odd terms are zero since we expand around equilibrium. This is equivalent to assuming that fluctuations of a free extensive variable are Gaussian around its equilibrium value. In the picture of Einstein the entropy is a potential, for which the

maximum is the equilibrium. This analogy means that any perturbation out of equilibrium will experience a force proportional to the gradient of the entropy potential. We consider here only changes of a single extensive thermodynamical variable[4]. The flux of the free extensive variable (J) back to equilibrium is given by,

$$J(\xi,t) = \frac{d\xi}{dt} = LX(\xi,t) = L\frac{\partial S}{\partial \xi} = L\left(\frac{\partial^2 S}{\partial \xi^2}\right)_0 \xi, \tag{3.10}$$

where X is the restoring force and L is the proportionality constant. Note, that Eq. (3.10) is a Taylor expansion around small forces, and we will throughout this chapter assume that thermodynamical forces are small. Solving Eq. (3.10) the common single exponential relaxation dynamics is recovered with additional insight into the nature of the characteristic relaxation time, τ.

$$\xi(t) = A\ exp\left(tL\left(\frac{\partial^2 S}{\partial \xi^2}\right)_0\right) = \xi_0\ exp\left(-\frac{t}{\tau}\right), \tag{3.11}$$

where A is the integration constant, ξ_0 is the target change and the characteristic relaxation time $\tau = -(L(\partial^2 S/\partial \xi^2)_0)^{-1}$. We continue with the example from section 3.1 with the enthalpy as the free extensive variable ($\xi = H$). From Eq. (2.12) and assuming constant pressure the change in entropy can be written as

$$\mathrm{d}S = \frac{1}{T}\mathrm{d}H. \tag{3.12}$$

From Eq. (3.12) we can write the characteristic relaxation time from Eq. (3.11) as

$$\tau = -(L(\partial^2 S/\partial \xi^2)_0)^{-1} = c_p T^2/L, \tag{3.13}$$

using $c_p = (\partial H/\partial T)_p$. Comparing Eq. (3.11), using Eq. (3.13), with Eq. (3.4) we see that

$$\Psi(t) = \exp\left(-t\frac{L}{T^2 c_p}\right). \tag{3.14}$$

We see from Eq. (3.14) that under the assumptions of Gaussian fluctuation of the free extensive thermodynamical variable the characteristic relaxation time is proportional to the appropriate susceptibility, here the heat capacity. Knowing the proportionality constant (L), for systems where the Gaussian assumption holds, we can predict the full dynamic behavior of the system from an equilibrium DSC experiment.

Using pressure jump calorimetry, Grabitz *et al.* [22] tested the applicability of Eq. (3.14) for the relaxation of lipid membranes in the vicinity of their lipid melting transition. They found within their available resolution remarkable agreement between the predicted proportionality between the characteristic relaxation time and the excess heat capacity throughout the transition region. For LUV of DPPC they found a proportionality constant of $L = 13.9 \cdot 10^8\ J \cdot K/(s \cdot mol)$, corresponding to a maximum relaxation time of $\tau_{max} \sim 3\ s$ at T_m . This proportionality is remarkable. It makes predictions about the dynamics of the membrane, spanning characteristic time scales from milliseconds outside the transition to seconds close to the melting temperature. The proportionality found between fluctuations in enthalpy, volume

[4]For a full derivation see treatment [45, 80]

(Eq. (2.18)) and area (Eq. (2.18)) further indicates that the membrane in the transition region only have a single free state variable and therefore a single relaxation behavior describing the enthalpy, area and volume of the lipid membrane.

The above linear non-equilibrium treatment illuminates the fundamental nature of single exponential relaxation behavior which is exhibited by many simple systems. We see from Eq. (3.9) that single exponential relaxation is a low order approximation for the dynamics of thermodynamical systems in general. Exotic materials and especially systems exhibiting a phase transition are however known to display advanced relaxation behavior often in the form of power law relaxation spanning several timescales. This is different from exponential relaxation which is a very rapid decaying function with an amplitude of practically zero for $t > 5\tau$. Experiments measuring the relaxation behavior of lipid membranes in the transition region show relaxation behavior beyond single exponential relaxation, which at T_m spans from sub milliseconds to seconds [7, 81–85]. Authors deal with the multi-scale nature of the membranes relaxation either by fitting multiple exponential relaxation terms as a empirical approach [81, 82, 84, 85] or attempting to adopt a Ginzburg-Landau free energy approach from liquid-crystals [83]. The latter mentioned has been somewhat successful in describing ultrasound ($> 100\ kHz$) attenuation data[5] from lipid vesicles but its applicability seems mainly to be empirical and it offers little insight on the underlying mechanism.

We will in the following take a different approach to understand the relaxation behavior of lipid membrane. We will look at heat exchange between a system and its environment as a potential underlying mechanism for abnormal relaxation. To understand this we consider the relation between thermodynamical fluctuations of a system and the size of its associated heat reservoir.

3.3 Finite heat reservoir

We are motivated to consider the relationship between the thermodynamical fluctuations of a system and its associated heat reservoir by the work of Halstenberg *et al.* [86]. Halstenberg *et al.* measured the speed of sound in a suspension of lipid vesicles and were able to predict this speed of sound at ultrasonic frequencies by considering the coupling between the membrane and the surrounding water. In describing their measurement they considered the sound velocity ($c^2 = 1/\rho\kappa_S$), which is a function of the density (ρ) and the adiabatic compressibility,

$$\kappa_S \equiv -\frac{1}{v}\left(\frac{\partial v}{\partial p}\right)_S = \kappa_T - \frac{T}{v\, c_p^{system}}\left(\frac{\partial v}{\partial T}\right)_p^2, \tag{3.15}$$

where c_p^{system} is the heat capacity of the total considered thermodynamical system. Considering a suspension of lipid vesicles the total thermodynamical system is the lipid membrane and the surrounding water. The above relation has

[5] Attenuation of sound in the vicinity of a phase transition is dominated by the slow relaxation in the system and is therefore connected to the relaxation of the membrane [79].

been derived using Maxwell's relations, following Wilson [87]. From Eq. (2.20) and assuming that $(\partial v/\partial T)_p$ in the lipid melting transition region is dominated by the volume changes in the membrane associated to the transition [86] one can rewrite Eq. (3.15) as,

$$\kappa_S \approx \kappa_{T,0} + \frac{\gamma_v^2 T}{v}\Delta c_p - \frac{\gamma_v^2 T}{v}\frac{\Delta c_p^2}{c_p^{system}} \tag{3.16}$$

$$= \kappa_{T,0} + \frac{\gamma_v^2 T}{v}\Delta c_p \left(1 - \frac{\Delta c_p}{c_p^{system}}\right), \tag{3.17}$$

where $\kappa_{T,0}$ is the part of the isothermal compressibility which is not related to the lipid melting transition, and Δc_p is the excess heat capacity of the lipid melting transition. Eq. (3.17) implies that the adiabatic and isothermal compressibilities of the membrane are related through the size of the thermodynamical system accessible (c_p^{system}) and we see that for an infinite total system they are the same. Arguing that at ultrasonic frequencies the membrane and its surrounding have no time to exchange energy, meaning that the total system is only the membrane, Halstenberg *et al.* [86] correctly predicted their measured speed of sound from Eq. (3.17). We note that Eq. (3.17) is functionally analogous to Eq. (2.20),

$$\kappa_S \approx \kappa_{T,0} + \frac{\gamma_v^2 T}{v}\Delta c_p^{eff}, \tag{3.18}$$

by writing

$$\Delta c_p^{eff} = \Delta c_p \left(1 - \frac{\Delta c_p}{c_p^{system}}\right), \tag{3.19}$$

which we will refer to as the effective heat capacity. The correctly predicted ultrasonic speed of sound by Halstenberg *et al.* [86] assuming that the total accessible system is only the membrane indicates that for the lipid membrane system the dynamic heat capacity depends on the coupling to the aqueous surrounds. This takes into account that the dynamic susceptibility can be viewed as an effective susceptibility, as the part of the equilibrium susceptibility accessible within the time available [88]. To understand the nature of the dynamics of the lipid membrane we need to understand the nature of this coupling and fundamentally how a thermodynamical system acts in a finite heat reservoir. Specifically, we are here interested in understanding the nature of the thermodynamical fluctuations which define both susceptibilities and dynamic timescales in a subsystem of a total system which is adiabatically shielded, following [89].

3.3.1 Modeling a finite heat reservoir

In an adiabatically shielded system the total enthalpy is strictly constant. However, the enthalpy of arbitrary subsystems contained within the total system can fluctuate by exchanging heat with the rest of the system, which we call "the reservoir". An example could be enthalpy and temperature fluctuations in a small water volume that is embedded into a larger water reservoir of finite size. One can also consider cases where the subsystem is of different physical nature than the reservoir. Such a subsystem could be a ice crystal that couples to surrounding water that serves as a reservoir. It could also, as considered

here, be a subsystem that is spatially separated from the reservoir and of different chemical nature than the reservoir, e.g., macromolecules or membranes suspended in an aqueous buffer.

When measuring the heat capacity using DSC, the instrument controls the temperature by removing or supplying heat to the system, effectively acting as an infinite heat reservoir with a constant temperature. In finite adiabatic systems (with constant total enthalpy), however, the temperature of the reservoir is not constant as a consequence of fluctuations in the subsystem. The restriction that the total enthalpy is constant means the any fluctuation in the subsystem (here, the membrane) will result in an appropriate fluctuation of the reservoir temperature. Thus, the temperature of the reservoir is only constant on average, with fluctuations that depends on the size of the reservoir. Furthermore, as a consequence the change in free energy of a fluctuation will have to include the free energy change of the reservoir. The change in free energy associated with a state change in the subsystem is given by,

$$\Delta G_s = \Delta H_s - T\Delta S_s, \tag{3.20}$$

where the s subscribe denote subsystem and T is the temperature of the total system. The change in enthalpy of the subsystem has to be buffered by the heat reservoir ($\Delta H_s = -\Delta H_r$) and the change in the free energy associated to reservoir buffering is given by,

$$\Delta G_r = \Delta H_r - T\Delta S_r, \tag{3.21}$$

where the r denotes heat reservoir and ΔS_r is the change in entropy of the reservoir associated to buffering. We can calculate the change in entropy of the reservoir upon buffering from the resulting temperature fluctuations of the reservoir using,

$$c_p^r = T\left(\frac{\partial S_r}{\partial T}\right)_p \Rightarrow \Delta S_r = \int_{T_r^a}^{T_r^b} \frac{c_p^r}{T}\mathrm{d}T, \tag{3.22}$$

where c_p^r is the heat capacity of the reservoir and T_r^a and T_r^b denotes respectively the reservoir temperature before and after the buffering[6]. Assuming that the heat capacity of the reservoir is constant, the change in the reservoir entropy (Eq. (3.22)) takes the form,

$$\Delta S_r = c_p^r \ln\left(\frac{T_r^b}{T_r^a}\right). \tag{3.23}$$

The change in the temperature of the reservoir upon buffering (ΔH_s) is

$$T_r^b = T_r^a + \frac{\Delta H_r}{c_p^r} = T_r^a - \frac{\Delta H_s}{c_p^r}, \tag{3.24}$$

using $\Delta H_r = c_p^r(T_r^b - T_r^a)$ and $\Delta H_s = -\Delta H_r$. From Eq. (3.23) and Eq. (3.24) the change in free energy of the reservoir (Eq. (3.21)) associated with buffering a state change in the subsystem is given by,

$$\Delta G_r = \Delta H_r - Tc_p^r \ln\left(\frac{T_r^b}{T_r^a}\right) = \Delta H_r - Tc_p^r \ln\left(1 - \frac{\Delta H_s}{T_r^a c_p^r}\right). \tag{3.25}$$

[6]With $\langle T_r^a\rangle = \langle T_r^b\rangle = T$, where the average is over time and T is the constant temperature of the total system which enters the Boltzmann factors.

We see that for an infinite heat reservoir ($c_p^r \to \infty$) the change in free energy of the reservoir upon buffering goes to zero for any finite ΔH_r. The total change in free energy (ΔG_t) associated with a change of state in the subsystem in a finite adiabatic system is given by the change of the free energy of the subsystem (Eq. (3.20)) plus the free energy change of the reservoir upon buffering this change (Eq. (3.25)),

$$\begin{aligned} \Delta G_t &= \Delta G_s + \Delta G_r && (3.26)\\ &= -T(\Delta S_s + \Delta S_r) && (3.27)\\ &= -T\left(\Delta S_s + c_p^r \ln\left(1 - \frac{\Delta H_s}{T_r^a c_p^r}\right)\right). && (3.28) \end{aligned}$$

We see that the change in the total free energy is entirely governed by the changes in entropy and we note that for $c_p^r \to \infty$, $\Delta G_t \to \Delta G_s$. In this limit, the fluctuations of the subsystem are independent of the nature of the reservoir. From Eq. (3.28) we also see that for finite c_p^r there is a maximum fluctuation that is possible for the system: $\Delta G_t \to \infty$ for $\Delta H_s \to c_p^r T_r^a$. That means that for vanishing reservoir size, no enthalpy fluctuations in the subsystem are possible. For finite adiabatic systems the fluctuations of a subsystem are coupled and limited by its surrounding heat reservoir.

The above considerations are general but we are here interested in understanding the coupling between the lipid melting transition and the surrounding aqueous medium. The membrane system is distinct from many other physical systems, being an approximate 2-dimensional subsystem embedded in a three-dimensional heat reservoir. Furthermore, the enthalpy difference between a lipid in the fluid and gel state ($\sim 40\ kJ/mol$) is substantially larger than the energy available in the lipid molecule itself ($c_p^{chain} \approx 1600\ J/mol \cdot K$ [90]), which means that almost the entire buffering of a state change must be facilitated by the aqueous surroundings. Underlining the key importance of the coupling between the membrane and its aqueous surrounding in the vicinity of the lipid melting transition. To explore the implications of a finite heat reservoir on the lipid melting transition we perform Monte Carlo simulations.

3.3.2 Monte Carlo simulation

The simulation performed is Metropolis Monte Carlo simulations. The core step of Metropolis Monte Carlo simulations is that a proposed state change is accepted with an acceptance probability so that the simulation effectively explore the systems phase space and converges towards equilibrium. The acceptance probability (based on the Glauber rejection algorithm) of a change in the state of the subsystem in a finite adiabatic system, is given by,

$$\alpha = \frac{K}{1+K}; \quad K = \exp\left(-\frac{\Delta G_t}{RT}\right), \tag{3.29}$$

which obeys detailed balance. A change is accepted if $\alpha \geq x$, where x is a random number drawn from a uniform distribution ($x \in [0:1]$).

Monte Carlo simulations have frequently been used to explore the properties

of the lipid melting transition [22, 91–94]. We will here use the model used by Ivanova *et al.* [60] for the lipid membrane. The model is Ising model inspired, considering the lipids to be in two states, fluid and gel, where only nearest neighbor interactions are included (last term in Eq. (3.30)). The free energy of each configuration of the lipid subsystem consisting of N lipids is given by,

$$G_s = G_g + N_f(\Delta H_0 - T\Delta S_0) + N_{fg}\omega_{fg}, \tag{3.30}$$

where the G_g is the free energy of the gel state, N_f is the number of lipids in the fluid state, N_{fg} is the number of fluid-gel neighbor interactions and ω_{fg} is the free energy cost of a fluid-gel interaction. ω_{fg} effectively plays the role of setting the cooperative nature of the lipid melting transition, like n in Eq. (2.22). To model the aqueous medium surrounding the membrane we associate to each lipid N_{water} water molecules acting as a shared heat reservoir for the membrane. Furthermore, we include the heat capacity of the lipid chains (c_p^{chain}) as being part of the available heat reservoir. The total heat capacity of the shared heat reservoir (c_p^r), is given by,

$$c_p^r = N(N_{water} \cdot c_p^{water} + c_p^{chain}). \tag{3.31}$$

See appendix A.3 for further details of the simulations.

We carried out Monte Carlo simulations throughout the lipid melting temperature ($T_m = 314.05\ K$) region for different water reservoir sizes. To monitor the enthalpy fluctuations of the membrane subsystem we introduce a measure for the fluctuation strength,

$$\Delta c_s = \frac{\sigma_{H_s}}{RT^2} = \frac{\langle \Delta H_s^2 \rangle - \langle \Delta H_s \rangle^2}{RT^2}. \tag{3.32}$$

In Fig. (3.1) are shown the Δc_s-profiles around the lipid melting transition for five different sizes of the aqueous reservoir: 500, 1000, 2000, 4000, and an infinite number of water molecules per lipid. We see from Fig. (3.1) and Fig. (3.2) that a reduction of the size of the available heat reservoir reduces the fluctuation strength Δc_s of the lipid membrane. This lowering is due to the suppression of large enthalpy fluctuations in the lipid membrane. In the limit of infinite reservoirs we recover the isothermal limit, i.e., the excess heat capacity Δc_p of the membrane. We see further from Fig. (3.1) that the center and width of the c_s-profiles for different reservoir sizes is unaltered, meaning that the damping of fluctuation with smaller reservoirs does not broaden the lipid melting transition.

Note that the excess enthalpy integrated over the melting transition is given by $\Delta H_0 = \int \Delta c_p \mathrm{d}T$. However, for finite reservoir $\Delta H_0 > \int \Delta c_s \mathrm{d}T$ and we see that the fluctuation strength is not a heat capacity.

In Eq. (3.18) we introduced the effective heat capacity (Eq. (3.19)), we called it effective heat capacity under the ansatz that it described the apparent/effective heat capacity of a system in a finite heat reservoir. Based on the simulations we test the validity of this ansatz by comparing the fluctuation strength (Δc_s) with the effective heat capacity, which can be done directly since both the heat capacity of the total system and the excess heat capacity (isothermal) are known. Fig. (3.2) shows the calculated effective heat capacity with the simulated fluctuation strength as a function of reservoir size for four different temperatures. We

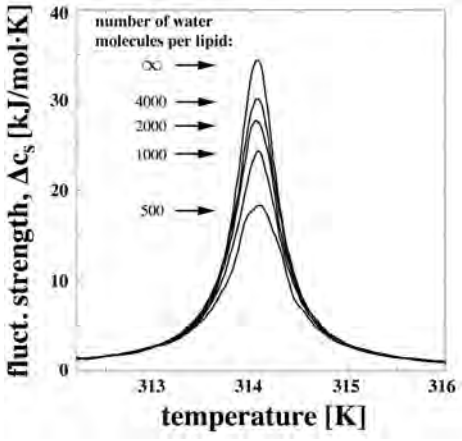

Figure 3.1: *Fluctuation strength, Δc_s, of the lipid membrane for five different sizes of associated water reservoirs. The isothermal limit corresponds to an infinite number of water molecules per lipid. The curves have been smoothed by cubic spline fitting. Error bars have been omitted for clarity. [89]*

see within the estimated error of the simulation (symbols) perfect agreement with the effective heat capacity (solid line). This indicates that the fluctuation strength of a subsystem in a finite heat reservoir is identical to the effective heat capacity: $\Delta c_p^{eff} = \Delta c_s$.

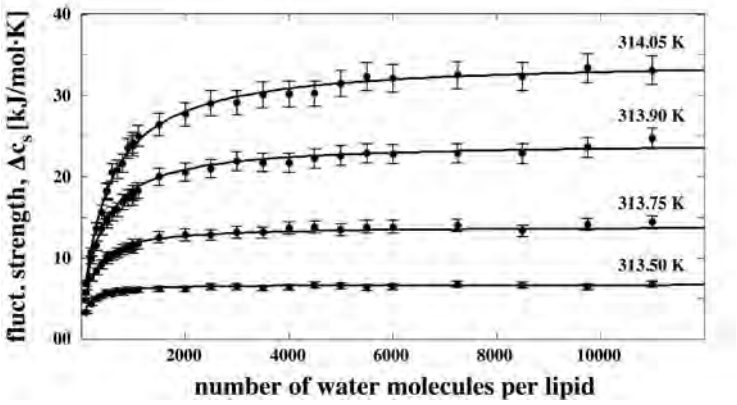

Figure 3.2: *Verification of the analytical ansatz. The effective heat capacity as a function of reservoir size calculated from Eq. (3.19) (solid lines) and the fluctuation strength, Δc_s, from the simulations (symbols) at four different temperatures. [89]*

3.3.3 Dynamic heat capacity

The success of Halstenberg *et al.* [86] in using the effective heat capacity to predict the dynamic heat capacity indicated that they might be identical for the lipid membrane system. This is further underlined by the fluctuation strength based on the fluctuation-dissipation theorem [88]. Effectively, this suggests that the time dependence of the dynamic heat capacity is governed by the size of the accessible heat reservoir which is time dependent. A possible form for the dynamic heat capacity of the lipid membrane in the vicinity of the lipid melting transition is,

$$\Delta c_p^{eff}(t) = \Delta c_p \left(1 - \frac{\Delta c_p}{c_p^{system}(t)}\right), \tag{3.33}$$

where $c_p^{system}(t)$ is the time dependence of the heat capacity of the total system and we assume that the underlying time dependence is due to a time dependence of the size of the accessible heat reservoir ($c_p^{system}(N_{water}(t))$). The simplest time dependence of the size of the accessible heat reservoir is diffusion. Considering the cooperative and pseudo 2-dimensional nature of lipid membranes we assume that the heat from and to the membrane is governed by 1-D diffusion ($N_{water}(t) \approx \sqrt{4D_Q t}$)[7] so that,

$$c_p^{system}(t) \approx c_p^{membrane} + \alpha \cdot t^{\frac{1}{2}}, \tag{3.34}$$

where α is a proportionality constant containing a measure for the heat diffusion constant and the heat capacity of water. $c_p^{membrane} = \Delta c_p + c_p^{chain}$ is the heat capacity of the membrane. For low frequencies ($\omega << 1\ MHz$) and close to the lipid melting transition, we approximate $c_p^{membrane} \approx \Delta c_p$. Using Eq. (3.34) considering low frequencies the here proposed dynamic heat capacity (Eq. (3.33)) of the lipid membrane in the vicinity of the lipid melting transition takes the form,

$$\Delta c_p^{eff}(t) \approx \Delta c_p \left(1 - \frac{\Delta c_p}{\Delta c_p + \alpha \cdot t^{\frac{1}{2}}}\right) \tag{3.35}$$

$$= \Delta c_p \left(1 - \frac{1}{1 + \frac{\alpha}{\Delta c_p} \cdot t^{\frac{1}{2}}}\right). \tag{3.36}$$

We note that this proposed dynamic heat capacity, like single exponential relaxation (Eq. (3.11)), only contains an amplitude and a free parameter, here α and for single exponential relaxation the τ.

Little low frequency relaxation data covering several decades reliably is available. Blume and collaborators have done a of number jump perturbation experiments with various lipid state recording methods [81, 82, 84, 85, 95]. They found systematically relaxation behavior spanning the full experimental available time spectra, using techniques covering from sub millisecond to seconds. In Fig. (3.3) we show the natural logarithm of the recorded optical density[8] as a function of time (red dots) after pressure jump for DPLA vesicles just above

[7] Assuming 1-D diffusion is equivalent to assuming that the diffusion length-scale is smaller then the area of the region of the membrane involved in a state change.

[8] The optical density is a proxy for the state of the lipid membrane.

the melting temperature ($T = 305\ K$) [81], along with a fit of Eq. (3.36) to the data (black line). We see that there is a quite good agreement between the proposed expression (Eq. (3.36)) for the dynamic susceptibility[9] especially noting the logarithmic y-axis. We find $\alpha/\Delta c_p \approx 12\ s^{-1/2}$ [10].

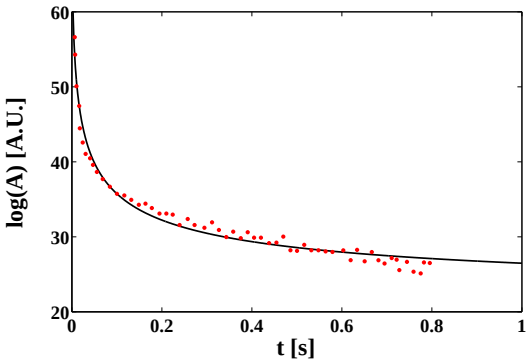

Figure 3.3: *The time dependence of the optical density A (red dots) after pressure jump for DLPA vesicles just above the melting temperature ($T = 305\ K$). The solid black line is the best fit using Eq. (3.36), estimating $\alpha/\Delta c_p \approx 12\ s^{-1/2}$. The data is taken from [81].*

Van Osdol *et al.* [96] used sinusoidal pressure perturbation to probe the frequency dependence of the dynamic heat capacity. As it is illustrated in Eq. (3.8), the frequency dependence of the dynamic heat capacity is given by the Laplace transform of the derivative of the time dependent dynamic heat capacity as

$$\Delta c_p^{eff}(\omega) = \int_0^\infty \frac{d\Delta c_p^{eff}(t)}{dt}\, e^{-st}\, \mathrm{d}t \tag{3.37}$$

where $s = i\omega$ is the complex argument of the Laplace transform. From Eq. (3.37) the frequency dependent dynamic heat capacity corresponding to Eq. (3.36) can be calculated using *Mathematica*. We have fitted Eq. (3.37) to the absolute value of the dynamic heat at $T_m = 314.15\ K$ of DPPC LUV, for four different perturbation frequencies $0.01\ Hz, 0.1\ Hz, 1\ Hz$ and $10\ Hz$ (red dots, Fig. (3.4)), from [96]. We find excellent agreement between fit and data, estimating $\alpha/\Delta c_p \sim 3\ s^{-1/2}$ [11], see Fig. (3.4). The full dynamic heat capacity profiles measured by Van Osdol *et al.* [96] are shown in Fig. (3.5), B. Using the estimated value for α we have calculated the dynamic heat capacity profiles based on the equilibrium heat capacity profiles generated using Eq. (2.24) (see Fig. (3.5), A) for comparison. We see again excellent agreement between the experimentally obtained dynamic heat capacity throughout the transition and the proposed form (Eq. (3.36)).

[9] Remember that the found proportionality relations between the different extensive variables (Eq. (2.20) and Eq. (2.21)) of the membrane lead to a single common dynamic susceptibility.

[10] 95 % confidence bounds: $8.1\ s^{-1/2}$, $15.7\ s^{-1/2}$.

[11] Note, that there is significant impact of the baseline correcting, resulting in an uncertainty on the determined $\alpha/\Delta c_p$ value.

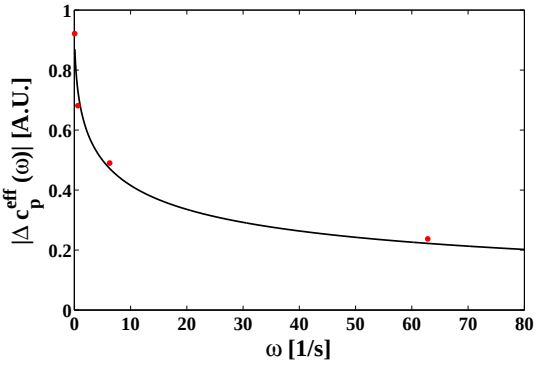

Figure 3.4: *The absolute value of the dynamic heat at* $T_m = 314.15\ K$ *of DPPC LUV (red dots), for four different perturbation frequencies (*$0.01\ Hz, 0.1\ Hz, 1\ Hz, 10\ Hz$*), taken from [96]. Zero order baseline corrections have been preformed on the data, assuming common baseline. Black line shows the best fit of Eq. (3.37) to the data, estimating* $\alpha/\Delta c_p \approx 3\ s^{-1/2}$.

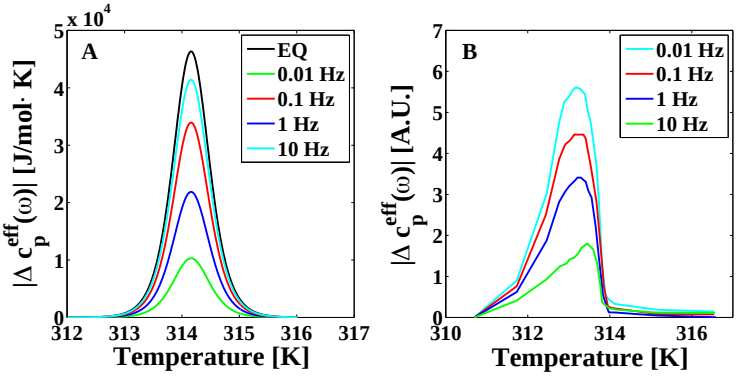

Figure 3.5: ***A****: Calculated dynamic heat capacities from Eq. (3.37) for four different perturbation frequencies, using the estimated* $\alpha/\Delta c_p$ *from Fig. (3.4). The equilibrium heat capacity profiles are generated using Eq. (2.24).* ***B****: The absolute value of the dynamic heat of DPPC LUV, as a function of temperature, for four different perturbation frequencies, taken from [96].*

3.4 Discussion of response behavior

In describing the response behavior of lipid membranes we introduced general linear response theory for the example of the enthalpy response to temperature perturbation. We saw that the response behavior is governed by the response function and the dynamic susceptibility of the system. The dynamic susceptibility is a generalization of the thermodynamical susceptibilities, describing the part of the susceptibility which is accessible within the time available. We showed that assuming Gaussian thermodynamical fluctuations, a system will show single exponential relaxation with the characteristic relaxation time being proportional to the appropriate equilibrium susceptibility. Grabitz *et al.* [22] showed that this assumption was sufficient to describe the relaxation of lipid membranes around the lipid melting transition in the long time relaxation limit, observing characteristic relaxation time around $\sim 3\ s$ at T_m. Several authors have however reported significant relaxation at smaller timescales than observed by Grabitz *et al.* spanning from seconds down below milliseconds [7, 81, 82, 84, 85, 95]. This indicates relaxation behavior beyond single exponential relaxation. We will however for simple examples in the proceeding chapters approximate the relaxation behavior of lipid membranes in the vicinity of the lipid melting transition by single exponential relaxation (Eq. (3.14)) as proposed by Grabitz *et al.* [22].

In attempting to describe the observed relaxation behavior, spanning several timescales, Blume and collaborators often use several exponentials (often 3) effectively aiming at parameterizing the relaxation (this approach is used consistently within the field). Beyond this, Halstenberg *et al.* [83] have successfully used a phenomenological description originally intended for describing ultrasonic attenuation in liquid crystals around their isotropic-to-nematic transition to describe ultrasonic attenuation in lipid membrane dispersions. Despite their success, the phenomenological nature of their approach does not illuminate the underlying physical mechanism and its applicability to a lower (biologically relevant) frequency regime is unknown. In earlier work, Halstenberg *et al.* [86] (different collaborators) succeeded in describing the ultrasonic attenuation in lipid membranes throughout the lipid melting region by considering the thermodynamical coupling between the membrane and the surrounding water. Motivated by this, we studied the fluctuations of a membrane surrounded by a finite amount of water (a finite heat reservoir) aiming to understand the underlying physical mechanism governing relaxation behavior in the transition region of lipid membranes [89]. We found through Monte Carlo simulations that the fluctuation strength (Eq. (3.32)) of the membrane in a finite reservoir is identical to the effective heat capacity (Eq. (3.19)) derived from the expression for the adiabatic compressibility (Eq. (3.18)). The previous success of using the effective heat capacity to describe ultrasonic attenuation in membranes [86] along with the coupling between the fluctuation strength and the effective heat capacity, indicates that the governing physics behind the observed relaxation behavior is through the size of the heat reservoir accessible in the available time. We assumed that the underlying time dependence of dynamic heat capacity is the time dependence of the size of the accessible heat reservoir. We assumed further that the size of the accessible heat reservoir is governed by 1-D heat diffusion. We found excellent agreement between the observed relaxation, from both jump

and sinusoidal experiments over the full available range, and the proposed dynamic heat capacity (Eq. (3.36)). Note, that proposed dynamic heat capacity fits the available data excellently with only a single free parameter. From the data of Van Osdol *et al.* [7] (Fig. (3.3)) we estimated $\alpha/\Delta c_p \approx 3\ s^{-1/2}$ at $T = T_m$. These experiments was done on DPPC LUV and knowing the excess heat capacity of DPPC (see Fig. (2.3)) we can estimate $\alpha \sim 120\ kJ/(K \cdot s^{1/2})$ per *mol* lipid. The experiment by Elamrani *et al.* [81] (Fig. (3.3)) was only available at one temperature, just above the lipid melting transition, and we estimated $\alpha/\Delta c_p \approx 12\ s^{-1/2}$. We can again from the known excess heat capacity (for DLPA vesicles) estimate α, and we find a value similar to one found for the Van Osdol *et al.* data set. That the only free parameter in the proposed dynamic heat capacity (α) is conserved cross different lipid membrane systems indicates that there is a universal role of the water-membrane interface, which underlines the potential generality of the proposed relaxation mechanism.

More experimental data spanning several timescales are though needed to further test our proposed form for the dynamic heat capacity. However, based on available data it seems to describe the advanced relaxation behavior of the lipid membrane close to the lipid melting transition excellently. Contrary to other efforts to understanding this behavior, our proposal have a clear underlying mechanism, being that the enthalpy of melting far exceeds the thermal energy available within the membrane and therefore needs the surrounding water to buffer the fluctuation. We note the similarity between the lipid melting transition and certain glass transitions [56], which could indicate that similar mechanisms can be important for the relaxation behavior of glasses.

Chapter 4

Lipid membranes as an electrical component

In chapter 2 we introduced the thermodynamical framework to describe the state of a lipid membrane. Our description targeted specifically a lipid membrane in the vicinity of the lipid melting transition, where we included the formalism to consider the effect of electrical fields across the membrane. In chapter 3 we extended the thermodynamical framework to include the dynamic properties of the lipid membrane. This enabled a description not only of equilibrium states of the membrane but also how the system dynamically progresses between these.

The foundation of electrophysiology, ion channels and also our understanding of the propagation of nerve signals rely on the techniques of current clamp and voltage clamp. By either clamping the current or the voltage across a cell membrane or artificial membrane, the electrical properties of the membrane as a whole can be investigated. The voltage clamp technique enabled Huxley and Hodgkin to characterize the electrical properties of the giant squid axon and from this derive their electrical model of nerve pulse propagation [24, 75]. They assumed, as it is common in the field, that the lipid membrane acts a simple capacitor (constant in value) and that the observed non-linear currents are due to protein ion-channels which can have sophisticated opening and closing mechanisms and be selective towards specific ions. In general, in the present paradigm, almost all sophisticated (non-linear) behaviors are assigned to specific proteins or protein classes and the membrane is believed to be inert.

4.1 Equivalent circuit of the membrane

The pure lipid membrane is commonly assumed to be permeable to small molecules like water and close to impermeable to larger molecules or ions[1]. In an electrolyte solution current is conducted by movement of ions rather then electrons. This means that the pure lipid membrane can be considered approximately as an insulator separating two electrically conductive compartments, the

[1] Ions atoms are very small but are in water always surrounded by a number of water molecules shielding the electrical field of the ion, effectively making the ion considerable in size.

electrolytic solution on the two sides of the membrane. The membrane is however not a perfect insulator and low conduction through it can be expected. The pure lipid membrane equivalent circuit therefore takes the form of a capacitor in parallel with a resistor, see Fig. (4.1)).

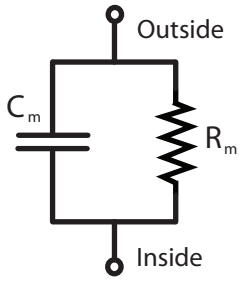

Figure 4.1: *The equivalent circuit of the lipid membrane, containing a resistor (R_m) and a capacitor (C_m) in paralel.*

In this chapter we will, based on our understanding of the lipid membrane, describe a appropriate equivalent circuit of pure lipid membranes. First, we will consider the lipid membrane as a capacitor based on our thermodynamical understanding of the membrane subject to electric fields. Secondly, we will describe the permeability to ions displayed by pure lipid membranes, so the lipid membrane as a resistor. We will for both the capacitance and the conductance of the membrane consider the electrical experiments commonly performed within the field of electrophysiology. We will consider two types of experiments, namely impedance spectroscopy and voltage jump experiments. We will see that the common approximation that the conductance and capacitance of the lipid membrane are constant, is far from valid in the vicinity of the lipid melting transition, and its validity is even questionable beyond this region.

4.2 Non-linear capacitor

In electrophysiology it is commonly assumed that the membrane acts as a simple capacitor, meaning that the capacitance is constant. As it will be shown here and has been shown by other authors, the membrane behaves rather as a non-linear capacitor [43,64,65], which changes the expected electrical response (of the membrane) significantly as we will see below. In voltage clamp experiments one makes a voltage perturbation and records the current response. Disregarding conduction for the moment, for a constant capacitance ($C = \varepsilon A/d$) the current response to a change in the applied voltage will be

$$I_C(t) = \frac{dq_C}{dt} = \frac{d(C \cdot \psi(t))}{dt} = C\frac{d\psi(t)}{dt}, \tag{4.1}$$

which is the charging or discharging of an ordinary capacitor (indicated by subscript C). Eq. (4.1) is based on Gauss's law which for a planar capacitor filled with a homogeneous dielectric takes the form,

$$q_C = v\,(\boldsymbol{\nabla} \cdot \mathbf{D}) = AD. \tag{4.2}$$

Assuming a linear dielectric medium, no offset polarization and constant geometry we recover Eq. (4.1). However, as we showed in section 2.3.2, the geometry of lipid membranes depends on the applied electric field and the membrane can furthermore display offset polarization such that $D = \varepsilon E + P_0$. Therefore, in the general case, the charges on the membrane capacitor takes the form

$$q_{C_m} = A(\varepsilon E + P_0) = \varepsilon \frac{A}{d}\psi + AP_0 = C_m\psi + AP_0, \tag{4.3}$$

where the capacitance (C_m), area (A), thickness (d) and offset polarization (P_0) of the membrane can all depend on the applied voltage (ψ)[2]. We will often refer to the last term in Eq. (4.3) as offset charges ($q_{offset} = AP_0$).

In chapter 2 we introduced a thermodynamic description of the lipid membrane melting transition including the thermodynamical implications of membranes being subject to applied electrical fields. Using the van't Hoff law based model for the lipid melting transition (see Eq. (2.22) and Eq. (2.23)) and the known expression for the free energy difference (Eq. (2.35)), we can calculate the change in charges on the membrane capacitor given a change in voltage (Eq. (4.3))[3]. Fig. (4.2) shows the number of charges on the membrane capacitor relative to the number of charges on a constant membrane capacitor ($q_{C_m,0}$) for different temperatures as a function of the applied voltage.

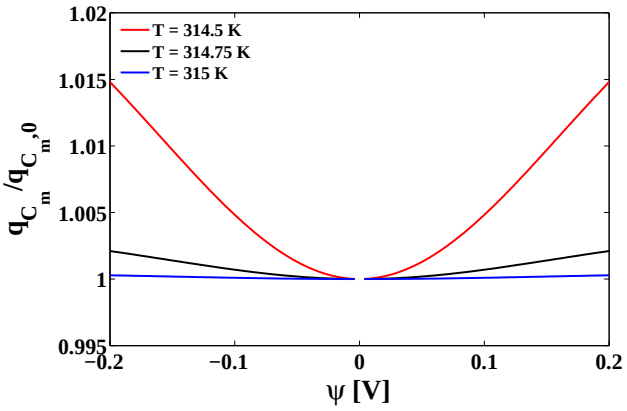

Figure 4.2: *The relative number of charges on the membrane capacitor as a function of applied voltage, shown for different temperatures above the lipid melting transition. Value used are from LUV of DPPC, where* $\Delta C \approx 656\ J/(mol \cdot V^2)$. *No offset polarization is assumed.*

We see from Fig. (4.2) that the non-linearity of the charges on the membrane capacitor (the capacitance) around the lipid melting transition is highly dependent on temperature.

Biological membranes commonly display a voltage difference between the inside and outside (Nernst potential) of around $\sim -100\ mV$. The inside electrode

[2]We used $\psi = E \cdot d$.

[3]Values used are from LUV made of DPPC, and can be see in appendix A.1.

is in electrophysiology conventionally defined as the positive electrode. Furthermore, experiments probing the electrical properties are commonly performed around a holding voltage (ψ_h). We see from Fig. (4.2), that experiments centered around a non-zero holding voltage will result in an asymmetric non-linear capacitance contribution. To illustrate this we consider the change in *non-linear charges* on the membrane capacitor which we define as

$$q_{C_m}^{non} \equiv (q_{C_m}(\psi_e) - q_{C_m}(\psi_h)) - C_m(\psi_h)\Delta\psi \tag{4.4}$$

where $q_{C_m}(\psi_e)$ and $q_{C_m}(\psi_h)$ is the charges on the membrane at respectively *end voltage* (ψ_e) and *holding voltage* (ψ_h), $C_m(\psi_h)$ is the capacitance at the holding voltage and $\Delta\psi = \psi_e - \psi_h$ is the change in voltage. We will consider changes in the end voltage while the holding voltage is fixed. In Fig. (4.3) we see the change in non-linear charges as a function of change in voltage from different holding voltages. The holding voltage result in asymmetry and we see for large changes in voltage that the change in non-linear charges can be against the the voltage change. In Fig. (4.2) and Fig. (4.3) no offset polarization was assumed. In Fig. (4.4) we consider the influence of offset polarization on the change in non-linear charges on the membrane capacitor in response to changes in end voltage (ψ_e). We see that the effect of the offset polarization can be very large especially for the case were the offset polarization is dependent on the state of the membrane and herby on the applied voltage (Fig. (4.4), ***right***).

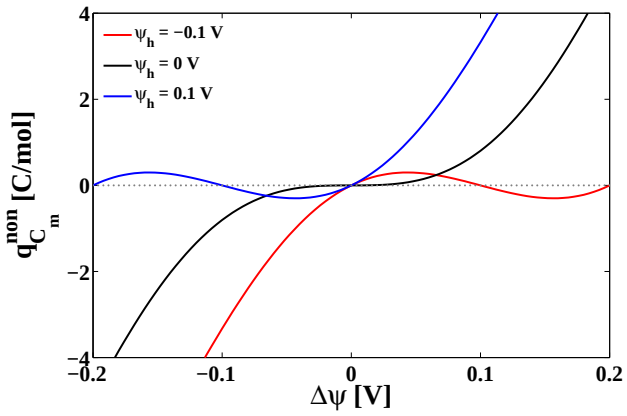

Figure 4.3: *The change in non-linear charges on the membrane capacitor as a function of changes in voltage, shown for three different fixed holding voltages (ψ_h). Values used are from LUV of DPPC, where $\Delta C \approx 656\ J/(mol \cdot V^2)$. No offset polarization is assumed and the temperature is $T = 314.5\ K$.*

We showed (in Fig. (4.2-4.4)) that change in non-linear charges on the membrane capacitor upon a voltage change are dependent on the state of membrane, holding voltage and the offset polarization. Note that the state of the membrane, specifically the vicinity to the melting transition, can affect the change in non-linear charges on the membrane capacitor by orders of magnitudes.

In this chapter we are interested in exploring the current response of membranes due to voltage perturbations. The capacitive current is the rate of change in the

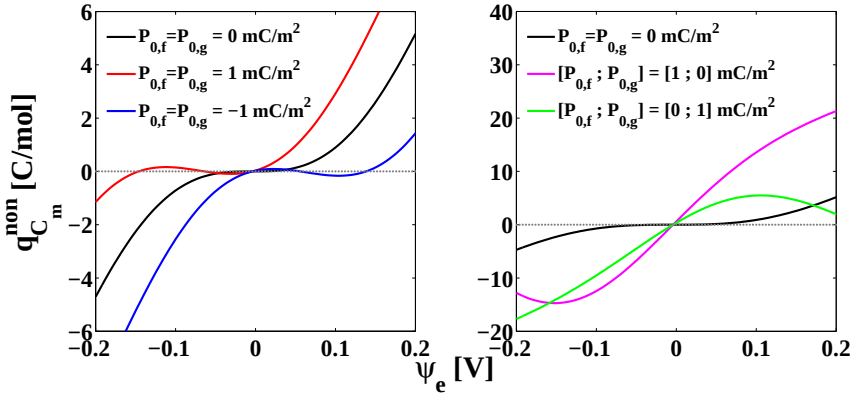

Figure 4.4: *The change in non-linear charges on the membrane capacitor as a function of end voltage (ψ_e). No holding voltage ($\psi_h = 0$) is assumed and the temperature is $T = 314.5\ K$. Values used are from LUV of DPPC, where $\Delta C \approx 656\ J/(mol \cdot V^2)$.* ***Left****, the change in non-linear charges on the membrane capacitor is shown for different offset polarizations, where the offset polarization is independent on the state of the membrane.* ***Right****, the change in non-linear charges is shown for different offset polarizations were the polarization is membrane state dependent.*

charges on the membrane capacitor. For the membrane the capacitive current response to a change in the applied voltage takes the form,

$$I_{C_m}(t) = \frac{dq_{C_m}}{dt} = \frac{d(C_m\psi + AP_0)}{dt}, \tag{4.5}$$

where the capacitance, applied voltage, area and offset polarization can depend on time.

4.2.1 Applied to common experiments

As is was discussed in section 3.1, perturbation experiments are mainly carried out by jump or sinusoidal perturbations. This is also the case for experiments probing the electrical properties of membranes. First we will consider the case of low amplitude sinusoidal perturbation experiments (referred to as impedance spectroscopy) and after we will consider jump experiments. We will consider voltage clamp experiments, originally introduced by Kenneth Cole [97], where the voltage across the membrane is locked (or clamped) and the current needed to keep the voltage is monitored.

Electrical impedance

The first type of electrical perturbation experiments we consider is electrical impedance spectroscopy, where the membrane is perturbed by a low amplitude sinusoidal applied voltage and the amplitude and the phase of the response current is measured to determine the impedance (Z).

$$Z(\omega) \equiv \frac{\psi(\omega)}{I(\omega)} = R(\omega) + iX(\omega), \tag{4.6}$$

where real part (R) is the resistance and the imaginary part (X) is the reactance. Only low amplitude perturbations are applied in impedance spectroscopy to linearize the response. To estimate the response of a lipid membrane to this type of perturbation we Taylor-expand the change in charges on the membrane capacitor (Eq. (4.3)) to the first order around the holding voltage:

$$\Delta q_{C_m} \approx \left(C_{m,0} + \psi_h \left(\frac{\partial C_m}{\partial \psi} \right)_{\psi_h} + \left(\frac{\partial (AP_0)}{\partial \psi} \right)_{\psi_h} \right) \Delta\psi, \tag{4.7}$$

where $C_{m,0}$ is the constant part of the capacitance for the given state of the membrane, ψ_h is the fixed holding voltage, $(\partial C_m/\partial\psi)_{\psi_h}$ and $(\partial(AP_0)/\partial\psi)_{\psi_h}$ are respectively the voltage dependence of the membrane capacitance and of the offset charge, both evaluated around the holding voltage (ψ_h).

In chapter 3 we introduced linear response theory, which describes the dynamics of a thermodynamic system between two equilibrium states. Using linear response theory we can estimate the time dependence of changes in the membrane. For simplicity, we assume that the change of offset charges and of the membrane capacitance follow the dynamics of the membrane directly. We further assume that the lipid membrane is well approximated by the single exponential response function of the form Eq. (3.14) [4]. Based on these assumptions, the time dependent change in the charges on the membrane capacitor, assuming low amplitude sinusoidal perturbations, takes the form,

$$\Delta q_{C_m}(t) = C_{m,0}\Delta\psi(t) + \int_{-\infty}^{t} C_0 \left(1 - \Psi_m(t-t')\right) \frac{d\psi(t')}{dt'} \mathrm{d}t' \tag{4.8}$$

where $\Psi_m(t)$ is the response function of the membrane (Eq. (3.14)) and $C_0 \equiv \psi_h(\partial C_m/\partial\psi)_{\psi_h} + (\partial(AP_0)/\partial\psi)_{\psi_h}$. Taking the time derivative of Eq. (4.8) we find the linear current response to a voltage perturbation. Including the sinusoidal nature of the applied voltage perturbation ($\Delta\psi(t) = \Delta\psi \exp(i\omega t)$) and using the assumption of single exponential relaxation, the frequency dependent current response of the membrane capacitor (I_{C_m}) takes the form,

$$I_{C_m}(\omega) = i\omega C_{m,0}\Delta\psi(\omega) + \frac{i\omega C_0}{1 + i\omega\tau}\Delta\psi(\omega), \tag{4.9}$$

where ω is the angular frequency of the perturbation, $\Delta\psi(\omega)$ is the Fourier transform of the applied voltage perturbation and τ is the characteristic relaxation timescale. For derivation see appendix A.4. From Eq. (4.9) the impedance of the membrane capacitor takes the form,

$$Z_{C_m}(\omega) = \left(i\omega C_{m,0} + \frac{i\omega C_0}{1 + i\omega\tau} \right)^{-1} \tag{4.10}$$

Note that the impedance of the membrane capacitor takes the form of a capacitor in parallel with a so-called lossy capacitor, which is a capacitor in series with a resistor, see Fig. (4.5).

[4] The area, thickness and offset polarization of the membrane can all be expected to follow the dynamics of the membrane. Furthermore, we saw in the previous chapter that lipid membranes display "abnormal" relaxation behavior. However, we are here interested in the general behavior and the detailed dynamics is beyond our scope.

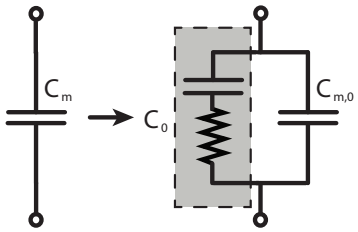

Figure 4.5: *Equivalent circuit representation of the impedance of the membrane capacitor, a capacitor in parallel with a lossy capacitor, see Eq. (4.10).*

This configuration of a capacitor (the membrane) in parallel with a lossy capacitor is often used in electrophysiology to fit the impedance of biological membranes [98, 99]. Interestingly, in electrophysiology, the phenomenological lossy capacitor is speculated to originate from voltage dependent capacitive components which is due to charge movement within the membrane (the movement of gating charges in protein channels). We predict the lossy capacitive term likewise from voltage dependent capacitive components originating however from geometrical and offset polarization changes of the membrane, no protein being considered. As it is indicated by considering the change in non-linear charges on the membrane (Fig. (4.4)), C_0 depends on the nature of the offset polarization, on the state of the membrane and on the holding voltages. We see in Fig. (4.6) that C_0 is positive and can have amplitudes of around 10 % of C_m ($\sim 1\ \mu F/cm^2 \sim 1600\ F/mol$).

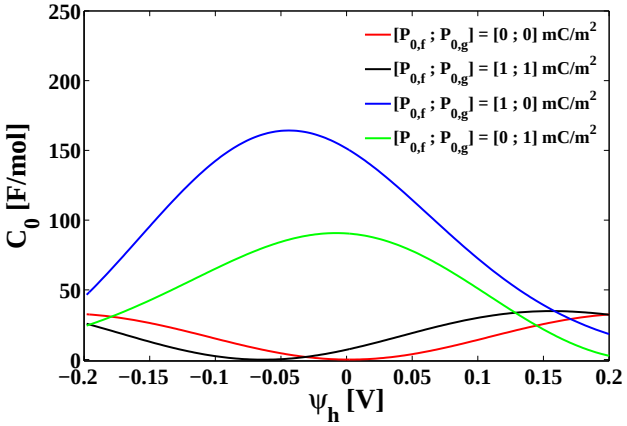

Figure 4.6: *The first order term of the voltage dependence of the membrane capacitance (C_0), including offset polarization, as a function of holding voltages shown for different offset polarizations. Values used are from LUV of DPPC, where $\Delta C \approx 656\ J/(mol \cdot V^2)$ and the temperature is $T = 314.5\ K$.*

As will be discussed in detail in the next section (4.3), the lipid membrane is not entirely impermeable to ions. The conduction of ions through the membrane is, like the capacitance, not constant in the vicinity of the lipid melting transition. However, we here assume that the conduction is constant to illus-

trate the effect of the non-linearity of the membrane capacitance. Including a resistor in parallel with the membrane capacitor the impedance takes the form,

$$Z_m = \left(\frac{1}{Z_{C_m}} + \frac{1}{Z_\Omega}\right)^{-1} \tag{4.11}$$

$$= \left(\left(i\omega C_{m,0} + \frac{i\omega C_0}{1+i\omega\tau}\right) + \frac{1}{R_m}\right)^{-1}, \tag{4.12}$$

where we have used that the impedance of a resistor is given by $Z_\Omega = R$. Using values for the resistance of a membrane estimated from the literature [75, 100] and C_0 from Fig. (4.6) we can calculate the impedance of the membrane, which is shown in a Nyquist plot in Fig. (4.7).

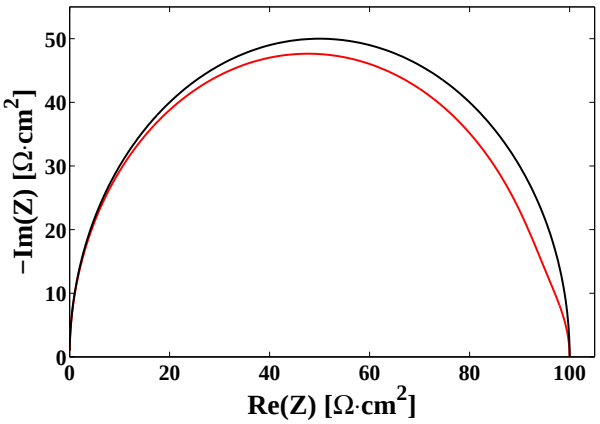

Figure 4.7: *Nyquist plot of the impedance of a lipid membrane.* ***Red****, shows the impedance profile assuming* $C_0 \approx 0.5 \cdot C_{m,0}$ *and* ***black*** *shows the impedance profile assuming* $C_0 = 0$*. We have assumed a resistance of the membrane of* $R_m = 100\ \Omega \cdot cm^2$*, membrane capacitance is* $C_{m,0} = 1\ \mu F/cm^2$ *and a characteristic relaxation time* $\tau = 1\ ms$*.*

We have assumed a characteristic relaxation time constant of $\tau = 1\ ms$, which is based on the characteristic timescales observed in biological membranes. We have in Fig. (4.7) assumed $C_0 = 0.5 \cdot C_{m,0}$ which is high compared to values shown in Fig. (4.6) but within achievable values for a pure lipid membrane.

We see that the non-linearity of the membrane capacitor takes the form of an additional capacitive term which is known in electrophysiology as a lossy capacitor. Interestingly, this could indicate that the common experimentally found lossy capacitive term can originate from the non-linearity of the membrane capacitor and not, as commonly speculated, from gating currents.

Voltage jump

The second type of electrical perturbation experiments commonly performed is jump experiments. Using voltage jump experiments Hodgkin and Huxley [75] characterized the electrical response of the squid giant axon, enabling them to propose their model for its action potential [24]. The voltage jump technique is widely used especially in characterizing the functionality of protein ion channels, and understanding the response of the membrane is therefore essential for correctly associating function to specific proteins.

A voltage jump experiment is carried out by performing a fast jump in voltage, from a holding voltage (ψ_h) to end voltage (ψ_e) and measuring the current response of the system. We assume the jump to be performed at $t = 0$ and that any change in the applied voltage is instantaneous. In dealing with the impedance spectroscopy we could apply linear response theory since only small perturbations were considered and we could linearize the response. Here, however, we are not limited to small perturbations and the response of the membrane is not guarantied to be linear. By assuming that the applied voltage jump is instantaneous, the problem of the non-linear response can be simplified to considering the equilibration of the system from the initial equilibrium charges on the membrane to the new equilibrium after the jump. We assume that equilibration of the membrane, its capacitance and polarization charges, follow single exponential relaxation as for the impedance calculations. Using these assumptions we can calculate the current response using Eq. (4.3) and Eq. (3.5) for $t > 0$[5],

$$\begin{aligned} I_{C_m}(t) &= \frac{d}{dt}\left(q_{C_m}^{non}(t)\right) = \frac{d}{dt}\left(\left(\Delta C_m \psi_e + \Delta(AP_0)\right)\left(1 - \Psi_m(t)\right)\right) \\ &= \left(\Delta C_m \psi_e + \Delta(AP_0)\right)\frac{\exp\left(-\frac{t}{\tau}\right)}{\tau}, \end{aligned} \tag{4.13}$$

where $\Delta(AP_0)$ and ΔC_m is respectively the change in offset charges and the change in membrane capacitance associated with the change in applied voltage ($\Delta\psi = \psi_e - \psi_h$). We see that the non-linear capacitive current is set by the change in non-linear charges on the membrane. From Fig. (4.8) we see that the non-linear current response of a membrane may not follow the change in voltage.

The current in Fig. (4.8) is given in the units $[A/mol]$ (mol of lipid) which is equivalent to 1 $A/mol \sim 2/3\ nA/cm^2$, assuming an area per mol lipid of $A \sim 1.5 \cdot 10^5\ m^2/mol$ [6] [51]. From this and Fig. (4.8) we can expect current responses of up to 20 $\mu A/cm^2$ after a voltage jump which originate from the non-linearity of the lipid membrane. Note that these values highly depend on the vicinity of the lipid melting transition and at the center of the transition we can expect responses up to 60 $\mu A/cm^2$ and that the current response is inversely proportional to the characteristic relaxation time. We see from this that the capacitive non-linear current response to a voltage jump can be significant on the

[5] The derivative of a step function is a Dirac delta function at the point of the step. We consider $t > 0$ to ignore the part of the capacitive current which is associated to the linear part of the membrane capacitor. In experiments compensation circuits are commonly used to remove the linear capacitive spike and it is not shown in recordings.

[6] We are considering a constant number of lipids which changes their size and direct conversion can therefore not be done. However, we can consider the conversion valid in equilibrium, such that units are $[\mu A/cm^2]$ in equilibrium.

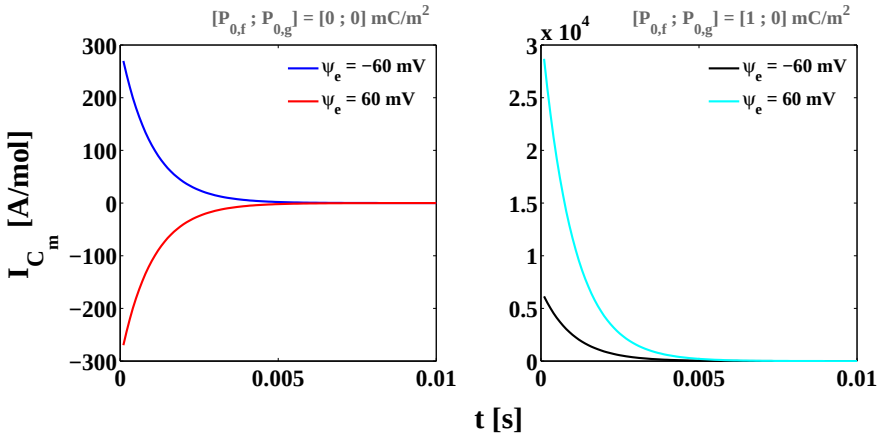

Figure 4.8: *The capacitive current response to a change in applied voltage from a holding voltage $\psi_h = -100\ mV$ to respectably $\psi_e = -60\ mV$ and $\psi_e = 60\ mV$. **Left**, shown for membrane with no offset polarization assumed. **Right**, shown for a polar membrane with $P_{0,f} = 1\ mC/m^2$ and $P_{0,g} = 0\ mC/m^2$. Values used are from LUV of DPPC, where $\Delta C \approx 656\ J/(mol \cdot V^2)$, the temperature is $T = 314.5\ K$ and $\tau = 1\ ms$ is assumed.*

level of electrophysiological recordings, especially compared to gating currents which will be considered in the discussion.

4.3 Lipid ion channels

Lipid membranes are electrically modeled as a resistor in parallel with a capacitor (see Fig. (4.1)). In the previous section (4.2) we described the behavior of the charges on the membrane capacitor, which is non-linear due to the softness of the membrane and its potential offset polarization. In subsection 4.2.1 we assumed that the resistance of the membrane was constant. In this section we describe the nature of the membrane conductance, especially in regard to the lipid melting transition, and consider its implications for electrophysiological experiments.

Lipid membranes have been shown to be able to conduct ions in a fashion similar to the conduction of protein ion channels. The similarity spans several aspects of protein conduction: quantized conduction events, gating due to drugs, temperature, pH and ions (especially calcium) and voltage [31–33]. The lipid ion channels can be seen as defects in the membrane through which ions can pass. In the literature two types of lipid ion channels have been proposed: hydrophobic pores and hydrophilic pores. Hydrophobic pores are defect in the membrane where the hydrophobic chains of the lipids are exposed to the pore. On the other hand, in hydrophilic pores lipids rearrange themselves within the pore to shield the hydrophobic lipid chains by lining the pore [7]. The conduction

[7] For further details on lipid pores see [33].

of pure lipid membranes has been shown to follow the magnitude of the fluctuations of the membrane. Hence, conduction follows the excess heat capacity profile of the membrane [101, 102]. There can be two mechanisms behind this, which are internally coupled: area fluctuations can directly lead to defects and, secondly, the large fluctuations also mean that the thermodynamical susceptibilities are high, including the various compressibilities (thickness, area and volume), so the work needed to form a pore (defect) is low. The direct connection between the lipid melting transition and permeability of the membrane has been confirmed by Andersen *et al.* [103]. They showed that the membrane becomes highly permeable in the regions which are in the transition and have very low permeability outside this region (both for gel and fluid regions).

The simplest way of modeling the voltage dependence of the creation of a pore in the membrane is through electrostriction. The charges on the membrane capacitor squeeze the membrane until a pore is created and the tension can be relieved, which can be seen as local dielectric breakdown of the membrane. From these considerations the free energy for forming a pore must dependent on the voltage squared [32],

$$\Delta G_{pore} = \Delta G_{pore,0} + \alpha\psi^2, \tag{4.14}$$

where $\Delta G_{pore,0}$ is the free energy of forming a pore at no applied electric field and α describes the coupling between the applied field and the formation of a pore. Both $\Delta G_{pore,0}$ and α must depend on the state of the lipid membrane due to the relation between the conduction of the membrane and the excess heat capacity. We note the similarity between the last term in Eq. (4.14) and the electrical enthalpy described in Eq. (2.35). As we showed for the free energy of the lipid membrane (Eq. (2.35)), an offset polarization leads to an additional term in Eq. (4.14),

$$\Delta G_{pore} = \Delta G_{pore,0} + \alpha\psi^2 + \beta\psi, \tag{4.15}$$

where β describe the difference in offset charges between a closed and an open pore. Blicher and Heimburg [32] assumed that the "voltage offset" (ψ_0, given in Eq. (2.32)) is constant. Using this assumption we can rewrite Eq. (4.15)

$$\Delta G_{pore} = \Delta G_{pore,0} + \alpha\psi^2 + 2\alpha\psi_0\psi. \tag{4.16}$$

The form of Eq. (4.16) is different from the form proposed by Blicher and Heimburg [32], however the two forms are equivalent.

We assume that a conducting pore through the membrane can be found only in two states, either closed (not existing) or open. From Eq. (4.16) the probability of an open pore can be calculated in a Boltzmann fashion,

$$P_{open} = \frac{K_{pore}}{1 + K_{pore}} = \frac{\exp\left(-\frac{\Delta G_{pore}}{kT}\right)}{1 + \exp\left(-\frac{\Delta G_{pore}}{kT}\right)} \tag{4.17}$$

where K_{pore} is the equilibrium constant between an open and a closed state of one pore. The quantized nature of single channel recordings, from both lipid

and protein ion channels, show that conduction through a single open channel is constant [32]. Using that the conductance of a single channel is constant, the current through such a channel takes the form,

$$I_\Omega = \gamma_p \psi P_{open} \tag{4.18}$$

where γ_p is the conductance of a single pore. The subscript Ω is used to indicate resistive current. Note that ψ is the total applied voltages which include the Nernst potential, if present. Blicher and Heimburg [32] used Eq. (4.18) to very successfully describe the current-voltage relationship in membranes made of DMPC:DLPC (10 : 1), see Fig. (4.9) (left). In Fig. (4.9) (right) is shown the current-voltage relationships for two types of TRP channels (Transient Receptor Potential channels) for which Eq. (4.18) likewise describes the relationship very well. We will discuss this further in the discussion section of the present chapter.

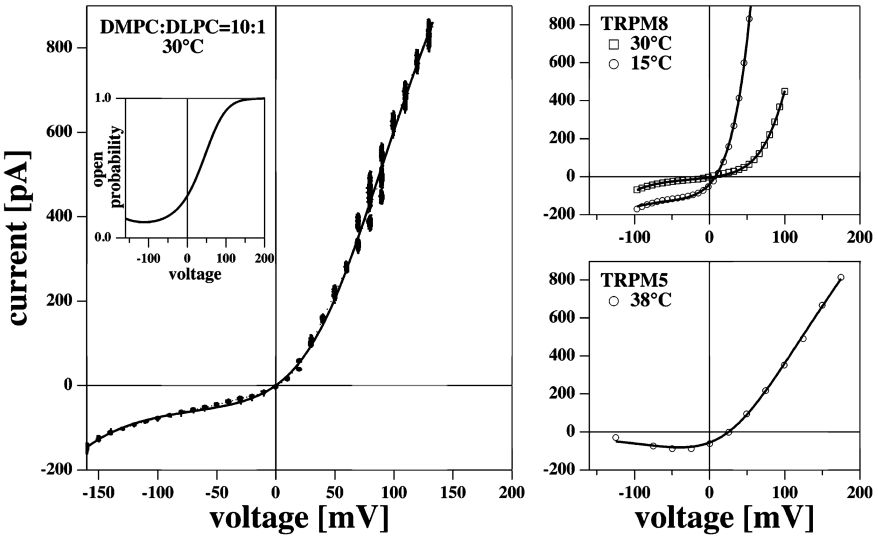

Figure 4.9: *Current-voltage relationships.* ***Left****, for a pure lipid membrane of DMPC:DLPC* (10 : 1) *at* $T = 303.15\ K$*. Insert shows the calculated probability of a pore being open.* ***Right****: (top) is for TRPM8 channels, and bottom is for TRPM5 channels both from HEK cells. Solid lines represent fits to data using Eq. (4.18). The figure is taken from [33]*

In fitting the current-voltage relationship in Fig. (4.9) (left) we allowed for a voltage offset, which was fitted to 110 mV. As was argued by Blicher and Heimburg [32] the voltage offset could originate from curvature of the membrane, as discussed in 2.3.2. The experiments were done using the patch pipette method where small pressure differences between the pipette and the outside can result in significant curvature. Note that by releasing the assumption of a constant offset voltage (Eq. (4.15)) the initial offset voltage can be smaller than the estimated 110 mV, since β can be bigger than 2α.

The conductance of lipid membranes depends both on the state of the membrane, especially in regard to the lipid melting transition, and is a non-linear function of the applied voltage. The permeability of the membrane has been

shown to be approximately proportional to the excess heat capacity profile of membrane. However, the detailed dependence of the non-linearity of the conduction on the state of the membrane has yet to be worked out. We are here interested in exploring the electrical response of lipid membranes and assume therefore for simplicity that the non-linearity of conduction of lipid membranes is well represented by the non-linearity of the current-voltage relationship shown in Fig. (4.9) (left). The main feature of interest, as we shall see below, for the electrical response of the non-linearity of the conduction of the membrane originates from the non-linearity having a time dependence. The time dependence results in a temporal separation between the linear and non-linear components in the electrical response. That the conduction of pure lipid membranes follows the magnitude of the membrane fluctuations, the excess heat capacity profile, indicates, through the Fluctuation-Dissipation theorem, that the dynamics of the pores must follow the relaxation/fluctuation dynamics of the membrane.

4.3.1 Applied to common experiments

We will again address two types of perturbation methods, impedance and voltage jump experiments, for conduction of lipid membranes.

Electrical impedance

The current response due to low amplitude sinusoidal perturbation (first order Taylor expansion around ψ_h), using linear response theory, takes the form,

$$I_\Omega \approx \int_{-\infty}^{t} \left(\sigma_{m,\psi_h} + \left(\frac{\partial \sigma_m}{\partial \psi} \right)_{\psi_h} (1 - \Psi_m(t-t')) \right) \frac{d\psi(t')}{dt'} \mathrm{d}t' \quad (4.19)$$

$$= \left(\sigma_{m,\psi_h} + \left(\frac{\partial \sigma_m}{\partial \psi} \right)_{\psi_h} \frac{1}{1+i\omega\tau} \right) \psi(\omega), \quad (4.20)$$

where $\sigma_{m,0}$ is the conductance of the membrane at ψ_h, $(\partial\sigma_m/\partial\psi)_{\psi_h}$ is the voltage dependence of the conduction evaluated around ψ_h and $\psi(\omega) = \psi_h + \Delta\psi(\omega)$. For simplicity of notation $(\partial\sigma_m/\partial\psi)_{\psi_h} \equiv \zeta_h$. Note that for a linear (constant) membrane conductance the last term in Eq. (4.20) is zero. From Eq. (4.20) the impedance of the membrane considering only conduction takes the form

$$Z_\Omega = \left(\sigma_{m,\psi_h} + \frac{\zeta_h}{1+i\omega\tau} \right)^{-1}. \quad (4.21)$$

Note that the conductance is defined as $\sigma \equiv 1/R$, R being the resistance.

The impedance of the full equivalent circuit (see Fig. (4.1)) of the lipid membrane in the vicinity of the lipid melting transition, using Eq. (4.10) and Eq. (4.21), takes the form,

$$Z_m = \left(\frac{1}{Z_\Omega} + \frac{1}{Z_{C_m}} \right)^{-1}$$

$$= \left(\left(\sigma_{m,\psi_h} + \frac{\zeta_h}{1+i\omega\tau} \right) + \left(i\omega C_{m,0} + \frac{i\omega C_0}{1+i\omega\tau} \right) \right)^{-1} \quad (4.22)$$

Based on the experimentally found current-voltage relationship (Fig. (4.9), (left)) we can estimate $\zeta_h/\sigma_{m,\psi_h} \approx 2$ for $\psi_h = -0.1\ V$[8]. Assuming as before that $1/\sigma_{m,\psi_h} = R_m = 100\ \Omega/cm^2$ and using the values for the membrane capacitance from Fig. (4.7) we can estimate the impedance profile of the lipid membrane in the vicinity of its lipid melting transition, see Fig. (4.10).

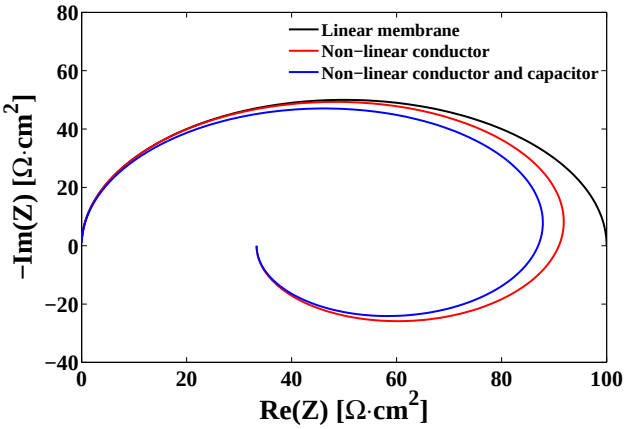

Figure 4.10: *Nyquist plot of the impedance of a lipid membrane (Eq. (4.22)) shown for different degrees of non-linearity:* ***black****, $\zeta_h = 0$ and $C_0 = 0$,* ***red****, $\zeta_h = 2 \cdot \sigma_{m,0}$ and $C_0 = 0$,* ***blue****, $\zeta_h = 2 \cdot \sigma_{m,0}$ and $C_0 = 0.5 \cdot C_{m,0}$. We have assumed a resistance of the membrane of $1/\sigma_{m,\psi_h} = R_m = 100\ \Omega/cm^2$, a membrane capacitance of $C_{m,0} = 1\ \mu F/cm^2$ and a characteristic relaxation time $\tau = 1\ ms$.*

From Fig. (4.10) and Eq. (4.21) the impedance of the non-linear membrane conduction interestingly takes the form of a resistor in parallel with an inductor and a resistor in series. A similar point was made by Mauro [104] in connection to the anomalous spiraling impedance profile of nerve membranes recorded by Cole and Baker [100]. He showed, similarly to our derivation, that a resistor going from low conducting state to a high conducting state with a finite relaxation time will produce a spiraling impedance profile characteristic of circuits containing a inductor. We see that for the impedance profile of the total equivalent circuit (Fig. (4.10)) of a membrane the non-linearity of the capacitor plays a minor role which could be overlooked in analyzing experimental data.

Voltage jump

As for the capacitive response to a voltage jump, we assume that the jump is instantaneous and that we can consider the dynamics of the conduction through the lipid membrane as a relaxation between two equilibrium states. We also assume that the equilibration follows the equilibration dynamics of the lipid membrane. Using these assumptions the current response to a voltage jump takes the following form,

$$I_\Omega(t) = \left(\sigma_{m,0} + \Delta\sigma_m \left(1 - e^{-\frac{t}{\tau}}\right)\right)\psi \tag{4.23}$$

[8] $\zeta_h/\sigma_{m,0}$ is strongly dependent on the holding voltage (ψ_h) and can for the lipid ion channels shown in Fig. (4.9) range from $\sim 2 - 20$.

where $\sigma_{m,0}$ is the background conduction or background leak, $\Delta\sigma_m$ is the change in conduction as a response to the voltage jump ($\Delta\psi = \psi_e - \psi_h$) and $\psi = \psi_e - \psi_{Nernst}$ is the potential felt by the ions, accounting for a Nernst potential. From Eq. (4.23) and Eq. (4.13) we can write the current response of the lipid membrane in the vicinity of the lipid melting transition to a voltage jump (for $t > 0$) as,

$$I_m(t) = \left(\sigma_{m,0} + \Delta\sigma_m \left(1 - e^{-\frac{t}{\tau}}\right)\right)\psi + \left(\Delta C_m \psi_e + \Delta(AP_0)\right)\frac{\exp\left(-\frac{t}{\tau}\right)}{\tau} \tag{4.24}$$

Notice the functional similarities between conduction and the non-linear capacitance contribution. From the literature we find that biological membranes have a background conductance of around $\sigma_{m,0} \sim 1\ mS/cm^2$ and open channel conductance of around $\Delta\sigma_m \sim 0.01\ S/cm^2$ [75, 100]. The resistive current through the membrane (Eq. (4.23)) is shown in Fig. (4.11), where we have assumed a characteristic relaxation time $\tau = 1\ ms$.

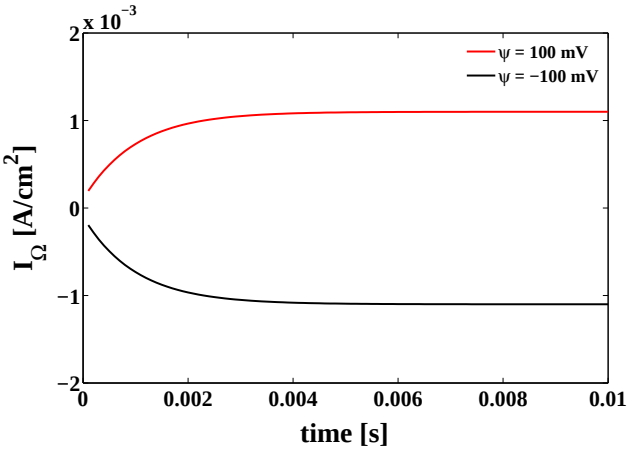

Figure 4.11: *The resistive current response to a voltage jump from $\psi_h = 0$ to respectively $\psi = 100\ mV$ and $\psi = -100\ mV$. The assumed conductance is $\sigma_{m,0} = 1\ mS/cm^2$ and $\Delta\sigma_m = 10\ mS/cm^2$, and the characteristic relaxation time is $\tau = 1\ ms$. No polarization or holding voltage is assumed.*

We see from comparing Fig. (4.8) and Fig. (4.11) that the resistive current is around 500 times greater then the peak of the capacitive current. We note though that the capacitive current is inversely proportional to the relaxation time and hence if we assume a characteristic relaxation time of $\tau = 0.1\ ms$ we see a ten-fold increase in the capacitive current.

4.4 Discussion of the electrical response

The treatment of the electrical response of lipid membranes has been carried out utilizing a number of simplifying assumptions, especially in regard to the ideal nature of the jump experiments and the assumed relaxation behavior of the membrane. We have used these assumptions to illuminate the consequences of the known non-linear nature of both the membrane capacitance and conduction, on common electrophysiological experiments.

We have shown that in the vicinity of the lipid melting transition the commonly made assumptions that the electrical properties of the lipid membrane are constant is an oversimplification. The capacitance is non-linear and additionally the offset polarization of membranes introduces an extra level of non-linearity, both of which are time dependent. The conduction through lipid membrane is likewise non-linear, where the non-linearity also is time dependent. Interestingly, the capacitive currents are strikingly similar to gating currents and the conduction shows great similarities with the conducting properties commonly associated with protein ion channels, both will be the focus of the following paragraphs.

4.4.1 Gating currents

In their model for the propagation of nerve signals in giant squid axons Hodgkin and Huxley [24] had predicted that the ion channels driving the signal must have a voltage-dependent gating mechanism. This gating mechanism must originate from a charged part of the protein which feels electric fields and effectively gates the channels. The gating should therefore produce a current signal, however small. Applying various experimental tricks, mainly involving lowering the conductive currents of the nerve membrane, a small capacitive current after a voltage jump have in fact experimentally been found, showing maximum height of about 30 $\mu A/cm^2$ and temporal width of around 0.1 ms [105, 106]. These findings greatly supported the nerve model of Hodgkin and Huxley.

We showed that the impedance of the non-linear part of the membrane capacitance takes the electrophysiologically familiar form of a so-called lossy capacitor. The lossy capacitor is commonly associated with the capacitive response of gating charges in membrane associated proteins (mainly protein ion channels). This indicates a similarity between the response of the non-linearity of the lipid membrane and gating currents. We further showed that the non-linear capacitance can lead to a variety of current responses to a voltage jump, depending on the state of the membrane and the offset polarization. These non-linear capacitive currents are temporally separable from the current of the constant part of the capacitance, due to the relaxation time of the membrane. We predict non-linear capacitive peak currents of between $1 - 60$ $\mu A/cm^2$, where the high currents only are achievable close to T_m, assuming a characteristic relaxation time of $\tau = 1$ ms. That the measured gating current could be due to the non-linearity of the membrane capacitor rather then the movement of gating charges was explored by Blatt [107]. Blatt considered only the electrostrictive effect, and found that the non-linear capacitive current was of the same order of magnitude as the gating current. However, he predicted the non-linear capacitive current to be in

the opposite direction of the gating current, which was already pointed out by Keynes and Rojas [106]. Only considering electrostriction we predict the same direction for the non-linear capacitive current as Blatt. However, considering a membrane with an offset polarization, excluding the possibility of the recorded gating current being due to non-linear capacitive current of the membrane is no longer possible and a detailed investigation is needed. The biological relevance of our predictions is underlined by the experiments by Farrell *et al.* [65], which show significant non-linearity of the capacitance of HEK cells (human embryonic kidney) including offset polarization effects following our predictions (see 2.4).

We should note that in our treatment of the non-linearity of the electrical properties of lipid membranes, we have implicitly assumed that the compressibilities goes to zero far from the lipid melting transition. This assumptions is acceptable since we have only considered the membrane in the vicinity of the transition. However, the compressibilities are not zero outside the transition, especially in the fluid phase, and we therefore expect non-linear capacitive currents outside the transition region.

4.4.2 Conduction effects

As was shown by among others Blicher and Heimburg [32] (see Fig. (4.9), left) lipid membranes show high conductivity close to the lipid melting transition. Furthermore, the membrane ion channels show similar conduction features as those commonly associated to specific ion channel proteins, including strongly voltage dependent conductance, response to chemical species, notably anesthetics [101] and temperature dependent conduction. Any factor which influences the lipid melting transition will influence the membrane conduction [102]. Arguing that the membrane conduction must follow the dynamics of the fluctuations of the lipid membrane, we showed that the temporal conduction behavior of lipid ion channels is similar to the behavior of voltage-gated proteins such as the potassium channel from Hodgkin and Huxley [75]. We see that we can expect lipid ion channels not only to show amplitude of conduction similar to that of proteins but also their dynamical properties mimics the protein ion channel dynamics, both on macroscopic level (discussed here) and on a microscopic level [32]. The similarity between the conduction of lipid channels and protein channels fundamentally complicates the association of conduction properties with a specific protein[9]. As shown in Fig. (4.9) (right), we see that the proposed model for the non-linear conduction of lipid ion channels describes the conduction of two groups of TRP channels. One can thus argue that a lipid membrane is capable to reproduce their conduction behavior, underlining the complication of differentiating protein conduction from lipid conduction. We see that lipid ion channels conduction behavior can encompass a great number of protein channels behavior, however the behavior of lipid channels seems far less regulated and is mainly prevalent in the vicinity of the lipid melting transition. Interestingly, commonly used artificial lipid membranes to successfully reconstitute channel proteins[10] have a lipid melting transition in the vicinity of

[9] We should however note that selective conduction of lipid ion channels is not expected.
[10] Successfully reconstituted means that they show conduction.

room temperature [108], indication a mutual influence between the membrane and proteins.

4.4.3 Protein-membrane interactions

It is well known that the electrical properties of a biological membrane can be disrupted by the misfolding or mutation of the proteins. An example of this is that targeted mutations of the gating groups, of a protein ion channel, can disrupt the gating of the conduction of the protein. This type of experiments strongly underlines the supposed protein gating mechanism and the central role of the protein in conduction through the membrane. Furthermore, when studying reconstituted protein ion channels, it is common procedure to measure the conduction of the used pure lipid membrane to reliably associate any change in conduction or function to the reconstituted protein. However, as it has been shown by several authors, membrane proteins affect their surrounding lipid membrane and vice versa (the membrane affects the associated proteins) [53, 108, 109][11]. This naturally also means that removing the proteins from a biological membrane can change the properties of the lipid part of the membrane. We have shown in our lab (unpublished[12]), that the heat capacity profile of a extracted membrane from a rat brain displays a shift in its heat capacity profile after denaturing the membrane proteins. This shows that the proteins influence the bulk properties of the membrane. Likewise, the coupling also means that the activity of a protein can be tuned by the physical properties of the surrounding membrane [108].

We have explored on a more local (though still thermodynamical) level the influence of a protein on the lipid membrane by Monte Carlo simulations[13]. In the simulations, a protein was modeled as a circle of the size of 7 lipids which is interacting with the surrounding lipids through nearest neighbor interactions. The protein is assumed to only have one state which has an energy penalty for neighbor lipids being in the fluid state of $\omega_{p,f} = 1326\ J/mol$ and no penalty for the neighbor lipids being in the gel state (interacting as a gel-lipid). This corresponds to a low interaction gel-loving protein. We see in Fig. (4.12) that the protein (black) above T_m induces local high fluctuations (yellow) and below acts by stabilizing the membrane (lowering fluctuations, red). The protein acts on the membrane by promoting the gel state locally. Hereby, inducing high fluctuations locally above T_m and stabilizing below T_m.

We have quantified the fluctuations[14] induced by the presence of a gel-loving protein as a function of distance from the protein in Fig. (4.13). We see that the influence of the protein close to the melting transition spans several layers of lipids in a decaying fashion. Similar effects were predicted by Jähnig [109].

We see from our simulation results (Fig. (4.12) and (4.13)) that even for a weak interacting protein which only has one state, the local lipid membrane can be affected substantially. We see that locally induced fluctuation levels can

[11] Furthermore, membrane proteins are very tedious to purify and will almost always bring with them a bit of their native membrane

[12] Experiments done by S. B. Madsen.

[13] The simulation is carried out using the model lipid model described in 3.3.3.

[14] The fluctuations are quantified by the variance of the probability of a state change of the lipid ($\langle s \rangle^2 - \langle s^2 \rangle$, s being the probability of a state change), which takes maximum value of 0.25 for the state changing in each Monte Carlo cycle.

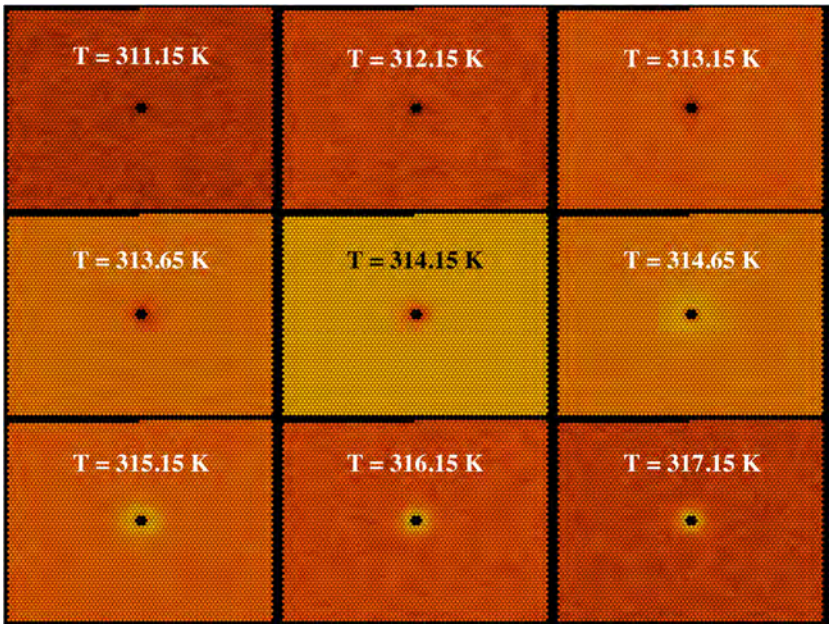

Figure 4.12: *Visualization of lipid state fluctuations, yellow indicates high fluctuation and red indicates low fluctuations, shown for different temperature around* $T_m = 314.15\ K$*. In the center of each panel is the protein shown in black.*

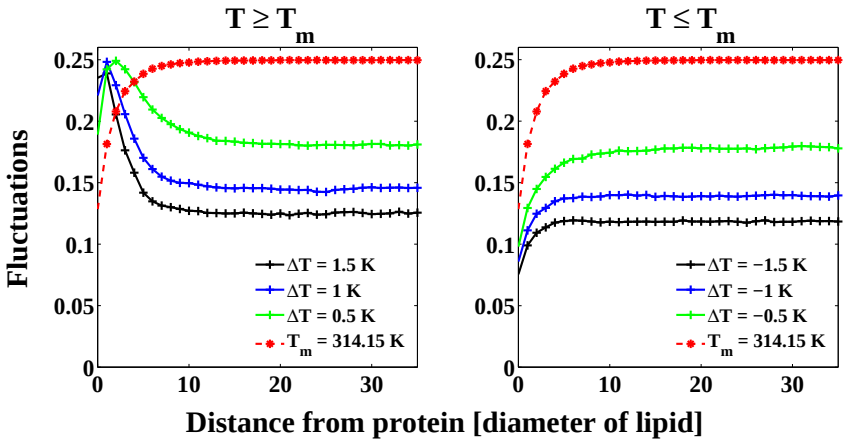

Figure 4.13: *The fluctuations of lipid state as a function of distance from the protein shown for different temperatures around* T_m*. The fluctuations are defined as* $\langle s \rangle^2 - \langle s^2 \rangle$*, where* s *is the probability of a state change.*

be similar to those in the transition even if the bulk membrane is far from the transition. This indicates that proteins could harness the transition properties of the lipid membrane without the bulk membrane being in the transition. This could potentially explain the similarity between the conduction of some class of proteins and the pure lipid membrane [33], by proposing that the protein locally

induces a transition in a region and the conduction is through this region rather than actually through the protein. We have only considered a minimalistic protein model, with low interactions and one state. Many membrane proteins, however, are known to have several states and to contain charged regions for which one can expect strong electrostatic interaction with their surrounds. For such proteins one can expect much more dramatic effects on the surrounding membrane including the possibility of drastic responses due to state changes of the protein.

From these considerations, assuming that the properties of the lipid membrane before and after reconstituting proteins can be highly speculative. To correctly associate a property to a specific protein one needs to know the detailed interaction between the given protein and the membrane, in practice rendering this very difficult. Likewise, we can not expect the interactions between protein and membrane to be unaffected by mutations. This means that mutation essays mapping the functions of different groups of proteins again becomes difficult.

We have mainly considered the implication of proteins for conduction however their interaction with the lipid membrane indicate implications also for the membrane capacitance. We have seen that membrane proteins can acts as controllers of the surrounding membrane and we could speculate if it is possible that they can even acts as property amplifiers. Additionally one can speculate how proteins influence the ionic environment close to the membrane and how this influences the state of the membrane and its properties. The implications of the interactions between membrane and proteins is interesting and can potentially solve an number of questions within cell biology.

Chapter 5

Dispersion in the Soliton model

The studies presented in this thesis have been motivated by the recently proposed alternative model for the propagation of nerve signals, the Soliton model. The Soliton model describes the nerve signals as a consequence of the thermodynamical/mechanical macroscopic properties of nerve membranes, rather than the properties of individual constituents of the membrane. In the framework of the Soliton model a nerve signal can be viewed as a lateral density soliton, a localized pulse.

Solitons are self-reinforced waves that propagate with constant velocity without attenuating. The prerequisite for propagation of solitons is that the non-linear and dispersive effects in the medium counteract each other. Systems displaying solitons require a source of non-linearity, this non-linearity can be due to a wide spectrum of phenomena, e.g. the Kerr effect in optics. In the soliton description of nerve pulse propagation the nonlinearity originates from the empirically known lipid melting transition, which results in a non-linear relationship between the speed of sound and the lateral density, see section 1.2.2. The second prerequisite for the propagation of solitons is dispersion. For the soliton description of nerve pulses the relevant dispersion effect is the frequency dependence of the speed of sound. Dispersion in lipid membranes is a rarely treated problem and little work has been done on it. As a consequence, in the present formulation of the Soliton model dispersion is included as an ad hoc term. In this chapter we will address the frequency dependence of the speed of sound in lipid membranes and show that it depends on the relaxation behavior of the membrane [79]. From the found frequency dependence of the speed of sound we will estimate the dispersion and consider the implications of the found dispersion for the Solition model. First we address the role of dispersion in the present formulation of the Soliton model [26].

Soliton model

The Soliton model, as described in section 1.2.2, is based on longitudinal sound propagation in a cylindrical medium. We remind the reader that the Soliton model is described by the following PDE (Eq. (1.4))

$$\frac{\partial^2 \Delta\rho^A}{\partial t^2} = \frac{\partial}{\partial x}\left(\left(c^2(\Delta\rho^A)\right)\frac{\partial \Delta\rho^A}{\partial x}\right) - h\frac{\partial^4 \Delta\rho^A}{\partial x^4}, \tag{5.1}$$

where $\Delta\rho^A$ is the change in the lateral density, $c^2(\Delta\rho^A)$ is the lateral speed of sound[1], the last term is the dispersion term and h is the dispersion coefficient. The lateral speed of sound is a non-linear function of the lateral density and in the Solition model it is approximated by (Eq. (1.3))

$$c^2(\Delta\rho^A) \approx c_0^2 + p\Delta\rho^A + q(\Delta\rho^A)^2, \tag{5.2}$$

where c_0 is the speed of sound in the fluid phase, far from the transition, p and q are the Taylor expansion coefficients[2]. If we consider the low-amplitude periodic solution of Eq. (5.1) ($\Delta\rho^A(x,t) = \Delta\rho_0^A \exp(i\omega(t - x/c_0))$), assuming $c(\Delta\rho_0^A) \approx c_0$, the nature of the dispersion term (last term in Eq. (5.1)) becomes apparent from the consequent dispersion relation

$$c^2(\omega) = c_0^2 + A\omega^2 \approx c_0^2 + \frac{h}{c_0^2}\omega^2\,. \tag{5.3}$$

We see that the dispersion constant (or coefficient) acts as the second order Taylor expansion coefficient of the frequency dependent speed of sound, around $\omega = 0$. The first order term in Eq. (5.3) is zero due to the symmetry of the frequency dependence of the squared speed of sound. Heimburg and Jackson [26] made the conservative assumption of using a dispersion term in Eq. (5.1) which represents the lowest order expansion of the frequency dependence of the speed of sound and assumed the dispersion to be independent of the state of the membrane. They made these assumptions since little insight on the propagation of low frequency sound in lipid membranes was available.

Under the assumptions used to derive Eq. (5.1), the sole role of the dispersion coefficient (h) is to set a linear scale for the solitons. This is illustrated in Fig. (5.1) where the Soliton model has been solved for different dispersion coefficients assuming constant propagation velocity. The chosen value of the dispersion coefficient by Heimburg and Jackson corresponds to a width of the soliton of $\sim 10\ cm$ ($h = 2\ m^4/s^2$) [26].

[1] Lateral speed of sound and speed of sound is used interchangeably in this chapter.
[2] For LUV of DPPC: $c_0 = 176.6\ m/s$, $p = -16.6 \cdot c_0^2/\rho_0^A$ and $q = 79.5 \cdot c_0^2/(\rho_0^A)^2$.

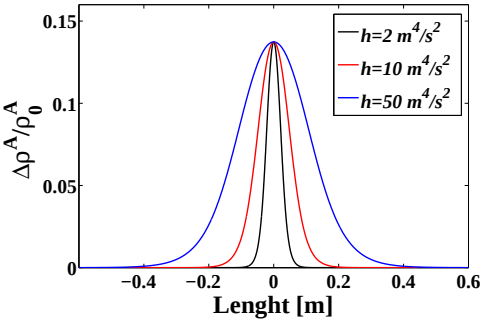

Figure 5.1: *Solitons calculated for different dispersion constants using Eq. (1.6). Parameters are from LUV of DPPC and the propagation velocity is* $v = 0.7\, c_0$.

In the present formulation of the Soliton model the dispersion is considered independent of the state of the membrane and the non-linearity and the dispersion are completely decoupled. However, as we will justify below, dispersion depends strongly on the state of the membrane and it is tightly coupled to the non-linearity of the speed of sound. The freedom in estimating dispersion and thereby regulation of the width of predicted solitons is therefore limited.

5.1 Sound propagation in membranes

The propagation of sound is the propagation of a low-amplitude adiabatic density wave. The adiabatic nature of sound means that the density wave is accompanied by a temperature wave. Sound propagation is a macroscopic phenomenon which is governed by the equation of sound[3]

$$\frac{\partial^2 \rho^A}{\partial t^2} = \hat{c}^2 \frac{\partial^2 \rho^A}{\partial x^2}, \tag{5.4}$$

where $\hat{c} = (\rho^A \kappa_S^A)^{-1/2}$ is the speed of sound. Ideally, the speed of sound is a constant. However, for sound propagation in any real medium, the speed of sound is a complex quantity, whose real part causes a phase shift (resulting in dispersion) and the imaginary part leads to a decrease of the amplitude (or intensity) of the sound as it propagates (attenuation) [79]. We note that, for non-ideal propagation of sound, the effective speed of sound (i.e. the speed of sound that one would measure) is different from the real part of the speed of sound ($\hat{c}$). The effective speed of sound is given by [79],

$$c = \left(\frac{Re(\hat{c})}{|\hat{c}|^2} \right)^{-1}. \tag{5.5}$$

We see that for ideal propagation of sound, where the imaginary part of the speed of sound is zero, the effective speed of sound (c) is equal to the speed of sound ($\hat{c}$). In fact, even for non-ideal propagation, the effective speed of sound is

[3]For the case of 1-dimensional longitudinal sound propagation

often referred to as just the speed of sound, which is also the case i.e. in Eq. (5.3). The non-ideal propagation of sound can be caused by a number of effects such as internal friction, heat conduction and finite relaxation times of the system. The latter will cause hysteresis and dissipation of heat due to the internal degrees of freedom being unable to keep up with the external propagating wave. We saw in chapter 3 that, in the vicinity of the lipid melting transition, the characteristic relaxation time of thermodynamical fluctuations is drastically extended. The magnitude of the slow-down allows us to assume it to be the main contributor to dispersion and attenuation in the vicinity of the transition in the lipid membrane system [79]. In other words, we consider the dispersion in lipid membranes to be caused by the slow relaxation in vicinity of the lipid melting transition. From this we investigate the response of the membrane to a sound wave. We start by considering how changes in lateral pressure (π) and temperature (T) couples to the change in entropy of the membrane.

$$\mathrm{d}S = \left(\frac{\partial S}{\partial T}\right)_{\pi} \mathrm{d}T + \left(\frac{\partial S}{\partial \pi}\right)_{T} \mathrm{d}\pi. \tag{5.6}$$

Considering only small changes in lateral pressure and temperature and writing the changes as rates (e.g. $\dot{T}$), we can write the time dependent change in entropy (as in Eq. (3.4)),

$$\Delta S(t) = \int_{-\infty}^{t} \left[c_{p0} + \Delta c_p \left(1 - \Psi_{c_p}(t - t')\right)\right] \left(\frac{\dot{T}(t')}{T_0} - \gamma_A \dot{\pi}(t')\right) dt', \tag{5.7}$$

where we have used the proportionality between changes in area and enthalpy (Eq. (2.21)), and we assumed that perturbations in temperature are small so that T_0 can be considered a constant. The transfer function is the dynamic heat capacity, where c_{p0} is the part of the heat capacity which relaxes much faster than the considered perturbation, Δc_p is the excess heat capacity, which is the part of the heat capacity that we assume to relaxe slowly, and Ψ_{c_p} is the relaxation function. We used that the extensive thermodynamical variables for the lipid membrane system are proportional to each other during the lipid melting transition to justify that the transition is well described by a single relaxation function Ψ_{c_p}. We will here again assume for simplicity, that the thermodynamical fluctuations of the lipid membrane in the vicinity of the melting transition are well described by a single exponential relaxation

$$\Psi_{c_p}(t) = \exp\left(-t\frac{L}{T^2 \Delta c_p}\right),$$

where the characteristic relaxation time ($\tau = T^2 \Delta c_p / L$) is proportional to the excess heat capacity (Eq. (3.14)) and L is a phenomenological proportionality constant. Sound is sinusoidal in nature, so the transfer function (dynamic heat capacity), can be written as a Debye term (following Eq. (3.8))

$$\Delta c_p(\omega) = \Delta c_p \left(\frac{1 - i\omega\tau}{1 + (\omega\tau)^2}\right). \tag{5.8}$$

Considering how changes in lateral pressure and temperature couple to change in the entropy of the membrane we found that the appropriate transfer function

is the dynamic heat capacity (Eq. (5.8)). Using Eq. (3.18)[4], which couples the adiabatic compressibility with the effective heat capacity, and the fact that the dynamic heat capacity can be identified with the available (or effective) heat capacity at a given frequency (see 3.3.3), we can calculate the frequency dependent adiabatic lateral compressibility,

$$\kappa_S^A(\omega) = \kappa_T^{A,0} + \frac{\gamma_A^2 T}{A}\Delta c_P(\omega) = \kappa_T^{A,0} + \frac{\gamma_A^2 T}{A}\Delta c_p \left(\frac{1 - i\omega\tau}{1 + (\omega\tau)^2}\right), \tag{5.9}$$

where $\kappa_T^{A,0}$ is the part of the isothermal lateral compressibility which is independent of the melting transition and we have used the dynamic heat capacity from Eq. (5.8). From the adiabatic lateral compressibility (Eq. (5.9)) the effective speed of sound (Eq. (5.5)) takes the form

$$c^2(\omega, \rho^A) = (\rho^A)^{-1} \frac{2}{Re(\kappa_S^A(\omega, \rho^A)) + |\kappa_S^A(\omega, \rho^A)|}, \tag{5.10}$$

Note that the effective speed of sound is a function of both the lateral density and the frequency. The non-linearity in Soliton model is contained within the lateral density dependence of the effective speed of sound, and the dispersion is contained within its frequency dependence.

We see that the frequency dependence of the speed of sound is strictly coupled to the variance of the thermodynamical fluctuations (the heat capacity) of the lipid membrane through the characteristic relaxation time. This means that the dispersion and non-linearity of the speed of sound are tightly coupled through their dependency on the state of the lipid membrane.

5.1.1 Dispersion

The dispersion describes the frequency dependence of the speed of sound. By Taylor expanding the effective speed of sound (Eq. (5.10)), around $\omega = 0$, up to second order, we find that we can write the expansion in the same form as Eq. (5.3) where the dispersion coefficient is now given by

$$h(\rho^A) = c^6(0)\frac{3c_1^2 + 4c_2^2}{4c_2^2(c_1^2 + c_2^2)}\tau^2, \tag{5.11}$$

where

$$c_1^2 \equiv c^2(\omega \to \infty, \rho^A) \equiv \left(\rho^A \kappa_T^{A,0}\right)^{-1}, \tag{5.12}$$

$$c_2^2 \equiv \left(\rho^A \frac{\gamma_A^2 T}{A}\Delta c_p\right)^{-1}, \tag{5.13}$$

$$c^2(0) \equiv c^2(\omega \to 0, \rho^A) \equiv \left(c_1^{-2} + c_2^{-2}\right)^{-1}. \tag{5.14}$$

Here, c_1 is the high frequency limit for the speed of sound, c_2 is the component of the speed of sound related to the lipid melting transition and $c(0)$ is the low frequency limit of the speed of sound, see Fig. (5.2). Note that c_1, c_2 and $c(0)$ are all dependent on the lateral density but not on frequency.

[4]The functional form of the volume and area compressibility is the same.

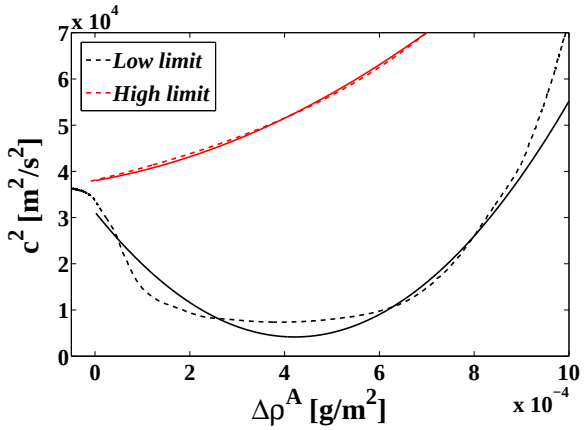

Figure 5.2: *The speed of sound squared as a function of lateral density, shown for the high (Eq. (5.12)) and low (Eq. (5.14)) frequency limit calculated from the heat capacity of LUV of DPPC (dashed lines) [79], along with the corresponding approximations for the high (red solid line) and low (black solid line) frequency limits using respectively Eq. (5.2) and Eq. (5.16).*

We see from Eq. (5.11) that the dispersion coefficient is no longer a constant but depends on the lateral density through the dependency of the speed of sound and the characteristic relaxation time on lateral density. Using the coupling between the heat capacity and the characteristic relaxation time ($\tau = T^2 \Delta c_p / L$) and Eq. (5.13) we can write the relaxation time as

$$\tau(\Delta\rho^A) = \frac{m_l T}{\gamma_A^2 L (\rho^A)^2} \frac{1}{c_2^2}\,, \tag{5.15}$$

where m_l is the mass of a lipid pair. Using the strict coupling between the heat capacity, the relaxation time and the speed of sound we can fully describe the dispersion coefficient (Eq. (5.11)) from the low frequency and the high frequency limits of the speed of sound. Instead of considering the explicit dependence of c_1 on the lateral density (Eq. (5.12)) we approximate it, by a second order polynomial (like the low frequency limit in Eq. (5.2) for the formulation of the Soliton model), for simplicity

$$c_1^2(\Delta\rho^A) \approx k \cdot c_0^2 + f\Delta\rho^A + g(\Delta\rho^A)^2. \tag{5.16}$$

Appropriate parameters of unilamellar vesicles of DPPC are $f = 2.3\, c_0^2/\rho_0^A$, $g = 20.9\, c_0^2/(\rho_0^A)^2$ and $k = 1.22$[5]. In Fig. (5.2) the high and low frequency limits of the speed of sound squared for unilaminar vesicles of DPPC are shown along with their approximated forms (Eq. (5.2) and Eq. (5.16)). Using the approximated forms for the high and low frequency limits we can calculate the dispersion coefficient as a function of lateral density, which is shown in Fig. (5.3).

[5]The low and high frequency limits are taken from [79]

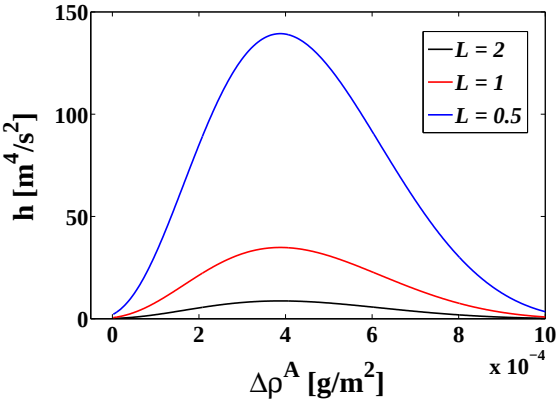

Figure 5.3: *The dispersion coefficients (h), as a function of lateral density for LUV of DPPC, calculated using Eq. (5.11) for different values of the phenomenological constant (L), which is given in units of* $10^{12}\ J \cdot K/(s \cdot mol)$.

5.2 Extending the Soliton Model

We have in the above shown that nonlinearity and dispersion in lipid membranes both originate from the lipid melting transition and are strictly coupled. This puts strong constrains on the dispersion coefficient. In the following, we extend the soliton model by including the found density dependent dispersion coefficient. We will show that the extended model can lead to solitons and that the timescale of thermodynamical fluctuations sets the scale for these solitons.

We can exchange the original constant dispersion coefficient with the found density dependent dispersion coefficient (Eq. (5.11)) without further assumptions in Eq. (5.1).

$$\frac{\partial^2 \Delta\rho^A}{\partial t^2} = \frac{\partial}{\partial x}\left(\left(c_0^2(\Delta\rho^A)\right)\frac{\partial \Delta\rho^A}{\partial x}\right) - h(\Delta\rho^A)\frac{\partial^4 \Delta\rho^A}{\partial x^4}\,. \tag{5.17}$$

Considering solitonic solutions that propagate with constant velocity of the form $\Delta\rho^A(z)$ with $z = x - vt$, we can simplify Eq. (5.17) to

$$v^2\frac{\partial^2 \Delta\rho^A}{\partial z^2} = \frac{\partial}{\partial z}\left(\left(c_0^2(\Delta\rho^A)\right)\frac{\partial \Delta\rho^A}{\partial z}\right) - h(\Delta\rho^A)\frac{\partial^4 \Delta\rho^A}{\partial z^4}\,. \tag{5.18}$$

This non-linear fourth order ordinary differential equation can be solved numerically assuming that soliton is exponentially localized as in [26]. We used the numerical ODE solver in *Mathematica*. The solution is shown in Fig. (5.4) for different values of the phenomenological constant (L).

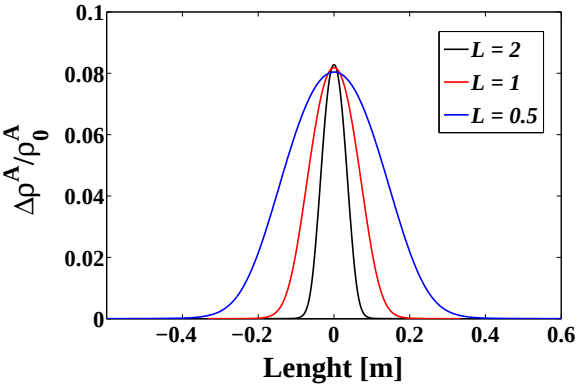

Figure 5.4: *Solitons predicted based on the coupling between non-linearity and dispersion (Eq. (5.18)), using different phenomenological constant (L), which is given in units of* $10^{12}\ J \cdot K/(s \cdot mol)$. *The predicted propagation velocity is set to* $v \approx 171\ m/s$ *for all three solitons.*

5.3 Discussion

In our treatment of solitons facilitated by the lipid melting transition we see that the coupling between heat capacity (the variance) and the characteristic relaxation time of thermodynamical fluctuation both define and set the scale for the soliton. This shows that solitons in lipid membranes are fully described by the close to equilibrium thermodynamical properties of the system. We have shown the coupling assuming a single exponential relaxation behavior. As was discussed in chapter 3, the relaxation behavior of the lipid membrane in the vicinity of the lipid melting transition is rather complicated, spanning several timescales. For all timescales, the characteristic relaxation times scales with the magnitude of the thermodynamical fluctuations of the system (the excess heat capacity). We therefore expect the relaxation behavior to still be coupled to the magnitude of the thermodynamical fluctuations. The conclusion that the membrane can facilitate solitons and that these are fully defined by the thermodynamical properties of the membrane in the transition is general and should not be specific to the chosen single exponential relaxation.

Relaxation experiments on lipid membranes using calorimetry have shown that relaxation is a single exponential with a phenomenological constant of $L = 1.39\ 10^9 J \cdot K/(s \cdot mol)$ for LUV of DPPC. This corresponds to relaxation times around $\sim 3\ s$ which predict solitons with a width of the order of $z \approx 125\ m$. These values represent the slow limit of the experimentally found relaxation timescales. Timescales found for the dynamics of pores in lipid membranes are rather on the millisecond regime which predict solitons with a width of $z \approx 10\ cm$ for $L = 1.39\ 10^{12} J \cdot K/(s \cdot mol)$. Nerve pulses in myelinated axons have a width of the order of $z \approx 10\ cm$ which seems within the predicted range. Note that biological membranes have a much less pronounced lipid transition which, in turn, will lower the width further without drastically changing other properties of the predicted solitons.

The relaxation behavior of lipid membrane along with the behavior of biological membranes is still an open field. Further insight into the relaxation behavior of lipid membranes will allow us to make detailed predictions regarding the propagation of solitons in lipid membranes and nerve membranes. The relaxation behavior of the thermodynamical fluctuations sets the scale for solitons which can propagate in the lipid membranes.

Chapter 6

Nerve experiments

The central motivation for investigating the properties of lipid membranes is that they represent a good model system for biological membranes. More specifically, within the context of this thesis we are interested in understanding the properties of the excitable membrane of nerve cells.

The current general understanding of nerve signal (action potential) generation and propagation in nerves is based on the Hodgkin and Huxley model [24]. However, there are a number of experimental findings in the literature, which are either not included in the Hodgkin and Huxley framework or which are directly contradicting it (see section 1.2). Examples of these findings are the measured mechanical component of nerve signals and the reversible nature of nerve signals heat signature. These findings lead Heimburg and Jackson [26] to propose the Soliton model as an alternative model for the propagation of nerve signals. The two theories are fundamentally different, the Hodgkin and Huxley model being entirely electrical and the Soliton model being fundamentally mechanical in nature. The Soliton model predicts that a nerve signal results in a thickness change of the axon membrane in-phase with the electrical nerve signal whereas Hodgkin and Huxley predict only an electrical nerve signal. Furthermore, within the Hodgkin and Huxley framework it is assumed that two nerve pulses annihilate upon collision. The Soliton model on the other hand predicts that two colliding nerve pulses penetrate each other [110].

The experimental effort described in this chapter aims at testing the predictions of respectively the Soliton model and the Hodgkin and Huxley model. In order to do so we have built a neurophysiology lab and preformed two types of experiments: The first type involves measurements of the electrical nerve signal, preformed to investigate the effect of collision of two nerve pulses in the same axon. The second type instead involves simultaneous measurements of both the electrical and mechanical components of a nerve signal. [1]

[1] The experiments presented in this chapter have been done in close collaboration with Dr. Alfredo Gonzalez-Perez, Dr. Rima Budvytyte and Prof. Edgar Villagran Vargas.

6.1 Nerve samples

Establishing a neurophysiology lab involves several aspects: sample preparation, recording of the nerve signal and data analysis. As a model system we used different nerve samples from invertebrates. The nervous system of invertebrates are well described in the literature and they are easily attainable.

We worked mainly with nerve samples from earthworms (*Lumbricus terrestris*) and from lobsters (*Homarus americanus*). Specifically we worked mainly with the ventral cord of the earthworms (see Fig. (6.1), a-c) and the thorax and the abdominal part (see Fig. (6.1), d-f) of the ventral cord of the lobster.

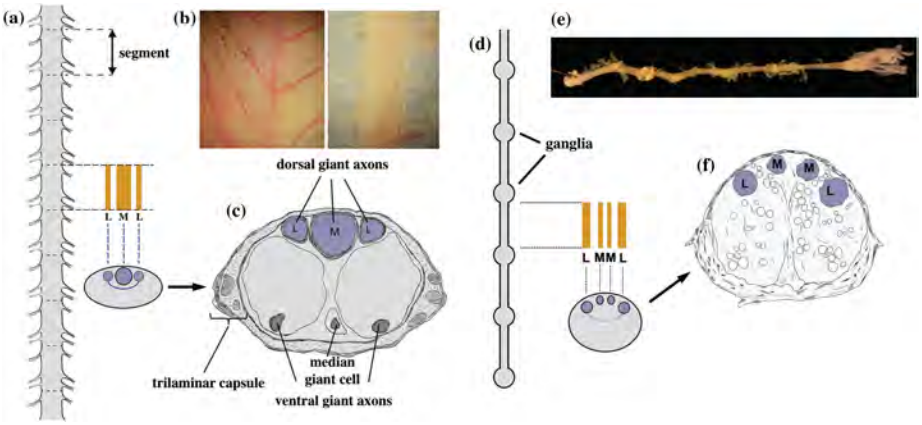

Figure 6.1: ***(a)*** *Schematic representation of the ventral cord of a earthworm,* ***(b)*** *ventral cord with and without muscular tissue of a earthworm and* ***(c)*** *schematic representation of cross-section of the ventral cord of earthworm.* ***(d)*** *Schematic representation of abdominal part of lobster ventral cord with six ganglia,* ***(e)*** *extracted abdominal ventral cord from lobster tail, and* ***(f)*** *cross-section of abdominal ventral cord of lobster. Median and lateral giant axons are marked with M and L. Figure is adopted from [110].*

The ventral cord of an earthworm is segmented along the length of the worm, each segment being $1-1.5\ mm$ and electrotonically[2] connected. The earthworms ventral cord contains three giant axons, two lateral axons which are connected and behave as one, and one median axon, see Fig. (6.1). The abdominal part of the ventral cord from lobster has four giant axons which are divided in two (ideally) identical parts, each containing a median and a lateral axon. The two parts are connected electrotonically at the ganglia, see Fig. (6.1). In the abdominal part of the ventral cord the signals from the two parts can be almost identical, if the two parts similar enough. In the thorax part, the two parts of the ventral cord splits in two separate nerves, each containing a median and a lateral giant axon. This part is called the circumesophageal connective (or connective) and is the part that connects the brain and the first ganglia in the ventral cord of a lobster. The giant axons in the earthworm is partially myelinated[3], whereas the

[2] Directly electrically connected.

[3] As a course grain division there exist myelinated and non-myelinated nerves. Myelin is a supporting tissue which is wrapped around the length of the axon of myelinated nerves. Myelinated nerves have higher signal propagation velocities than non-myelinated nerves.

giant axons in the lobster are non-myelinated. Methods of extraction of nerve samples can be found in [110].

The giant axons are experimentally interesting due to their size, allowing for "easy" identification and manipulation. Furthermore, the electrical strength of the nerve signal in giant axons is particularly strong, allowing for easier electrical detection. The strong electrical signal is due to the large circumference of the axon. This connection between strong electrical signal and axon circumference is both in the Hodgkin and Huxley model and in the Soliton model attributed to a coupling between surface area and electrical signal.

6.2 Electrical measurement

In this section the measurement of the electrical signal from nerves is described. We are interested in recording the nerve signals from giant axons. The electrical signal strength from giant axons varies greatly, depending on the nerve but also on the individual preparation[4]. The common signal range is between 20 μV and 2 mV in external recordings. We measured the nerve signal as a potential difference between two spatially separated electrodes on the surface of the nerve (purple and blue in Fig. (6.3))[5]. This is referred to as external recording, oppose to intercellular recording where one electrode is inside the axon. Note that by measuring the potential difference between two spatially separated electrodes, one effectively measure a proxy for the "derivative" of the nerve signal, we will therefore record a bi-phased pulse for a mono-phased nerve signal.

In our experiments, the signal propagating along the nerve, that we aim at detecting, is produced by external stimulation rather than the nerve self-stimulating. We can externally stimulate the nerve by applying a short ($5 - 20$ μs) square voltage pulse[6] between two spatially separated electrodes on the surface of the nerve (see stimulation electrodes in Fig. (6.3), shown in red and black). For self-stimulation the nerve is firing (nerve signal) spontaneously, this however can only occur for certain preparations. By using external stimulation we can control when the nerve is firing, which allows for easy detection and for averaging of the nerve signal. All used nerves contained several axons and the association of a signal with an axon can be complicated. However, it has been shown experimentally that the propagation velocity, like the signal strength, scales with the thickness of the axon[7], so that action potentials in thicker axons propagates faster. This allows one to associate signals to axons in simple nerve preparations, when using external stimulation, by the arrival time after stimulation at the recording electrodes, see Fig. (6.2). For self-stimulations, determining the origin of a signal is complicated and it has to be done by grouping signals using signal strength and shape (see i.e. [111]).

[4] Here preparation is used as synonym for sample.

[5] A recording can also be done with a single electrode and using ground as reference. Using ground as reference can however result in substantial electrical noise since electrical noise is not uniform in a setup.

[6] Also current pulses can be used for stimulation.

[7] This is true under physiological conditions, when comparing non-myelinated nerves with non-myelinated nerves and myelinated nerves with myelinated nerves. Propagation velocities for the used samples are between $2 - 20$ m/s

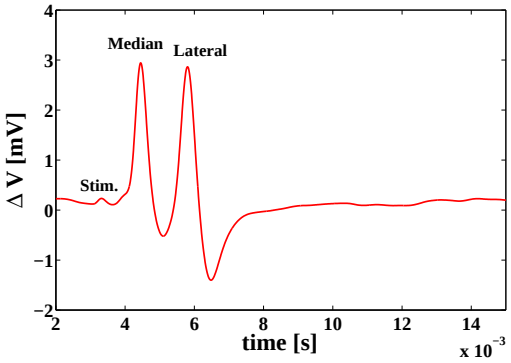

Figure 6.2: *Example of a nerve signal (external recording) from ventral cord of a earthworm (Lumbricus terrestris) using external stimulation. First pulse from the left is the stimulation artifact, the second pulse is from the median axon, and the last pulse is from the lateral axons.*

External stimulation has two disadvantages: it requires a long nerve and stimulations artifacts. For external stimulation the nerve preparation has to be of a certain length since both the two stimulation electrodes and the two recording electrodes have to be spatially separated and the stimulation site has to be away from the recording site, see Fig. (6.3). The second disadvantage of external stimulations is the possibility of a stimulation artifact, which is the stimulation pulse propagating in the surface water of the nerve to the recording electrodes. To limit the extent of the stimulation artifact, a ground electrode is placed between the stimulation site and the recording site, see Fig. (6.3) in green.

6.2.1 Electrical recording instrumentation

To record the voltage signal from the nerve we used a pre-amplifier with a low and a high-pass filter. The used differential amplifier is *DP-304* from *Warner Instruments*. The amplification settings commonly used are: AC-mode, gain $x1000$, 10 Hz high-pass filter and 10 kHz low pass filter[8]. Alternatively a 300 Hz high-pass filter can be used to lower the noise, though this might result in filtering distortion of the action potential profile. As can be seen from Fig. (6.2) the recorded nerve pulses are usually bi-phased with an approximate width of $1-3$ ms. The power spectrum of the action potential spans $200-2000$ Hz[9]. This means that any filtering in the vicinity of this range can distort the pulse and lead to artifacts depending on the type of filter.

The pre-amplified signal is fed to a *PowerLab 8/35* unit, see Fig. (6.3), from *ADInstruments*. The PowerLab unit is used as a analog-to-digital converter (16 bit, max. sampling 200 kHz) acting as a digital oscilloscope. The used PowerLab unit features software (LabChart) controlled filters (both hardware and software), AC-coupling, adjustable bit resolution and sampling frequency

[8] Both filters are -3 dB.

[9] A wider frequency range can in some experiments be relevant due to action potentials from different axons overlapping.

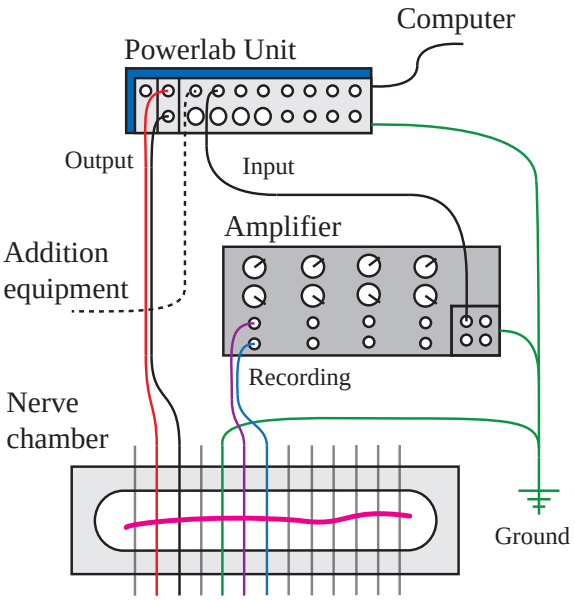

Figure 6.3: *Schematic representation of electrical neurophysiology setup, where the nerve is depicted as a thick pink line in the nerve chamber.*

(commonly using 40 kHz) on 8 independent channels. The PowerLab unit also includes software controlled output channels used for external stimulation. All data acquisition is done in LabChart using a self-build template, which includes the possibility of averaging nerve signals. The 8 channels allows for multiple simultaneous action potential recordings which can be used to accurately determine pulse propagation velocity and can also be used to acquire analog input from additional instrumentation. As we see in section 6.3, we have connected an Atomic Force Microscopy (AFM) unit to measure the mechanical component of a nerve signal simultaneous with electric measurements. Alternatively, a *PowerLab 26T* unit (*ADInstruments*) which is an easy-use unit with in-build bio-amplifier has been used. The protocol and the software template used for the 26T unit are as described above. The 26T unit was used for the collision experiments.

The nerve chambers we used are build after our specification in plexiglass and include a lid for minimizing dehydration of the nerve sample. The electrodes are stainless steel pins with a width of 0.5 mm spaced 2.5 mm apart. The nerve chambers are shown in Fig. (6.3) and Fig. (6.7) (bottom) for, respectively, the setup where only electrical recordings were preformed and for the electrical and mechanical recordings setup.

6.2.2 Collision of action potentials

The Soliton model, unlike the Hodgkin and Huxley model, predicts that nerve signal propagating down the same axon can pass through one another without annihilation [42, 110]. Assessing whether colliding nerve pulses annihilate or

penetrate each other is a crucial point in understanding the nature of nerve pulses. Despite its relevance for understanding nerve signals, collision of nerve pulses have received surprisingly little attention. Tasaki [112] showed in 1949 that two nerve pulses annihilated upon collision, which followed the predictions of the Hodgkin and Huxley framework. Little work have been done since, that explores collision though annihilation is what is generally assumed to occur in neuroscience.

We have conducted collision experiments to test the hypothesis that nerve pulses annihilate upon collision. We have preformed collision experiments in the ventral cord of earthworms, in the thorax and abdominal part of the ventral cord of lobsters and in walking legs of lobsters.

Nerve pulses are under physiological conditions generally believed to propagate from the nerve cell body down the axon to the nerve terminals, so-called orthodromic propagation. However, nerve pulses can be stimulated at any point throughout the axon (or in the dendrites) and nerve signals can also propagate in the opposite direction, called antidromic propagation. We can therefore, by simultaneously applying stimulation in the two ends of the nerve, produce both an orthodromic and an antidromic nerve pulses hereby enforce a collision. We place the recording electrode off center[10] where the orthodromic pulse arrives first, so that we can determine if the pulses annihilate or penetrate each other. In case of annihilation only the orthodromic pulse will be recorded whereas if the pulses penetrate each other both the orthodromic and the antidromic pulse is going to be recorded, see Fig. (6.4) for schematic representation.

The nerves we used for the collision experiments, contain several axons. The ventral cord of earthworms contains many small axons, however only two pulses, one from the median and one from the lateral giant axons, give distinct and strong electrical signal. Likewise, the abdominal part of the ventral cord from the lobster contain multiple small axons and four giant axons. Here, we will only discuss the collision experiments done in earthworms. For details on collision experiments done in the abdominal ventral cord of lobster see Gonzalez-Perez *et al.* [110]. The multiple axons in the investigated nerves makes it more complicated to ensure that the nerve pulses from the two sides propagate in the same axon. To rule out this possibility we needed to identify the various stimulation thresholds for all axons (e.g. the median and the lateral giant axons in earthworms) for both antidromic and orthodromic propagation, so to make sure to work in a stimulation regime that allows for ready identification of the axon the pulse is propagating in. We did so by increasing the stimulus by small voltage steps[11] and using the fact that above the stimulation threshold the nerve pulses are stable and unchanged in shape and position (time of arrival at recording site). We saw that threshold is slightly higher for the antidromic side. For the ventral cord in earthworms the median giant axon is larger then the laterals giant axons throughout the full length of the worm. The median giant axon therefore has a lower threshold, a stronger electrical signal and a

[10] Recording electrode is place approximately 1/3 of the distance between the two stimulation sights from the orthodromic side.

[11] The stimulation threshold is determine by applying a low stimulation voltage, often 0.5 V for 5 μs, and increasing the amplitude until the nerve fires at each stimulation. This voltage is referred to as the stimulation threshold.

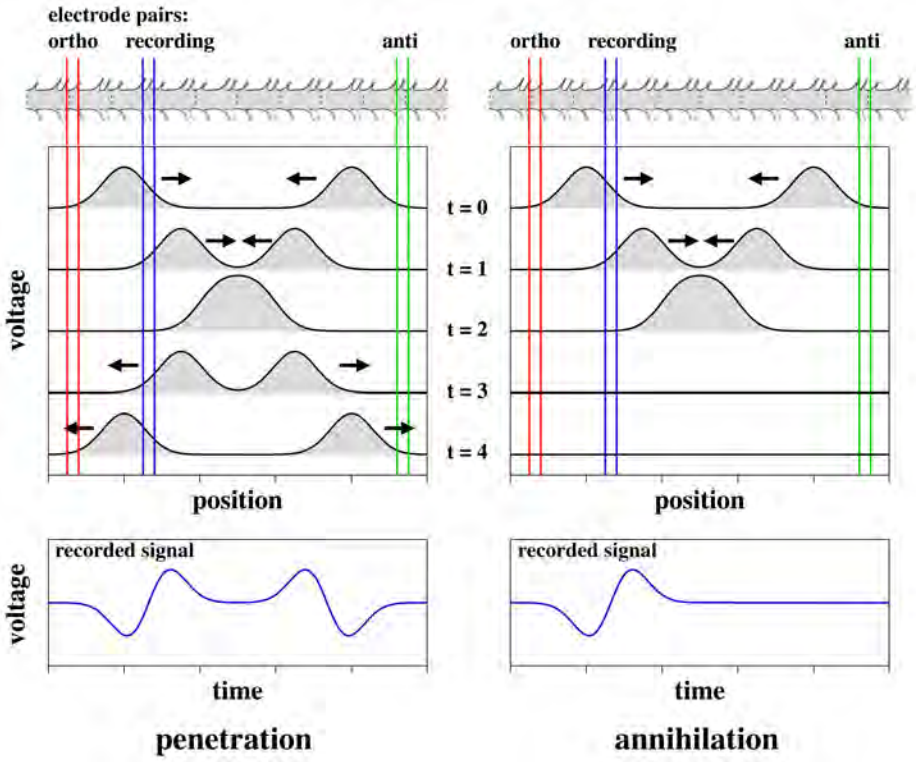

Figure 6.4: *A schematic representation of the outcomes of the collision experiments at t_0, t_1, t_2 and t_3. The nerve pulses are generated simultaneously in both ends of the nerve at t_0. At t_1 the orthodromic pulse reaches the recording electrodes. At t_2 the pulses collide. At t_3 the antidromic pulse potentially reaches the recording electrodes depending on penetration or annihilation. In the top a earthworm ventral cord is schematically shown along with electrodes. [110]*

higher propagation velocity and can be distinguished from the lateral giant axons [113]. Having identified the axons from both sides and lowering the stimulus to just above the median thresholds the collision experiment can be carried out following the scheme in Fig. (6.4), see Fig. (6.5).

For our interpretation to be valid, identification of the median and lateral axons in both directions is necessary. To rule out any possibility of misinterpretation, we carried out the collision experiment at higher voltages, were both the median and lateral axons are firing in the orthodromic direction whereas only one axon is firing in the antidromic direction. All three nerve pulses arrive at the recording electrodes, unambiguously showing penetration of nerve pulses [110]. Collision experiments were carried out on more then 30 samples all showing penetration. Stimulation close to the ends of the nerve seemed like it could lead to apparent annihilation, however through repositioning of the nerve sample penetration was recovered. Similarly, we showed that nerve pulses in the abdominal part of the ventral cord of a lobster also does not annihilate upon collision [110]. Additionally, we showed the same results for the walking leg nerve bundle and connective from lobster (unpublished).

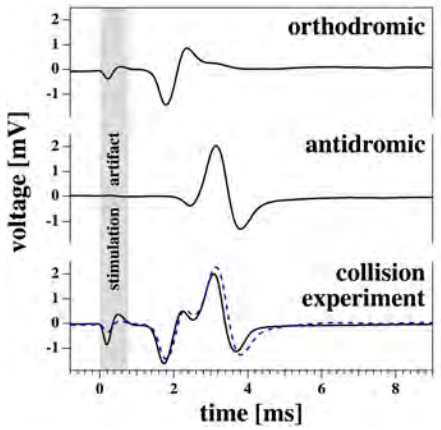

Figure 6.5: *Pulse collision experiment in the ventral cord of an earthworm.* ***Top****: Nerve pulse from orthodromic stimulation.* ***Center****: Nerve pulse from antidromic stimulation.* ***Bottom****: Simultaneous stimulation, both orthodromic and antidromic, showing penetration. The sum of the orthodromic and antidromic signal is shown in blue for comparison. The stimulation artifact is shaded gray. [110]*

We demonstrated that nerve pulses can penetrate each other in both myelinated preparations (earthworms) and in non-myelinated preparations (lobster). Penetration is predicted by the Soliton model, whereas it seems contradictory with respect to the prediction of the Hodgkin and Huxley model.

6.3 Mechanical nerve signal

The Soliton model proposes that nerve signals are lateral density pulses in the membrane of the nerve axon, which due to the piezoelectric nature of the membrane have an electrical component. Several studies have shown, using both optical and mechanical methods, that nerve fibers swell during the nerve pulse [37–39, 114, 115]. However, these mechanical changes are though to be a product of the electrical signal, being a secondary effect. On the other hand in the Soliton model the mechanical changes are the one that cause the electrical signal and they represent two aspects of the same pulse.

We are going to measure the thickness change of the axon associated with a nerve pulse. Our goal is to confirm the mechanical component of the nerve signal in a direct measurement, while simultaneously measuring the electrical component, in order to explore the mechanical nature of the nerve signals and the coupling between its electrical and mechanical components.

The Soliton model predicts a mono-phased change in the membrane thickness, with a maximum change in thickness of $0.5 - 1\ nm$ and a temporal width of the nerve signal ($1 - 3\ ms$). Both the spacial and temporal size of the nerve signal are challenging to measure directly. Kim *et al.* [115] used an AFM to measure the mechanical changes accompanying an action potential at a nerve terminal. The mechanical change at the nerve terminal is the combined signal from a large

number of axons resulting in a broad signal ($\sim 5\ ms$) with a large change in thickness ($\sim 10\ nm$). This is more then 10 times the signal amplitude we can expect from a single axon but the temporal width is close to that of the signal from a single axon. Zhang *et al.* [116] showed that a HEK (Human Embriodic Kidney) cell display deflection of an AFM cantilever of $\sim 0.5\ nm$ upon changing the voltage across the cell membrane. This shows that an AFM can achieve the spacial accuracy needed on a biological sample. These experiments motivated us to used AFM to measure the mechanical component of nerve signals.

6.3.1 Mechanical measurement instrumentation

The working principle of an AFM is the following: a spring like cantilever is placed in the close vicinity of the surface of a sample; interactions with the sample cause a deflection of the cantilever which is detected. The deflection is detected by a laser beam being reflected of the back of the cantilever on to a photodetector, see Fig. (6.6). From the displacement of the laser beam on the photodetector, the height of the sample can be measured. The cantilever is mounted on a "head" which can move up and down perpendicular to the plane where the sample is arranged. The head is moved up and down using a feedback loop which ensures that cantilever is constantly in contact with the surface of the sample. This mode of operation is referred to as contact mode. There are several alternative modes of operations of an AFM, depending on the actual AFM setup, an example is tapping mode where a vibrating cantilever is used to tap the sample. We however exclusively used contact mode.

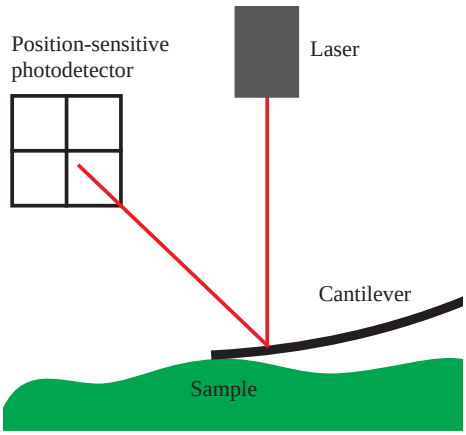

Figure 6.6: *Schematic representation of the working principle of an AFM. A cantilever interacts with the surface of the sample and is deflected. The deflection is detected by a laser beam which reflected onto a photodetector.*

The standard use of an AFM is to move the cantilever along the surface of the sample, so to scan the topography of the sample surface. We are interested in measuring the thickness change of a axon during a nerve pulse. We therefore used a slightly different configuration: we placed the cantilever on the surface of the axon in a fixed position and measured the change in height at the fixed position as the nerve signal propagates down the axon, see Fig. (6.7).

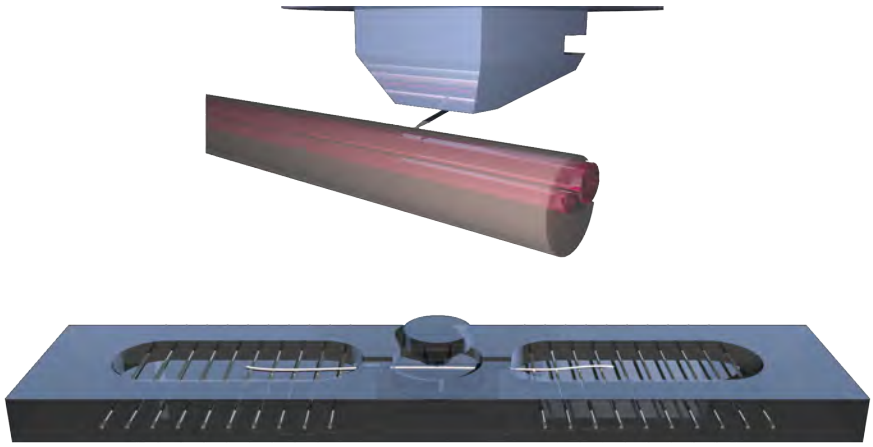

Figure 6.7: *The nerve chamber for simultaneous electrical and mechanical recording.* ***Top****, AFM cantilever touching the surface of the nerve, the axons are colored glassy red.* ***Bottom****, the full nerve chamber including AFM head and nerve (shown in light pink).*

Our AFM is a *NanoWizard II* from *JPK Instruments* which has a direct analog output from the Z-sensor (height). The output signal is in the range $-8\ V$ to $8\ V$ which scales linearly with the height, with a scaling factor of $-904.35\ nm/V$, corresponding to a $\sim 15\ \mu m$ range. The height signal from the AFM was given as an input to the PowerLab 8/35 unit (described in 6.2.1), so that we could simultaneously record both the electrical and mechanical signal. Note that the A/D in the PowerLab is 16 bit, so that the effective bit resolution on the height measurement (using $\pm 10\ V$ range) is about $0.27\ nm$. Applying a low frequency high-pass filter we can filter out slow baseline movements allowing us to use a narrower voltage range, commonly between $\pm 0.5\ V$ and $\pm 2\ V$, hereby increasing the bit resolution to below $0.06\ nm$. Beyond the issue of bit resolution, the mechanical noise, even using an anti-vibration table, is around $2\ nm$ on the soft axon. This poses a problem since the mechanical component of the nerve signal has an expected maximum amplitude of about $1\ nm$. In order to overcome the high noise levels, between 100 and 200 nerve signals have been averaged, which is possible due to the controlled external stimulation of the nerve and the simultaneous electrical recording. By averaging the recordings we achieved a mechanical noise level around $0.1\ nm$. We use tip-less cantilevers[12] to avoid interaction with specific molecules on the surface of the axon, but rather get an average response of a larger area of the membrane. The experiments were done using two types of tip-less cantilevers from μmash (Nanoworld) with force constants of $0.3\ N/m$ (HQ:CS37) and $0.03\ N/m$ (HQ:CS38).

Beyond the fact that change in membrane thickness due to the nerve signal is small, the nerve signal will pass a recording site in the span of $1 - 3\ ms$

[12]For scanning the surface of samples usually a cantilever with an atomic fine tip is used for accurate interaction with the sample.

(so it is temporally short). The analog output from the AFM is sampled by the PowerLab unit at 40 kHz, however the feedback loop adjusting the height position of the AFM cantilever can only keep up with frequencies up to around $\sim$ 300 Hz (according to *JPK Instruments*). This mean that the AFM, when using the feedback loop, has issues keeping up with changes that occur on a smaller scale than around 3 ms. This is slightly slow compared to the temporal width of nerve signals. However, given that the height measurement is continuous the speed of the feedback loop should effectively not limit the measurement of small changes in height, although a slight smoothing of the mechanical signal can be expected. In conclusion the nerve signal is within the measurement range of the AFM but close to both the height measurement accuracy limit and the temporal accuracy limit. This means that any sources of of noise and artifacts needs to be minimized, see appendix A.5.

The nerve signals are temporally short but extend over a long distance, of the order of mm to cm, meaning orders of magnitude larger the the thickness of the axon, even for giant axons. It is therefore irrelevant if the cantilever is positioned with an angle with respect to the length of the axon. On the other hand, the AFM cantilever is smaller than thickness of the investigated giant axons, and therefore the correct positioning of the cantilever on the surface of the axon is important. The positioning of the nerve sample in the nerve chamber is done as shown in Fig. (6.7), bottom, where the central section of the chamber (for the AFM) is lifted to support the nerve. The stimulation is done on one side of the mechanical measurement site (distance $\sim$ 1 cm) and the electrical recording is done on the other (again distance $\sim$ 1 cm). This allow for a simultaneous mechanical and electric measurement of the nerve signal. The nerve is grounded right after the stimulation site to limit stimulation artifacts.

6.3.2 Electro-mechanical measurements

The mechanical measurements were preformed on circumesophageal connectives (or simply connectives) from lobster. The connective is chosen due to its rather simple structure, two easily distinguishable giant axons, and its robustness. The axons of connectives are surrounded by protective sheaths. The sheaths is opened, around the area of the mechanical measurement, to expose the median giant axon (diameter $150 - 200$ μm) using micro-scalpels under a microscope. The connective is placed in the nerve chamber with the exposed axon facing the AFM cantilever, see Fig. (6.7). The chamber is closed with a lid (with an opening for access of the AFM head) to limit dehydration. Before approaching the axon with the AFM, the nerve preparation is tested electrically in order to determine the stimulation thresholds for both axons. The median giant axon of the connective is thicker and has a lower stimulation threshold, higher propagation velocity and stronger electrical signal. In the mechanical measurements we only stimulated the median giant axon to identify the mechanical signal from a single axon. The AFM is positioned manually above the exposed axon and the approach (engagement) is done using a routine in the control software of the AFM[13]. After a successful approach the AFM reports the height of the

[13]The nerve sample is soft and fragile so much care have to be made in the approach, to avoid damage of the sample and the cantilever.

nerve/axon to the PowerLab unit. The stimulation threshold of the median giant axon is reconfirmed and any needed adjustment is done. The electrical and mechanical signal associated with a change in height of the nerve is recorded simultaneously and averaged over 100 or 200 stimulations cycles.

We found a height change of between $0.2 - 1.2\ nm$ in the form of a monophase pulse of temporal width around $2 - 4\ ms$ from the median giant axon. An example of the measured electrical signal, the "true" electrical signal[14] and the mechanical signal is shown in Fig. (6.8).

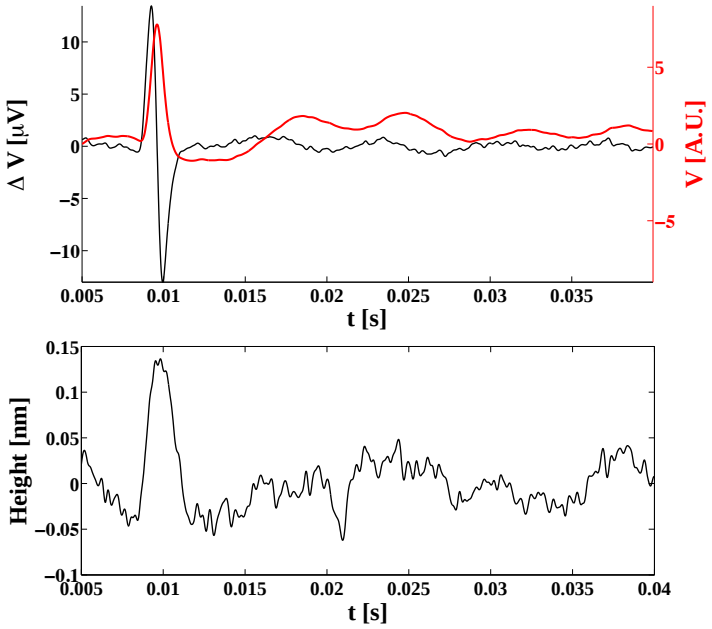

Figure 6.8: ***Top**: Electrical recording of the action potential from the median giant axon in the circumesophageal connective of a lobster, shown in black. Shown in red is the integrated electrical signal, which approximate the true electrical signal. **Bottom**: The height change due to the nerve signal (the mechanical signal). The mechanical signal has been temporally aligned and digitally filtered (50 Hz high-pass and 3 kHz low-pass).*

Three additional examples of the measured mechanical signal, from three different lobster samples, are shown in Fig. (6.9). We also observed higher amplitude mechanical signals for samples where more than one axon was firing (data not shown).

We show that the presence of a mechanical component is a consistent property of nerve signals. Within the available accuracy we observed no obvious causality between the electrical and mechanical signal. The mechanical and electrical signal seems to be contemporary. Note that there may be a slight smearing of the mechanical signal do to the instrumentation. Furthermore, we

[14]The measured electrical signal is the potential difference at two specially separated electrodes. The spacing being smaller than the spacial width of the pulse allow us to approximate with a differential. The "true" signal is therefore the integral of the measured electrical signal.

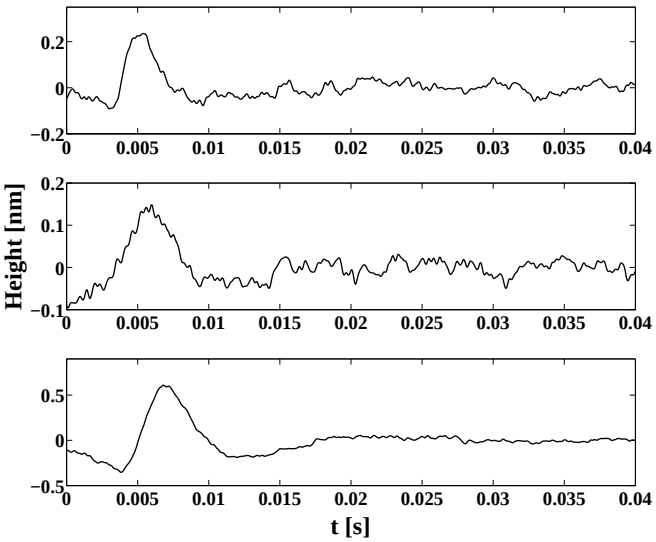

Figure 6.9: *The measured mechanical nerve signal from three different connective preparations from lobster. The mechanical signals have been digitally filtered (*50 Hz *high-pass and* 3 kHz *low-pass).*

can not exclude that there is a small amount of tissue between the axon and the cantilever which also can distort the mechanical signal. Considering these limitations we found strong similarity between the "true" electrical signal and the mechanical signal. Note that we found no mechanical signal accompanying the stimulation artifact, ruling out an electrical interaction between the sample and the cantilever.

6.4 Discussion of nerve experiments

The motivation for the presented experiments on nerves was to understand the mechanism underlying the propagation of nerve signals. More specifically, we wanted to address the two mechanisms that have been proposed so far: the Hodgkin and Huxley framework and the Soliton model by Heimburg and Jackson. To be able to identify the underlying mechanism of propagation of nerve signals, rigorous testing of the prediction of the models are needed. The Soliton model proposes the nerve pulse to be an adiabatic electro-mechanical density pulse, which is characterized by a thickening of the membrane, a reversible heat signature and an electrical signal. The framework based on the Hodgkin and Huxley model is, a priori, entirely electrical in nature and does not explicitly contain mechanical or temperature changes. However, the Hodgkin and Huxley model is based on resistive currents, therefore one would assume an intrinsic dissipative nature of nerve signal propagation. This contradicts the measured reversible heat release associated with a nerve signal [34, 36, 117]. The goal of the experiments described in this chapter was to further test the predictions of Hodgkin and Huxley model and the Soliton model.

6.4.1 Mechanical experiment

Iwasa and Tasaki [39] were the first to report thickness changes associated to nerve pulses. Tasaki and collaborators proposed that the thickness change associated to nerve pulses is caused by ion fluxes, which facilitated the uptake of water in a gel surrounding the axon and hereby a swelling [37]. Tasaki based his proposal on the framework of Hodgkin and Huxley and assumes that the mechanical signal is caused by the electrical signal. This is opposite to what is stated by the Soliton model, where it is the electrical component that is caused by the mechanical pulse. We have confirmed the thickness change associated to a nerve signal experimentally and, within the available accuracy, observe no phase difference between the mechanical and electrical signal. This observation indicate that the swelling does not occur through a secondary mechanism, like the uptake of water. Additionally we found that the measured changes in thickness fits with the changes expected within the Soliton model, whereas an estimation can not be made in the Hodgkin and Huxley framework.

From an experimental perspective, our measurement of the changes in height of the nerve sample (a proxy for the change in the thickness of the axon membrane) are direct and the only limitation is the temporal resolution due to the feedback loop of the AFM. To overcome this limitation the feedback loop can be removed and the height can be measured without temporal limitation beyond the vibrational limitation of the used cantilever ($> 10\ kHz$). However, this was not done since this would constrain the height position of the AFM head and limit the active height range of the cantilever (a few μm) which could be problematic in case of slight movement of the sample. Our results show that the characteristic time of the mechanical signal was similar to one of the electrical signal. However, we can not exclude that the mechanical signal is narrower than what we can measure. Furthermore, although we have used low force feedback settings to minimize perturbation of the membrane, we can not fully exclude that the observed change of height associated with nerve signal is due to changes in surface tension, rather than changes in membrane thickness [116].

6.4.2 Collision experiments

The Soliton model predicts that two colliding nerve pulses penetrates one another without major distortions in shape and propagation velocity [110]. On the other hand the properties of neurons in the Hodgkin and Huxley framework cannot easily generalized, since no general theory for the function of the involved protein ion channels exits. We can therefore not exclude that there is a possibility for penetration upon collision within this framework. However, for nerve which has a refractory period[15] Hodgkin and Huxley predicts annihilation. We showed that nerve pulses in the ventral cord of earthworms penetrates each other upon collision. This finding contradicts the prediction of the Hodgkin and Huxley model, since the giant axons in ventral cord of earthworm has a refractory period of about 1 ms [113]. We should however note that the ventral

[15]The refractory period is the delay between two successive nerve pulses in the same axon. In the Hodgkin and Huxley model the refractory period originates from the relaxation of protein ion-channels and in the Soliton model it originate from the conservation of lateral density in the axon.

cord of the earthworm is often considered slightly special, since it is segmented in connected segments of $1 - 1.5\ mm$ along the length of the ventral cord. Interestingly, the segments are significantly shorter then the spacial extension of the nerve pulse ($\sim 10\ mm$), underlying the macroscopic nature of nerve signals. We showed additionally that nerve pulses penetrated each other upon collision in non-segmented single axons in various lobster samples, contradicting the previous notion that all nerve pulses annihilate upon collision. We showed this in both myelinated and non-myelinated nerves indicating that penetration of colliding nerve signals is not a special case but could be a more generic feature.

Our experimental efforts in testing the prediction of nerve propagation, both the mechanical component of the nerve signal and the penetration upon collision, shows results compatible with what is predicted by the Soliton model. However, we can not fully dismiss the Hodgkin and Huxley framework since the generalized predictions possible within this framework is so limited.

Chapter 7

Concluding remarks

During the three years of my PhD I have had the chance to work on quite different projects within the field of lipid membranes, that are presented in this thesis. Despite the differences they are all motivated by the attempt to produce a description of the functional behavior and biological role of membranes, that would stem naturally from a deep understanding of the physical properties of a lipid membrane.

With this idea in mind in chapter 2 we developed a general thermodynamical framework that allows us to deduce commonly observed electrical properties of membrane, such as the existence of an offset voltage, electrostriction, flexoelectrical and piezoelectrical effects, as special cases of our general description.

We then expanded our horizon in chapter 3, where we attempt to extend this thermodynamical description in order to address non-equilibrium properties of lipid membranes. More specifically, we built a description of the relaxation behavior of lipid membranes in the vicinity of the lipid melting transition using linear response theory. We concluded that the multi-scale relaxation behavior observed in the vicinity of the lipid melting transition is governed by heat exchange between the membrane and the surrounding water.

In chapter 4 we finally combined the insights we gained on dynamical properties of a lipid membranes with our thermodynamical description of its electrical properties so that we could provide an alternative interpretation for several non-linear electrical behavior observed in biological membranes. These behaviors are commonly assumed to be due to the action of proteins embedded in the membranes, but we show that this non-linear effects can be fully explained for a "pure" lipid membrane as well, once we abandon the vision of the membrane as an inert electrical structure and instead view it as a non-linear electrical component.

Ultimately, our efforts to address the biological functionality of membranes from a physical perspective, aims at contributing to the open discussion regarding the nature of nerve signals. Currently the most widely accepted interpretation of the propagation of signals in nerves assumes the signals to be purely electrical in nature and is due to the Hodgkin-Huxley model. However several existing experimental findings cannot be explained within this framework, such as the measured mechanical component of nerve signals. The Soliton Model, proposed by Heimburg and Jackson [26], is the main alternative model for nerve signals

propagation and identifies nerve pulses with a localized density wave (soliton).

We use the results of the efforts made to address the dynamical properties of lipid membranes in the vicinity of the lipid melting transition to extend the Soliton model. In chapter 5 we show how the relaxation behavior in the lipid melting transition couples to the dispersion in lipid membranes. We then include this coupling in the Soliton model and show that we can then characterize the solitonic solution in lipid membrane in the vicinity of the lipid melting transition uniquely from the close-to-equilibrium thermodynamical properties of the membrane.

Finally in chapter 6 we address experimentally a number of the predictions of the Soliton model on the nature of nerve signals. We established a neurophysiology lab and performed experiments that show that nerve signals propagating in the same axon penetrate each other upon collision, rather than annihilate, as it is commonly believed and suggested by the Hodgkin-Huxley model. We furthermore show that nerve signal is both electrical and mechanical in nature, without an obvious causality, which is particularly important, as we discard the common argument that the mechanical signal is caused by the propagating electrical signal.

So far we have taken crucial steps towards understanding how the properties of lipids relate to the function of biological membranes in living organisms and with the experimental efforts we made, we have improved the way we understand the nature of nerve signals. However several problems remain open. The relaxation behavior of lipid membranes in the vicinity of their melting transition, for example, is still not fully understood and at this point collecting more experimental data is one of the crucial challenges for achieving substantial progress on this topic. Furthermore, in order to deepen our comprehension of the functional behavior of "real" biological membranes we need to face two challenges in the understanding of the model system of lipid membranes: we need to explore in detail the coupling between the membrane and ions as well as the thermodynamical coupling between proteins embedded in the membrane and the lipid membrane itself, focusing on the implications of the presence of these proteins for the membrane.

Bibliography

[1] Cell. Invitrogen: http://invitrogen.com.

[2] Overton, E. 1899. On the general osmotic properties of cell, their probable origin, and their significance for physiology. Vierteljahrschrift der Naturforschende Gesselschaft (Zürich) 44:88–135.

[3] Gorter, E. M. D., and F. Grendel. 1925. on Bimolecular Layers of Lipoids on the Chromocytes of the Blood. J. Exp. Med. 41:439–443.

[4] Danielli, J. F., and E. N. Harvey. 1935. The tension at the surface of mackerel egg oil, with remarks on the nature of the cell surface. J. Cell. Comp. Physiol. 5:483–494.

[5] Singer, S. J., and G. L. Nicolson. 1972. The fluid mosaic model of the structure of cell membranes. Science 175:720–31.

[6] Mouritsen, O. G., and M. Bloom. 1984. Mattress model of lipid-protein interactions in membranes. Biophys. J. 46:141–153.

[7] Van Osdol, W. W., and R. L. Biltonen. 1989. Measuring the kinetics of membrane phase transitions. J. Biochem. Bioph. Methods 20:1–46.

[8] Heimburg, T., 2007. Thermal biophysics of membranes. Wiley-VHC.

[9] Hazel, J. R. 1979. Influence of thermal acclimation on membrane lipid composition of rainbow trout liver. Am. J. Physiol. 236:R91–R101.

[10] DeLong, E. F., and A. A. Yayanos. 1985. Adaptation of the membrane lipids of a deep-sea bacterium to changes in hydrostatic pressure. Science 228:1101–1103.

[11] Eisenberg, M., and S. Mclaughlin. 1976. Lipid Bilayers Membranes. BioScience 26:436–443.

[12] Lakhdar-Ghazal, F., J. Tichadou, and J. Tocanne. 1983. Effect of pH and monovalent cations on the ionization state of phosphatidylglycerol in monolayers. Eur. J. Biochem. 134:531–537.

[13] Petrov, A. G. 2001. Flexoelectricity of model and living membranes. Biochim. Biophys. Acta 1561:1–25.

[14] Heimburg, T., and A. D. Jackson, 2008. Thermodynamics of the nervous impulse. In Structure and dynamics of membranous interfaces, John Wiley and Sons, Inc, chapter 12, 318–335.

[15] Verkleij, A. J., R. F. Zwaal, B. Roelofsen, P. Comfurius, D. Kastelijn, and L. L. van Deenen. 1973. The asymmetric distribution of phospholipids in the human red cell membrane. A combined study using phospholipases and freece-etch electron microscopy. Biochim. Biophys. Acta 323:178–193.

[16] Rothman, J. E., and J. Lenard. 1977. Membrane asymmetry. Science 195:743–753.

[17] Marsh, D. 1991. General features of phospholipid phase transitions. Chem. Phys. Lipids 57:109–120.

[18] Janiak, M., D. Small, and G. Shipley. 1979. Temperature and compositional dependence of the structure of hydrated dimyristoyl lecithin. J. Biol. Chem. 254:6068–6078.

[19] Heimburg, T. 2000. A model for the lipid pretransition: coupling of ripple formation with the chain-melting transition. Biophys. J. 78:1154–1165.

[20] Nagle, J. F. 1980. Theory of the main lipid bilayer phase transition. Annu. Rev. Phys. Chem. 31:157–196.

[21] Cevc, G. 1991. Isothermal lipid phase transitions. Chem. Phys. Lipids 57:293–307.

[22] Grabitz, P., V. P. Ivanova, and T. Heimburg. 2002. Relaxation kinetics of lipid membranes and its relation to the heat capacity. Biophys. J. 82:299–309.

[23] Schrader, W., S. Halstenberg, R. Behrends, and U. Kaatze. 2003. Critical Slowing in Lipid Bilayers. J. Phys. Chem. B 107:14457–14463.

[24] Hodgkin, A. L., and A. F. Huxley. 1952. A quantitative description of membrane current and its application to conduction and excitation in nerve. J. Physiol. 117:500–544.

[25] Howells, J., L. Trevillion, H. Bostock, and D. Burke. 2012. The voltage dependence of I_h in human myelinated axons. J. Physiol. 590:1625–1640.

[26] Heimburg, T., and A. D. Jackson. 2005. On soliton propagation in biomembranes and nerves. Proc. Natl. Acad. Sci. U. S. A. 102:9790–9795.

[27] Cole, K. S., and H. J. Curtis. 1939. Electric Impedance of the Squid Giant Axon During Activity. J. Gen. Physiol. 22:649–670.

[28] Kobatake, Y., I. Tasaki, and A. Watanabe. 1971. Phase transition in membrane with reference to nerve excitation. Adv. Biophys. 2:1–31.

[29] Tasaki, I. 1999. Evidence for phase transition in nerve fibers , cells and synapses. Ferroelectrics 220:305–316.

[30] Tasaki, I., A. Watanabe, and I. Singer. 1966. Excitability of squid giant axons in the absence of univalent cations in the external medium. Proc. Natl. Acad. Sci. U. S. A. 56:1116–1122.

[31] Laub, K. R., K. Witschas, A. Blicher, S. B. Madsen, A. Lückhoff, and T. Heimburg. 2012. Comparing ion conductance recordings of synthetic lipid bilayers with cell membranes containing TRP channels. Biochim. Biophys. Acta 1818:1123–1134.

[32] Blicher, A., and T. Heimburg. 2013. Voltage-gated lipid ion channels. PloS one 8:e65707.

[33] Mosgaard, L. D., and T. Heimburg. 2013. Lipid ion channels and the role of proteins. Acc. Chem. Res. 46:2966–2976.

[34] Abbott, B. C., A. V. Hill, and J. V. Howarth. 1958. The positive and negative heat production associated with a nerve impulse. Proc. R. Soc. B 148:149–187.

[35] Tasaki, I., and P. Byrne. 1992. Heat production associated with a propagated impulse in bullfrog myelinated nerve fibers. Jpn. J. Physiol. 42:805–813.

[36] Ritchie, J. M., and R. D. Keynes. 1985. The production and absorption of heat associated with electrical activity in nerve and electric organ. Q. Rev. Biophys. 18:451–476.

[37] Tasaki, I., K. Kusano, and P. M. Byrne. 1989. Rapid mechanical and thermal changes in the garfish olfactory nerve associated with a propagated impulse. Biophys. J. 55:1033–1040.

[38] Iwasa, K., I. Tasaki, and R. C. Gibbons. 1980. Swelling of nerve fibers associated with action potentials. Science 210:338–339.

[39] Iwasa, K., and I. Tasaki. 1980. Mechanical changes in squid giant axons associated with production of action potentials. Biochem. Biophys. Res. Commun. 95:1328–1331.

[40] Heimburg, T., and A. D. Jackson. 2007. The thermodynamics of general anesthesia. Biophys. J. 92:3159–3165.

[41] Mendes, P. M., W. Lu, H. Tseng, S. Shinder, T. Iijima, M. Miyaji, C. M. Knobler, and J. F. Stoddart. 2006. A soliton phenomenon in langmuir monolayers of amphiphilic bistable rotaxanes. J. Phys. Chem. B 110:3845–3848.

[42] Lautrup, B., R. Appali, A. D. Jackson, and T. Heimburg. 2011. The stability of solitons in biomembranes and nerves. Eur. Phys. J. E 34:1–9.

[43] Heimburg, T. 2012. The capacitance and electromechanical coupling of lipid membranes close to transitions: the effect of electrostriction. Biophys. J. 103:918–929.

[44] Einstein, A. 1910. The theory of the opalescence of homogeneous fluids and liquid mixtures near the critical state. Ann. Phys. 33:1275–1298.

[45] Onsager, L. 1931. Reciprocal Relations in Irreversible Processes. I. Phys. Rev. 37:405–426.

[46] Kondepudi, D., and I. Prigogine, 1999. Modern thermodynamics. From heat engines to dissipative structures. Wiley-VHC.

[47] Callen, H. B., 1960. Thermodynamics. Wiley-VHC.

[48] Träuble, H., and H. Eibl. 1974. Electrostatic effects on lipid phase transitions: membrane structure and ionic environment. PNAS 71:214–219.

[49] McLaughlin, S. G., G. Szabo, and G. Eisenman. 1971. Divalent ions and the surface potential of charged phospholipid membranes. J. Gen. Physiol. 58:667–687.

[50] Böckmann, R. A., A. Hac, T. Heimburg, and H. Grubmüller. 2003. Effect of sodium chloride on a lipid bilayer. Biophys. J. 85:1647–1655.

[51] Heimburg, T. 1998. Mechanical aspects of membrane thermodynamics. Estimation of the mechanical properties of lipid membranes close to the chain melting transition from calorimetry. Biochim. Biophys. Acta 1415:147–162.

[52] Antonov, V. F., E. Y. Smirnova, and E. V. Shevchenko. 1990. Electrical field increases the phase transtion temperature in the bilayer membrane of phosphatidic acid. Chem. Phys. Lipids 52:251–257.

[53] Ivanova, V. P., I. M. Makarov, T. E. Schäffer, and T. Heimburg. 2003. Analyzing heat capacity profiles of peptide-containing membranes: cluster formation of gramicidin A. Biophys. J. 84:2427–2439.

[54] Seeger, H. M., M. L. Gudmundsson, and T. Heimburg. 2007. How anesthetics, neurotransmitters, and antibiotics influence the relaxation processes in lipid membranes. J. Phys. Chem. B 111:13858–66.

[55] Ebel, H., P. Grabitz, and T. Heimburg. 2001. Enthalpy and volume changes in lipid membranes. I. The proportionality of heat and volume changes in the lipid melting transition and its implication for the elastic constants. J. Phys. Chem. B 105:7353–7360.

[56] Pedersen, U. R., G. H. Peters, T. B. Schrøder, and J. C. Dyre. 2010. Correlated volume-energy fluctuations of phospholipid membranes: a simulation study. J. Phys. Chem. B 114:2124–2130.

[57] Steppich, D., J. Griesbauer, T. Frommelt, W. Appelt, A. Wixforth, and M. F. Schneider. 2010. Thermomechanic-electrical coupling in phospholipid monolayers near the critical point. Phys. Rev. E 81:1–5.

[58] Dimova, R., B. Pouligny, and C. Dietrich. 2000. Pretransitional effects in dimyristoylphosphatidylcholine vesicle membranes: optical dynamometry study. Biophys. J. 79:340–356.

[59] Mosgaard, L. D., 2011. Propagation of Sound in Lipid Membranes.

[60] Ivanova, V. P., and T. Heimburg. 2001. Histogram method to obtain heat capacities in lipid monolayers, curved bilayers, and membranes containing peptides. Phys. Rev. E 63:1914–1925.

[61] Wodzinska, K., A. Blicher, and T. Heimburg. 2009. The thermodynamics of lipid ion channel formation in the absence and presence of anesthetics. BLM experiments and simulations. Soft Matter 5:3319–3330.

[62] Petrov, A. G., 1975. Flexoelectric model for active transport. In Physical and Chemical Bases of Biological Information Transfer (Vassileva-Popova, J. G., editor), Plenum Press, New York, 111–125.

[63] Frank, H. S. 1955. Thermodynamics of a Fluid Substance in the Electrostatic Field. J. Chem. Phys. 23:2023–2032.

[64] Alvarez, O., and R. Latorre. 1978. Voltage-dependent capacitance in lipid bilayers made from monolayers. Biophys. J. 21:1–17.

[65] Farrell, B., C. D. Shope, and W. E. Brownell. 2006. Voltage-dependent capacitance of human embryonic kidney cells. Phys. Rev. E 73:1–29.

[66] Petrov, A. G., and P. N. R. Usherwood. 1994. Mechanosensitivity of cell membranes. Eur. Biophys. J. 23:1–19.

[67] Antonov, V. F., E. V. Shevchenko, E. T. Kozhomkulov, A. A. Mol'ar, and E. Y. Smirnova. 1985. Capacitive and ionic currents in BLM from phosphatidic acid in Ca^{2+}-induced phase transition. Biochem. Biophys. Res. Commun. 133:1098–1103.

[68] Binder, H., and O. Zscho. 2002. The effect of metal cations on the phase behavior and hydration characteristics of phospholipid membranes. Chem. Phys. Lipids 115:39 – 61.

[69] Sturtevant, J. M. 1998. The effect of sodium chloride and calcium chloride on the main phase transition of dimyristoylphosphatidylcholine. Chem. Phys. Lipids 95:163 – 168.

[70] Träuble, H., M. Teubner, P. Woolley, and H. Eibl. 1976. Electrostatic interactions at charged lipid membranes. 1. Effects of pH and univalent cations on membrane structure. Biophys. Chem. 4:319–342.

[71] Träuble, H., 1977. Membrane electrostatics. In Struct. Biol. Membr. (Abrahamsson, S., and I. Pascher, editors), Plenum Press, NY, 509–550.

[72] Woolley, P., and M. Teubner. 1979. Electrostatic interactions at charged lipid membranes. Calcium binding. Biophys. Chem. 10:335–350.

[73] Sapia, P., and L. Sportelli. 1994. Effect of main high electrolyte of DPPC cooperativity of the main phase-transition of DPPC. J. Phys. II France 4:1107–1116.

[74] Ambjörnsson, T., M. A. Lomholt, and P. Lyngs Hansen. 2007. Applying a potential across a biomembrane: Electrostatic contribution to the bending rigidity and membrane instability. Physical Review E 75:051916.

[75] Hodgkin, A. L., and A. F. Huxley. 1952. Currents carried by sodium and potassium ions through the membrane of the giant axon of loligo. J. Physiol. 116:449–472.

[76] Greene, R. F., and H. B. Callen. 1951. On the formalism of thermodynamic fluctuation theory. Phys. Rev. 83:1231–1235.

[77] Kubo, R. 1957. Statistical-mechanical theory of irreversible processes. I. General theory and simple applications to magnetic and conduction problems. J. Phys. Soc. Jpn. 12:570–586.

[78] Eigen, M. 1954. Methods for investigation of ionic reactions in aqueous solutions with half-times as short as 10ˆ-9 sec. Discuss. Faraday Soc. 17:194–205.

[79] Mosgaard, L. D., A. D. Jackson, and T. Heimburg. 2012. Low-frequency sound propagation in lipid membranes. Adv. Planar Lipid Bilayers Liposomes 16:51–74.

[80] Onsager, L. 1931. Reciprocal Relations in Irreversible Processes. II. Phys. Rev. 38:2265–2279.

[81] Elamrani, K., and A. Blume. 1983. Phase transition kinetics of phosphatidic acid bilayers. A pressure-jump relaxation study. Biochemistry 22:3305–3311.

[82] Blume, A., and M. Hillmann. 1986. Dimyristoylphosphatidic acid/ cholesterol bilayers. Thermodynamic properties and kinetics of the phase transition as studied by the pressure jump relaxation technique. Eur. Biophys. J. 13:343–353.

[83] Halstenberg, S., W. Schrader, P. Das, J. K. Bhattacharjee, and U. Kaatze. 2003. Critical fluctuations in the domain structure of lipid membranes. J. Chem. Phys. 118:5683–5691.

[84] Schiewek, M., and A. Blume. 2009. Pressure jump relaxation investigations of lipid membranes using FTIR spectroscopy. Eur. Biophys. J. 38:219–228.

[85] Schiewek, M., and A. Blume. 2010. Phase transition kinetics of lipid bilayer membranes studied by time-resolved pressure perturbation calorimetry. Eur. Biophys. J. 39:815–824.

[86] Halstenberg, S., T. Heimburg, T. Hianik, U. Kaatze, and R. Krivanek. 1998. Cholesterol-induced variations in the volume and enthalpy fluctuations of lipid bilayers. Biophys. J. 75:264–271.

[87] Wilson, A. H., 1957. Thermodynamics and Statistical Mechanics. Cambridge University Press, chapter 3. 1st edition.

[88] Nielsen, J. K., and J. C. Dyre. 1996. Fluctuation-dissipation theorem for frequency-dependent specific heat. Phys. Rev. B 54:15754–15761.

[89] Mosgaard, L. D., A. D. Jackson, and T. Heimburg. 2013. Fluctuations of systems in finite heat reservoirs with applications to phase transitions in lipid membranes. J. Chem. Phys. 125101:1–8.

[90] Blume, A. 1983. Apparent molar heat capacities of phospholipids in aqueous dispersion. Effects of chain length and head group structure. Biochemistry 22:5436–5442.

[91] Doniach, S. 1978. Thermodynamic fluctuations in phospholipid bilayers. J. Chem. Phys. 68:4912–4916.

[92] Mouritsen, O. G., A. Boothroyd, R. Harris, N. Jan, T. Lookman, L. MacDonald, D. A. Pink, and M. J. Zuckermann. 1983. Computer simulation of the main gel-fluid phase transition of lipid bilayers. J. Chem. Phys. 79:2027–2041.

[93] Sugar, I. P., R. L. Biltonen, and N. Mitchard. 1994. Monte Carlo simulations of membranes: Phase transition of small unilamellar dipalmitoylphosphatidylcholine vesicles. Methods Enzymol. 240:569–593.

[94] Heimburg, T., and R. L. Biltonen. 1996. A Monte Carlo simulation study of protein-induced heat capacity changes and lipid-induced protein clustering. Biophys. J. 70:84–96.

[95] Gruenewald, B., A. Blume, and F. Watanabe. 1980. Kinetic investigations on the phase transition of phospholipid bilayers. Biochim. Biophys. Acta 597:41–52.

[96] Van Osdol, W. W., M. L. Johnson, Q. Ye, and R. L. Biltonen. 1991. Relaxation dynamics of the gel to liquid-crystalline transition of phosphatidylcholine bilayers. Effects of chainlength and vesicle size. Biophys. J. 59:775–785.

[97] Cole, K. S., 1968. Membranes, ions and impulses. University of California Press.

[98] Fernandez, J. M., F. Bezanilla, and R. E. Taylor. 1982. Distribution and kinetics of membrane dielectric polarization. II, frequency domain studies of gating currents. J. Gen. Physiol. 79:41–67.

[99] Santos-Sacchi, J. 1991. Reversible inhibition of voltage-dependent motility and capacitance. J. Neurosci. 11:3096–3110.

[100] Cole, K. S., and R. F. Baker. 1941. Longitudinal impedance of the squid giant axon. J. Gen. Physiol. 24:771–88.

[101] Blicher, A., K. Wodzinska, M. Fidorra, M. Winterhalter, and T. Heimburg. 2009. The temperature dependence of lipid membrane permeability, its quantized nature, and the influence of anesthetics. Biophys. J. 96:4581–4591.

[102] Gallaher, J., K. Wodzinska, T. Heimburg, and M. Bier. 2010. Ion-channel-like behavior in lipid bilayer membranes at the melting transition. Phys. Rev. E 81:1–5.

[103] Andersen, T., A. Kyrsting, and P. M. Bendix. 2014. Local and transient permeation events are associated with local melting of giant liposomes. Soft matter 10:4268–4274.

[104] Mauro, A. 1961. Anomalous impedance, a phenomenological property of time-variant resistance. An analytic review. Biophys. J. 1:353–72.

[105] Armstrong, C. M., and F. Bezanilla. 1973. Currents related to movement of the gating particles of the sodium channels. Nature 242:459–461.

[106] Keynes, R. D., and E. Rojas. 1973. Characteristics of the sodium gating current in the squid giant axon. J. Physiol. 233:P28–P30.

[107] Blatt, F. J. 1977. Gating currents: the role of nonlinear capacitative currents of electrostrictive origin. Biophys. J. 18:43–52.

[108] Seeger, H. M., L. Aldrovandi, A. Alessandrini, and P. Facci. 2010. Changes in single K^+ channel behavior induced by a lipid phase transition. Biophys. J. 99:3675–3683.

[109] Jähnig, F. 1981. Critical effects from lipid-protein interaction in membranes. I. Theoretical description. Biophys. J. 36:329–345.

[110] Gonzalez-Perez, A., R. Budvytyte, L. D. Mosgaard, S. Nissen, and T. Heimburg. 2014. Penetration of action potentials during collision in the median and lateral giant axons of invertebrates. Phys. Rev. X 4:031047.

[111] Quiroga, R. Q., Z. Nadasdy, and Y. Ben-Shaul. 2004. Unsupervised spike detection and sorting with wavelets and superparamagnetic clustering. Neural Computation 16:1661–1687.

[112] Tasaki, I. 1949. Collision of two nerve impulses in the nerve fibre. Biochim. Biophys. Acta 3:494–497.

[113] Kao, C. Y., and H. Grundfest. 1957. Postsynaptic electrogenesis in septate giant axons. I. Earthworm median giant axon. J. Neurophysiol. 20:553–573.

[114] Yao, X., D. M. Rector, and J. S. George. 2003. Optical lever recording of displacements from activated lobster nerve bundles and Nitella internodes. Appl. opt. 42:2972–2978.

[115] Kim, G. H., P. Kosterin, A. L. Obaid, and B. M. Salzberg. 2007. A mechanical spike accompanies the action potential in Mammalian nerve terminals. Biophys. J. 92:3122–3129.

[116] Zhang, P., A. M. Keleshian, and F. Sachs. 2001. Voltage-induced membrane movement. Nature 413:428–432.

[117] Howarth, J. V., R. D. Keynes, and J. M. Ritchie. 1968. The origin of the initial heat associated with a single impulse in mammalian non-myelinated nerve fibres. J. Physiol. 194:745–793.

Appendix A

Supplementary notes

A.1 List of values of variables

List of commonly used values. Values are taken from DPPC LUV.

T_m	Melting temperature	$(T_m = 314.15\ K)$
ΔS_0	Melting entropy	$(\Delta S_0 = 124.14\ J/mol \cdot K)$
ΔH_0	Melting enthalpy	$(\Delta H_0 = 39\ kJ/mol)$
v_g	Volume of lipid in gel state	$(v_{gel} = 0.947\ cm^3/g$ [51])
v_f	Volume of lipid in fluid state	$(v_{fluid} = 0.999\ cm^3/g$ [51])
A_g	Area of lipid in gel state	$(A_{gel} = 0.474\ nm^2$ pr. lipid [51])
A_f	Area of lipid in fluid state	$(A_{fluid} = 0.629\ nm^2$ per lipid [51])
d_g	Thickness of lipid in gel state	$(d_{gel} = 4.79\ nm$ [51])
d_f	Thickness of lipid in fluid state	$(d_{fluid} = 3.92\ nm$ [51])
n	Cooperative unite size	$(n = 170)$
γ_v	Proportionality constant $(v - H)$	$(\gamma_v = 8.6 \cdot 10^{-10}\ m^3/J$ [51])
γ_A	Proportionality constant $(A - H)$	$(\gamma_A = 0.89\ m^2/J$ [51])
ε	Dielectric constant	$(\varepsilon = 4 \cdot \varepsilon_0)$
ΔC	Capacitance difference	$(\Delta C = 656\ J/(mol \cdot V^2))$

A.2 Thermodynamical susceptibilities

At equilibrium the extensive variables of a system will fluctuate around their equilibrium value. From these fluctuations the susceptibilities of the system can be found, e.g. the heat capacity. At constant pressure, the heat capacity, c_p, is given by (Eq. (2.16))

$$c_P = \left(\frac{dH}{dT}\right)_P. \tag{A.1}$$

Using the statistical mechanical approach to thermodynamics, the thermodynamics variables can be considered as average values.

$$\langle H \rangle = \frac{\sum_i H_i \cdot e^{-H_i/RT}}{\sum_i e^{-H_i/RT}} = \frac{\sum_i H_i \cdot e^{-H_i/RT}}{Z}, \tag{A.2}$$

where R is the gas constant, T is the temperature and Z is the partition sum. The sums are over all possible states of the system. Using Eq. (A.2),

$$\begin{aligned} c_p &= \left(\frac{d}{dT}\frac{\sum_i H_i \cdot e^{-H_i/RT}}{Z}\right)_p \\ &= \frac{\sum_i H_i^2 \cdot e^{-H_i/RT}}{RT^2 \cdot Z} - \frac{1}{RT^2}\frac{\sum_i H_i \cdot e^{-H_i/RT}}{Z}\frac{\sum_j H_j \cdot e^{-H_j/RT}}{Z} \\ &= \frac{\langle H^2\rangle - \langle H\rangle^2}{RT^2}. \end{aligned} \tag{A.3}$$

A similar derivation can be carried out for the isothermal lateral compressibility:

$$\begin{aligned} \kappa_T^A &= -\left(\frac{1}{\langle A\rangle}\cdot\frac{d\langle A\rangle}{d\pi}\right)_T, \qquad \langle A\rangle = \frac{\sum_i A_i \cdot e^{-H_i/RT}}{\sum_i e^{-H_i/RT}} \\ &= -\frac{1}{\langle A\rangle}\left(\frac{d}{d\pi}\frac{\sum_i A_i \cdot e^{-H_i/RT}}{Z}\right)_T \\ &= \frac{\langle A^2\rangle - \langle A\rangle^2}{\langle A\rangle RT}, \end{aligned} \tag{A.4}$$

where π is the lateral pressure.

Using the proportionality relation, $\Delta A = \gamma_A \cdot \Delta H$ (Eq. (2.19)), between changes in area and changes in enthalpy, the excess isothermal lateral compressibility can be found from the excess heat capacity:

$$\begin{aligned} \Delta\kappa_T^A &= -\frac{1}{\langle A\rangle}\left(\frac{d}{d\pi}\frac{\sum_i \Delta A_i \cdot e^{-H_i/RT}}{Z}\right)_T \\ &= \frac{\sum_i (\gamma_A \Delta H_i)^2 \cdot e^{-H_i/RT}}{\langle A\rangle RT \cdot Z} - \frac{1}{\langle A\rangle RT}\left(\frac{\sum_i \gamma_A \Delta H_i \cdot e^{-H_i/RT}}{Z}\right)^2 \\ &= \gamma_A^2 \frac{\langle \Delta H^2\rangle - \langle \Delta H\rangle^2}{\langle A\rangle RT} = \frac{\gamma_A^2 T}{\langle A\rangle}\Delta c_P. \end{aligned} \tag{A.5}$$

This relation is "unique" to the lipid membrane, where the proportionality relation holds. Note that similar relations can be made using the proportionality relation between volume and enthalpy.

A.3 Monte Carlo simulation specifics

In the Metropolis Monte Carlo simulations carried out in this thesis, a lipid membrane patch is simulated as a 100 × 100 triangular grid with periodic boundary conditions. Each grid point represent one lipid which can be in either a gel or fluid state. All simulations have been equilibrated for more the 30 times the correlation time of the simulation before sampling, corresponding to more then $6 \cdot 10^4$ Monte Carlo cycles in the transition maximum. For the finite heat reservoir simulations the equilibration was done assuming constant temperature (infinite reservoir). After the initial equilibration temperature fluctuations was allowed and the equilibration was repeated.

In the simulations, we used the following parameters for modeling the heat capacity profiles of DPPC large unilamellar vesicles (LUV): $\Delta H_0 = 36400\ J/mol$ (melting enthalpy), $\Delta S_0 = 115.9\ J/mol \cdot K$ (melting entropy), and $\omega_{fg} = 1326.0\ J/mol$ [89] leading to a melting temperature of $T_m = 314.05\ K$ and a transition half width of about 1 K. The heat capacity of water was taken to be $c_p^{water} = 75\ J/K \cdot mol$ which corresponds to the value of 1 $cal/g \cdot K$ for bulk water. The heat capacity of the lipid chains was set to $c_p^{chain} = 1600 \cdot J/K \cdot mol$ which was determined experimentally for gel state DPPC [90]. The total heat reservoir is shared by all lipids in the lipid membrane. The minimum number of water molecules per lipid considered in any simulation is 100. The simulated heat capacity profiles have been smoothed using cubic spline fits and the error is estimated using the Jackknife method.

A.4 Capacitive current response function

Derivation of the frequency dependent response function used in Eq. (4.9).

$$r(t) = \frac{d}{dt}\left(\int_{-\infty}^{t} g(t-t')\frac{d\psi(t')}{dt'}\mathrm{d}t'\right) = g(t-t)\frac{d\psi(t)}{dt} + \int_{-\infty}^{t}\frac{dg(t-t')}{dt}\frac{d\psi(t')}{dt'}\mathrm{d}t', \tag{A.6}$$

where $r(t)$ is the response function to a perturbation ($\psi(t)$) and g is the relaxation function. We assume that the relaxation function can be described by single exponential relaxation.

$$g(t-t') = a\left(1 - e^{\frac{t-t'}{\tau}}\right). \tag{A.7}$$

For simplicity of notation we write,

$$h(t-t') = \frac{dg(t-t')}{dt}. \tag{A.8}$$

Using these we can write Eq. (A.6),

$$r(t) = \int_{-\infty}^{t} h(t-t')\frac{d\psi(t')}{dt'}\mathrm{d}t' \tag{A.9}$$

Using partial integration,

$$\begin{aligned} r(t) &= \left[h(t-t')\int\frac{d\psi(t')}{dt'}\mathrm{d}t'\right]_{-\infty}^{t} - \int_{-\infty}^{t}\frac{dh(t-t')}{dt'}\psi(t')\mathrm{d}t' && \text{(A.10)}\\ &= h(0)\psi(t) - h(\infty)\psi(-\infty) - \int_{-\infty}^{t}\frac{dh(t-t')}{dt'}\psi(t')\mathrm{d}t' && \text{(A.11)}\\ &= \frac{a}{\tau}\psi(t) - \int_{-\infty}^{t}\frac{dh(t-t')}{dt'}\psi(t')\mathrm{d}t' && \text{(A.12)} \end{aligned}$$

We continue the derivation with the last term which we name $r'(t)$. Change variables $t'' = t - t'$ [1]

$$r'(t) = -\int_{-\infty}^{t}\frac{dh(t-t')}{dt'}\psi(t')\mathrm{d}t' = \int_{0}^{\infty}\frac{dh(t'')}{dt''}\psi(t-t'')\mathrm{d}t'' \tag{A.13}$$

[1] note: $\frac{d}{dt'} = \frac{d}{dt''}\frac{dt''}{dt'} = -\frac{d}{dt''}$, $\mathrm{d}t'' = -\mathrm{d}t'$

Preforming a Fourier transform on Eq. (A.13)

$$r'(\omega) = \int_{-\infty}^{\infty}\int_{0}^{\infty}\frac{dh(t'')}{dt''}\psi(t-t'')\mathrm{d}t''e^{-i\omega t}\mathrm{d}t \tag{A.14}$$

$$= \int_{0}^{\infty}\frac{dh(t'')}{dt''}\int_{-\infty}^{\infty}\psi(t-t'')e^{-i\omega t}\mathrm{d}t\mathrm{d}t'' \tag{A.15}$$

Changing variables again $t' = t - t''$.

$$r'(\omega) = \int_{0}^{\infty}\frac{dh(t'')}{dt''}\int_{-\infty}^{\infty}\psi(t')e^{-i\omega(t'+t'')}\mathrm{d}t'\mathrm{d}t'' \tag{A.16}$$

$$= \int_{0}^{\infty}\frac{dh(t'')}{dt''}e^{-i\omega t''}\mathrm{d}t''\int_{-\infty}^{\infty}\psi(t')e^{-i\omega t'}\mathrm{d}t' \tag{A.17}$$

$$= \int_{0}^{\infty}\frac{dh(t'')}{dt''}e^{-i\omega t''}\mathrm{d}t''\psi(\omega) \tag{A.18}$$

$$= -\frac{a}{\tau}\frac{1}{1+i\omega\tau}\psi(\omega) \tag{A.19}$$

From Eq. (A.19) and the Fourier transform of the first term in the last line of Eq. (A.12) we get,

$$r(\omega) = \frac{a}{\tau}\psi(\omega) - \frac{a}{\tau}\frac{1}{1+i\omega\tau}\psi(\omega) = a\frac{i\omega}{1+i\omega\tau}\psi(\omega) \tag{A.20}$$

A.5 Sources of artifacts and noise

The main source of noise in our electrical and mechanical measurement of nerve signals is the electrical noise at 50 Hz from the power cables and sockets. Additional electrical noise comes from light and other electrical devices. To limit the electrical noise all cables and instrumentation have to be carefully grounded[2]. Even with careful grounding removing all electrical noise is difficult, especially the substantial 50 Hz noise and its higher harmonics. Non-periodic noise can be cancelled by averaging. However, periodic noise is not cancelled if the frequency of the noise is a harmonic of the repetition frequency when averaging. To insure cancellation by averaging we choose a repetition frequency which does not have 50 Hz or its higher harmonics as higher harmonics. Due to the maximum succession rate for stimulation of nerves being around 10 Hz we used 6.28 Hz as repetition frequency. This becomes important since we do averaging over min. 100 repetitions, to achieve the desired mechanical accuracy. Failing to do this leads to structured artifacts in the recording.

Beyond noise issues, instrumental cross-talk can also lead to artifacts. When using a common interface, like the PowerLab, cross-talk between the different channels is possible, especially when the voltage signal in the different channels are of different order of magnitude. For our setup the pre-amplified electrical recording of a nerve signal can be around 1 V (remembering the gain $x1000$) whereas the voltage output of the mechanical nerve signal is of the order of 1 mV or smaller. Cross-talk often show up as similar signals showing up in multiple

[2] Then grounding is done using the same ground and avoiding creating any grounding loops.

channels. The mechanical and electrical nerve signal should in our setup be temporally separated since the point of measurement is spatially separated, which help ruling out cross-talk issues.

Appendix B

Publications

CHAPTER TWO

Low-Frequency Sound Propagation in Lipid Membranes

Lars D. Mosgaard, Andrew D. Jackson, Thomas Heimburg[1]
Membrane Biophysics Group, The Niels Bohr Institute, University of Copenhagen, Copenhagen, Denmark
[1]Corresponding author: e-mail address: theimbu@nbi.dk

Contents

Abstract

In the recent years, we have shown that cylindrical biological membranes such as nerve axons under physiological conditions are able to support stable electromechanical pulses called solitons. These pulses share many similarities with the nervous impulse, for example, the propagation velocity as well as the measured reversible heat production and changes in thickness and length that cannot be explained with traditional nerve models. A necessary condition for solitary pulse propagation is the simultaneous existence of nonlinearity and dispersion, that is, the dependence of the speed of sound on density and frequency. A prerequisite for the nonlinearity is the presence of a chain-melting transition close to physiological temperatures. The transition causes a density dependence of the elastic constants which can easily be determined by an experiment. The frequency dependence is more difficult to determine. The typical timescale of a nerve pulse is 1 ms, corresponding to a characteristic frequency in the range up to 1 kHz. Dispersion in the sub-kilohertz regime is difficult to measure due to the very long wave lengths involved. In this contribution, we address theoretically the dispersion of the speed of sound in lipid membranes and relate it to experimentally accessible relaxation times by using linear response theory. This ultimately leads to an extension of the differential equation for soliton propagation.

Advances in Planar Lipid Bilayers and Liposomes, Volume 16
ISSN 1554-4516
http://dx.doi.org/10.1016/B978-0-12-396534-9.00002-7

© 2012 Elsevier Inc.
All rights reserved.

ABBREVIATIONS

DPPC dipalmitoyl phosphatidylcholine
DSC differential scanning calorimetry

1. INTRODUCTION

Biological membranes are ubiquitous in the living world. Despite their diversity in composition, membranes of different cells or organelles are remarkably similar in structure and exhibit similar thermodynamic properties. They exist as thin, almost two-dimensional lipid bilayers whose primary function is to separate the interior of cells and organelles (subcellular compartment) from their external environments. This separation leads in turn to the creation of chemical and biological gradients which play a pivotal role in many cellular and subcellular processes, for example, adenosine triphosphate production. A particularly important feature of biomembranes is the propagation of voltage signals in the axons of neurons, which allows cells to communicate quickly over long distances, an ability that is vital for higher lifeforms such as animals [1,2].

Biological membranes exhibit a phase transition between an ordered and a disordered lipid phase near physiological conditions [3]. It has been shown that organisms alter their detailed lipid composition in order to maintain the temperature of this phase transition despite different growth conditions [4–6]. The biological implications of membrane phase transitions continue to be an area of active research. Near a phase transition, the behavior of the membrane changes quite drastically: The thermodynamic susceptibilities, such as heat capacity and compressibility, display a maximum, and the characteristic relaxation times of the membrane show a drastic slowing down [7–11].

The melting transition in lipid membrane is accompanied by a significant change of the lateral density by about −20%. Thus, the elastic constants are not only temperature dependent, but they are also sensitive functions of density. Together with the observed frequency dependence of the elastic constants (dispersion), this leads to the possibility of localized solitary pulse (or soliton) propagation in biomembrane cylinders such as nerve axons. With the emergence of the soliton theory for nerve pulse propagation, the investigation of sound propagation in lipid membranes close to the lipid melting transition has become an important issue [2]. The soliton model

describes nerve signals as the propagation of adiabatic localized density pulses in the nerve axon membrane. This view is based on macroscopic thermodynamics arguments in contrast to the well-known Hodgkin–Huxley model for the action potential that is based on the nonadiabatic electrical properties of single protein molecules (ion channels).[1] Using this alternative model, we have been able to make correct predictions regarding the propagation velocity of the nerve signal in myelinated nerves, along with a number of new predictions regarding the excitation of nerves and the role of general anesthetics [12]. In addition, the soliton model explains a number of observations about nerve signal propagation, which are not included in the Hodgkin and Huxley model, such as changes in the thickness of the membrane, changes in the length of the nerve, and the existence of phase-transition phenomena [13]. The solitary wave is a sound phenomenon which can take place in media displaying dispersion and nonlinearity in the density. Both of these criteria are met close to the main lipid transition. However, the magnitude of dispersion in the frequency regime of interest for nerve pulses (up to 1 kHz) is unknown [2]. Exploring sound propagation in lipid membranes is thus an important task for improving our understanding of mechanical pulse propagation in nerves. All previous attempts to explore sound propagation in lipid membranes have focused on the ultrasonic regime [9,14–16], and it has clearly been demonstrated that dispersion exists in this frequency regime. Furthermore, the low-frequency limit of the adiabatic compressibility of membranes (which determines the sound velocity) is equal to the isothermal compressibility, which is significantly larger than the compressibility in the megahertz regime. With the additional knowledge that relaxation times in biomembranes are of the order of milliseconds to seconds, it is quite plausible to expect significant dispersion effects in the frequent regime up to 1 kHz.

Theoretical efforts to describe sound propagation in lipid membranes near the lipid melting transition in the ultrasonic regime have been based on scaling theory, which assumes critical relaxation behavior during the transition [16,17]. However, a number low-frequency experiments, pressure jump experiments [10,18], and stationary perturbation techniques [11,19] all show noncritical relaxation dynamics. These findings have led us to propose a noncritical thermodynamical description of sound propagation in lipid membranes near the lipid melting transition for low frequencies based on linear response theory.

[1] For a comparison of the Hodgkin–Huxley model and the soliton theory, see Chapter 9.

In this chapter, we present a theoretical derivation of the magnitude of dispersion for membranes close to lipid melting transitions. The goal is to modify the wave equation for solitons in biomembranes. This will ultimately lead to a natural timescale for the pulse length, which we will explore in future work.

2. THE PROPAGATING SOLITON IN NERVE MEMBRANES

In the following, we present the hydrodynamic equations that govern the propagation of density waves in cylindrical membranes, in general, and in nerve membranes close to the chain-melting transition, in particular.

In it simplest formulation, the wave equation for compressible fluids assumes the form[2]:

$$\frac{\partial^2 \rho}{\partial t^2} = \nabla(c^2 \nabla \rho), \tag{2.1}$$

where

$$c = \sqrt{\left(\frac{\partial p}{\partial \rho}\right)_{S,0}} = \frac{1}{\sqrt{\kappa_S \rho}} \tag{2.2}$$

is the speed of sound for low-amplitude waves ($\Delta\rho \ll \rho_0$), κ_S is the adiabatic compressibility, and $\rho(x, t)$ is the density. If the speed of sound is roughly independent of density, this equation simplifies to

$$\frac{\partial^2 \rho}{\partial t^2} = c^2 \nabla^2 \rho. \tag{2.3}$$

The wave equation in one dimension is then given by

$$\frac{\partial^2 \rho}{\partial t^2} = \frac{\partial}{\partial x}\left(c^2 \frac{\partial}{\partial x}\rho\right). \tag{2.4}$$

For low-amplitude sound, we further assume that there is dispersion of the form

$$c^2 = c_0^2 + h_0 \omega^2 + \cdots, \tag{2.5}$$

[2] A derivation of the equation of sound, based on fluid dynamics, can be found in Ref. [20]. There are two basic assumptions in the derivation of the equation of sound: Perturbations are small, and sound propagation is an adiabatic process.

which corresponds to a Taylor expansion of the sound velocity with respect to frequency. The parameter h_0 indicates the magnitude of the dispersion. Due to symmetry arguments, only even power terms appear in this expansion. One way to generate this frequency dependence is to add a dispersion term to the wave equation

$$\frac{\partial^2\rho}{\partial t^2}=\frac{\partial}{\partial x}\left(c^2\frac{\partial}{\partial x}\rho\right)-h\frac{\partial^4}{\partial x^4}\rho. \tag{2.6}$$

The density of a small amplitude plane wave can be written as

$$\begin{aligned}\rho(x,t)&=\rho_0+\Delta\rho \quad \text{with} \quad \Delta\rho=A\sin(kx-\omega t)\\ &\equiv A\sin(k(x-ct)).\end{aligned} \tag{2.7}$$

The amplitude of this plane wave is A, and its velocity is $c=\omega/k$. Inserting this into Eq. (2.4) yields the dispersion relation in Eq. (2.5) with $h_0=h/c_0^2$. We have shown experimentally that the sound velocity close to melting transitions in lipid membranes is a sensitive nonlinear function of density. Thus, we expand

$$c^2=c_0^2+p\Delta\rho+q(\Delta\rho)^2+\cdots. \tag{2.8}$$

The parameters p and q describe the nonlinear elastic properties of membranes. At temperatures slightly above the melting transition, lipid membranes have negative values for the parameter p and positive values for the parameter q. The final wave equation is given by

$$\frac{\partial^2\rho}{\partial t^2}=\frac{\partial}{\partial x}\left((c_0^2+p\Delta\rho+q(\Delta\rho)^2)\frac{\partial}{\partial x}\rho\right)-h\frac{\partial^4}{\partial x^4}\rho. \tag{2.9}$$

We have shown that this equation possesses analytical solitary solutions that in many aspects resemble the nerve pulse (see Fig. 2.1).

While the above equation makes use of the fact that the speed of sound is a known function of density, the dispersion constant h must be regarded as an adjustable parameter due to the absence of quantitative empirical data regarding dispersion in the low-frequency regime. The magnitude of h sets the width and the timescale of the mechanical pulse. In previous publications, it was adjusted to $h=2\,\mathrm{m}^4/\mathrm{s}^2$ in order to match the observed width of the nerve pulse, which is about 10 cm. However, we will argue below that h is expected to be density dependent and that its functional form can be approximated using experimental knowledge about relaxation timescales and elastic constants. This will ultimately lead to a wave equation for

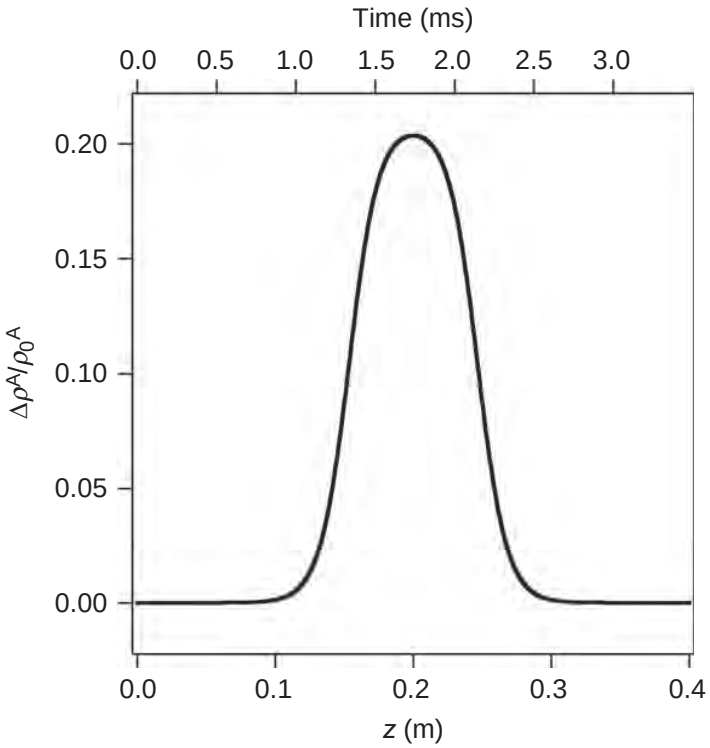

Figure 2.1 The propagating soliton using parameters appropriate for unilamellar DPPC vesicles and a dispersion constant $h = 2\text{m}^4/\text{s}^2$ (from Ref. [21]). The soliton has a width of about 10 cm and a duration of about 1 ms, which is very similar to action potentials in myelinated nerves.

the mechanical pulse in nerve axons that is free of adjustable parameters and has a timescale that is fixed by the thermodynamics of the system.

3. BRIEF OVERVIEW OF SOUND

Sound is a propagating low-amplitude density wave in compressible medium which, due to its adiabatic nature, is accompanied by a corresponding temperature wave. The equation governing sound propagation is universal. This generality implies that sound propagation is determined solely by the macroscopic thermodynamical properties of the system.

As mentioned above, the equation of sound for low-amplitude waves has the following form:

$$\frac{\partial^2 p}{\partial t^2} = c^2 \nabla^2 \rho.$$

The general solution has the following form:

$$\rho = A \exp(i\omega(t - x/\hat{c})), \tag{2.10}$$

which is merely Eq. (2.7) in complex notation. Due to dispersion and the absorption of sound in a real medium, the effective speed of sound, $\hat{c}$, is a complex quantity. The real part of the speed of sound will cause a phase shift (as a result of dispersion), and the imaginary part will lead to a decrease in the amplitude or intensity of the sound as it propagates (attenuation). This can be seen by inserting the complex speed of sound into Eq. (2.10).

$$\rho = A\exp(i\omega(t - x\mathrm{Re}(\hat{c})/|\hat{c}|^2))\exp(-x\omega\mathrm{Im}(\hat{c})/|\hat{c}|^2), \tag{2.11}$$

where

$$u = \left(\frac{\mathrm{Re}(\hat{c})}{|\hat{c}|^2}\right)^{-1} \tag{2.12}$$

is the effective speed of sound which would be measured in an experiment.

In 1928, Herzfeld and Rice extended the theory of sound by arguing that internal vibrational modes of polyatomic molecules require time to approach thermal equilibrium with translational degrees of freedom [22]. If the timescale of the density (or pressure) perturbation is similar to or less than the timescale of these internal relaxation times, the temperature response of the system will lag behind that of the perturbation. This will prevent the internal degrees of freedom from taking up all the heat and will result in a decrease in the effective heat capacity.[3] This decrease in the effective heat capacity results in hysteresis and in dissipation of heat.

In 1962, Fixman applied the basic ideas of Herzfeld and Rice to describe the viscosity of critical mixtures [23]. He was motivated by the intimate relation between viscosity and attenuation. Critical mixtures of fluids display a second-order transition which is indicated by a critical slowdown of the relaxation rates of the order parameters. In contrast to Herzfeld and Rice, Fixman did not limit his attention to the rates of translational and internal degrees of freedom but rather considered a continuum of long-wavelength fluctuations in the order parameter. With this change of perspective, he made the connection between the transfer rates and relaxation rates of order parameters in viscous systems. The slowdown during a transition means large changes in the dynamic heat capacity of the system and thereby in the speed of sound.

Following the argument of Fixman, the slowing down of the characteristic relaxation rate during the lipid melting transition will cause hysteresis

[3] Note that the effective heat capacity will be referred to as the dynamic heat capacity.

and dissipation of heat. Even in the absence of critical phenomena, internal friction and heat conduction as introduced by Stokes [24] and Kirchhoff [25], respectively, can cause hysteresis and dissipation. However, within cooperative transitions, these are secondary effects and we will disregard them for low frequencies.

4. SYSTEM RESPONSE TO ADIABATIC PRESSURE PERTURBATIONS

Sound is the propagation of a pressure wave that is followed by a temperature wave as a consequence of its adiabatic nature. Thermodynamically, changes in pressure (dP) and temperature (dT) couple to a change in the entropy (dS) of the system:

$$dS = \left(\frac{\partial S}{\partial T}\right)_p dT + \left(\frac{\partial S}{\partial p}\right)_T dp, \tag{2.13}$$

where $c_p = T(\partial S/\partial T)_p$ is the heat capacity at constant pressure. Using a well-known Maxwell relation, $(\partial S/\partial p)_T$ can be rewritten as $(\partial S/\partial p)_T = -(\partial V/\partial T)_p$,

$$\begin{aligned}\left(\frac{\partial S}{\partial p}\right)_T &= -\left(\frac{\partial V}{\partial T}\right)_p \\ &= -\left(\frac{\partial S}{\partial T}\right)_p \left(\frac{\partial V}{\partial S}\right)_p \\ &= -\frac{c_p}{T}\left(\frac{\partial V}{\partial S}\right)_p.\end{aligned} \tag{2.14}$$

Another Maxwell relation, $(\partial V/\partial S)_p = (\partial T/\partial p)_S$, allows us to write Eq. (2.14) as

$$\left(\frac{\partial S}{\partial p}\right)_T = -\frac{c_p}{T}\left(\frac{\partial T}{\partial p}\right)_S. \tag{2.15}$$

Constant entropy implies that no heat is dissipated into the environment but only moved between different degrees of freedom within a closed system. At transitions, the Clausius–Clapeyron relation[4] can be used:

[4] The use of the Clausius–Clapeyron relation can be justified by the weak first-order nature of the lipid melting transition [26].

$$\left(\frac{\partial p}{\partial T}\right)_S = \frac{\Delta H}{T\Delta V}, \tag{2.16}$$

where ΔH and ΔV are the enthalpy (or excess heat) and volume changes (excess volume) associated with the transition [11]. Note that these are constant system properties for a given transition that can be determined experimentally.

The change in entropy (Eq. 2.13) can now be written as

$$\mathrm{d}S = c_p(T,p)\left(\frac{\mathrm{d}T}{T} - \left(\frac{\Delta V}{\Delta H}\right)\mathrm{d}p\right). \tag{2.17}$$

It is clear from Eq. (2.17) that the heat capacity acts as a transfer function that couples adiabatic changes in pressure to changes in entropy.

Equation (2.17) governs the equilibrium properties of the thermodynamical system. However, here we consider the propagation of sound, which is a nonequilibrium process. The theory of sound considers the limit of small changes in pressure and temperature for which close-to-equilibrium dynamics can be assumed. This implies linear relations between perturbations and system responses. For this reason, it is also called linear response theory.

In any real system, transfer rates are finite and changes happen in finite time. Thus, the changes in pressure and temperature can be represented as rates, and Eq. (2.17) can be rewritten as

$$\Delta S = \int \mathrm{d}S = \int c_p(t)\left[\frac{\dot{T}(t)}{T_0} - \left(\frac{\Delta V}{\Delta H}\right)\dot{p}(t)\right]\mathrm{d}t, \tag{2.18}$$

where $\dot{T} = \partial T/\partial t$ and $\dot{p} = \partial p/\partial t$ are rates. Note that $T_0 = T_{\text{equilibrium}}$, which holds if absolute changes in temperature upon pressure changes are very small.

If changes in pressure or temperature happen faster than the transfer rate (or relaxation rate), the energy transferred during this change will be only a part of the amount otherwise transferred. Considering Eq. (2.17), the finite transfer rate will lower the effective transfer function, in this case the heat capacity. This means that also the heat capacity must contain a relaxation term, $(1-\Psi_{c_p})$, with $0 \le \Psi_{c_p} \le 1$. This function describes the equilibration of the system. As the system approaches equilibrium, $(1-\Psi_{c_p})$ approaches unity. Below, we will assume that the function Ψ_{c_p} is an exponentially decaying function of time. Equation (2.18) must then be written as a convolution:

$$\Delta S(t) = \int_{-\infty}^{t} \left[c_p(\infty) + \Delta c_p(1 - \Psi_{c_p}(t - t'))\right] \left(\frac{\dot{T}(t')}{T_0} - \frac{\Delta V}{\Delta H}\dot{p}(t')\right) \mathrm{d}t', \tag{2.19}$$

where $\Delta S(t)$ is the time-dependent change in entropy, $c_p(\infty)$ is the part of the heat capacity that relaxes more rapidly than the changes in the pressure and temperature considered. In the lipid bilayer system, $c_p(\infty)$ is the heat capacity contribution from lipid chains, which we consider as a background contribution. Δc_p is the part of the heat capacity which relaxes on timescales of a similar order or longer than the perturbation timescale. In the lipid membrane system this is the excess heat capacity. In Eq. (2.19), it has been assumed that the mechanisms of relaxation are the same for pressure and temperature. This assumption has been justified experimentally and numerically in the literature [10,14,27,28].

After partial integration of Eq. (2.19), subsequent Fourier transformation and the use of the convolution theorem, Eq. (2.19) can be transformed into (see Appendix)

$$\Delta S(\omega) = c_p(\omega)\left(\frac{T(\omega)}{T_0} - \frac{\Delta V}{\Delta H}p(\omega)\right). \tag{2.20}$$

$T(\omega)$ and $p(\omega)$ can be regarded as periodic variations of temperature and pressure, respectively. We have also now introduced the frequency-dependent heat capacity,

$$c_p(\omega) = c_p(\infty) - \Delta c_p \int_0^{\infty} \mathrm{e}^{-i\omega t}\dot{\Psi}_{c_p}(t)\mathrm{d}t. \tag{2.21}$$

From Eq. (2.21), the frequency-dependent transfer function (dynamic heat capacity)[5] can be found, giving a full description of how a lipid bilayer responds to adiabatic pressure perturbations. Both $c_p(\infty)$ and Δc_p are experimentally available using differential scanning calorimetry (DSC). The only unknown is the relaxation function, Ψ_{c_p}.

[5] It is important note to the difference between the dynamic heat capacity (frequency dependent) and the normally known equilibrium heat capacity. The equilibrium heat capacity is a constant system property, whereas the dynamic heat capacity is an effective heat capacity that can be less than or equal to the equilibrium heat capacity as a consequence of the finite transfer rates in real systems.

4.1. Relaxation function

The relaxation function of the heat capacity is related to the rate of energy transfer from the membrane to the environment. The fluctuation–dissipation theorem ensures that the rate of energy transfer is equivalent to the relaxation behavior of energy fluctuations. Since the heat capacity is a measure of enthalpy fluctuations, the relaxation function of the heat capacity must be the relaxation function of the enthalpy fluctuations [11].

The relaxation behavior of the fluctuations of enthalpy in pure lipid vesicles has been considered theoretically, numerically, and experimentally, showing that the relaxation of enthalpy is well described by a single exponential function [10,18]:

$$(H-\langle H\rangle)(t)=(H-\langle H\rangle)(0)\exp\left(-\frac{t}{\tau}\right), \tag{2.22}$$

where $(H-\langle H\rangle)(0)$ serves only as a proportionality constant and τ is the relaxation time. For various pure lipid membranes close to melting transitions, it was further found that relaxation times are proportional to the excess heat capacity,

$$\tau=\frac{T^2}{L}\Delta c_p, \tag{2.23}$$

where L is a phenomenological coefficient. For large unilamellar vesicles (LUV) of dipalmitoyl phosphatidylcholine (DPPC), $L=13.9\times10^8$ JK/(s mol) [10].

4.2. Response function

Using the relaxation function of the enthalpy fluctuation as the relaxation function of the dynamic heat capacity,

$$\Psi_{c_p}=\exp\left(-\frac{t}{\tau}\right). \tag{2.24}$$

Equation (2.21) can be solved and the dynamic heat capacity can be determined as

$$\begin{aligned} c_p(\omega)&=c_p(\infty)-\Delta c_p\int_0^\infty \mathrm{e}^{-i\omega t}\left(-\frac{1}{\tau}\right)\mathrm{e}^{-t/\tau}\mathrm{d}t \\ &=c_p(\infty)+\Delta c_p\left(\frac{1-i\omega\tau}{1+(\omega\tau)^2}\right). \end{aligned} \tag{2.25}$$

Note that the above derivations can be carried out with lateral pressure instead of pressure; the choice of using pressure is entirely for notational convenience.

5. ADIABATIC COMPRESSIBILITY

In estimating the speed of sound in the plane of a lipid membrane during the melting transition, the response of the membrane to sound (the dynamic heat capacity) must be related to the lateral adiabatic compressibility. The adiabatic lateral compressibility is defined as

$$\kappa_S^A = -\frac{1}{A}\left(\frac{\partial A}{\partial \Pi}\right)_S, \tag{2.26}$$

where Π is the lateral pressure. The adiabatic lateral compressibility can be rewritten in the following form [29]:

$$\kappa_S^A = \kappa_T^A - \frac{T}{A c_p^{\text{system}}}\left(\frac{\partial A}{\partial T}\right)_\Pi^2, \tag{2.27}$$

where

$$\kappa_T^A = -\frac{1}{A}\left(\frac{\partial A}{\partial \Pi}\right)_T = \kappa_T^A(\infty) + \frac{\gamma_A^2 T}{A}\Delta c_p \tag{2.28}$$

is the isothermal lateral compressibility, $\kappa_T{}^A(\infty)$ is the part of the isothermal lateral compressibility that relaxes faster than changes in the pressure and temperature considered, and $c_p{}^{\text{system}}$ is the heat capacity of the total thermodynamical system, that is, the lipid membrane plus the accessible surrounding aqueous medium that serves as a buffer for heat transfer. In the last equality, the empirical proportionality $\Delta A = \gamma_A \Delta H$ has been used [2,27], with $\gamma_A = 0.893\,\text{m}^2/\text{J}$ for a lipid bilayer of DPPC.

In the literature on attenuation and dissipation of sound in critical media, a different form of Eq. (2.27) is often used to relate the dynamic heat capacity and the adiabatic compressibility, using the dynamic heat capacity as the heat capacity of the total system [17,30]. This can be done in a straight forward manner by employing the Pippard–Buckingham–Fairbank relations [31,32]. The main difference between this approach and the one adopted here is that their compressible medium is three dimensional, and the system heat capacity is that of this medium. In contrast, the lipid membrane system is

a pseudo-two dimensional (the bilayer) embedded in a three-dimensional aqueous medium that serves as a heat reservoir (see Fig. 2.2). Therefore, the aqueous medium contributes significantly to the features of the membrane in a frequency-dependent manner.

Imagine a standing temperature wave in the bilayer. The transfer of heat from the wave to the surrounding water will be time dependent, see Fig. 2.2 for visualization. In the limit of $\omega \to 0$, the amount of water (heat reservoir) participating will effectively go to infinity. In the other extreme, $(\omega \to \infty)$, no heat will be transferred to the surrounding heat reservoir. Evidently, the heat capacity of the total system is frequency dependent:

$$c_p^{\text{system}}(\omega) = c_p^{\text{lipid}} + c_p^{\text{reservoir}}(\omega) \tag{2.29}$$

where $c_p{}^{\text{lipid}} = \Delta c_p + c_p(\infty)$ is the complete heat capacity (in equilibrium) of the lipid membrane and $c_p{}^{\text{reservoir}}(\omega)$ is the heat capacity of the participating heat reservoir. In this approach, it is the size of the contributing heat reservoir that is frequency dependent.

Using the proportionality relation $\Delta A = \gamma_A \Delta H$ in Eq. (2.27) and assuming that $(\partial A/\partial T)_\Pi$ in the chain-melting transition region is completely dominated by the transition-associated change in area, the following approximation can be made [14]:

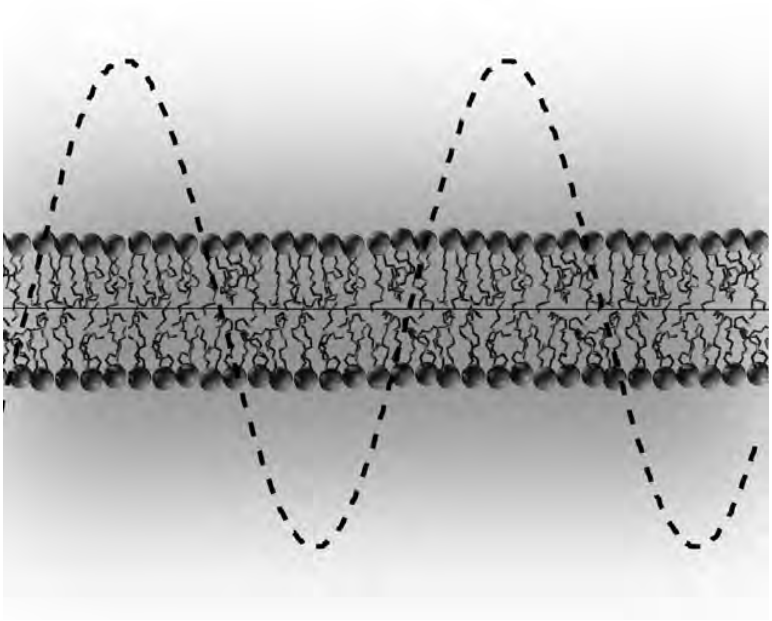

Figure 2.2 Visualization of temperature wave in the plane of a lipid bilayer. The coloring indicates heat penetrating into the surrounding water.

$$\begin{aligned}\kappa_S^A &\approx \kappa_T^A(\infty) + \frac{\gamma_A^2 T}{A}\Delta c_p - \frac{\gamma_A^2 T}{A}\frac{(\Delta c_p)^2}{c_p^{\text{system}}} \\ &= \kappa_T^A(\infty) + \frac{\gamma_A^2 T}{A}\left(\Delta c_p - \frac{(\Delta c_p)^2}{c_p^{\text{system}}}\right).\end{aligned} \tag{2.30}$$

The parenthesis has the units of a heat capacity and is frequency dependent through the frequency dependence of the size of the associated heat reservoir. We pose as an ansatz here that this parenthesis is the effective heat capacity of the lipid membrane in a finite adiabatically isolated heat reservoir, which is equivalent to the dynamic heat capacity of the lipid membrane following the above argument:

$$\Delta c_p(\omega) = \Delta c_p - \frac{(\Delta c_p)^2}{c_p^{\text{system}}}. \tag{2.31}$$

Numerical justification of this ansatz will be published at a later point.

Using this ansatz, the dynamic heat capacity can be related directly to the adiabatic lateral compressibility through Eq. (2.30):

$$\kappa_S^A = \kappa_T^A(\infty) + \frac{\gamma_A^2 T}{A}\Delta c_p(\omega), \tag{2.32}$$

where the $\Delta c_p(\omega)$ is the dynamic heat capacity without background. In this equation, we use the area of the lipid bilayer.

6. RESULTS—THE SPEED OF SOUND

The goal is to estimate the speed of sound and its frequency dependence in the plane of a lipid membrane. From the estimated dynamic heat capacity equation (2.25), the adiabatic lateral compressibility can found using the proposed relation (Eq. 2.32). The lateral speed of sound can then be estimated using Eq. (2.2) as

$$c^A = \frac{1}{\sqrt{\kappa_S^A \rho^A}},$$

where ${\kappa_S}^A$ is a function of the frequency, ω. The effective speed of sound is given by Eq. (2.12)

$$u = \left(\frac{\mathrm{Re}(c^A)}{|c^A|^2} \right)^{-1}.$$

Using the previous two equations, one can show that

$$u^2(\omega) = (\rho^A)^{-1} \frac{2}{\mathrm{Re}(\kappa_S^A) + |\kappa_S^A|}. \tag{2.33}$$

Inserting the estimated adiabatic lateral compressibility from Eqs. (2.32) and (2.25) into Eq. (2.33), the effective speed of sound squared takes the analytic form:

$$u^2(\omega) = \frac{2}{\frac{1}{c_1^2} + \frac{1}{c_2^2} \frac{1}{(1+(\omega\tau)^2)} + \sqrt{\left(\frac{1}{c_1^2} + \frac{1}{c_2^2} \frac{1}{(1+(\omega\tau)^2)} \right)^2 + \left(\frac{1}{c_2^2} \frac{\omega\tau}{(1+(\omega\tau)^2)} \right)^2}}, \tag{2.34}$$

with the notation

$$c_1^2 \equiv \left(\rho^A \kappa_T^A(\infty) \right)^{-1} \tag{2.35}$$

and

$$c_2^2(\omega) \equiv \left(\rho^A \frac{\gamma_A^2 T}{A} \Delta c_p(\omega) \right)^{-1}. \tag{2.36}$$

Here, c_1 is the lateral speed of sound of the membrane outside the transition, and c_2 is the component of the lateral speed of sound related to the lipid melting transition.

All variables in Eq. (2.34) can be found from the excess heat capacity of the lipid melting transition and the fluid fraction,[6] which can be obtained using DSC. The area, the lateral density, and the background isothermal compressibility are all directly related to the fluid fraction [28]. The relaxation time can be estimated from its phenomenological proportionality relation to the excess heat capacity, Eq. (2.23). The proposed analytic expression for the effective speed of sound (Eq. 2.34) is shown in Fig. 2.3, where the excess heat capacity and the fluid fraction are taken from Monte Carlo simulations of the lipid melting transition in LUV of DPPC. The simulation has been carried out in a manner similar to that described in Ref. [33].

[6] The fluid fraction is the fraction of a considered lipid system that is in the fluid phase.

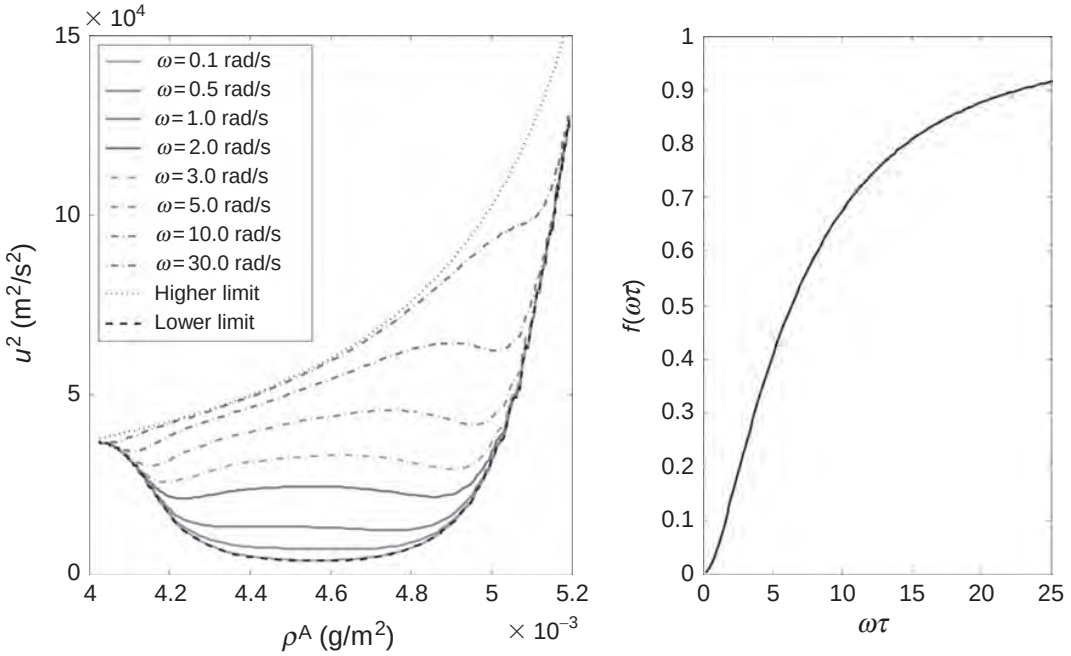

Figure 2.3 *Left*: The effective lateral speed of sound squared as a function of density at different angular frequencies along with the limiting cases: $\omega \to 0$ and $\omega \to \infty$. *Right*: The generic function, $f(\omega\tau)$, that takes the effective lateral speed of sound squared, at a given lateral density, from the low-frequency limit ($f(\omega\tau \to 0) = 0$) to the high-frequency limit ($f(\omega\tau \to \infty) = 1$).

The frequency dependence of the speed of sound is described by the function, $f(\omega\tau)$ with $0 \leq f(\omega\tau) \leq 1$, defined by

$$u^2(\omega\tau) = u_0^2 + (u_\infty^2 - u_0^2) f(\omega\tau) \tag{2.37}$$

where $u_0 \equiv u(\omega\tau \to 0)$ and $u_\infty \equiv u(\omega\tau \to \infty)$. From Eq. (2.34) we see that

$$\begin{aligned} u_0^2 &= \left(\frac{1}{c_1^2} + \frac{1}{c_2^2} \right)^{-1} \\ u_\infty^2 &= c_1^2. \end{aligned} \tag{2.38}$$

See Fig. 2.3 (right). The generic function f was chosen to be a function of the dimensionless quantity $\omega\tau$ rather than ω in order to render it independent of the lateral density.

6.1. Dispersion relation

In the soliton model described by Eq. (2.4), dispersion was assumed to be small and independent of the lateral density due to the lack of detailed information of the frequency dependence of the speed of sound as a function

of density. Using the considerations of the previous sections, we can now estimate the dispersion in lipid membranes. In the soliton model, the extent of dispersion is described by the parameter, h. Assuming that dispersion is small, h can be related to the lateral speed of sound as

$$u^2 \approx u_0^2 + \frac{h\omega^2}{u_0^2} + \cdots. \tag{2.39}$$

Equation (2.39) corresponds to a Taylor expansion of the lateral speed of sound squared to second order.[7] Expanding Eq. (2.34) to second order,

$$u^2 \approx u_0^2 + u_0^4 \frac{3c_1^2 + 4c_2^2}{4c_2^2(c_1^2 + c_2^2)} \omega^2 \tau^2, \tag{2.40}$$

we see that the dispersion parameter has the following form:

$$h = u_0^6 \frac{3c_1^2 + 4c_2^2}{4c_2^2(c_1^2 + c_2^2)} \tau^2. \tag{2.41}$$

Using the excess heat capacity and the fluid fraction for large unilamellar vesicles of DPPC as used in Fig. 2.3, we can estimate the density dependence of the dispersion parameter $h(\rho_A)$ as shown in Fig. 2.4.

Here, the density of the fluid phase is approximately 4×10^{-3} g/m^2, the maximum of the dispersion parameter corresponds to the chain-melting

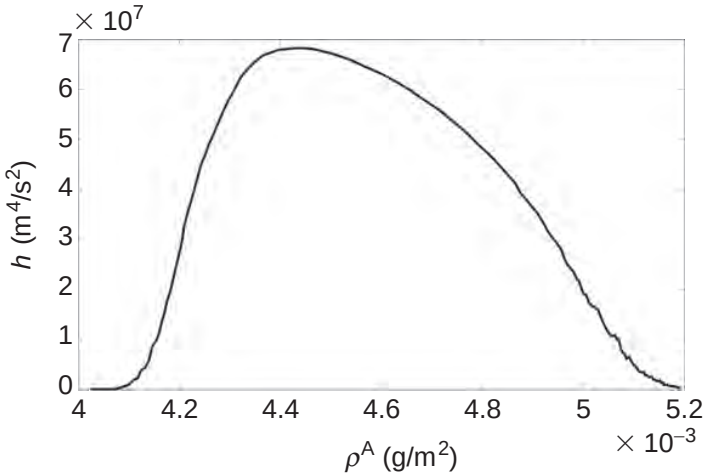

Figure 2.4 The dispersion parameter, h, as a function of lateral density for LUV of DPPC, based on the proposed expression for the lateral speed of sound.

[7] The first-order term is zero since the speed of sound squared is symmetric around $\omega = 0$.

transition maximum, and the density of the gel phase is 5×10^{-3} g/m^2. It is clear that the dispersion parameter is strongly dependent on the lateral density of the membrane.

The density-dependent dispersion parameter, $h(\rho^A)$, will finally enter the differential equation (Eq. 2.4) for the propagating nerve pulse. In the original treatment, h was considered an adjustable constant that determined the timescale of a solitary pulse in nerve axons. In the present extension, $h(\rho^A)$ is fully determined by the cooperative nature of the membrane system and does not contain adjustable parameters. Preliminary calculations indicate that this dispersion parameter will yield a natural timescale for the propagating soliton in nerve axons.

7. DISCUSSION

The response of lipid membranes to adiabatic periodic pressure perturbations (sound) is closely related to the relaxation behavior of the system [22,23]. Using thermodynamics and linear response theory, we have described the response of the lipid membrane to a perturbation with the assumption that the relaxation function has a simple exponential dependence on time. We obtain a form for the dynamic heat capacity which can be understood as the effective heat capacity when the lipid membrane is subject to periodic adiabatic pressure perturbations. The dynamic heat capacity was then related to the adiabatic lateral compressibility using the idea that the size of the associated water reservoir is frequency dependent [14]. The adiabatic lateral compressibility was then used to obtain an expression for the effective speed of sound as a function of frequency.

The major assumption in our approach concerns the nature of the relaxation function. We have previously studied the relaxation behavior of the lipid membrane in the vicinity of the melting transition at low frequencies.[8] This means that the lipid melting transition is assumed to be *non*critical. The single exponential relaxation behavior should, however, only be considered as a low-frequency approximation. In a number of ultrasonic experiments, it has been shown that a single exponential is insufficient to describe the dynamics of the cooperative processes involved in lipid melting in the ultrasonic regime [9,14–16]. In these ultrasonic experiments, some phase-transition phenomena are even apparent in the megahertz regime. Single

[8] The time resolution of experiments from our group is 0.3 s corresponding to 3.3 Hz. Relaxation profiles on longer time scales are well approximated by a single exponential decay [10,18].

exponential relaxation behavior, and thereby the validity of the estimated speed of sound, is thus limited to frequencies comparable to the relaxation rate or lower.

van Osdol *et al.* [19] have made adiabatic pressure perturbation experiments on unilaminar and multilaminar vesicles of DPPC. They studied relaxation behavior of the lipid membrane by measuring the frequency dependence of the effective heat capacity and the compressibility as a function of frequency. Although the data available for unilamellar vesicles are very limited and have large errors, it can still serve to illustrate qualitative tendencies of the effective heat capacity, see Fig. 2.5, that are similar to the theoretical results reported here. The effective frequency dependence of the speed of sound shown in Fig. 2.3 is dominated by the cooperative properties of the lipid melting transition of DPPC. In this model system, the relaxation time during the transition is as slow as seconds. In biological membranes such as membranes of nerves, realistic characteristic relaxation times can be assumed to be of the order of 1–100 ms. This change in

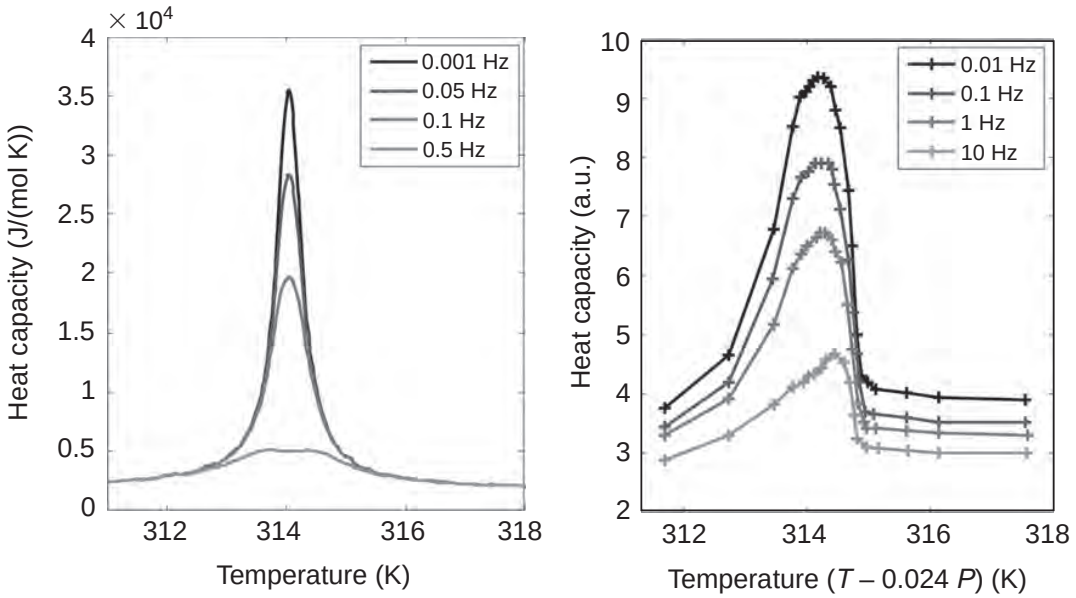

Figure 2.5 *Left*: The calculated dynamic heat capacity for LUV of DPPC at different frequencies. *Right*: The effective heat capacity profiles for LUV of DPPC at different frequencies, measured by van Osdol *et al.* [19]. The measured effective heat capacities have not been corrected for contributions from the experimental setup, and a direct comparison is therefore not possible. The theoretical dynamic heat capacity shows the same qualitative features as the measurements—a dramatic decrease in the height of the excess heat capacity with increasing frequency and a relatively constant width. The difference in frequency scales seen in the two panels is due to an estimated difference of more than a factor of 10 in the characteristic relaxation time. Frequencies are given in units of Hz = $(1/2\pi)$ rad/s.

relaxation times between the model system and biological membrane expands the upper limit of the frequency range for which our approach is likely to be valid from the hertz to kilohertz regime, assuming that the general behavior of pure lipid and biological membranes is otherwise similar. Since the duration of a nerve pulse is roughly 1 ms, the relevant frequency components contained in a nerve pulse can be estimated to be 1 kHz or less. The relevant frequency range for nerve pulses is thus covered by our proposed expression for the effective speed of sound. The present results may thus provide useful insights regarding sound propagation in an otherwise inaccessible regime and can extend our understanding of the nature of nerve signals.

In future studies, the linear response theory described in this chapter will help to define an intrinsic length scale of the electromechanical soliton proposed by us as an alternative description for the nervous impulse.

APPENDIX A. DERIVATION OF THE DYNAMIC HEAT CAPACITY USING THE CONVOLUTION THEOREM

The purpose of this appendix is to provide additional details in the derivation of the frequency-dependent heat capacity given in Eq. (2.25) starting from Eq. (2.19). The change in entropy is a convolution of the applied perturbation and the relaxation of the transfer function—the effective heat capacity. The perturbation is well defined at all times and can safely be assumed to be zero for $t \to -\infty$. The relaxation function is only defined from $[0, \infty]$, where $t = 0$ is the time at which the system starts to equilibrate. The relaxation function, Ψ, is chosen such that $\Psi(t \to 0) = 1$ and $\Psi(t \to \infty) = 0$. To accommodate the chosen form of the relaxation function, the convolution can be written as follows:

$$\Delta S(t) = \int_{-\infty}^{t} (c_p(\infty) + \Delta c_p(1 - \Psi(t - t'))) \left(\frac{\dot{T}(t')}{T_0} - \frac{\Delta V}{\Delta H} \dot{p}(t') \right) \mathrm{d}t', \quad \text{(A.1)}$$

$$\Delta S(t) = \int_{-\infty}^{t} g(t - t') \dot{f}(t') \mathrm{d}t', \quad \text{(A.2)}$$

where $g(t - t')$ is the transfer function and $\dot{f}(t')$ is the perturbation. Note that $\dot{f}(t) = \mathrm{d}f(t)/\mathrm{d}t$, $c_p(\infty)$ is the component of the heat capacity not associated with the melting transition, and T_0 is the equilibrium temperature.

Integration by parts allows us to rewrite Eq. (A.2) to the following form:

$$\Delta S(t) = \left[g(t') \int \dot{f}(t') \mathrm{d}t' \right]_{-\infty}^{t} - \int_{-\infty}^{t} \left(\int \dot{f}(t'') \mathrm{d}t'' \right) \dot{g}(t - t') \mathrm{d}t'. \tag{A.3}$$

The first term in Eq. (A.3) takes the form:

$$\begin{aligned} \left[g(t') \int \dot{f}(t') \mathrm{d}t' \right]_{-\infty}^{t} &= [g(t') f(t')]_{-\infty}^{t} \\ &= g(t) f(t) - g(-\infty) f(-\infty), \end{aligned} \tag{A.4}$$

where

$$f(t') = \frac{(T(t') - T_0)}{T_0} - \frac{\Delta V}{\Delta H} (p(t') - p_0).$$

Assuming that the system is in equilibrium as $t' \to -\infty$ and $f(t' \to -\infty) = 0$, simplifies Eq. (A.4):

$$g(t) f(t) - g(-\infty) f(-\infty) = c_p(\infty) f(t). \tag{A.5}$$

The second term in Eq. (A.3) can be rewritten by changing the variable to $t'' = t - t'$

$$\int_{-\infty}^{t} \left(\int \dot{f}(t') \mathrm{d}t' \right) \dot{g}(t - t') \mathrm{d}t' = - \int_{0}^{\infty} f(t - t'') \dot{g}(t'') \mathrm{d}t'', \tag{A.6}$$

where the integration limits have been changed accordingly.

Since we are interested in sinusoidal perturbations, we consider the Fourier transform of Eq. (A.1) and find:

$$\Delta \hat{S}(\omega) = \int_{-\infty}^{\infty} \Delta S(t) \mathrm{e}^{-i\omega t} \mathrm{d}t, \tag{A.7}$$

$$\Delta \hat{S}(\omega) = \int_{-\infty}^{\infty} \left(c_p(\infty) f(t) + \int_{0}^{\infty} f(t - t'') \dot{g}(t'') \mathrm{d}t'' \right) \mathrm{e}^{-i\omega t} \mathrm{d}t. \tag{A.8}$$

The Fourier transform of the first term in Eq. (A.8) can be carried out without complications:

$$c_p(\infty) \int_{-\infty}^{\infty} f(t) \mathrm{e}^{-i\omega t} \mathrm{d}t = c_p(\infty) \hat{f}(\omega). \tag{A.9}$$

The second term of Eq. (A.8) can be rewritten as follows:

$$\int_{-\infty}^{\infty} \int_{0}^{\infty} f(t - t'') \dot{g}(t'') \mathrm{e}^{-i\omega t} \mathrm{d}t'' \mathrm{d}t = \int_{0}^{\infty} \dot{g}(t'') \int_{-\infty}^{\infty} f(t - t'') \mathrm{e}^{-i\omega t} \mathrm{d}t \mathrm{d}t''. \tag{A.10}$$

Changing variables again, $t' = t - t''$, the Fourier transform of the second term in Eq. (A.8) can be split into two terms:

$$\begin{aligned}\int_0^\infty \dot{g}(t'')\int_{-\infty}^\infty f(t-t'')\mathrm{e}^{-i\omega t}\mathrm{d}t''\mathrm{d}t &= \int_0^\infty \dot{g}(t'')\int_{-\infty}^\infty f(t')\mathrm{e}^{-i\omega(t'+t'')}\mathrm{d}t'\mathrm{d}t'' \\ &= \int_0^\infty \dot{g}(t'')\mathrm{e}^{-i\omega t''}\mathrm{d}t''\int_{-\infty}^\infty f(t')\mathrm{e}^{-i\omega t'}\mathrm{d}t' \\ &= \hat{f}(\omega)\int_0^\infty \mathrm{e}^{-i\omega t}\dot{g}(t)\mathrm{d}t. \end{aligned} \tag{A.11}$$

This is known as the convolution theorem. From Eqs. (A.11) and (A.9), Eq. (A.7) can be written as

$$\Delta\hat{S}(\omega) = \left(c_p(\infty) + \int_0^\infty \mathrm{e}^{-i\omega t}\dot{g}(t)\mathrm{d}t\right)\hat{f}(\omega), \tag{A.12}$$

where

$$\hat{f}(\omega) = \frac{\hat{T}(\omega)}{T_0} - \frac{\Delta V}{\Delta H}\hat{p}(\omega) \text{ and } \dot{g}(t) = -\Delta c_p \dot{\Psi}(t).$$

The Fourier transform of Eq. (A.2) takes the final form:

$$\Delta\hat{S}(\omega) = \left(c_p(\infty) - \Delta c_p\int_0^\infty \mathrm{e}^{-i\omega t}\dot{\Psi}(t)\mathrm{d}t\right)\left(\frac{\hat{T}(\omega)}{T_0} - \frac{\Delta V}{\Delta H}\hat{p}(\omega)\right) \tag{A.13}$$

$$\Delta\hat{S}(\omega) = c_p(\omega)\left(\frac{\hat{T}(\omega)}{T_0} - \frac{\Delta V}{\Delta H}\hat{p}(\omega)\right). \tag{A.14}$$

Using $\Psi(t) = \exp(-t/\tau)$, the dynamic heat capacity, $c_p(\omega)$, is found to be

$$c_p(\omega) = c_p(\infty) + \frac{\Delta c_p}{\tau}\int_0^\infty \mathrm{e}^{-i\omega t}\mathrm{e}^{-t/\tau}\mathrm{d}t \tag{A.15}$$

$$c_p(\omega) = c_p(\infty) + \Delta c_p\left(\frac{1 - i\omega\tau}{1 + (\omega\tau)^2}\right), \tag{A.16}$$

which has the form of a Debye relaxation term.

REFERENCES

[1] A.L. Hodgkin, A.F. Huxley, A quantitative description of membrane current and its application to conduction and excitation in nerve, J. Physiol. 117 (1952) 500–544.
[2] T. Heimburg, A.D. Jackson, On soliton propagation in biomembranes and nerves, Proc. Natl. Acad. Sci. U.S.A. 102 (2005) 9790–9795.
[3] D.L. Melchior, H.J. Morowitz, J.M. Sturtevant, T.Y. Tsong, Characterization of the plasma membrane of Mycoplasma laidlawii. VII. Phase transitions of membrane liquids, Biochim. Biophys. Acta 219 (1970) 114–122.

[4] J.R. Hazel, Influence of thermal acclimation on membrane lipid composition of rainbow trout liver, Am. J. Physiol. Regul. Integr. Comp. Physiol. 287 (1979) R633–R641.
[5] E.F. DeLong, A.A. Yayanos, Adaptation of the membrane lipids of a deep-sea bacterium to changes in hydrostatic pressure, Science 228 (1985) 1101–1103.
[6] T. Heimburg, Thermal Biophysics of Membranes, Wiley VCH, Berlin, Germany, 2007.
[7] T.Y. Tsong, T.-T. Tsong, E. Kingsley, R. Siliciano, Relaxation phenomena in human erythrocyte suspensions, Biophys. J. 16 (1976) 1091–1104.
[8] T.Y. Tsong, M.I. Kanehisa, Relaxation phenomena in aqueous dispersions of synthetic lecithins, Biochemistry 16 (1977) 2674–2680.
[9] S. Mitaku, T. Date, Anomalies of nanosecond ultrasonic relaxation in the lipid bilayer transition, Biochim. Biophys. Acta 688 (1982) 411–421.
[10] P. Grabitz, V.P. Ivanova, T. Heimburg, Relaxation kinetics of lipid membranes and its relation to the heat capacity, Biophys. J. 82 (2002) 299–309.
[11] W.W. van Osdol, R.L. Biltonen, M.L. Johnson, Measuring the kinetics of membrane phase transition, J. Bioener. Biophys. Methods 20 (1989) 1–46.
[12] T. Heimburg, A.D. Jackson, On the action potential as a propagating density pulse and the role of anesthetics, Biophys. Rev. Lett. 2 (2007) 57–78.
[13] S.S.L. Andersen, A.D. Jackson, T. Heimburg, Towards a thermodynamic theory of nerve pulse propagation, Prog. Neurobiol. 88 (2009) 104–113.
[14] S. Halstenberg, T. Heimburg, T. Hianik, U. Kaatze, R. Krivanek, Cholesterol-induced variations in the volume and enthalpy fluctuations of lipid bilayers, Biophys. J. 75 (1998) 264–271.
[15] W. Schrader, H. Ebel, P. Grabitz, E. Hanke, T. Heimburg, M. Hoeckel, M. Kahle, F. Wente, U. Kaatze, Compressibility of lipid mixtures studied by calorimetry and ultrasonic velocity measurements, J. Phys. Chem. B 106 (2002) 6581–6586.
[16] S. Halstenberg, W. Schrader, P. Das, J.K. Bhattacharjee, U. Kaatze, Critical fluctuations in the domain structure of lipid membranes, J. Chem. Phys. 118 (2003) 5683–5691.
[17] J.K. Bhattacharjee, F.A. Ferrell, Scaling theory of critical ultrasonics near the isotropic-to-nematic transition, Phys. Rev. E 56 (1997) 5549–5552.
[18] H.M. Seeger, M.L. Gudmundsson, T. Heimburg, How anesthetics, neurotransmitters, and antibiotics influence the relaxation processes in lipid membranes, J. Phys. Chem. B 111 (2007) 13858–13866.
[19] W.W. van Osdol, M.L. Johnson, Q. Ye, R.L. Biltonen, Relaxation dynamics of the gel to liquid crystalline transition of phosphatidylcholine bilayers. Effects of chainlength and vesicle size, Biophys. J. 59 (1991) 775–785.
[20] L.D. Landau, E.M. Lifshitz, Fluid Mechanics, Course of Theoretical Physics, vol. 6, second ed., Pergamon Press, Oxford, 1987.
[21] T. Heimburg, A.D. Jackson, Thermodynamics of the nervous impulse, in: K. Nag (Ed.), Structure and Dynamics of Membranous Interfaces, Wiley, Hoboken, NJ, 2008, pp. 317–339.
[22] K.F. Herzfeld, F.O. Rice, Dispersion and absorption of high frequency sound waves, Phys. Rev. 31 (1928) 691–695.
[23] M. Fixman, Viscosity of critical mixtures: dependence on viscosity gradient, J. Chem. Phys. 36 (1962) 310–318.
[24] C.G. Stokes, On the theories of the internal friction of fluids in motion, and of the equilibrium and motion, Trans. Cambridge Phil. Soc. 8 (1845) 287–305.
[25] G. Kirchhoff, Über den Einfluss der Wärmeleitung in einem Gase auf die Schallbewegung, Ann. Phys. 210 (1868) 177–193.
[26] J.F. Nagle, Theory of the main lipid bilayer phase transition, Annu. Rev. Phys. Chem. 31 (1980) 157–196.

[27] H. Ebel, P. Grabitz, T. Heimburg, Enthalpy and volume changes in lipid membranes. I. The proportionality of heat and volume changes in the lipid melting transition and its implication for the elastic constants, J. Phys. Chem. B 105 (2001) 7353–7360.
[28] T. Heimburg, Mechanical aspects of membrane thermodynamics. Estimation of the mechanical properties of lipid membranes close to the chain melting transition from calorimetry, Biochim. Biophys. Acta 1415 (1998) 147–162.
[29] A.H. Wilson, Thermodynamics and Statistical Mechanics, Cambridge University Press, Cambridge, 1957.
[30] M. Barmatz, I. Rudnick, Velocity and attenuation of first sound near the lambda point of helium, Phys. Rev. 170 (1968) 224–238.
[31] A.B. Pippard, Thermodynamic relations applicable near lambda-transition, Philos. Mag. 1 (1956) 473–476.
[32] M.J. Buckingham, W.M. Fairbank, Progress in Low Temperature Physics, North-Holland Publishing Co., Amsterdam, 1961.
[33] T. Heimburg, R.L. Biltonen, A Monte Carlo simulation study of protein-induced heat capacity changes, Biophys. J. 70 (1996) 84–96.

ACCOUNTS
of chemical research

Lipid Ion Channels and the Role of Proteins

LARS D. MOSGAARD AND THOMAS HEIMBURG*
Niels Bohr Institute, University of Copenhagen, Copenhagen, Denmark

RECEIVED ON FEBRUARY 27, 2013

CONSPECTUS

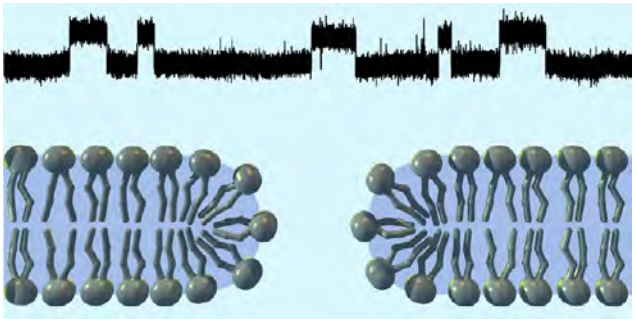

In the absence of proteins, synthetic lipid membranes can display quantized conduction events for ions that are virtually indistinguishable from those of protein channels. The phenomenological similarities between typical conductances are striking: they are of equal order and show similar lifetime distributions and current histograms. They can include conduction bursts, flickering, and multistep conductance. Lipid channels can be gated by voltage and blocked by drugs. They respond to changes in lateral membrane tension and temperature. Thus, they behave like voltage-gated, temperature-gated, and mechano-sensitive protein channels, or like receptors.

The similarity between lipid and protein channels poses an important problem for the interpretation of protein channel data. For example, the Hodgkin–Huxley theory for nerve pulse conduction requires a selective mechanism for the conduction of sodium and potassium ions. To this end, the lipid membrane must act both as a capacitor and as an insulator. Nonselective ion conductance by mechanisms other than the gated protein channels challenges the proposed mechanism for pulse propagation. Nevertheless, textbooks rarely describe the properties of the lipid membrane surrounding the proteins in their discussions of membrane models.

These similarities lead to important questions: Do these similarities in lipid and protein channels result from a common mechanism, or are these similarities fortuitous? What distinguishes protein channels from lipid channels, if anything?

In this Account, we document experimental and theoretical findings that show the similarity between lipid and protein channels. We discuss important cases where protein channel function strongly correlates with the properties of the lipid. Based on statistical thermodynamics simulations, we discuss how such correlations could come about. We suggest that proteins can act as catalysts for lipid channel formation and that this hypothesis can explain some of the unexplained correlations between protein and lipid membrane function.

1. Introduction

The observation of channel-like conduction events in pure lipid membranes is not new but has not received appropriate attention. Yafuso et al. described them in oxidized cholesterol membranes as early as 1974. Further evidence was provided by Antonov and collaborators and by Kaufmann and Silman in the 1980s. It was shown that channel formation is influenced by temperature and pH. Goegelein and Koepsell showed in 1984 that one can block such lipid channels with calcium, and Blicher et al. showed that one can block lipid membrane channels with general anesthetics. They may be mildly selective for ions following the Hofmeister series (the above is reviewed in Heimburg[1]). Further, lipid channels can be gated by voltage.[2] In the past decade, Colombini and collaborators described channel-like events in membranes containing ceramides and sphingolipids.[3]

Synthetic lipid membranes can display melting transitions of their chains.[4] The transition is accompanied by an absorption of heat, and a change in entropy due to the disordering of the lipid chains. Biological membranes possess such melting transitions, too, typically at temperatures about 10 degrees below physiological temperature.[4] Chain

Published on the Web 07/31/2013 www.pubs.acs.org/accounts
10.1021/ar4000604 © 2013 American Chemical Society

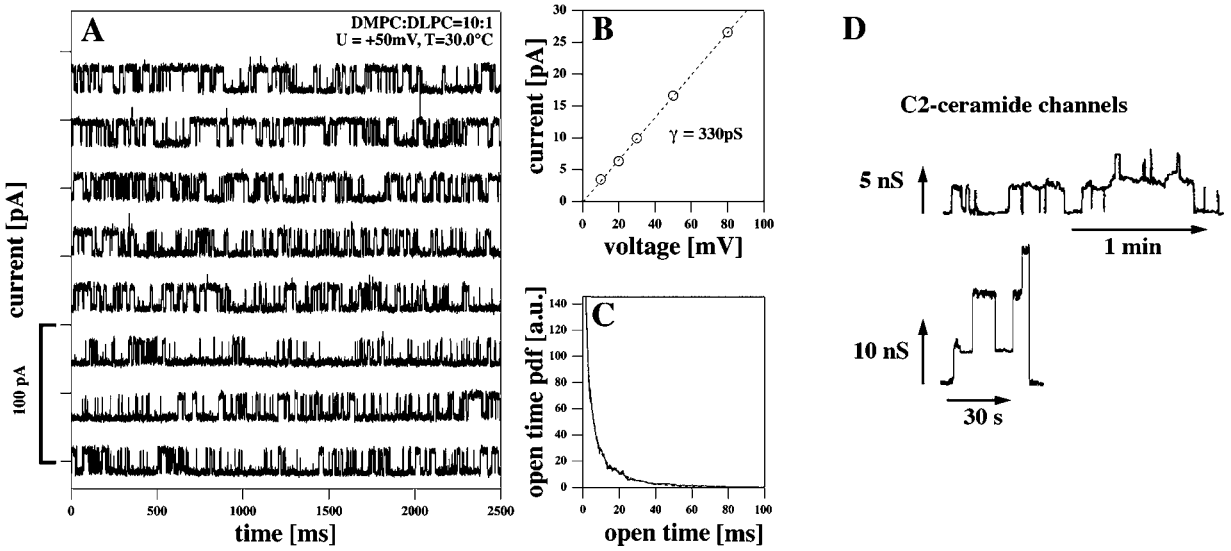

FIGURE 1. Lipid ion channels in a synthetic membrane (DMPC/DLPC = 10:1 in 150 mM KCl, 30 °C). (A) Characteristic current trace recorded at 50 mV. It was stable for more than 30 min. (B) The single-channel $I-V$ profile is linear, resulting in a conductance of 330 pS. (C) Lifetime distribution of the channels. Adapted from from ref 10, Copyright 2012, with permission from Elsevier. (D) Ceramide channels in soybean lipids (asolectin) in 1 M KCl.[3,11] From refs 3 and 11, Copyright 2002 and 2003, with permission from The American Society for Biochemistry and Molecular Biology and Elsevier, respectively.

melting has been described for several bacterial membranes but also for lung surfactant and nerve membranes. Electrophysiological experiments on synthetic membrane suggest that the spontaneous appearance of pores in membranes is related to thermal fluctuations, which are known to approach a maximum in the transition regime. The likelihood of pore opening and the respective open lifetimes are characterized well by the well-known fluctuation–dissipation theorem (FDT)[5] and its applications to membrane pores.[1] In essence, the FDT establishes connections between the fluctuations of extensive variables such as enthalpy, volume and area, and the conjugated susceptibilities: heat capacity, isothermal volume and area compressibility, respectively. For instance, wherever the heat capacity is high, the fluctuations in enthalpy are large. Similarly, large volume and area fluctuations imply a high volume or lateral compressibility. Volume and area fluctuations are strongly coupled to the enthalpy fluctuations.[4] Therefore, the membrane becomes highly compressibly (i.e., soft) close to transition, and the formation of defects is facilitated. For this reason, close to transitions one expects the spontaneous formation of pores in the lipid membrane, and a significant increase of the permeability for ions and small molecules. Such changes in permeability close to transitions were in fact observed experimentally.[1] The presence of melting transitions in biological membranes therefore makes it highly likely that lipid ion channels are also present in living cells. An important implication of the FDT is that fluctuations are directly coupled to fluctuation lifetimes,[6] which implies that the open lifetime of lipid membrane pores is maximum close to the transition.

Changes in experimental conditions can shift the melting point. For instance, drugs such as the insecticide lindane or the anesthetic octanol lower transition temperatures and therefore influence the permeability of membranes.[1] Due to their effect on the physics of membranes, such drugs can "block" lipid channels without binding to any particular receptor. Similarly, hydrostatic pressure shifts transitions upward.[4]

It seems to be increasingly accepted that the composition of lipid membranes can influence the channel activity of proteins.[7] Interestingly, critical phenomena such as the ones described above for synthetic membranes have also been found for protein channels embedded in synthetic lipid membranes. The characteristics of some of these channels are highly correlated with the chain melting transition in the surrounding membrane. For instance, the KcsA potassium channel when reconstituted into a synthetic membrane displays a mean conductance that exactly reflects the heat capacity profile of the membrane.[8] Simultaneously, the open lifetime of the channel is maximum in the membrane transition. Thus, the properties of membranes containing this channel protein accurately reflect the physics of the fluctuations in the lipid membrane. Very similar phenomena were found for the sarcoplasmic reticulum calcium channel.[9]

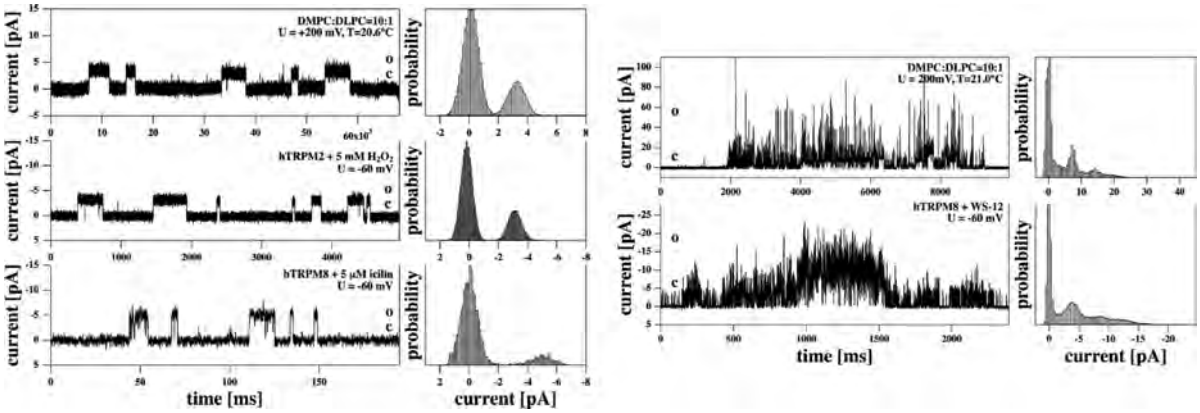

FIGURE 2. Comparison of channel events from synthetic lipid membranes (top) and from protein-containing cell membranes (center, TRPM2; bottom, TRPM8) demonstrate the phenomenological similarity of both stepwise conductance and probability distribution of current events.[10] Conduction burst in a synthetic membrane (top) and in a HEK cell membrane containing the TRPM8 channel (bottom).[10] The current histograms are nearly identical. Reprinted from ref 10, Copyright 2012, with permission from Elsevier.

2. Lipid Ion Channels

2.1. Single Channels in Protein-Free Membranes. Figure 1A shows a typical channel event in a synthetic lipid membrane (DMPC: DLPC = 10:1, 150 mM NaCl) recorded around 30 °C.[10] These channels display a conductance of about 330 pS and lifetimes on the order of 1−100 ms. Such conductances and lifetimes are not untypical for protein channels, too. In fact, it would be difficult to distinguish the traces in Figure 1 from protein channels in the absence of independent information available. Further examples were reviewed in Heimburg.[1] Figure 1D shows recordings from so-called ceramide channels. Such channels have been investigated in much detail by the Colombini group from the University of Maryland. Channel events in protein-free membranes containing a small amount of ceramide lipids look similar to the lipid pores in Figure 1. Ceramide channels seem to be distinct from other lipid membrane pores since they display much larger conductances and much longer lifetimes than the data in Figure 1A−C.

2.2. Comparison of Lipid and TRP Protein Ion Channels. The literature contains copious examples for protein channel conductance. As mentioned, many of these data are similar in appearance to the lipid channels. This is demonstrated in the following for TRP channels that were overexpressed in human embryonic kidney (HEK) cells.[10] Figure 2 (left) shows short but representative time-segments of channel recordings from a synthetic lipid preparation (top trace), HEK cells containing the TRPM2 (center trace) and TRPM8 (bottom trace) channels (data from Laub et al.[10]). The order of magnitude of the conductance and the current histograms are very similar. Equally similar traces were found for conduction bursts, flickering traces and other phenomena typical for protein conductance.[10] On the right-hand side of Figure 2, a conduction burst in a synthetic membrane (top) is compared to a burst of the TRPM8 channel activity. The current histogram of the two bursts is very similar, both in absolute currents and in the peak areas. It is again difficult to distinguish the data from the synthetic and cell membranes without independent experimental evidence. It is likely that this statement is generally true.

2.3. Pore Geometries. Lipid pores are transient in time and probably due to area fluctuations in the membrane. There exists no experimental evidence for a well-defined pore geometry and size from electron microscopy or other nanoscopic techniques. Glaser and collaborators[12] proposed two kinds of pores: the hydrophobic pore shown in Figure 3A (left) and the hydrophilic pore shown in Figure 3A (right). The hydrophobic pore is a area density fluctuation without major rearrangement of its lipids. Water in the pore is in contact with hydrophobic hydrocarbon chains. The hydrophilic pore (Figure 3A, right) is linked to a rearrangement of the lipids so that contact with water is avoided. Such pores are thought to be more stable and long-lived. Based on elastic considerations, the pore diameter was estimated to be of order 1 nm,[12] suggesting a well-defined channel conductance. Both, hydrophilic and hydrophobic pores have been found in MD simulations[13] (Figure 3B). Application of voltage across the membrane initially forms a hydrophobic pore which subsequently develops into a hydrophilic pore. Due to the lack of direct observation, these geometries must be regarded as tentative. The proposed structure of ceramide channels consists rather of a stable geometry with well-defined molecular order. Considering their longer lifetimes and larger conductance, it is not clear whether these

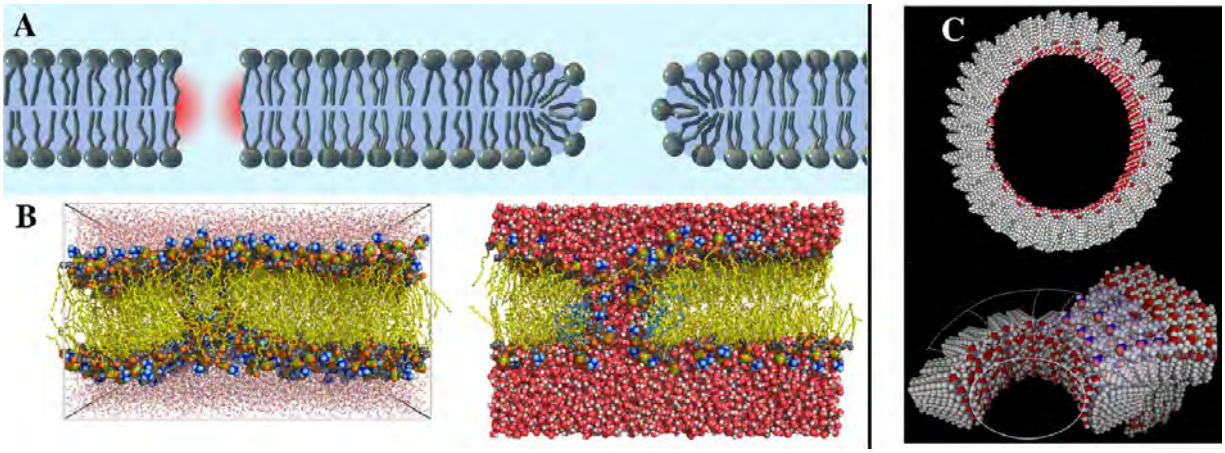

FIGURE 3. Hydrophobic and hydrophilic pores in lipid membranes. (A) Schematic drawing with hydrophobic pore on the left and hydrophilic pore on the right. (B) Molecular dynamics simulation of a membrane subject to a voltage difference of 2 V.[13] Reprinted from ref 13, Copyright 2008, with permission from Elsevier. Here, the hydrophobic pore (left) consists of a file of water molecules spanning through the membrane. Such pores are thought to be dynamic structures caused by fluctuations in the lipid bilayer. (C) Hypothetical structure of a ceramide channel.[14] Reprinted from ref 14, Copyright 2011, with permission from Elsevier.

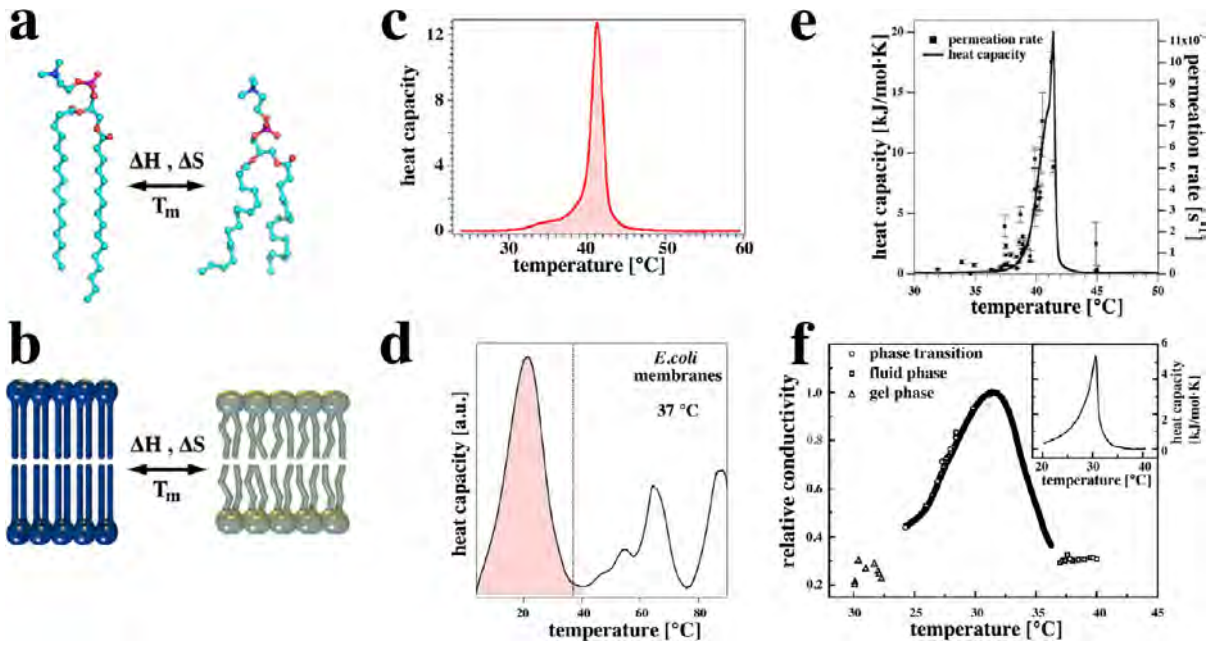

FIGURE 4. Melting of lipid membranes and permeability changes. (a, b) Schematic representation of the melting process in a lipid membrane.[4] (c) Calorimetric melting profile of a dipalmitoyl phosphatidylcholine (DPPC) membrane. (d) Melting profile of native *E. coli* membranes.[4] The peak shaded in red is the lipid melting peak, situated about 10−15 degrees below growth temperature (dashed line). (e) Permeability of a synthetic lipid membrane for a fluorescence dye compared to its heat capacity.[15] Reprinted from ref 15, Copyright 2009, with permission from Elsevier. (f) Conductance of a synthetic lipid membrane for ions compared to the heat capacity.[16] Reprinted from ref 16, Copyright 2009, with permission from Elsevier.

events are comparable to the lipid ion channel events described in Figure 1.

3. Transitions in the Membrane and Permeability Maxima

Lipid membranes display melting transitions. In these transitions, the membranes remain intact, but enthalpy ΔH and entropy ΔS change at a defined temperature $T_m = \Delta H/\Delta S$. This is schematically displayed in Figure 4a, b. One can investigate such transitions in calorimetry by recoding the heat capacity, $c_p = (dH/dT)_p$. The heat capacity profile shown in panel (c) is from synthetic vesicles of dipalmitoyl phosphatidylcholine (the lipid in panel a) with a melting temperature of ~41 °C. Panel (d) (shaded area) shows the c_p-profile of

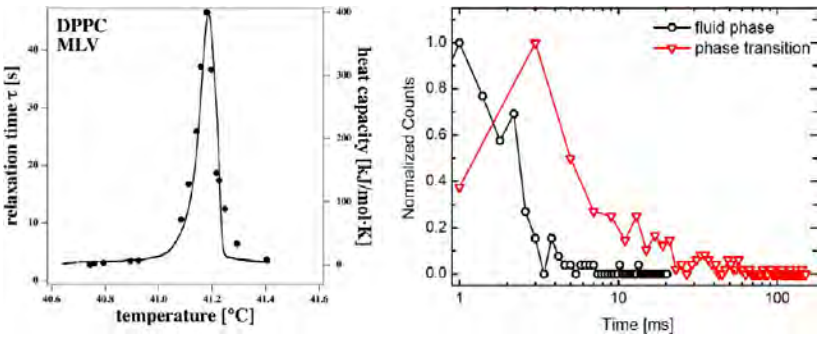

FIGURE 5. Left: Relaxation time scale of DPPC MLV compared to the heat capacity.[6] Right: Open lifetimes of channel events in a D15PC: DOPC = 95:5 mixture in the fluid phase and in the phase transition.[16] Reprinted from ref 16, Copyright 2009, with permission from Elsevier.

native *E. coli* membranes with a lipid melting peak close to physiological temperatures ($T_m \approx 22$ °C). This has also been reported for other bacterial membranes, for lung surfactant,[4] and for nerve membranes from rat brains, where the heat capacity maximum is always found in the range from 20 to 30 °C. It seems likely that chain melting close to physiological conditions is a generic property of cells. The integrated heat capacity yields both ΔH and the ΔS. Simultaneously, the volume of the membrane changes by about 4% and the area by about 24%.[17] The fluctuation−dissipation theorem (FDT) states that heat capacity c_p, volume and area compressibility κ_T^V and κ_T^A are given by

$$c_p = \frac{\langle H^2\rangle - \langle H\rangle^2}{RT^2}; \quad \kappa_T^V = \frac{\langle V^2\rangle - \langle V\rangle^2}{\langle V\rangle RT};$$

$$\kappa_T^A = \frac{\langle A^2\rangle - \langle A\rangle^2}{\langle A\rangle RT} \tag{1}$$

that is, they are related to enthalpy, volume, and area fluctuations.

Empirically, it was found that

$$\kappa_T^V = \gamma_V c_p; \quad \kappa_T^A = \gamma_A c_p \tag{2}$$

where $\gamma_V \approx 7.8 \times 10^{-10}$m^2/N and $\gamma_A \approx 0.89$ m/N are material constants.[17−19] As a consequence, membranes become very soft in transitions. The application of the FDT to lipid membranes is discussed in detail by Heimburg.[1]

Several previous studies reported that membranes become more permeable in the transition regime.[1] In order to create a pore, work $\Delta W(a)$ has to be performed:

$$\Delta W(a) = \frac{1}{2\kappa_T^A A_0} a^2 \tag{3}$$

where a is the area of the pore and A_0 is the area of the overall membrane. Here, the line tension of the pore circumference[12,20] is not explicitly contained for reasons discussed in Blicher et al.[15] Since κ_T^A has a maximum in the transition, the likelihood of finding a pore is enhanced and the permeability is high. This is shown for fluorescence dyes and ions in Figure 4e and f.

3.1. Relaxation Time Scales and Lipid Channel Lifetimes. The lifetime of fluctuations is also described by the fluctuation−dissipation theorem.[5] Generally, larger fluctuations are associated with larger time scales. In the case of single lipid membranes close to transitions, it has been shown that relaxation times are reasonably well described by an single-exponential process with a time constant of

$$\tau = \frac{T^2}{L} \Delta c_p \tag{4}$$

where L is a phenomenological coefficient with $L = 6.6 \times 10^8$ J K/mol s for multilamellar lipid vesicles (MLV) of synthetic lipids.[6] In nonequilibrium thermodynamics, it is assumed that the relaxation and the fluctuation time scales are identical. Therefore, the time scale τ is intimately related to the mean open time of lipid channels. Figure 5 (left) shows that DPPC MLV display a Δc_p maximum of about 400 kJ/(mol K), leading to a relaxation time τ of 45 s. The half width of this transition is of the order of 0.05−0.1 K.

The half width of the heat capacity profile of lung surfactant is much broader (order 10 K). The heat capacity at maximum is about 300 times smaller than for DPPC, and one expects a maximum relaxation time on the order of 100 ms. Similar numbers are expected for the transitions in *E. coli* and other bacterial membranes, and the membranes of nerves. Interestingly, 1−100 ms is the time scale of the open lifetime of protein channels as well as that of lipid channels. The right-hand panel of Figure 5 shows the distribution of lipid channel lifetimes within and above the melting range of a synthetic lipid mixture.[16] It can be seen that the lifetime

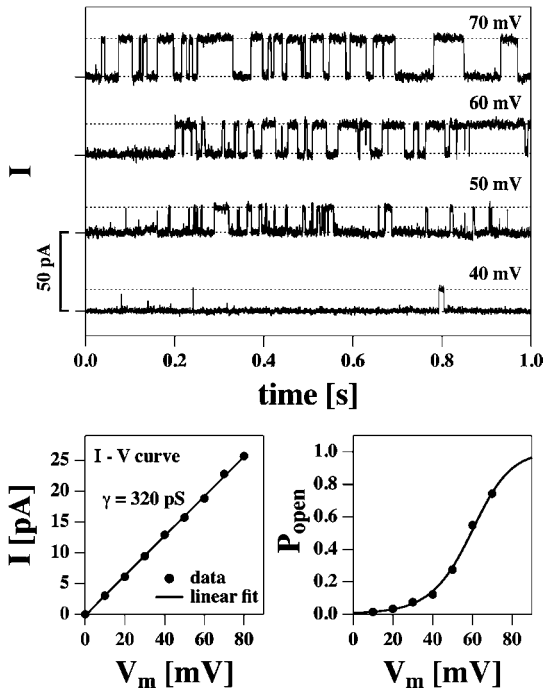

FIGURE 6. Voltage-gating in a DMPC/DLPC = 10:1 membrane at 30 °C in 150 mM KCl. Top: Current traces at four voltages showing an increase of single-channel conductance with voltage and an increased likelihood of channel formation. Bottom, left: The corresponding linear single-channel current–voltage relation indicating a single-channel conductance of $\gamma =$ 320 pS. Bottom, right: Open probability as a function of voltage.

increases 5- to 10-fold in the transition range, which is consistent with the above considerations. Below, we will show that the KcsA potassium channel displays similar dependence on the melting transition in the surrounding membrane.

3.2. Gating of Lipid Channels. The likelihood of finding lipid pores depends on experimental conditions due to the dependence of the melting point on all intensive thermodynamic variables.

The permeability must be considered as primarily due to pore formation. Therefore, the likelihood of finding channels is correlated with changes in the intensive variables. In analogy with the nomenclature of protein channels, we will call this effect "gating". Gating implies that the open probability of lipid channels depends in a very general sense on the intensive thermodynamic variables. It has been shown experimentally that lipid channels can be gated by[1]

- temperature (temperature-sensing)
- lateral pressure or tension (mechanosensitive-gating)
- general anesthetics (gating by drugs)
- calcium and pH, i.e., chemical potential differences of calcium and protons
- voltage (voltage-gating), discussed below

Note that these variables have also been reported to control protein channels, for example, the temperature sensitive TRP channels,[21] mechanosensitive channels,[22] the effect of general anesthetics on the nicotinic acetyl choline receptor,[23] calcium channels,[9] and the pH-dependent[8] and voltage-gated[7] KcsA potassium channels.

3.3. The Effect of Voltage. At suitable voltages, one can induce single channel events in the synthetic membrane (Figure 6). In contrast to the conductance of the overall membrane, the single channel conductance is constant and leads to a linear current–voltage relation. The open probability increases as a function of voltage.

The phase diagram of a membrane as a function of voltage was recently given by Heimburg.[24] If one regards the membrane as a capacitor, one can calculate the force on the membrane due to electrostatic attraction. This force can reduce the thickness of the membrane. It can thus change the melting temperature and potentially create holes above a threshold voltage.[20,25] The electrostatic force, $\mathscr{F}$, exerted by voltage on a planar membrane is given by

$$\mathscr{F} = \frac{1}{2}\frac{C_m {V_m}^2}{D} \tag{5}$$

where C_m is the membrane capacitance, V_m is the transmembrane voltage, and D is the membrane thickness.[24] This force reduces the thickness of the membrane.[2] The electrical work performed on the membrane by a change in thickness from D_1 to D_2 is

$$\Delta W_{el} = \int_{D_1}^{D_2} \mathscr{F} dD \propto {V_m}^2 \tag{6}$$

It can thus be assumed that the free energy of pore formation, ΔG, is related to the square of the voltage and to the elastic constants of the membrane[2] with

$$\Delta G = \Delta G_0 + \alpha {V_m}^2 \tag{7}$$

where ΔG_0 is the free energy difference between open and closed pores in the absence of voltage and α is a constant. ΔG_0 reflects the elastic properties of the membrane that depend on composition, temperature and pressure. For asymmetric membranes one obtains

$$\Delta G = \Delta G_0 + \alpha (V_m - V_0)^2 \tag{8}$$

where the offset voltage V_0 is due to membrane curvature or to a different lipid composition in the two membrane leaflets.[27] The probability, $P_{open}(V_m)$, of

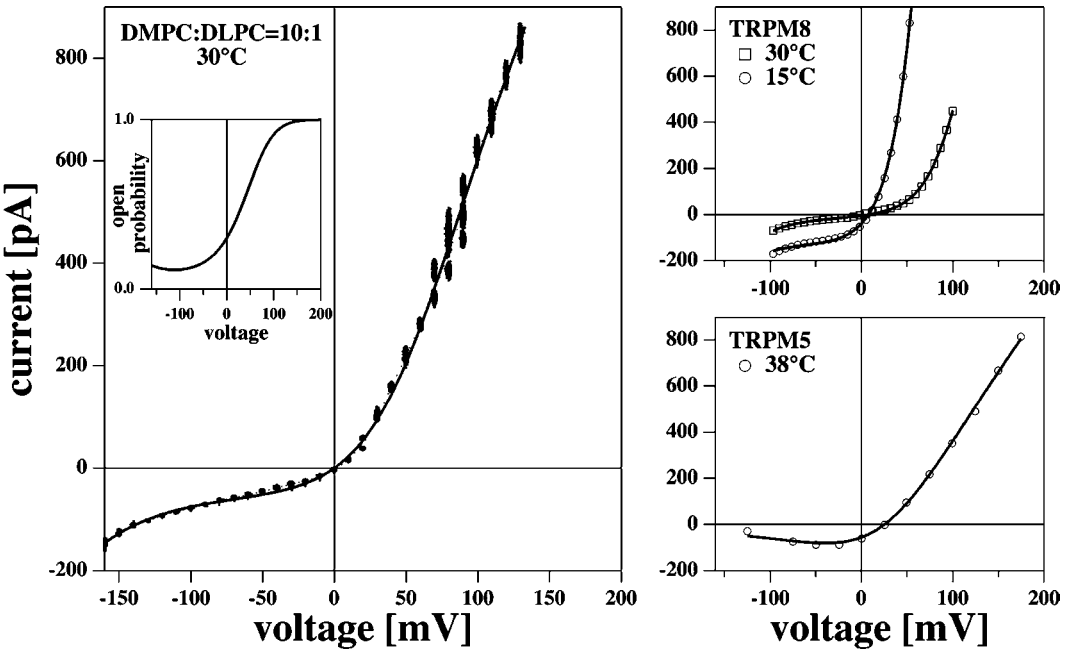

FIGURE 7. Current−voltage relations. Left: A synthetic membrane (DMPC/DLPC = 10:1). The inset is the open probability of a membrane pore. The solid line represents a fit to eq 10 with $E_0 = 0$ V. Right: $I-V$ profiles of TRPM8 channels in HEK cells, adapted from Voets et al.[21] (top panel) and of TRPM5 in HEK cells, adapted from Talavera et al. 2005.[26] The solid lines are fits to eq 10.

finding an open pore in the membrane at a fixed voltage is given by

$$P_{\text{open}}(V_{\text{m}}) = \frac{K(V_{\text{m}})}{1 + K(V_{\text{m}})}; \quad K(V_{\text{m}}) = \exp\left(-\frac{\Delta G}{kT}\right) \qquad (9)$$

where $K(V_{\text{m}})$ is the voltage-dependent equilibrium constant between open and closed states of a single pore.

The current−voltage relation for the lipid membrane is proportional to the likelihood of finding an open channel for a given voltage:

$$I_{\text{m}} = \gamma_{\text{p}} P_{\text{open}}(V_{\text{m}} - E_0) \qquad (10)$$

where γ_{p} is the conductance of a single pore and $E_0 =$ is the Nernst potential. While the voltage V_0 reflects the asymmetry of the membrane, E_0 reflects the asymmetry of the ion concentrations of the buffer solution. If the aqueous buffer is the same on both sides of the membrane, the Nernst potential is zero.

Figure 7 (left) shows the $I-V$ profile of a lipid membrane made of a mixture of DMPC and DLPC[10] and a fit given by the formalism given by eqs 8−10 ($V_0 = -110$ mV, $\gamma_m =$ 6.62 nS, $\Delta G_0 = 5.2$ kJ/mol, and $a = -248$ kJ/mol·V^2). This fit reproduces the experimental profile. For comparison, the right-hand panel of Figure 7 shows the current−voltage relationships of two proteins from the TRP family. Members of this family of ion channels have been reported to respond to environmental stimuli such as temperature, membrane tension, pH, and various drugs.[28] No particular structure for these channels is known, and no very well-defined selectivities for ions have been reported. Figure 7 (right panels) show data for the current−voltage relationship of TRPM8 at two temperatures and TRPM5 adapted from publications of Nilius' group.[21,26] The $I-V$ profiles look quite similar to that obtained from the synthetic membrane. The solid lines in Figure 7 (right panels) are fits to the above formalism using parameters of similar order of magnitude as used for the synthetic membrane. The quality of these fits indicates that the TRP channel conductance is well described as unspecific pore formation in an asymmetric membrane caused by the charging of the membrane capacitor.

4. The Role of Proteins

Here, we consider several cases where proteins and lipid pores display similar dependences on intensive variables.

4.1. Temperature Dependence of Lipid Pores, Temperature Sensing Protein Channels, and van't Hoff Law. Sensitivity to temperature is one of the most prominent properties of the TRP channels.[26] Such channels display a temperature sensitivity over a temperature range of 10 K that is similar to the width of melting transitions in many biomembranes. For instance, the TRPM8 channel is activated at temperatures about 10 degrees below body temperature,

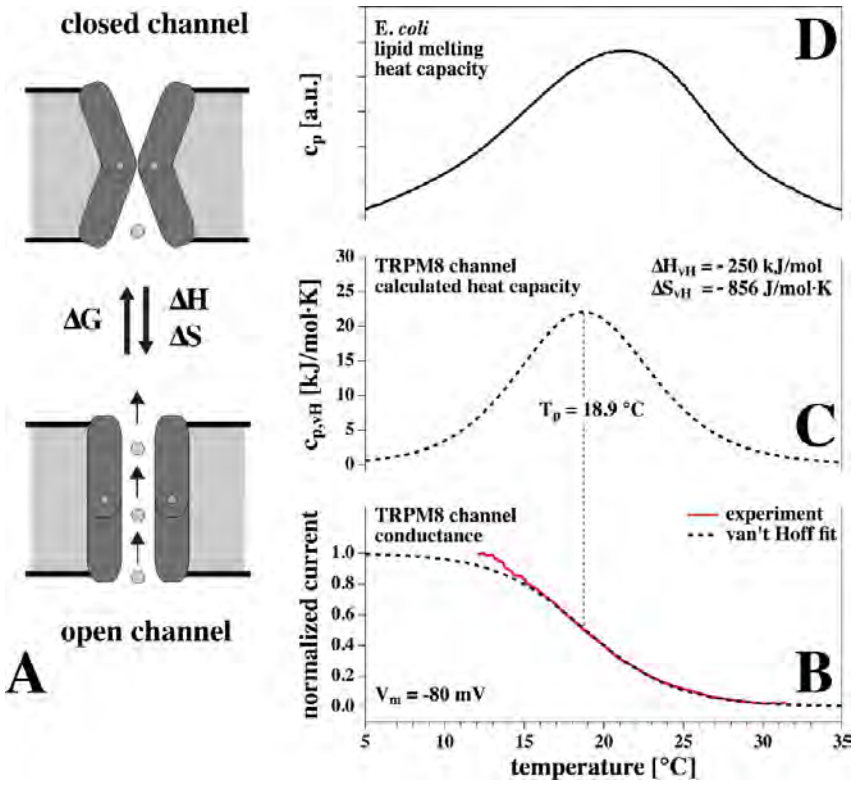

FIGURE 8. (A) Schematic drawing of a possible equilibrium between an open and a closed state of a channel protein. The equilibrium is defined by Gibbs free energy, enthalpy, and entropy differences (ΔG, ΔH, and ΔS, respectively). (B) Van't Hoff analysis of the temperature dependent conductance of a TRPM8 channel in HEK cells at −80 mV (adapted from ref 21). It leads to ΔH of −250 kJ/mol and $\Delta S = -859$ J/mol·K for the two-state equilibrium. (C) From the analysis in panel B one obtains a heat capacity profile of the transition with a midpoint at 18.9 °C. (D) For comparison, the lipid melting profile of native *E. coli* membranes is shown. It displays similar transition width and midpoint.

just where the maximum of the melting profile of many cell membranes is found. While this may be coincidental, the assumption of temperature-sensing macromolecules is problematic as we discuss below.

Assume a channel protein with open and closed states as shown in Figure 8A. These states correspond to distinct protein conformations. The equilibrium constant between the two states is $K = \exp(-\Delta G/RT)$ with $\Delta G = \Delta H - T\Delta S$. The likelihood for finding open and closed states is

$$P_{\text{open}} = \frac{K}{1+K} \quad \text{and} \quad P_{\text{closed}} = \frac{1}{1+K} \qquad (11)$$

respectively (van't Hoff's law). On this basis, Talavera et al. reported activation enthalpies on the order of 200 kJ/mol for TRPM4, TRPM5, TRPM8, and TRPV1 channels.[26] Figure 8B shows a fit of the conductance of a TRPM8 channel[21] to eq 11. The corresponding transition enthalpy is $\Delta H = -250$ kJ/mol, and the entropy $\Delta S = -856$ J/mol·K. Figure 8C displays the corresponding heat capacity of the transition in the protein with a maximum at 18.9 °C. It is given by the derivative of the fit in Figure 8B multiplied with the van't Hoff enthalpy. These numbers are comparable to the total heat of protein unfolding. Typical values are: about 350 kJ/mol for staphylococcal ribonuclease, 200 kJ/mol for lysozyme, and 200−500 kJ/mol for metmyoglobin. However, such transition enthalpies seem highly unlikely for the small conformational change from an open to a closed state. The conformational change from closed to open state of a protein should have a much smaller enthalpy change and should thus have a much smaller temperature dependence. Similarly, the claimed difference in the entropy of closed and open states is too large. According to Boltzmann's equation, $S = k \ln \Omega$ (with Ω being the degeneracy of states), an entropy difference of −856 J/(mol K) corresponds to a change of the number of states by a factor of $\Omega = 5 \times 10^{44}$. A change of this magnitude is plausible for protein denaturation where there is no well-defined unfolded structure but one well-defined native conformation. It is not reasonable for a transition between two states with well-defined function and geometry. Due to cooperative behavior,

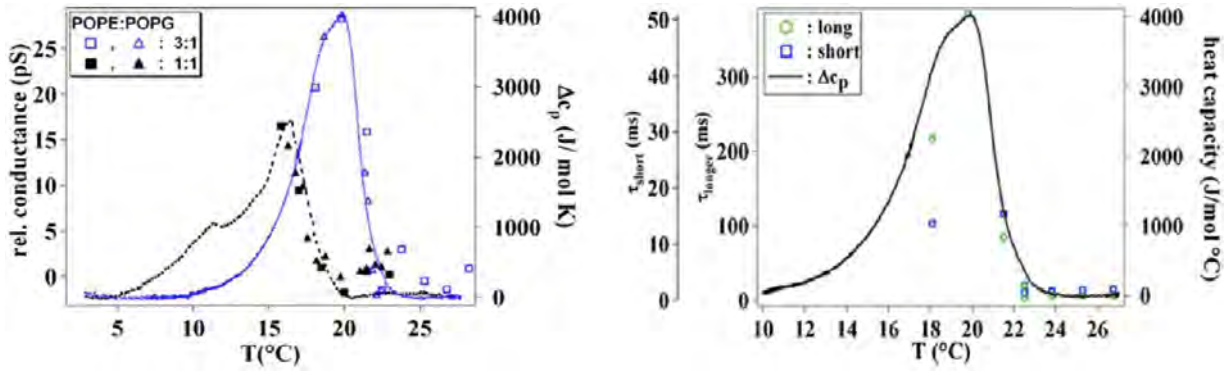

FIGURE 9. Dependence of KcsA channels on the phase transition of its host membrane. Left: The conductance of the channel in two lipid mixtures (symbols) compared to the respective heat capacity profile of the lipids (lines). Right: Open lifetimes of the KscA-channel (symbols) compared to the heat capacity profile (line).[8] Adapted from ref 8, Copyright 2010, with permission from Elsevier.

however, the melting of the lipid membrane can easily have enthalpies and entropies of the above order. Figure 8D shows the experimental melting profile of *E. coli* membranes. The activation profile of TRPM8 channels is apparently quite consistent with the melting profile of a cell membrane.

4.2. Channel Proteins and Phase Transitions in the Lipid Membrane. The KcsA potassium channels are pH- and voltage-gated. In order to measure their properties they are frequently reconstituted into synthetic membranes such as POPE/POPG = 3:1 mol/mol.[8] It is unclear why this particular lipid mixture is often chosen. Measurement of the heat capacity reveals that this lipid mixture has a melting profile with a maximum close to room temperature (blue line in Figure 9, left). Interestingly, the measurement of the mean conductance of the KcsA channel reconstituted into this membrane (blue symbols) exactly follows the heat capacity profile. This is not accidental, since a change in the lipid composition to POPE/POPG = 1:1 reveals that the conductance profile of the channel shifts in the same manner as the heat capacity curve (black symbols). A similar observation can be made for the KcsA channel open times. Typically, the open time distribution is fitted with a biexponential yielding two time constants. These two time constants are plotted in Figure 9 (right) for the POPE/POPG = 3:1 mixture as a function of temperature and compared with the respective heat capacity profiles. It was found that the lifetimes also follow the heat capacity profile. Very similar behavior was found for the sarcoplasmic reticulum calcium channel reconstituted into POPE/POPC mixtures at different ratios.[9] Close to the largest heat capacity events of the lipid mixture, the channel displayed maximum activity (highest conductance) and the longest open times.

The behavior described above is expected from the fluctuation dissipation theorem for the lipid transition itself. Both mean conductance and the lifetimes of conduction events accurately reflect the physics of the lipid membrane. Interestingly, in the case of the KcsA channel the conductance (and thus channel activity) is related to the total amount of protein in the membrane and is still inhibited by the potassium channel blocker tetraethylammonium (TEA). Channel conductance in these systems is apparently a property of the lipid−protein ensemble. In the following, we suggest one possible description for this behavior.

4.3. A Possible Catalytic Role of Membrane Proteins. There is ample evidence in the literature that membrane proteins can influence the thermodynamic properties of lipid membranes. This is true for both integral and peripheral proteins. Figure 10 (center, top) shows the calorimetric profiles of the band 3 protein of erythrocytes, and of cytochrome b_5 (Figure 10, center bottom) reconstituted into synthetic lipid membranes.[29,30] While band 3 protein increases the temperature regime of membrane melting in membranes, cytochrome b_b lowers it. Similar observations have been made with other proteins. *E. coli* membranes display a lipid transition around 22 °C (Figure 4d) while the extracted lipids (in the absence of proteins) display a transition around 12 °C. Since proteins influence melting points, they must also affect lipid membrane fluctuations and the occurrence of lipid channels. The influence of an integral protein on membrane melting is partially dictated by the so-called hydrophobic matching.[31] If the hydrophobic part of the protein is more extended than the hydrocarbon core of a fluid membrane, it will match better with ordered lipids. As a consequence, lipids tend to be more gel-like at the interface of the protein.[32] If the proteins have short hydrophobic cores (e.g., gramicidin A), it will favor fluid lipids in its vicinity (Figure 10, left). The first class of proteins will shift melting events toward higher temperatures, while the second class

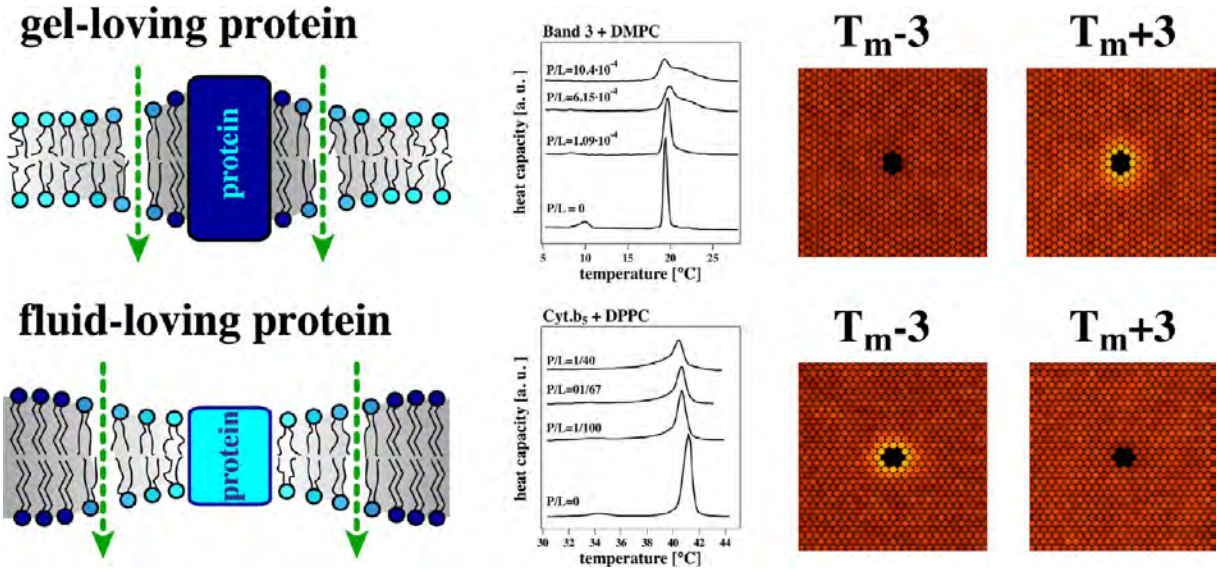

FIGURE 10. Interaction of proteins with lipid membranes and hydrophobic matching. The top row refers to a protein that favors the solid state, while the bottom row refers to a protein favoring the liquid state. Left: Schematic drawing of the lipid arrangement around proteins. Center: The influence of proteins on the heat capacity profile of a synthetic membrane (top, band 3 protein of erythrocytes in DMPC shifts heat capacity profiles toward higher temperatures; bottom, cytochrome b_5 in DPPC shifts c_p profiles toward lower temperatures). Right: Monte Carlo simulations of the local fluctuations (yellow indicates larger fluctuations) of the lipid membrane close to the protein. Top: Fluctuations are enhanced at the protein interface above the melting temperature T_m and unaffected below. Bottom: Fluctuations are enhanced below T_m and unaffected above the transition.

will shift it toward lower temperatures. This is shown for the experimental examples band 3 protein and cytochrome b_5 (Figure 10, center). Peripheral proteins can shift transitions, for instance by shielding electrostatic charges on the surface. If a protein that matches the gel state of the membrane is located in a fluid membrane, it tends to surround itself by a gel lipid layer. As a consequence, there is a regime of high fluctuations near the protein[32,33] meaning that both heat capacity and compressibility can be altered close to a protein. For this reason, the presence of a protein has the potential to locally induce lipid pores in its proximity. Another way of stating this is that proteins can catalyze lipid pores at their outer interface. Figure 10 (right) shows Monte Carlo simulations of such a simulation.[32,33] The simulations show a protein (black) in a membrane at temperatures below and above the melting regime. Dark red shades indicate small fluctuations, while bright yellow shades display large fluctuations. It can be seen that a protein that favors the fluid lipid state would tend to create regimes of large fluctuations in its environment at temperatures below the melting temperature (top panels).

It thus seems likely that proteins can catalyze channel activity without being channels themselves. This is due to the effect of the proteins on the cooperative fluctuations in the lipid membrane. It should generally be possible to estimate this effect from the influence of the protein on melting transitions.

5. Summary

The aim of this Account has been to characterize lipid ion channels and to illustrate the similarity of ion conduction events and protein channel activity. We have shown that the appearance of lipid channels is rooted in the fluctuation dissipation theorem. It is thus strictly coupled to the thermodynamics of the membrane and influenced by changes in the thermodynamics variables such as temperature, pressure, voltage, and so forth.

Many (but not all) properties of protein channels are practically indistinguishable from lipid channels. These include:

- Single channel conductances and lifetimes.
- The current–voltage relations of some proteins such as TRPM8 and the synthetic membrane.
- The activation of TRP channels by temperature.
- The conductance and the lifetimes of KcsA and calcium channels embedded in membranes with transitions. However, a few important properties are difficult to reconcile with the pure lipid membrane:
- The effect of mutations in the protein.
- The action of strong poisons such as tetrodotoxin or tetraethylammonium. Tedrodotoxin in high concentrations (mM regime) only displays a very minor influence on the melting profiles of zwitterionic membranes (unpublished data from Master's thesis of S. B. Madsen, NBI 2012).

- The selectivity of the ion conduction, for instance, of the potassium channel (about 10 000 times higher conductance for potassium over sodium). Lipid channels seem to display a mild selectivity only, following the Hofmeister sequence.[34]

Nevertheless, there exist a number of cases where one can demonstrate clear correlations of protein behavior with the lipid membrane physics, in particular the KcsA channels and calcium channels.

It seems likely that a view will eventually emerge in which the conductance of biomembrane is seen as a feature of a lipid−protein ensemble rather than as a feature of single proteins. This implies a strong coupling to the macroscopic thermodynamics of the biological membrane as a whole.

Thanks to Andrew D. Jackson from the Niels Bohr International Academy for a critical reading of the manuscript. This work was supported by the Villum Foundation (VKR022130).

BIOGRAPHICAL INFORMATION

Lars Dalskov Mosgaard (*1986) is a Ph.D. student in the Membrane Biophysics Group, where he also received his Master's in 2011. He focusses on theoretical aspects of membrane fluctuations.

Thomas Heimburg (*1960) is the head of the Membrane Biophysics Group at the Niels Bohr Institute of the University of Copenhagen in Copenhagen. He graduated in 1989 under the supervision of Derek Marsh at the Max Planck Institute (MPI) for Biophysical Chemistry in Göttingen, Germany. From 1989 to 1990, he was a postdoctoral fellow with Rodney Biltonen in Charlottesville (VA), where he also was a guest lecturer in 1992. In 1997, he received a Heisenberg fellowship of the German Science Foundation. From 1997 to 2003, he headed an independent research group at the MPI in Göttingen. He has been an associate professor at the University of Copenhagen since 2003. The focus of his work is the thermodynamics of biomembranes. He authored a textbook on "Thermal Biophysics of Membranes" in 2007.

FOOTNOTES

*To whom correspondence should be addressed. E-mail: theimbu@nbi.dk.
The authors declare no competing financial interest.

REFERENCES

1 Heimburg, T. Lipid ion channels. *Biophys. Chem.* **2010**, *150*, 2–22.
2 Blicher, A.; Heimburg, T. Voltage-gated lipid ion channels. PLOS ONE **2013**, *8*, e65707.
3 Siskind, L. J.; Kolesnick, R. N.; Colombini, M. Ceramide channels increase the permeability of the mitochondrial outer membrane to small proteins. *J. Biol. Chem.* **2002**, *277*, 26796–26803.
4 Heimburg, T. *Thermal biophysics of membranes*; Wiley VCH: Berlin, Germany, 2007.
5 Kubo, R. The fluctuation-dissipation theorem. *Rep. Prog. Phys.* **1966**, *29*, 255–284.
6 Grabitz, P.; Ivanova, V. P.; Heimburg, T. Relaxation kinetics of lipid membranes and its relation to the heat capacity. *Biophys. J.* **2002**, *82*, 299–309.
7 Schmidt, D.; Jiang, Q.-X.; MacKinnon, R. Phospholipids and the origin of cationic gating charges in voltage sensors. *Nature* **2006**, *444*, 775–779.
8 Seeger, H. M.; Alessandrini, A.; Facci, P. KcsA Redistribution Upon Lipid Domain Formation in Supported Lipid Bilayers and its Functional Implications. *Biophys. J.* **2010**, *98*, 371a.
9 Cannon, B.; Hermansson, M.; Györke, S.; Somerharju, P.; Virtanen, J. A. Regulation of calcium channel activity by lipid domain formation in planar lipid bilayers. *Biophys. J.* **2003**, *85*, 933–942.
10 Laub, K. R.; Witschas, K.; Blicher, A.; Madsen, S. B.; Lückhoff, A.; Heimburg, T. Comparing ion conductance recordings of synthetic lipid bilayers with cell membranes containing TRP channels. *Biochim. Biophys. Acta* **2012**, *1818*, 1–12.
11 Siskind, L. J.; Davoody, A.; Lewin, N.; Marshall, S.; Colombini, M. Enlargement and contracture of C2-ceramide channels. *Biophys. J.* **2003**, *85*, 1560–1575.
12 Glaser, R. W.; Leikin, S. L.; Chernomordik, L. V.; Pastushenko, V. F.; Sokirko, A. I. Reversible breakdown of lipid bilayers: Formation and evolution of pores. *Biochim. Biophys. Acta* **1988**, *940*, 275–287.
13 Böckmann, R.; de Groot, R.; Kakorin, S.; Neumann, E.; Grubmüller, H. Kinetics, Statistics, and Energetics of Lipid Membrane Electroporation Studied by Molecular Dynamics Simulations. *Biophys. J.* **2008**, *95*, 1837–1850.
14 Samanta, S.; Stiban, J.; Maugel, T. K.; Colombini, M. Visualization of ceramide channels by transmission electron microscopy. *Biochim. Biophys. Acta* **2011**, *1808*, 1196–1201.
15 Blicher, A.; Wodzinska, K.; Fidorra, M.; Winterhalter, M.; Heimburg, T. The temperature dependence of lipid membrane permeability, its quantized nature, and the influence of anesthetics. *Biophys. J.* **2009**, *96*, 4581–4591.
16 Wunderlich, B.; Leirer, C.; Idzko, A.; Keyser, U. F.; Myles, V.; Heimburg, T.; Schneider, M. Phase state dependent current fluctuations in pure lipid membranes. *Biophys. J.* **2009**, *96*, 4592–4597.
17 Heimburg, T. Mechanical aspects of membrane thermodynamics. Estimation of the mechanical properties of lipid membranes close to the chain melting transition from calorimetry. *Biochim. Biophys. Acta* **1998**, *1415*, 147–162.
18 Ebel, H.; Grabitz, P.; Heimburg, T. Enthalpy and volume changes in lipid membranes. I. The proportionality of heat and volume changes in the lipid melting transition and its implication for the elastic constants. *J. Phys. Chem. B* **2001**, *105*, 7353–7360.
19 Pedersen, U. R.; Peters, G. H.; der, T. B. S.; Dyre, J. C. Correlated volume-energy fluctuations of phospholipid membranes: A simulation study. *J. Phys. Chem. B* **2010**, *114*, 2124–2130.
20 Winterhalter, M.; Helfrich, W. Effect of voltage on pores in membranes. *Phys. Rev. A* **1987**, *36*, 5874–5876.
21 Voets, T.; Droogmans, G.; Wissenbach, U.; Janssens, A.; Flockerzi, V.; Nilius, B. The principle of temperature-dependent gating in cold- and heat-sensitive TRP channels. *Nature* **2004**, *430*, 748–754.
22 Suchyna, T. M.; Tape, S. E.; Koeppe, R. E., II; Andersen, O. S.; Sachs, F.; Gottlieb, P. A. Bilayer-dependent inhibition of mechanosensitive channels by neuroactive peptide enantiomers. *Nature* **2004**, *430*, 235–240.
23 Bradley, R. J.; Sterz, R.; Peper, K. The effects of alcohols and diols at the nicotinic acetylcholine receptor of the neuromuscular junction. *Brain Res.* **1984**, *295*, 101–112.
24 Heimburg, T. The capacitance and electromechanical coupling of lipid membranes close to transitions. The effect of electrostriction. *Biophys. J.* **2012**, *103*, 918–929.
25 Crowley, J. M. Electrical breakdown of bimolecular lipid membranes as an electromechanical instability. *Biophys. J.* **1973**, *13*, 711–724.
26 Talavera, K.; Yasumatsu, K.; Voets, T.; Droogmans, G.; Shigemura, N.; Ninomiya, Y.; Margolskee, R. F.; Nilius, B. Heat activation of TRPM5 underlies thermal sensitivity of sweet taste. *Nature* **2005**, *438*, 1022–1025.
27 Alvarez, O.; Latorre, R. Voltage-dependent capacitance in lipid bilayers made from monolayers. *Biophys. J.* **1978**, *21*, 1–17.
28 Wu, L.-J.; Sweet, T.-B.; Clapham, D. E. International Union of Basic and Clinical Pharmacology. LXXVI. Current progress in the mammalian TRP ion channel family. *Pharmacol. Rev.* **2010**, *62*, 381–404.
29 Morrow, M. R.; Davis, J. H.; Sharom, F. J.; Lamb, M. P. Studies of the interaction of human erythroyte band 3 with membrane lipids using deuterium nuclear magnetic resonance and differential scanning calorimetry. *Biochim. Biophys. Acta* **1986**, *858*, 13–20.
30 Freire, E.; Markello, T.; Rigell, C.; Holloway, P. W. Calorimetric and fluorescence characterization of interactions between cytochrome b_5 and phosphatidylcholine bilayers. *Biochemistry* **1983**, *28*, 5634–5643.
31 Mouritsen, O. G.; Bloom, M. Mattress model of lipid-protein interactions in membranes. *Biophys. J.* **1984**, *46*, 141–153.
32 Ivanova, V. P.; Makarov, I. M.; Schäffer, T. E.; Heimburg, T. Analizing heat capacity profiles of peptide-containing membranes: Cluster formation of Gramicidin A. *Biophys. J.* **2003**, *84*, 2427–2439.
33 Seeger, H.; Fidorra, M.; Heimburg, T. Domain size and fluctuations at domain interfaces in lipid mixtures. *Macromol. Symp.* **2005**, *219*, 85–96.
34 Antonov, V. F.; Anosov, A. A.; Norik, V. P.; Smirnova, E. Y. Soft perforation of planar bilayer lipid membranes of dipalmitoylphosphatidylcholine at the temperature of the phase transition from the liquid crystalline to gel state. *Eur. Biophys. J.* **2005**, *34*, 155–162.

THE JOURNAL OF CHEMICAL PHYSICS **139**, 125101 (2013)

Fluctuations of systems in finite heat reservoirs with applications to phase transitions in lipid membranes

Lars D. Mosgaard, Andrew D. Jackson, and Thomas Heimburg[a)]
The Niels Bohr Institute, University of Copenhagen, Blegdamsvej 17, 2100 Copenhagen Ø, Denmark

(Received 16 May 2013; accepted 6 September 2013; published online 25 September 2013)

In an adiabatically shielded system, the total enthalpy is conserved. Enthalpy fluctuations of an arbitrarily chosen subsystem must be buffered by the remainder of the total system which serves as a heat reservoir. The magnitude of these fluctuations depends on the size of the reservoir. This leads to various interesting consequences for the physical behavior of the subsystem. As an example, we treat a lipid membrane with a phase transition that is embedded in an aqueous reservoir. We find that large fluctuations are attenuated when the reservoir has finite size. This has consequences for the compressibility of the membrane since volume and area fluctuations are also attenuated. We compare the equilibrium fluctuations of subsystems in finite reservoirs with those in periodically driven systems. In such systems, the subsystem has only finite time available to exchange heat with the surrounding medium. A larger frequency therefore reduces the volume of the accessible heat reservoir. Consequently, the fluctuations of the subsystem display a frequency dependence. While this work is of particular interest for a subsystem displaying a transition such as a lipid membrane, some of the results are of a generic nature and may contribute to a better understanding of relaxation processes in general. © *2013 AIP Publishing LLC*. [http://dx.doi.org/10.1063/1.4821837]

INTRODUCTION

The enthalpy fluctuations of an adiabatically shielded system are zero by definition. The enthalpy of arbitrary subsystems contained within the total system can only fluctuate by the exchange of heat with the rest of the system which we call "the reservoir." In a simple homogeneous system, this leads to temperature fluctuations in both the subsystem and the "reservoir" that are trivially related and that depend only on the size of the two parts of the system. An example would be enthalpy and temperature fluctuations in a small water volume that is embedded into a larger water reservoir of finite size. One can also consider cases where the subsystem is of different physical nature than the reservoir. Such a subsystem could be a particular vibrational mode in a macromolecule that couples to the rest of the molecule that serves as a reservoir. One may also consider subsystems that are spatially separated from the reservoir, e.g., macromolecules or membranes dissolved in an aqueous buffer. The purpose of this paper is to treat this problem in all generality and apply it to the particularly interesting case of a subsystem that can undergo a phase transition while embedded in a homogeneous medium that displays no transition. In particular, we discuss the case of a lipid membrane with a melting transition when the membrane is in contact with a finite aqueous volume that serves as a heat reservoir.

When varying temperature, lipid membranes display cooperative melting transitions in which both enthalpy and entropy of the individual molecules change at a melting temperature, T_m.[1] At this temperature, the heat capacity has a maximum. According to the fluctuation-dissipation theorem, at constant temperature the heat capacity is proportional to the enthalpy fluctuations of the membrane and closely related to the fluctuation time-scales.

Heat capacity is typically measured in a differential scanning calorimeter (DSC). A DSC controls the temperature very precisely and records the heat absorbed by the sample when the temperature is changed. Therefore, the temperature of the reservoir is fixed by the instrumental setup, which is intended to behave like an infinite reservoir with constant temperature. In finite adiabatic systems (with constant total enthalpy), however, the temperature of the reservoir is not constant because it exchanges heat with the subsystem due to fluctuations. Consequently, there are fluctuations of the reservoir temperature that are completely correlated with the enthalpy fluctuations of the subsystem (here, the membrane). Thus, the temperature of the reservoir is only constant on average with fluctuations that can be either large or small depending on the size of the reservoir. In this publication, we show that the size of the (water) reservoir has a significant effect on the magnitude of the fluctuations and the relaxation time scales of the subsystem (the lipid membrane).

There have been very few attempts to model systems in a finite reservoir,[2,3] and these are of limited generality and not applicable to the lipid membrane system. The lipid membrane is distinct from many other systems due to its pseudo two-dimensional nature. While the membrane is effectively two-dimensional, it is embedded in a three-dimensional reservoir with which it can exchange heat. The overall system thus consists of two coupled systems with a total enthalpy that is constant but fluctuating for each of the two sub-systems. Here, we present a statistical mechanics framework for modeling the lipid melting transition in a finite heat reservoir, i.e.,

a)theimbu@nbi.dk. URL: http://membranes.nbi.dk.

 © 2013 AIP Publishing LLC

Downloaded 25 Sep 2013 to 130.225.212.4. This article is copyrighted as indicated in the abstract. Reuse of AIP content is subject to the terms at: http://jcp.aip.org/about/rights_and_permissions

a membrane in a very small water volume. This problem is of more than academic interest.

The heat capacity c_p is an equilibrium property of a system and therefore does not possess a timescale. When a system is probed for finite times (or when the system is driven by an external periodic force), it may not be possible to establish equilibrium with the entire reservoir. Such non-equilibrium systems can be approximated by an equilibrated adiabatic system consisting of the membrane and a reservoir of finite size. Adiabaticity ensures that the total enthalpy fluctuations of this combined system are precisely zero. The fluctuation-dissipation theorem cannot be used to calculate the heat capacity, and other methods must be used. It is, however, possible to calculate the enthalpy fluctuations for the membrane alone. In the limit of large reservoirs, these fluctuations describe the usual equilibrium heat capacity. For smaller reservoirs unable to support large enthalpy fluctuations, the fluctuations in the enthalpy of the membrane will necessarily be reduced. Such effects should be most pronounced near the maximum of the equilibrium heat capacity. It is very important to point out that this argument holds for all fluctuations of extensive quantities such as volume and area of the subsystem, which are closely related to the enthalpy fluctuations. Therefore, our considerations can be extended to the elastic properties of the subsystem that are determined by the volume and area fluctuations. Our analysis contains a reinterpretation of the adiabatic compressibility.

We note that some authors[4] have performed calculations in systems driven externally at a well-defined frequency to determine a "dynamic heat capacity" or "frequency dependent heat capacity." The authors (Nielsen and Dyre[4]) suggest that the frequency dependent heat capacity can be understood as an equilibrium property of the system. In the limit of an arbitrarily small frequency, which corresponds to an infinite reservoir, this dynamic heat capacity is identical to the usual equilibrium heat capacity. For finite frequencies, it is closely related to the enthalpy fluctuations of membranes in finite size reservoirs studied here using Monte Carlo simulations. We discuss our finding of reservoir-size dependent membrane fluctuations in the context of the frequency dependence of the heat capacity of membranes determined in periodic perturbation experiments[5,6] and with the frequency dependence of sound.[7,8] Our findings suggest a close connection between the frequency dependence of both the compressibility and the sound velocity of membranes and the size of the available water reservoir.

THEORY

Fluctuations in finite reservoirs

Enthalpy is strictly conserved in an adiabatically insulated system. Any heat released or absorbed by a subsystem must be exchanged with the surrounding system which we call the reservoir. Consequently, the properties of the reservoir will also fluctuate. Typically, one considers the fluctuations of a small system in an infinite heat reservoir (for the example of a membrane embedded into an aqueous reservoir, see Fig. 1, left) that effectively keeps the temperature of the reservoir constant. This is also the situation in calorimetric experiments. In such an infinite system, temperature fluctuations of the reservoir vanish. This is not the case for a finite system (Fig. 1, right), where care is required to guarantee that the enthalpy is strictly conserved. As shown below, this implies that the temperature of the reservoir fluctuates in correlation with fluctuations of the subsystem.

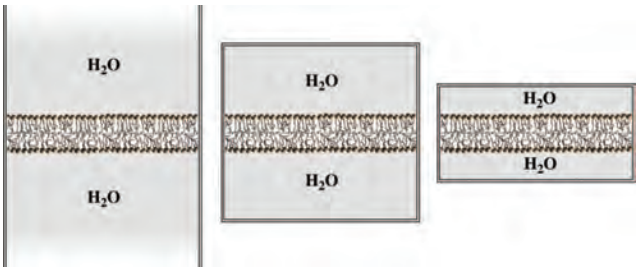

FIG. 1. Three scenarios for a lipid membrane subsystem in an aqueous reservoir: (Left) The membrane is embedded in an infinite water reservoir with constant temperature. (Center and right) The membrane is embedded in a finite size water reservoir. The total system consisting of membrane and water is adiabatically shielded. Thus, enthalpy fluctuations of the membrane now are coupled to both fluctuations in enthalpy and temperature of the water reservoir.

The Gibbs free energy change associated with a state change in the subsystem is

$$\Delta G_s = \Delta H_s - T\Delta S_s, \tag{1}$$

where the index "s" denotes the subsystem. During this change in state, heat is transferred from the subsystem to the reservoir.

The free energy change of the reservoir ΔG_r (the index "r" denoting the reservoir) upon the absorption of the heat $\Delta H_r = -\Delta H_s$ is given by

$$\Delta G_r = \Delta H_r - T\Delta S_r, \tag{2}$$

where ΔH_r is the change in enthalpy of the reservoir and ΔS_r is the associated entropy change in the reservoir. T is the temperature, and $\Delta G = \Delta G_s + \Delta G_r$ the free energy change of the total system. If the reservoir absorbs heat from a fluctuation of the subsystem, the change in the enthalpy of the reservoir is naturally fixed to exactly this amount since the total system conserves enthalpy.

From the local fluctuations of temperature, the change in the reservoir's entropy associated with the transfer of enthalpy internally between the two sub-ensembles can be calculated as follows:

$$c_p^r = T\left(\frac{\partial S_r}{\partial T}\right)_P \quad \Rightarrow \quad \Delta S_r = \int_{T_r^a}^{T_r^b} \frac{c_p^r}{T} dT, \tag{3}$$

where c_p^r is the heat capacity of the reservoir and ΔS_r is the corresponding change in entropy. The heat capacity of the reservoir is assumed to be constant. The reservoir temperature T_r before the change in the state of the subsystem is defined as

Downloaded 25 Sep 2013 to 130.225.212.4. This article is copyrighted as indicated in the abstract. Reuse of AIP content is subject to the terms at: http://jcp.aip.org/about/rights_and_permissions

T_r^a and after the change as T_r^b (with $\langle T_r^a \rangle = \langle T_r^b \rangle = T$, averaged over time, T is the constant temperature of the total system that enters the Boltzmann factors). The entropy change of the reservoir is then given by

$$\Delta S_r = c_p^r \ln \frac{T_r^b}{T_r^a}, \tag{4}$$

where $(T_r^b - T_r^a)$ is the temperature change of the reservoir associated to absorbing a given amount of heat, ΔH_r. Since $c_p^r(T_r^b - T_r^a) = \Delta H_r$ for constant c_p^r, the temperature T_r^b of the reservoir after absorbing ΔH_r is given by

$$T_r^b = \frac{\Delta H_r}{c_p^r} + T_r^a. \tag{5}$$

Using Eq. (4), Eq. (2) can be rewritten as

$$\begin{aligned} \Delta G_r &= \Delta H_r - T c_p^r \ln \frac{T_r^b}{T_r^a} \\ &= \Delta H_r - T c_p^r \ln \left(\frac{\Delta H_r / c_p^r + T_r^a}{T_r^a} \right). \end{aligned} \tag{6}$$

Note that in the limit $c_p^r \to \infty$ the free energy $\Delta G_r \to 0$ independently of the magnitude of ΔH_r.

The probability of a state change in a finite reservoir

We can now determine the acceptance probability of a change in the state of the subsystem in a finite adiabatic system. It is given by

$$p = \frac{K}{1+K}; \quad K = \exp\left(-\frac{\Delta G_s + \Delta G_r}{RT} \right), \tag{7}$$

which obeys detailed balance. If it is decided to allow a change of state of the subsystem during a Monte Carlo simulation, the enthalpy associated with this change is absorbed or supplied by the reservoir. T_r^a of the reservoir is updated to the value of T_r^b.

Since $\Delta H_s + \Delta H_r = 0$, the equilibrium is completely governed by entropy differences

$$\Delta G = -T(\Delta S_s + \Delta S_r) = -T \left(\Delta S_s + c_p^r \ln \left(1 - \frac{\Delta H_s}{c_p^r T_r^a} \right) \right). \tag{8}$$

In the limit of $c_p^r \to \infty$, $\Delta G \to \Delta G_s$, as expected. In this limit, the fluctuations of the subsystem are independent of the nature of the reservoir. It is also obvious that for finite c_p^r there is a maximum fluctuation that can be carried by the system: $\Delta G \to \infty$ for $\Delta H_s \to c_p^r \cdot T_r^a$. For vanishing reservoir size, no enthalpy fluctuations in the subsystem are possible.

It is important to point out that the results of these considerations are general. In any physical system, the probability of heat transfer from any arbitrarily chosen subsystem "s" to a reservoir "r" consisting of the rest of the total system is a function of the heat capacity of the reservoir.

MODELING LIPID MEMBRANE FLUCTUATIONS IN A FINITE AQUEOUS RESERVOIR

Below, we apply these concepts to the fluctuations in lipid membranes embedded into an aqueous reservoir. In particular, we consider the case of the cooperative melting transition from an ordered gel to a disordered fluid membrane.

Monte Carlo simulations have frequently been used to analyze the cooperative behavior of membranes. Some early applications can be found in Refs. 9–12. Enthalpy fluctuations are the central element in such simulations. The parameters for the simulation are the melting enthalpies and entropies of the lipid components and the nearest neighbor interactions. The overall temperature is assumed to be constant and identical to that of the aqueous reservoir. The enthalpy fluctuates during the simulation. The heat capacity at constant pressure can be calculated from the enthalpy fluctuations and yields $c_p = (\langle H^2 \rangle - \langle H \rangle^2)/RT^2$, where $\langle \dots \rangle$ denotes the statistical average and T is the (constant) temperature of the reservoir. The fluctuation relation can easily be calculated from a canonical ensemble of N identical systems that are allowed to exchange heat. Due to ergodicity, the time evolution of a single system at absolutely constant temperature leads to the same distribution of states. The latter can be studied in Monte Carlo simulations, and it is meaningful to determine the heat capacity of a membrane from the fluctuations observed in such simulations.

The assumption of constant reservoir temperature and the resultant neglect of reservoir temperature fluctuations are only permissible if the size of the reservoir is infinite. In a finite reservoir, the separation of the membrane from its surroundings is not permissible because the enthalpy fluctuations of the membrane and of the reservoir are correlated. Nevertheless, considering the fluctuations of the membrane alone can provide meaningful insights into the behavior of a membrane. The Gibbs free energy of each configuration of the lipid subsystem consisting of N lipids is given by

$$G_s = G_g + N_f(\Delta H - T\Delta S) + N_{gf}\omega_{gf}, \tag{9}$$

where G_g denotes the Gibbs free energy of the ground state (with all lipids in the ordered gel state). ΔH and ΔS are the molar excess enthalpy and entropy of the melting transition, which can be obtained from the calorimetric experiment. N_f is the number of lipids in the fluid state, N_{gf} is the number of unlike nearest neighbor contacts associated with an interfacial enthalpy contribution. The parameter ω_{gf} describes unlike nearest-neighbor interactions and is typically positive. It is responsible for the cooperativity of the transition, i.e., the half width of the melting transition and the size of domains in the transition regime.

We further assume that each lipid is associated with N_{water} water molecules with which the membrane exchanges heat during the simulation. Further, the lipid chains possess a heat capacity, c_p^{chain}, which is due to vibration within the molecular bonds. This heat capacity is also part of the heat reservoir. Thus, the total heat capacity per lipid of the reservoir, c_p^r, is given by

$$c_p^r = N_{water} \cdot c_p^{water} + c_p^{chain}. \tag{10}$$

Downloaded 25 Sep 2013 to 130.225.212.4. This article is copyrighted as indicated in the abstract. Reuse of AIP content is subject to the terms at: http://jcp.aip.org/about/rights_and_permissions

This number has to be multiplied by the total number of lipids to obtain the total heat capacity of the reservoir. For more details and parameter values, see Appendix A.

RESULTS

Simulations of a lipid membrane in a finite heat reservoir

We first consider the effect of the finite heat reservoir on the lipid melting transition. In order to illustrate the coupling between the membrane enthalpy H_s and the reservoir temperature T_r, we performed a Monte Carlo simulation at the melting temperature (314.05 K) with 1000 water molecules per lipid. This is shown in Fig. 2. Due to Eq. (5), H_s and ΔT_r are exactly proportional functions.

Subsequently, we calculated the fluctuations of the enthalpy of the membrane and determined the function $\Delta c_s = (\langle \Delta H_s^2 \rangle - \langle \Delta H_s \rangle^2)/RT^2$, which we call the fluctuation strength of the membrane. In Fig. 3, it is shown close to the transition temperature. We show the c_s-profiles for five different sizes of the aqueous reservoir: 500, 1000, 2000, 4000, and an infinite number of H_2O molecules per lipid. The latter case corresponds to the isothermal limit, i.e., to the heat capacity Δc_p of the membrane. It can be seen that a reduction of the size of the available heat reservoir also reduces the fluctuation strength Δc_s of the lipid membrane. This lowering is due to the suppression of large enthalpy fluctuations in the lipid membrane. In the limit of infinite reservoirs, the excess heat integrated over the melting transition is given by $\Delta H = \int c_p dT$. For finite reservoirs, however, $\int c_s dT < \Delta H$. For this reason, we do not call c_s a heat capacity.

The dependence of the fluctuation strength on reservoir size is also shown in Fig. 5 for 4 different temperatures close to the transition temperature. Fig. 3 shows that the position and width of the fluctuation function profile in the melting transition are unaltered, meaning that the depletion of the fluctuation strength with smaller heat reservoirs occurs without broadening the transition. For comparison, the inset of Fig. 3 shows experimental data for frequency-dependent heat capacities from van Osdol and collaborators adapted from Ref. 6. The relation between finite size systems and frequency dependence is considered in the Discussion section.

In order to demonstrate the robustness of our approach, we show in Appendix B that these results are independent of the overall system size as long as the number of water molecules per lipid is constant.

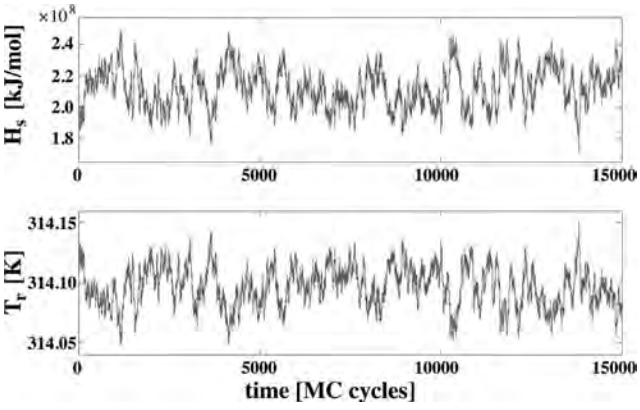

FIG. 2. Traces of membrane enthalpy, H_s, and reservoir temperature, T_r, from Monte Carlo simulations (100 × 100 matrix). (Top) Fluctuations in enthalpy H_s of a lipid membrane with 1000 water molecules associated to each lipid. The enthalpy is given for the total lipid matrix (molar units). (Bottom) Temperature fluctuations in the aqueous reservoir. The water molecules serve as a reservoir for the heat released from the membrane. The membrane enthalpy and the temperature are correlated due to the adiabatic boundary conditions. ΔH_s and ΔT_r are exactly proportional functions.

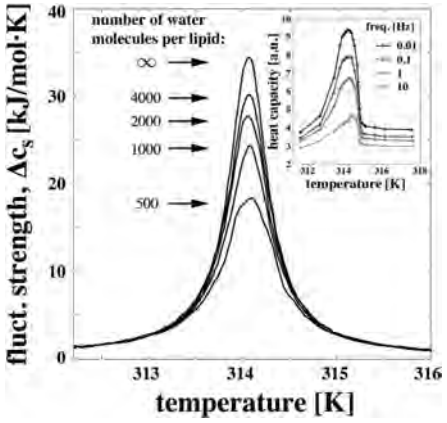

FIG. 3. Fluctuation strength, Δc_s, of the lipid membrane for five different sizes of associated water reservoirs. The isothermal limit corresponds to an infinite number of water molecules per lipid. The curves have been smoothed by cubic spline fitting. Error bars have been omitted for clarity (cf. error bars in Figs. 6 and 5). The inset shows frequency dependent heat capacities, $c_p(\omega)$, measured by van Osdol *et al.* Adapted from Ref. 6.

Fluctuation timescales in finite systems

Fig. 4 shows the probability distribution of enthalpy fluctuations close to the transition temperature for various reservoir sizes. It can be seen that the distributions

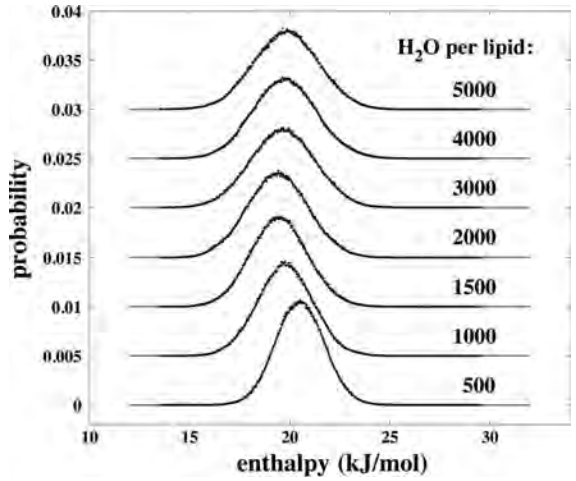

FIG. 4. Probability distribution of enthalpy states close to the transition maximum for different reservoir sizes. The simulated distribution (symbols) is well described by a Gaussian distribution (solid gray lines) with a half width that is closely related to the fluctuation strength.

Downloaded 25 Sep 2013 to 130.225.212.4. This article is copyrighted as indicated in the abstract. Reuse of AIP content is subject to the terms at: http://jcp.aip.org/about/rights_and_permissions

are Gaussian,

$$P(H_s) = \frac{1}{\sqrt{2\pi\sigma^2}} \exp\left(-\frac{(H_s - \langle H_s\rangle)^2}{2\sigma^2}\right), \tag{11}$$

where the variance of the fluctuations, $\sigma^2 = \langle H_s^2\rangle - \langle H_s\rangle^2$, is directly related to the fluctuation strength ($c_s = \sigma^2/RT^2$). Following Einstein,[13] this implies that entropy fluctuations of the system are harmonic with

$$S(H_s) \approx -R\frac{(H_s - \langle H_s\rangle)^2}{2\sigma^2} + \text{const.} \tag{12}$$

with an entropy maximum at $H_s = \langle H_s\rangle$. The use of linear response theory allows us to conclude that, for a fixed reservoir size, the relaxation behavior of enthalpy fluctuations is described by a single exponential with a relaxation time constant, τ, given by Refs. 14 and 15

$$\tau = \frac{T^2}{L}\Delta c_s, \tag{13}$$

where L is a phenomenological coefficient setting the absolute time scale of the cooperative processes. This relation implies that the relaxation times in our simulations are directly proportional to the magnitude of the fluctuations. We also find this in a direct correlation analysis of the cooperative enthalpy fluctuations in the simulation (not shown, see Ref. 14, for examples). Smaller reservoir sizes result in a reduced fluctuation strength with a smaller fluctuation time constant, i.e., fluctuations are faster. We will discuss this feature in the context of frequency dependent heat capacities in the Discussion section.

Linking the effective heat capacity to the adiabatic compressibility

We now consider some consequences of the above results concerning the magnitude of volume or area fluctuations of the membrane in finite reservoirs, and their relation to the adiabatic compressibility. The results are especially instructive if the reservoir is a nearly incompressible medium such as water while the subsystem displays large volume or area fluctuations such as those shown by membranes close to transitions.

The specific isothermal area compressibility (i.e., infinite reservoir) is given by

$$\kappa_T^A = -\frac{1}{A}\left(\frac{\partial A}{\partial \Pi}\right)_T, \tag{14}$$

where Π is the lateral pressure and A is the membrane area. Close to the melting transition, the isothermal compressibility can be approximated by

$$\kappa_T^A \approx \kappa_{T,0}^A + \frac{\gamma_A^2 T}{A}\Delta c_p, \tag{15}$$

where Δc_p is the excess heat capacity.[16,17] In Eq. (15), we used the experimentally found relation $\Delta A = \gamma_A \Delta H$, with $\gamma_A = 0.89$ m^2/J for a lipid bilayer of dipalmitoyl phosphatidylcholine (DPPC).[16,18] The adiabatic area compressibility is related to the isothermal compressibility and is given by Ref. 19

$$\kappa_S^A \equiv -\frac{1}{A}\left(\frac{\partial A}{\partial \Pi}\right)_S = \kappa_T^A - \frac{T}{A\, c_p^{system}}\left(\frac{\partial A}{\partial T}\right)_\Pi^2. \tag{16}$$

This relation has been derived for equilibrium systems using the Maxwell relations.[19] Here, c_p^{system} is assumed to be the heat capacity of the total thermodynamic system, i.e., the excess heat capacity of the lipid membrane, Δc_p, plus the heat capacity of the reservoir, c_p^r (lipid chains and aqueous buffer),

$$c_p^{system} = \Delta c_p + c_p^r. \tag{17}$$

Assuming that $(\partial A/\partial T)_\Pi$ in the lipid melting transition region is completely dominated by the change in area associated with the transition, we obtain[20]

$$\begin{aligned}\kappa_S^A &\approx \kappa_{T,0}^A + \frac{\gamma_A^2 T}{A}\Delta c_p - \frac{\gamma_A^2 T}{A}\frac{\Delta c_p^2}{c_p^{\text{system}}} \\ &= \kappa_{T,0}^A + \frac{\gamma_A^2 T}{A}\Delta c_p \cdot \left(1 - \frac{\Delta c_p}{c_p^{\text{system}}}\right).\end{aligned} \tag{18}$$

It is easily seen that the term in brackets approaches unity when the heat capacity of the total system is much larger than the excess heat capacity of the lipid membrane. This implies that the adiabatic and isothermal compressibilities of the membrane are equal for a very large reservoir.

Following Halstenberg *et al.*,[20] we postulate that the effective heat capacity of the lipid membrane in a finite size reservoir is given by

$$\Delta c_p^{\text{eff}} = \Delta c_p \cdot \left(1 - \frac{\Delta c_p}{c_p^{\text{system}}}\right) \tag{19}$$

with an associated adiabatic compressibility of

$$\kappa_S^A = \kappa_{T,0}^A + \frac{\gamma_A^2 T}{A}\Delta c_p^{\text{eff}}, \tag{20}$$

which is formally similar to Eq. (15). The treatment for the isothermal and adiabatic volume compressibilities is absolutely analogous.

In order to test whether this is a reasonable definition of the membrane heat capacity, it is therefore interesting to compare the above heat capacity with the fluctuation strength of the membrane, Δc_s, obtained from the Monte Carlo simulations (Fig. 3). In the Monte Carlo simulation, the heat capacity of the total heat reservoir, c_p^r, is an input parameter. The excess heat capacity of the lipid melting transition in the isothermal case is known, because it corresponds to the standard Monte Carlo simulation with constant reservoir temperature.[11] We can therefore calculate the effective heat capacity analytically from Eq. (19) and compare it with the simulation results. Fig. 5 shows the fluctuation strength of the membrane from Monte Carlo simulation as a function of reservoir size (symbols) at four different temperatures. Due to the linear relation between fluctuation strength and fluctuation time scales discussed above, the time scales display the same dependence on reservoir size. The solid lines show the analytical calculation from Eq. (19). Within the estimated error,

Downloaded 25 Sep 2013 to 130.225.212.4. This article is copyrighted as indicated in the abstract. Reuse of AIP content is subject to the terms at: http://jcp.aip.org/about/rights_and_permissions

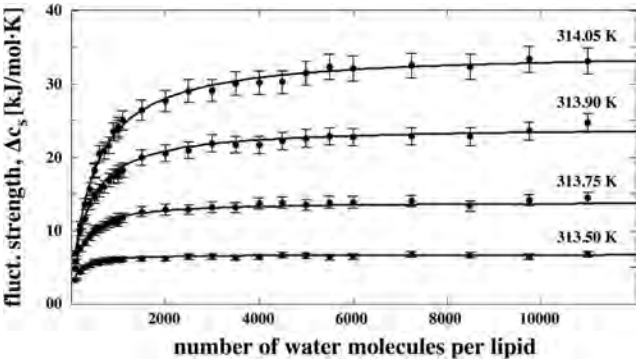

FIG. 5. Verification of the analytical ansatz. The effective heat capacity calculated as a function of reservoir size calculated from Eq. (19) (solid lines) and the fluctuation strength, Δc_s, from the simulations (symbols) at four different temperatures. The analytical formalism yields a very good approximation of the simulated data.

perfect agreement between Eq. (19) and the simulated fluctuation strength was found, indicating that these are identical functions: $\Delta c_p^{\text{eff}} = \Delta c_s$.

Our results also indicate that the isothermal and the adiabatic compressibility are not fundamentally different functions. They merely reflect different sizes of the available heat reservoir. They are equally related as the heat capacity and the fluctuation strength in finite reservoirs as seen from Eqs. (18) and (19).

DISCUSSION

Here, we have shown that the enthalpy fluctuations of an arbitrary part (subsystem) of an adiabatically insulated total system (total enthalpy is constant) depends on the entropy of the total system, i.e., it depends on the combined entropy of the subsystem and the reservoir. This entropy can be regarded as a harmonic potential which depends on the relative size of subsystem and reservoir (i.e., the rest of the total system). Linear response theory then leads to interesting connections between enthalpy fluctuations of the subsystem, its fluctuation lifetimes, and its adiabatic compressibility. While many of our considerations are general, we have applied them to the special case of lipid membranes surrounded by an aqueous reservoir. The fact that enthalpy, volume, and area fluctuations of lipid membranes are proportional functions[16] allows us to find very simple relations between seemingly different thermodynamic response functions.

In calorimetric experiments, membranes (in the form of a dispersion of vesicles) are coupled to an aqueous reservoir and the calorimeter itself. It is generally assumed that the calorimeter serves as an infinite heat bath guaranteeing a constant temperature of the reservoir. If the temperature of the reservoir is absolutely constant, it is meaningful to assign a heat capacity c_p to a subsystem, and the integral $\int_{T_1}^{T_2} c_p dT = \Delta H$ yields the enthalpy change of the subsystem upon a variation of the temperature. We have shown that this is not the case for a finite reservoir that necessarily has temperature fluctuations that are intimately coupled to the enthalpy fluctuations of the subsystem.

The mean square fluctuations of two systems cannot be added when they are correlated, and it is not meaningful to assign heat capacities to individual parts of the total system. However, one can consider enthalpy fluctuations of subsystems that we called the "fluctuation strength" Δc_s of the membrane. For finite size reservoirs, it is generally true that $\Delta c_s < \Delta c_p$. The integral of c_s over temperature does not yield the enthalpy difference of the system at different temperatures. For this reason, we do not call c_s a heat capacity.

Frequency dependent heat capacity and the relation to the finite reservoir

Experimentally, it is hard to test the dependence of the membrane fluctuations on the aqueous volume directly because at very low water content the phase diagrams of lipid membrane dispersions change. However, one can consider frequency-dependent processes where only a short time is available for the membrane system to exchange heat with the buffer. Under such circumstances, only a small volume of the aqueous buffer can contribute as a reservoir. As a result, the size of the volume that communicates with the membrane is frequency-dependent.

In periodic perturbation experiments, one can determine the amplitude of the periodic heat uptake. This function has often been called the "frequency-dependent" or "dynamic heat capacity," $c_p(\omega)$. This term has been coined in analogy with the definition of the equilibrium heat capacity dQ/dT. However, in periodic perturbation experiments both dQ and dT display a dependence on frequency. $c_p(\omega)$ is a complex function with an amplitude and a phase shift between $dQ(\omega)$ and $dT(\omega)$. This phase shift is absent at zero frequency. There are basically two ways of determining the frequency dependent heat capacity. The first consists of a periodic temperature variation imposed on the system from the outside, which is linked to a periodic uptake and release of heat, such as described by Ref. 21. The second method consists of a periodic variation of pressure of an adiabatically shielded volume. The observable is the periodic variation in reservoir temperature.[22] The frequency dependent heat capacity is determined indirectly using the Clausius-Clapeyron equation. What is actually observed in the case of lipid membranes is the transfer of heat from the membrane to the reservoir.[5,6] This situation is in fact comparable to our case that considers temperature fluctuations in the reservoir generated by enthalpy fluctuations in the membrane. For this reason, we compared the frequency dependent heat capacity by Ref. 6 with the fluctuation strength in finite reservoirs (Fig. 3). The inset of Fig. 3 shows the results of these experiments on DPPC vesicles for four frequencies between 0.01 and 10 Hz. They display a striking similarity to our simulations when varying reservoir size in two respects: 1. The half width of the excess heat capacity profile is unchanged but its amplitude decreases when increasing frequency or decreasing reservoir size. 2. The effect on amplitude is most pronounced in the transition, because the fluctuation time scales are much larger due to critical slowing-down.

In contrast to the enthalpy fluctuations, the equilibrium heat capacity does not possess an intrinsic time scale. Nielsen

Downloaded 25 Sep 2013 to 130.225.212.4. This article is copyrighted as indicated in the abstract. Reuse of AIP content is subject to the terms at: http://jcp.aip.org/about/rights_and_permissions

and Dyre[4] have thoroughly analyzed the frequency dependent heat capacity and its coupling to fluctuation relations. They define $c_p(\omega)$ as the fraction of the equilibrium fluctuations with time scales shorter than $\tau = 1/2\pi\omega$. Clearly, $c_p(\omega)$ captures only those equilibrium fluctuations that are faster than the characteristic time scale of the oscillation. In other words, it captures those heat transfer processes that have equilibrated within the time $t < \tau$. In the limit of $\omega \to 0$, the frequency dependent heat capacity $c_p(\omega)$ therefore approaches the equilibrium heat capacity, c_p. Our present simulation considers heat transfer into a finite reservoir in an equilibrium situation. The reduction in reservoir size attenuates the large fluctuations. By demonstrating the Gaussian nature of the fluctuations, we have also shown that fluctuation relaxation is single exponential with a time scale related to the size of the reservoir (Fig. 4). Thus, relaxation of heat into a finite reservoir resembles the relaxation of heat in finite time as discussed above.

Consider a membrane embedded in an infinite water reservoir (Fig. 1, left) that is subject to periodic variation of the lateral pressure applied to the membrane. It is reasonable to assume that this will lead to an exchange of heat with an adjacent layer of water that is finite due to the finite time scale for heat transport in water. In the first phase of the perturbation, heat is released into the aqueous layer; in the second phase, it is reabsorbed. The volume of the contributing water layer is likely to be directly related to the timescale of the oscillation.

In the past, we have demonstrated for lipid membranes that the equilibrium volume and area fluctuations are directly proportional to the enthalpy fluctuations[16,23] as are the relaxation times following temperature and pressure perturbations. This suggests a proportionality between equilibrium heat capacity and isothermal volume or area compressibility. The adiabatic compressibility is also an equilibrium property that can be derived from isothermal properties by using Maxwell relations. It is not intuitive why the concept of an adiabatic compressibility can successfully be used for describing dynamic or frequency dependent phenomena. While the frequency dependent heat capacity is not a thermodynamic function, we have shown here that one can nevertheless draw a reasonable analogy between a properly defined "frequency dependent heat capacity" and a "frequency dependent compressibility" and suggest a proportional relationship for the two. In analogy to Eq. (19), one can also postulate that the frequency dependent excess heat capacity of the membrane assumes the following form:

$$\Delta c_p^{\text{eff}}(\omega) = \Delta c_p \cdot \left(1 - \frac{\Delta c_p}{c_p^{\text{system}}(\omega)}\right), \tag{21}$$

where $c_p^{system}(\omega)$ is the reservoir size accessible in the finite time $\tau = 1/2\pi\omega$. The excess adiabatic compressibility is then given by

$$\Delta\kappa_S(\omega) = \frac{\gamma_A^2 T}{A}\Delta c_p^{\text{eff}}(\omega). \tag{22}$$

If $c_p^{\text{system}} \to \infty$, the frequency dependent heat capacity approaches the equilibrium excess heat capacity, and the adiabatic compressibility approaches the isothermal compressibility. Understanding the timescale of heat transfer from the membrane subsystem into the aqueous reservoir might help formulating dispersion relations.

While Eq. (22) expresses a tentative rather than a derived form of the frequency dependence of the compressibility, it has been used successfully in describing the ultrasonic frequency dependence of the three-dimensional sound velocity of lipids in the MHz regime. Halstenberg *et al.*[20] performed experiments on DPPC vesicles using a resonator with a frequency of 7.2 MHz, which corresponds to a timescale that is much faster than that of the cooperative domain size fluctuation in equilibrium. The speed of sound in the volume is given by

$$c = \sqrt{\frac{1}{\kappa_S^V \rho^V}}, \tag{23}$$

where κ_S^V is the adiabatic volume compressibility and ρ^V is the mass density. The experimentally measured speed of sound of lipid dispersions was correctly predicted by assuming that the heat capacity of the lipid chains is dominant at such high frequencies. Again, the rationale is that there is insufficient time for heat to diffuse into the aqueous volume at these frequencies.

The frequency dependence of sound is called "dispersion" and is of considerable importance for sound propagation phenomena in matter. We have previously proposed that electromechanical solitons with strong similarities to the action potential can propagate in biomembranes and nerves.[18,24–27] Such solitons are a consequence of the simultaneous presence of nonlinear elastic constants and dispersion close to melting transitions. Although many details remain to be understood, we have also shown that the dispersion relation is related to the thermodynamic behavior of membranes.[8] In particular, the dispersion relation sets a natural timescale for the propagating nerve pulse. Similarly, the fluctuation time scales correspond to the typical open-time of lipid channels.[28,29] It seems likely that the time scale of fluctuations is of significant biological relevance.

CONCLUSION

We have constructed a framework for modeling the fluctuations of arbitrary subsystems embedded in an adiabatically shielded reservoir. This method was applied to the lipid melting transition in a finite adiabatically insulated aqueous reservoir. We show that the magnitude of the cooperative fluctuations of the membranes depends on the size of the associated reservoir. As a consequence, the elastic constants of the membrane also depend on reservoir size. It seems plausible to compare this effect to frequency dependent measurements where only parts of the environment of a membrane can contribute as a reservoir for the heat transfer. We believe that the present considerations may contribute to the better understanding of relaxation processes in general and the dispersion relation of lipid membranes that is important for setting the time scale of dynamic processes such as nerve pulse propagation.

Downloaded 25 Sep 2013 to 130.225.212.4. This article is copyrighted as indicated in the abstract. Reuse of AIP content is subject to the terms at: http://jcp.aip.org/about/rights_and_permissions

ACKNOWLEDGMENTS

This work was supported by the Villum foundation (VKR 022130).

APPENDIX A: MONTE CARLO SIMULATIONS

We have modeled the melting transition of a single lipid membrane using the Doniach model,[9] which is a modified version of the Ising model with two lipid states, gel and fluid, instead of two spins. This differs from the Ising model in that the two lipid states are not only different in enthalpy but also in entropy. This is due to the higher degeneracy of states of each lipid molecule in the fluid phase. We used Monte Carlo simulations employing the Glauber algorithm for the individual simulation steps.[30] Such simulations are described in detail by Refs. 11 and 12.

Simulations were typically carried out on a triangular lattice with 100 × 100 sites with periodic boundary conditions. Each lattice point represents one lipid which can either be in the gel or the fluid state. All simulations were equilibrated for at least 30 times the correlation time before sampling, effectively meaning more than 6×10^4 Monte Carlo cycles at the transition maximum. The equilibration was carried out by assuming a constant water bath temperature in the first step. In a second step, we considered finite reservoir size using an algorithm described below. In analogy to the heat capacity, we defined the excess fluctuation strength $\Delta c_s = \left(\left\langle \Delta H_s^2 \right\rangle - \langle \Delta H_s \rangle^2\right)/RT^2$ that we calculated from the excess enthalpy fluctuations of the lipid membrane (enthalpy H_s) embedded into the finite reservoir. The statistical error was estimated using the Jackknife method. We emphasize that the fluctuation strength Δc_s is identical to the equilibrium excess heat capacity defined as $\Delta c_p = (dQ/dT)_p$ only in the limit of infinite reservoirs and constant reservoir temperature.

In the present simulation, we used the following parameters for modeling the heat capacity profiles of DPPC large unilamellar vesicles (LUV): $\Delta H = 36\,400$ J/mol (melting enthalpy), $\Delta S = 115.9$ J/mol K (melting entropy), and $\omega_{gf} = 1326.0$ J/mol[31] leading to a melting temperature of $T_m = 314.05$ K and a transition half width of about 1 K. The heat capacity of water was taken to be $c_p^{water} = 75$ J/K mol which corresponds to the value of 1 cal/g K for free water. The heat capacity of the chains was set to $c_p^{chain} = 1600$ J/K mol which was determined experimentally by Blume[32] for gel state DPPC. The total heat reservoir is shared by all lipids in the lipid membrane. The minimum number of water molecules per lipid considered in any simulation is 100.

The simulated heat capacity profiles and the estimated statistical errors were smoothed using cubic spline fits.

APPENDIX B: SYSTEM SIZE DEPENDENCE

Fig. 6 shows that the calculated fluctuation strength (per mole of lipid) is independent of the total number of lipids assuming a fixed reservoir size per lipid (here, 1000 H_2O molecules per lipid) within statistical error. This behavior was demanded in the Theory section and demonstrates the robustness of our approach.

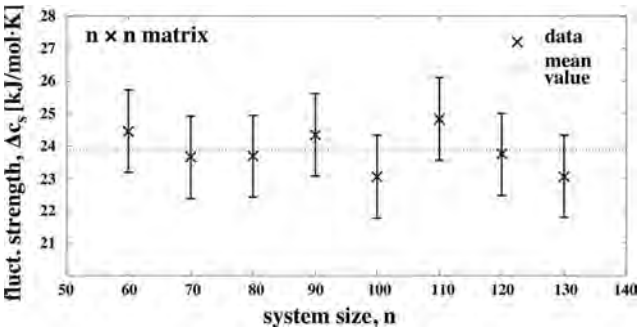

FIG. 6. Fluctuation strength, Δc_s, at the transition temperature T_m of the lipid membrane in a finite system with 1000 water molecules per lipid. The simulation was performed for different sizes, n, of the lipid membrane. A system size of n denotes a $n \times n$ matrix. The fluctuation strength per lipid is independent of system size within the error of the calculation.

[1] T. Heimburg, *Thermal Biophysics of Membranes* (Wiley VCH, Berlin, Germany, 2007).
[2] M. Creutz, Phys. Rev. Lett. **50**, 1411 (1983).
[3] A. Milchev, I. Gerroff, and J. Schmelzer, Z. Phys. B **94**, 101 (1994).
[4] J. K. Nielsen and J. C. Dyre, Phys. Rev. B **54**, 15754 (1996).
[5] W. W. van Osdol, R. L. Biltonen, and M. L. Johnson, J. Bioenerg. Biophys. Methods **20**, 1 (1989).
[6] W. W. van Osdol, M. L. Johnson, Q. Ye, and R. L. Biltonen, Biophys. J. **59**, 775 (1991).
[7] S. Halstenberg, W. Schrader, P. Das, J. K. Bhattacharjee, and U. Kaatze, J. Chem. Phys. **118**, 5683 (2003).
[8] L. D. Mosgaard, A. D. Jackson, and T. Heimburg, in *Advances in Planar Lipid Bilayers and Liposomes*, edited by A. Iglic (Elsevier, 2012), Vol. 16, pp. 51–47.
[9] S. Doniach, J. Chem. Phys. **68**, 4912 (1978).
[10] O. G. Mouritsen, A. Boothroyd, R. Harris, N. Jan, T. Lookman, L. MacDonald, D. A. Pink, and M. J. Zuckermann, J. Chem. Phys. **79**, 2027 (1983).
[11] I. P. Sugar, R. L. Biltonen, and N. Mitchard, Methods Enzymol. **240**, 569 (1994).
[12] T. Heimburg and R. L. Biltonen, Biophys. J. **70**, 84 (1996).
[13] A. Einstein, Ann. Phys. (Leipzig) **33**, 1275 (1910).
[14] P. Grabitz, V. P. Ivanova, and T. Heimburg, Biophys. J. **82**, 299 (2002).
[15] H. M. Seeger, M. L. Gudmundsson, and T. Heimburg, J. Phys. Chem. B **111**, 13858 (2007).
[16] T. Heimburg, Biochim. Biophys. Acta **1415**, 147 (1998).
[17] U. R. Pedersen, G. H. Peters, T. B. Schrøder, and J. C. Dyre, J. Phys. Chem. B **114**, 2124 (2010).
[18] T. Heimburg and A. D. Jackson, Proc. Natl. Acad. Sci. U.S.A. **102**, 9790 (2005).
[19] A. H. Wilson, *Thermodynamics and Statistical Mechanics* (Cambridge University Press, Cambridge, 1957).
[20] S. Halstenberg, T. Heimburg, T. Hianik, U. Kaatze, and R. Krivanek, Biophys. J. **75**, 264 (1998).
[21] O. L. Mayorga, W. W. van Osdol, J. L. Lacomba, and E. Freire, Proc. Natl. Acad. Sci. U.S.A. **85**, 9514 (1988).
[22] M. L. Johnson, T. C. Winter, and R. L. Biltonen, Anal. Biochem. **128**, 1 (1983).
[23] H. Ebel, P. Grabitz, and T. Heimburg, J. Phys. Chem. B **105**, 7353 (2001).
[24] T. Heimburg and A. D. Jackson, Biophys. Rev. Lett. **2**, 57 (2007).
[25] S. S. L. Andersen, A. D. Jackson, and T. Heimburg, Prog. Neurobiol. **88**, 104 (2009).
[26] B. Lautrup, R. Appali, A. D. Jackson, and T. Heimburg, Eur. Phys. J. E **34**, 57 (2011).
[27] E. Villagran Vargas, A. Ludu, R. Hustert, P. Gumrich, A. D. Jackson, and T. Heimburg, Biophys. Chem. **153**, 159 (2011).
[28] B. Wunderlich, C. Leirer, A. Idzko, U. F. Keyser, V. Myles, T. Heimburg, and M. Schneider, Biophys. J. **96**, 4592 (2009).
[29] J. Gallaher, K. Wodzinska, T. Heimburg, and M. Bier, Phys. Rev. E **81**, 061925 (2010).
[30] R. J. Glauber, J. Math. Phys. **4**, 294 (1963).
[31] V. P. Ivanova and T. Heimburg, Phys. Rev. E **63**, 041914 (2001).
[32] A. Blume, Biochemistry **22**, 5436 (1983).

Downloaded 25 Sep 2013 to 130.225.212.4. This article is copyrighted as indicated in the abstract. Reuse of AIP content is subject to the terms at: http://jcp.aip.org/about/rights_and_permissions

Penetration of Action Potentials During Collision in the Median and Lateral Giant Axons of Invertebrates

Alfredo Gonzalez-Perez, Rima Budvytyte, Lars D. Mosgaard, Søren Nissen, and Thomas Heimburg*

The Niels Bohr Institute, University of Copenhagen, Blegdamsvej 17, 2100 Copenhagen, Denmark

(Received 31 March 2014; revised manuscript received 3 July 2014; published 10 September 2014)

The collisions of two simultaneously generated impulses in the giant axons of both earthworms and lobsters propagating in orthodromic and antidromic direction are investigated. The experiments have been performed on the extracted ventral cords of *Lumbricus terrestris* and the abdominal ventral cord of a lobster, *Homarus americanus*, by using external stimulation and recording. The collision of two nerve impulses of orthodromic and antidromic propagation did not result in the annihilation of the two signals, contrary to the common notion that is based on the existence of a refractory period in the well-known Hodgkin-Huxley theory. However, the results are in agreement with the electromechanical soliton theory for nerve-pulse propagation, as suggested by Heimburg and Jackson [*On Soliton Propagation in Biomembranes and Nerves*, Proc. Natl. Acad. Sci. U.S.A. 102, 9790 (2005).].

DOI: 10.1103/PhysRevX.4.031047 Subject Areas: Biological Physics, Medical Physics

I. INTRODUCTION

The action potential in nerves consists of a transmembrane voltage pulse of approximately 100 mV that propagates along the neuronal axon. In 1952, Hodgkin and Huxley (HH) proposed that this pulse results from a selective voltage-dependent breakdown in membrane resistance for potassium and sodium [1]. Ions flow along the concentration gradients through channel proteins modeled as electrical resistors, and the HH model is thus intrinsically dissipative. Hodgkin compared the action potential to "a burning fuse of gunpowder" [2]. Time scales in the model, intended to describe relaxation processes in the proteins, are contained in the parametrization of the protein conductances. They lead to a refractory period following a pulse during which the nerve is not excitable. Thus, it is expected that nerve pulses traveling from opposite ends of a neuron will annihilate upon collision [3].

Because of its dissipative nature, the action potential in the Hodgkin-Huxley model should be accompanied by heat production. However, investigations of the initial heat resulted in the finding that, within experimental error, no such heat is released during the action potential [4–7]. A first phase of apparent heat release is followed by a second phase of heat absorption [8]. The emission and reabsorption of the initial heat is exactly in phase with the observed voltage changes, and the integrated heat associated with the action potential is zero within experimental accuracy. The data thus indicate that the action potential is an adiabatic (nondissipative) phenomenon such as, e.g., a sound wave. This finding is in conflict with the HH model, as acknowledged by Hodgkin (Ref. [2], p. 70).

The absence of net heat release combined with the experimental finding of mechanical dislocations during the action potential [9,10] provided the motivation for attempts to explain the action potential as a propagating electromechanical pulse [11–13]. Because of the presence of lipid-chain-order transitions just below physiological temperature, the elastic constants of biomembranes display a nonlinear dependence on both lateral density and dispersion [11], i.e., frequency dependence of the sound velocity. This was shown to result in solitary mechanical waves with properties surprisingly similar to those of the action potential. For instance, they propagate with a velocity of about 100 m/s (which is similar to the velocity of the action potential in the myelinated nerves of vertebrates) and display a reversible heat release as found in experiments. The change in nerve thickness associated with such solitary waves is approximately 1 nm, in agreement with the changes in membrane thickness associated with a phase change. Given the known capacitive properties of lipid membranes, this thickness change and the associated decrease in membrane area can produce voltage changes on the order of 100 mV without any transverse flow of charge. It was shown [11] that the thermodynamic properties of biological membranes support the propagation of solitary waves that display electric, thermal, and mechanical changes consistent with those found in experiments. In contrast to the Hodgkin-Huxley view, an electromechanical theory would not lead to annihilation of colliding pulses but rather to near-lossless penetration [14]. Given the

*theimbu@nbi.ku.dk; http://www.membranes.nbi.dk

Published by the American Physical Society under the terms of the Creative Commons Attribution 3.0 License. Further distribution of this work must maintain attribution to the author(s) and the published article's title, journal citation, and DOI.

difference between these predictions of the fate of colliding nerve pulses, it is important to investigate whether they annihilate or simply pass through each other.

It is generally believed that the action potential is generated in the neuron at the axon hillock [15]. Pulse propagation in the direction of the axon, the so-called orthodromic propagation, occurs from the soma towards the end of the synapses. However, in vertebrate and invertebrate nerve cells, the action potential can also be stimulated in regions remote from the axon hillock, e.g., ectopic sites located in axons or dendrites [16]. Pulse propagation in the opposite direction, called antidromic propagation, can occur [16]. In fact, orthodromic and antidromic impulse propagation in neurons and other excitable tissues can be induced by electrical stimulation in the vicinity of the soma or in the distal part of the axon, respectively.

The simultaneous stimulation of orthodromic and antidromic pulses can lead to collision events. As suggested above, such events can provide important information regarding the nature of signal transmission of information in neurons. In spite of its relevance for understanding neuronal function and behavior, surprisingly little attention has been given to such phenomena. The collision between two impulses was first investigated by Tasaki in 1949 [3] using the motor fibers innervating the sartorious muscle of the toad. From his experiments, Tasaki concluded that the collision of two impulses results in their mutual annihilation. Since this experiment was performed, little further work was done to confirm or to reject its finding. This may be due in part to the fact that the outcome of Tasaki's experiment is in agreement with the predictions of the HH model [1]. The importance of further investigation is emphasized by the fact that collision experiments, supplemented by the assumption that impulses always annihilate each other, are often used to identify axonal destinations of single cells in the central nervous system [17–19].

In the current work, we report on collision experiments using the ventral cords of earthworm *Lumbricus terrestris* and the abdominal ventral cord of a lobster *Homarus americanus* and show that the collision of two impulses generated simultaneously in orthodromic and antidromic directions does not result in their mutual annihilation. Instead, they penetrate each other and emerge from the collision without material alterations of their shape or velocity. The earthworm was chosen because of the properties of the median giant fibers (MGF) and because of the possibility of making simultaneous orthodromic and antidromic stimulation [20]. The electrotonic connections of the synapses and the neuronal syncytia permit the bidirectional propagation of the action potential along the array of giant neurons that form the MGF [21]. A similar situation is found in the median giant axons of the ventral cord of a lobster [22]. We compare these findings with simulations of the action potential, as suggested by the electromechanical soliton theory.

II. MATERIALS AND METHODS

Materials.—Earthworms (*Lumbricus terrestris*) were obtained from a local supplier. We used an earthworm saline solution adapted from Drewes *et al.* [23] consisting of 75 mM NaCl, 4 mM KCl, 2 mM $CaCl_2$, 1 mM $MgCl_2$, 10 mM Tris, and 23 mM glucose, adjusted to pH 7.4 with 8 mmol/l HCl. All the chemicals used in the preparation were purchased from Sigma-Aldrich.

Lobsters (*Homarus americanus*) were obtained from a local supplier. We used a lobster saline solution adapted from Ref. [24], with the following composition: 462 mM NaCl, 10 mM KCl, 25 mM $CaCl_2$, 8 mM $MgCl_2$, 10 mM Tris, and 11 mM Glucose, adjusted to pH 7.4 with NaOH.

Hardware and software.—The PowerLab 26 T data acquisition hardware was purchased from ADInstruments Europe (Oxford, UK). The instrument contains an internal bio-amplifier that allows us to record small electrical potential on the order of microvolts. The bio-amplifier contains two recording channels (see Ref. [25]). The Labchart software from ADInstruments was used to control the PowerLab 26 T sending the stimulation and recording the signals coming from the ventral cord.

Nerve chamber.—The self-built nerve chamber is composed of an array of 21 stainless-steel electrodes in a longitudinal cavity covered by a lid in order to protect the nerve once extracted. The lid also allows maintenance of a saturated water-vapor atmosphere in order to keep the moisture in the ventral cord. The nerve chamber is a 7×2.5-cm block of 1-cm height made on Plexiglas that contains a longitudinal channel of 6-cm length (depth of 0.5 cm and width of 0.5 cm). In the longitudinal aperture, an array of 21 perforations was created to place stainless-steel electrodes. The array was located about 0.25 cm from the top of the chamber. The distance between consecutive electrodes is 0.25 cm. The stainless-steel electrodes have a length of about 3.4 cm and a diameter of 0.5 mm and were fixed in the perforation along the chamber by using Reprorubber Thin Pur by Flexbar (Islandia, NY). A scheme of the nerve chamber is shown in Fig. 1.

Nerve preparation of an earthworm.—The earthworms (*Lumbricus terrestris*) were anesthetized by immersing them in a solution of 10% ethanol in tap water. The earthworm was left between 5 and 10 min in the anesthetic solution depending on its size. Once removed from the anesthetic solution, the earthworm was washed with tap water to remove remains of the anesthetic solution and fixed longitudinally in a dissecting pan using pins. The earthworm was pinned laterally with the ventral side facing the dissection pan. A small incision in the dorsal side was made by using a scalpel or small scissors. Subsequently, the incision was elongated along the entire length of the earthworm body. Using micro-scissors with a straight

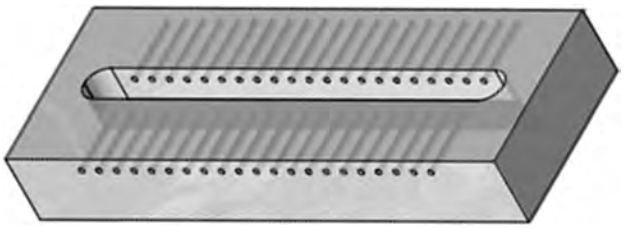

FIG. 1. The design of the recording chamber. The nerve is placed on top of 21 electrodes located slightly above an aqueous buffer. The chamber is closed with a lid to avoid drying of the nerve. The electrodes at the end are used for stimulation, while the center electrodes are used for recording the signal.

blade, we cut each septum to liberate the internal organs and pin down the loose skin with muscular tissue. Using curved micro-scissors, we removed the crop, gizzard, intestine, and the first 20 segments of the ventral cord including the brain. After this step, we cleaned the preparation with the saline solution, leaving the ventral cord and median ventral blood vessel exposed. In the final step, we cut each segment below the ventral cord, taking care to avoid damaging the sample. The blood vessels were removed before extracting the ventral cord. The extraction and all experiments were performed at room temperature (about 22 °C). A scheme of the internal and external structure of the ventral cord is shown in Fig. 2.

Electrical stimulation can be used to excite the median and lateral giant fibers (LGF) of intact anesthetized earthworms [27]. The signals coming from the small giant axons of the ventral side of the ventral cord cannot be detected using our setup. The signal from the three small giant axons require higher stimulation voltages and probably higher amplification. Note that even in the intact earthworm, the signals from the median and lateral axons can be detected in external recordings. This is not the case for the small giant axons [27].

However, earthworms can move during the experiment after several electrical stimulations. Additionally, an excessive amount of anesthetic preventing movements during the experiment will affect the excitation properties of the ventral cord as well as the propagation velocity. For this reason, we performed experiments on the extracted ventral cord.

The ventral cord from *Lumbricus terrestris* was used right after extraction, and special care was taken to remove any remaining tissue that did not belong to the ventral cord itself. The ventral cord was left in Ringer's solution for about 30 min, to relax. We proceeded to the next step after the ventral cord had reached a stable size. The ventral cord is very flexible and can be stretched without damaging its internal structure as a consequence of the trilaminar layer that protects the neurons filling the inside. After the equilibration period, the ventral cord was placed in the nerve chamber over the electrode array, and a few

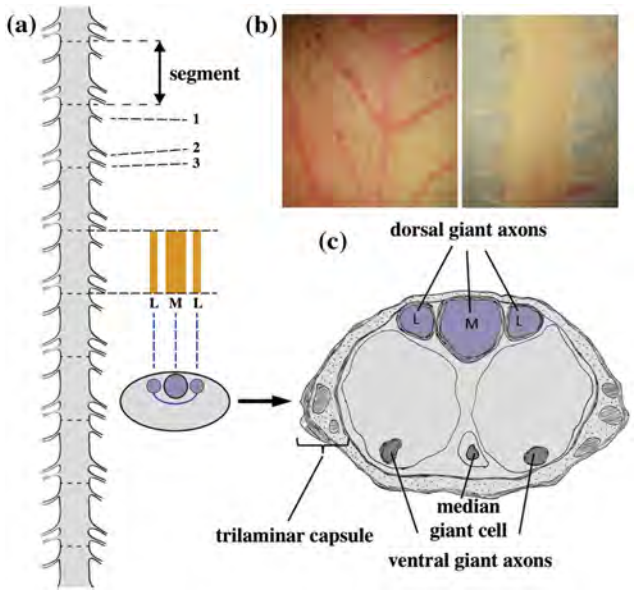

FIG. 2. (a) Schematic representation of an earthworm ventral cord with the segments and three pairs of roots, (b) ventral cord with and without muscular tissue, and (c) internal structure of the ventral cord redrawn from Ref. [26]. Median and lateral giant fibers are marked with M and L.

microliters of Ringer's solution were deposited at the bottom of the chamber. The nerve chamber was closed with a glass lid, allowing an atmosphere of saturated water vapor to accumulate. This prevented the loss of moisture by the ventral cord and the subsequent death of the nerve for several hours. The ventral cord was placed with the ventral side facing the electrode array, and the preparation was ready for the collision experiment. Two pairs of stimulation electrodes were placed close to the two ends of the extracted ventral cord. A single pair of recording electrodes was placed at about $1/3$ of the distance between the stimulation sites. As an initial step, we determined the voltage threshold for the generation of an action potential propagating orthodromically. We followed the conventional protocol by increasing the voltage in small intervals. The same protocol was followed by stimulating the ventral cord from the tail side to generate an action potential propagating antidromically. In all the experiments, we found that slightly higher voltages were needed to initiate antidromic action potential propagation. At voltages higher than the voltage threshold, the spike was stable and unchanged in shape and position. The observed differences in threshold voltage can be due to variations in diameter of the giant neurons along the MGF. The MGF becomes smaller in diameter towards the posterior end of the earthworm, and the LGF becomes smaller towards the anterior end of the animal [20]. According to Coggeshall [26], the diameter of lateral giant axons ranges between 4 μm in the anterior regions and 50 μm in the posterior regions of the nerve cord, while the diameter of the median

giant fiber in the posterior end is of the order of 100 μm. In order to have a relatively uniform diameter in the median giant axons, we used a fragment of the ventral cord starting at segment 20 with a total length of about 4 to 6 cm. Because the two LGFs are physically connected and fire in a synchronous way, we used only the MGF for the collision experiment [27]. We should note that voltage values higher than those used for the antidromic action potential for the MGF will generate an antidromic action potential for the LGF, which we wanted to avoid. The median giant axon has a larger diameter than the lateral giant axon over the full length of the ventral cord fragment used in our experiments. This results in faster signal propagation in the median giant axon [28] and makes it possible to distinguish the action potentials from the median and the lateral giant axons. In all cases, we verified for orthodromic and antidromic propagation that at higher voltages we could get a second signal with a bigger latency (corresponding to the LGF), ruling out any uncertainty in the spike identification.

Nerve preparation of lobster.—The lobster (*Homarus americanus*) was anesthetized by keeping the animal in the freezer for about 30 minutes. Once removed from the freezer, the animal was placed on the dissecting table and the head was severed in order to remove the brain. In a second step, a cut was made at the onset of the abdomen in order to separate the tail. The abdominal part of the ventral cord can be extracted by cutting both laterals of the ventral side of the animal and removing the soft shell. The abdominal ventral cord is attached to the soft shell and is easily removed with tweezers after cutting the nerves branching from the six ganglia. The ventral cord contains four giant axons. Two median giant axons run, as a single neuron, all the way through the abdominal ventral cord, and two lateral giant axons are formed by six neurons connected at the level of each ganglia [29]. In the abdominal part, the lateral giant axons display a larger diameter than the median giant axons [22]. They are excited at the lowest stimulation voltage. A cross section of the ventral cord is shown in Fig. 3. The giant axons of the ventral cord of the lobster are considered nonmyelinated [30].

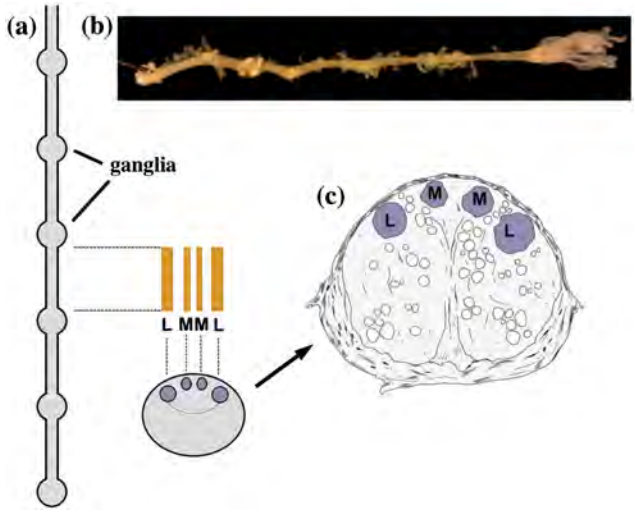

FIG. 3. (a) Schematic representation of a lobster ventral cord at the abdominal (tail) site with six ganglia, (b) abdominal ventral cord extracted from the lobster tail, and (c) internal structure of the ventral cord showing four giant axons.

III. RESULTS

A schematic description of key steps in the collision experiment is shown in Fig. 4. We stimulate the axon with two pairs of electrodes at the two ends of the nerve (shown in red and green). Two recording electrodes (shown in blue) are located at about 1/3 of the total length of the axon in the orthodromic direction. Since the difference in potential between these two electrodes is recorded, the resulting signal is approximately the first derivative of the true pulse shape. If two pulses are generated simultaneously at opposite ends of the nerve, the orthodromic pulse is recorded by these electrodes before the collision of the pulses, while the antidromic pulse is detected after the collision. If the two pulses penetrate each other, the recorded signal will show both the orthodromic pulse and the subsequent antidromic pulse (see Fig. 4, bottom left). If the two pulses annihilate, only the initial orthodromic pulse will be recorded (see Fig. 4, bottom right). The results for simultaneous stimulation at both ends can be compared with experiments in which only the orthodromic or only the antidromic pulse was stimulated. Although the schematic drawing in Fig. 4 suggests that orthodromic and antidromic

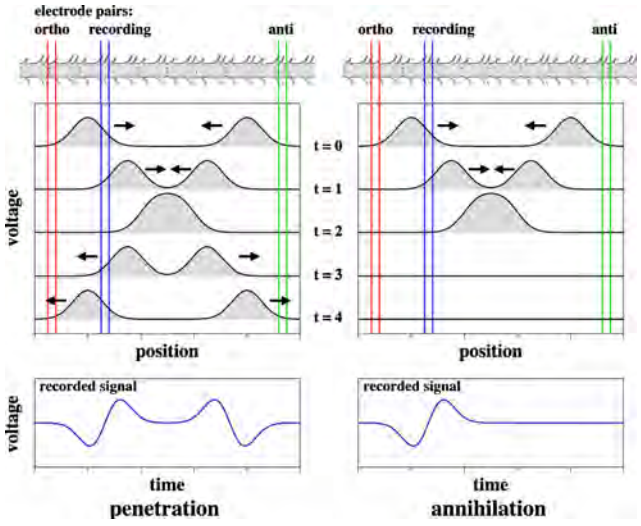

FIG. 4. A schematic representation of the different steps of the collision experiment at times t_0, t_1, t_2, and t_3. The action potentials (AP) are generated at t_0 by simultaneous stimulation in both ends of the ventral cord; the orthodromic AP reaches the recording electrodes at t_1; the APs collide at t_2; the antidromic AP reaches the recording electrodes at t_3.

pulses have the same shape, their shapes can differ in real nerves because the thickness of the axon is not constant along its full length.

A. Theory

Biological membranes display lipid-chain-melting transitions slightly below body temperature. In these transitions, the lateral compressibility of the membrane changes as a nonlinear function of the lateral mass density. The compression modulus is also a function of frequency. These two facts lead to the possibility of propagating mechanical solitons (or solitary pulses) [11]. The mathematical expression for a propagating soliton in such a membrane cylinder is given by

$$\frac{\partial^2}{\partial t^2}\Delta\rho = \frac{\partial}{\partial x}\left[(c_0^2 + p\Delta\rho + q(\Delta\rho)^2)\frac{\partial}{\partial x}\Delta\rho\right] - h\frac{\partial^4}{\partial x^4}\Delta\rho, \tag{1}$$

where x is the spatial coordinate along the membrane cylinder and t is time. Here, we use parameters appropriate for dipalmitoyl phosphatidylcholine (DPPC) membranes at 45 °C as given in Ref. [11]. The density variation, $\Delta\rho = \rho - \rho_0$, is the difference between the lateral mass density of the membrane and its empirical equilibrium value of $\rho_0 = 4.035 \times 10^{-3}$ g/m^2. The low-frequency sound velocity is $c_0 = 176.6$ m/s. The coefficients p and q were fitted to measured values of the sound velocity as a function of density. For the simulations here, $p = -16.6c_0^2/\rho_0$ and $q = 79.5c_0^2/(\rho_0)^2$, as found in Ref. [11]. If the membrane is slightly above the melting transition of the lipid chains, it is to be expected that $p < 0$ and $q > 0$. The dispersion coefficient h must be positive. The above equation possesses exponentially localized solutions of a fixed shape which propagate with an arbitrary constant velocity v that is smaller than c_0 and larger than a minimum limiting velocity $v_{\min}$. Equation (2) possesses analytic solutions given in Ref. [14].

The pulse amplitude reaches a maximum amplitude of

$$\Delta\rho_{\max} = \frac{|p|}{q} \tag{2}$$

as the velocity approaches the limiting value [11] of

$$\Delta v_{\min} = \sqrt{c_0^2 - \frac{p^2}{6q}}. \tag{3}$$

Thus, different velocities are associated with different pulse amplitudes and energies. For synthetic DPPC large unilamellar vesicle membranes slightly above their melting temperature, the minimum pulse velocity is $v_{\min} = 0.65c_0$ and the maximum amplitude change is $\Delta\rho_{\max}/\rho_0 = 0.209$. This corresponds to passing from the liquid to the solid phase of the membrane.

We have solved Eq. (1) numerically using the above parameters for DPPC and a velocity of $v = 0.7c_0$. The solid lipid phase has a maximum density that is 24.6% higher than that of the liquid state. In order to prevent densities higher than that of the solid lipid phase during pulse collision, we have introduced a soft barrier at $\Delta\rho/\rho_0 \approx 0.25$ (see Ref. [14] for details). The results are shown in Fig. 5. The top panel shows the pulses propagating before and after the collision at five different times t. The collision process leads to some dissipation of energy in the form of small amplitude noise that propagates with the speed of sound c_0 (i.e., faster than the velocity of the solitary pulse). The shape, velocity, and energy of the pulses are largely unaltered. During pulse collision, the density changes of both pulses do not have to add together, as one might intuitively assume. Instead, one finds a broadened intermediate collision state, which is wider than the individual solitons. In the soliton theory, collision obviously does not lead to annihilation of the colliding pulses. The fact that the individual pulses suffer a minor loss of energy during the collision merely indicates that we are considering solitary pulses rather than true solitons. The generation of small amplitude noise with very low energy content is mostly a consequence of not allowing the density change to exceed $\Delta\rho/\rho_0 = 0.25$.

Biomembranes can be regarded as charged capacitors [31]. Voltage changes are directly related to the density changes. Assuming that $\Delta\rho$ is proportional to a change in voltage, we can determine the voltage signal recorded by two hypothetical electrodes that are placed as shown in Fig. 4. These electrodes are shown as blue lines in Fig. 5 (top panel) and, in our simulation, they are separated by 1.6 cm (which is to be compared with the total pulse width of about 5 cm). Figure 5 (bottom panel) shows the recording by these electrodes for a single pulse from the left, a single pulse from the right, and for the calculated collision experiment. The dashed blue line is the sum of the two single pulses shown as a guide for the eye. It is clear that the second pulse is distorted by the collision process, as is expected from the analysis in the top panel.

The results of soliton theory described above can be compared with the well-known Hodgkin-Huxley model. Originally designed to describe a squid axon containing sodium and potassium channel proteins, the differential equation for the Hodgkin-Huxley model is given by

$$\frac{r}{2R_i}\frac{\partial^2}{\partial x^2}V = C_m\frac{\partial}{\partial t}V + g_K(V,t)(V - E_K) + g_{Na}(V,t)(V - E_{Na}), \tag{4}$$

where the transmembrane voltage V is the observable (instead of $\Delta\rho$), r is the radius of the axon, R_i is the resistance of the cytoplasm in the axon, C_m is the

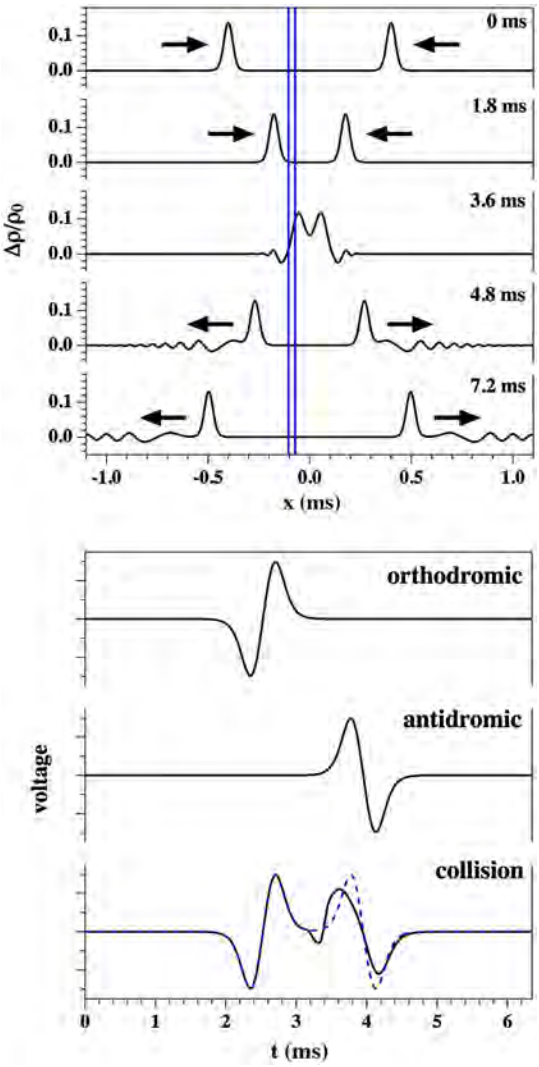

FIG. 5. Top panel: The collision of two pulses in the soliton theory of nerves for $v = 0.7c_0$. Parameters are given in the text. After collision, the shape of the solitary pulses is virtually unchanged. The two blue lines indicate the positions of two hypothetical recording electrodes with a distance of 16 mm. Bottom panel: The calculated voltage difference between the two electrodes shown in the top panel. The top trace shows the single orthodromic AP, the center trace shows the antidromic AP, and the bottom trace (solid) shows the recording of the two colliding pulses. The dashed blue line is the sum of the orthodromic and antidromic without a collision. It is added as a guide to the eye.

membrane capacitance, and E_K and E_{Na} are the Nernst potentials of potassium and sodium reflecting the differences in ion concentrations inside and outside of the neuron. The conductances of potassium and sodium ions, $g_K(V,t)$ and $g_{Na}(V,t)$, are complicated functions of voltage and time. If additional channel proteins are present, more conductance terms must be added to Eq. (4). Equation (4) has a structure similar to the wave equation (1). However, no general theory exists for the conductances $g_i(V,t)$. Their dependence on time and voltage must be determined empirically from voltage-clamp data [1]. This introduces many parameters into the above equation. Furthermore, not all nerves are as simple as the squid axon, and they may contain more than just two channel proteins. More terms containing the conductances of other proteins must be introduced, further increasing the number of parameters. In the literature, one finds models with up to 66 parameters [32]. Since different nerves contain different ion channels, it is not generally possible to make a generic statement about the pulse collision process. However, on the basis of numerical simulations for the squid axon, it is generally believed that the Hodgkin-Huxley model results in the annihilation of colliding pulses. Qualitatively, this is due to a refractory period introduced by time-dependent changes in protein structure during the nerve pulse that render the nerve unexcitable for a short period after the pulse. This will be explained further in the Discussion section.

B. Experimental results

1. Earthworm experiments

After confirming that we could stimulate the ventral cord from both ends independently, we performed a collision experiment by simultaneously stimulating both ends of the ventral cord. We proceeded by increasing the stimulating voltage in small intervals up to the values necessary to generate action potentials at both ends of the ventral cord fragment simultaneously. The recording electrodes are located closer to the site where the orthodromic pulse is generated. It is therefore necessary for the antidromic pulse to pass through the orthodromic pulse before it can reach the recording electrodes (cf. Fig. 4). Thus, if both the orthodromic and the antidromic pulse can be recorded, the two pulses must have passed through each other. If only the orthodromic pulse (but not the antidromic pulse) can be recorded, this is evidence for pulse annihilation.

A representative result is shown in Fig. 6. The top two traces show the orthodromic and antidromic pulses after individual stimulation. The antidromic signal arrives at the electrodes about 1.5 ms later than the orthodromic pulses. This interval is comparable to the width of the pulses. Therefore, one can recognize both pulses as separate events. The bottom trace shows the experiment where both orthodromic and antidromic pulses were generated simultaneously. We find that both pulses can be recorded and that they are unchanged in shape. As a guide to the eye, we show the sum of the individual orthodromic and antidromic pulses in the absence of a collision (dashed blue line). This signal is very similar to that recorded in the collision experiment, indicating that pulse collision does not generate much distortion of the signal. This experiment was reproduced in at least 30 different worm axons, and we always found pulse penetration. We observed infrequent events (less than 15%) in which we recorded only the

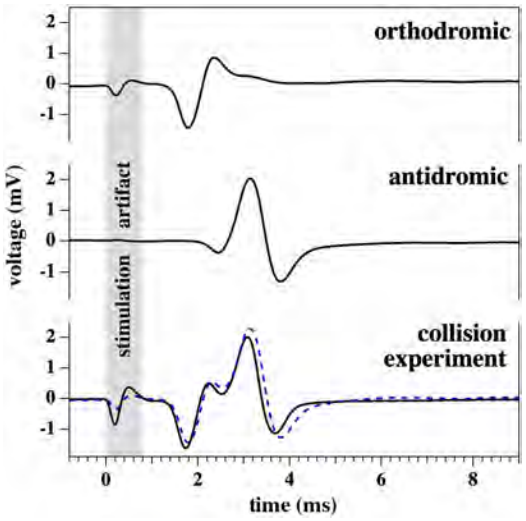

FIG. 6. Example of the pulse collision experiment in the ventral cord of an earthworm (sample #7 in Table I). Top: Action potential propagating orthodromically after stimulation at the top end of the nerve. Center: Action potential propagating antidromically after stimulation at the bottom end of the nerve. Bottom: Both action potentials generated by simultaneous stimulation at both ends (solid line). For comparison and a guide for the eye, the dashed line represents the sum of the individual pulses. This signal is similar to the observed trace. The region shaded in grey shows the stimulation artifact.

orthodromic pulse. This typically happened when the axon was moved such that the stimulation electrodes were close to the extreme ends of the axon. In all of these cases, relative movement of the same axon with respect to the electrodes reestablished pulse penetration.

In Table I, we report the results of a selection of ten different samples (out of the 30 different nerves) for which there was little or no overlap between the orthodromic and antidromic pulses. In these cases, the velocities of the individual pulses could be determined easily. The convention is to determine the velocities from the first extremum in each pulse recording. For completeness, we also give the velocities for the nodal point in each trace corresponding to the pulse maximum (values in brackets). These values are somewhat smaller but are also comparable for single pulses and pulses in the collision experiment. We show the velocities of both the orthodromic and the antidromic pulses in the case of single and of simultaneous stimulation. In general, the velocities of the antidromic pulses are lower. This lower velocity could be a result of diameter changes along the median giant axon. Pulse velocities range between 2.8 and 9.7 m/s. The earthworm MGF and LGF axons are considered myelinated (with varying degrees of myelin packing). The conduction speed is a few fold higher than that of nonmyelinated fibers of the same diameter [30]. Since the temporal width of the pulses is about 2 ms, this corresponds to a lateral extension of the

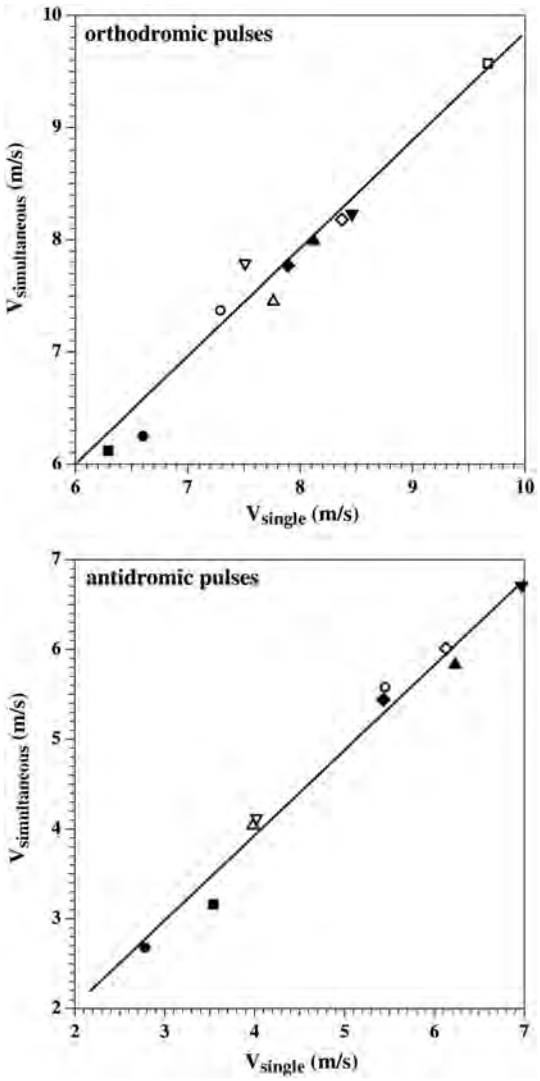

FIG. 7. Pulse velocities obtained in the collision experiment in the earthworm (simultaneous stimulation) versus the velocities of the single stimulation (using the first extremum of each pulse recording). Top panel: Orthodromic pulses. Bottom panel: Antidromic pulses. The same symbols in both panels indicate identical nerve preparation. The open square corresponds to the traces in Fig. 6 (sample #7). The experimental temperature was 22 ± 1 °C.

pulse of 4–17 mm. Thus, the pulse width is larger than the distance between the electrodes. It is also larger than the average neuron in the segmented giant axons which has a length of about 1–1.5 mm [21]. In Fig. 7, we plot both orthodromic and antidromic pulse velocities in the collision experiment versus the velocities in the single stimulation experiment. Within experimental error, we find that the propagation velocities are unaltered by the collision. Similarly, as can be seen in Fig. 6, the pulse shapes are unaltered by a collision. The pulse velocities are typically smaller in the antidromic direction as compared to the

TABLE I. Conduction velocity estimates in m/s from ten different collision experiments on the ventral cord of an earthworm. All measurements were carried out at $22 \pm 1\,^{\circ}\mathrm{C}$. The convention is to calculate the velocities by using the first extremum in each pulse recording. Values in parentheses correspond to velocities calculated for the nodal point in each pulse that corresponds to the pulse maximum. The recordings belonging to sample #7 are shown in Fig. 6.

	Single		Simultaneous	
Sample	Orthodromic	Antidromic	Orthodromic	Antidromic
1	6.60 (5.43)	2.78 (2.32)	6.25 (5.01)	2.68 (2.23)
2	6.29 (5.52)	3.54 (3.03)	6.12 (5.12)	3.16 (2.78)
3	8.12 (7.76)	6.23 (5.39)	7.99 (7.03)	5.83 (5.61)
4	8.46 (7.06)	6.97 (5.69)	8.23 (6.83)	6.71(5.41)
5	7.89 (6.63)	5.43 (4.82)	7.77 (6.48)	5.44 (4.91)
6	7.29 (6.65)	5.45 (4.71)	7.37 (6.77)	5.58 (4.91)
7	9.67 (7.81)	7.50 (6.66)	9.57 (7.77)	7.13 (6.69)
8	7.76 (6.46)	3.98 (3.28)	7.45 (6.21)	4.04 (3.38)
9	7.51 (7.01)	4.02 (3.59)	7.79 (7.35)	4.12 (3.79)
10	8.37 (7.36)	6.13 (5.27)	8.18 (7.16)	6.01 (5.10)

orthodromic direction. We believe that this is due to the change in diameter of the fibers along the worm axis.

The interpretation of the collision experiments shown in Fig. 6 and Table I rests on the assumption that in both the orthodromic and antidromic directions, the same fiber was stimulated. Early experiments from Refs. [33,34] on the neural cord of an earthworm show that the MGF displays a lower threshold voltage than the LGF. However, there is a finite possibility that in our collision experiments, we stimulate the MGF in one direction and the LGF in the other direction. Under such circumstances, the action potentials would trivially pass by each other and never collide at all. As a consequence, this would lead to a misinterpretation of the experiment.

To rule out this possibility, we performed another set of experiments using double stimulation of both MGF and LGF. In Fig. 8 (top left), we show the stimulation of the earthworm axon at two different stimulation voltages. At 0.25 V, one only observes an action potential in one of the fibers. According to the literature, this is likely to be the pulse in the MGF. At 0.45 V, one sees the pulse in both the MGF and the LGF. Both voltages are directly above threshold for single and double stimulation. Thus, in order to stimulate both fibers, nearly twice the stimulation voltage is required. A similar observation is made for the antidromic signal (Fig. 8, bottom left). Here, too, one nearly needs twice the voltage to stimulate both pulses. Next, we performed an experiment in which both fibers were stimulated in the orthodromic direction (Fig. 8, right, top trace), and only one fiber was stimulated in the antidromic direction (Fig. 8, right, center trace) [35]. After collision, one can still observe both action potentials in the orthodromic direction and the single action potential in the antidromic direction. Independent of which fiber was

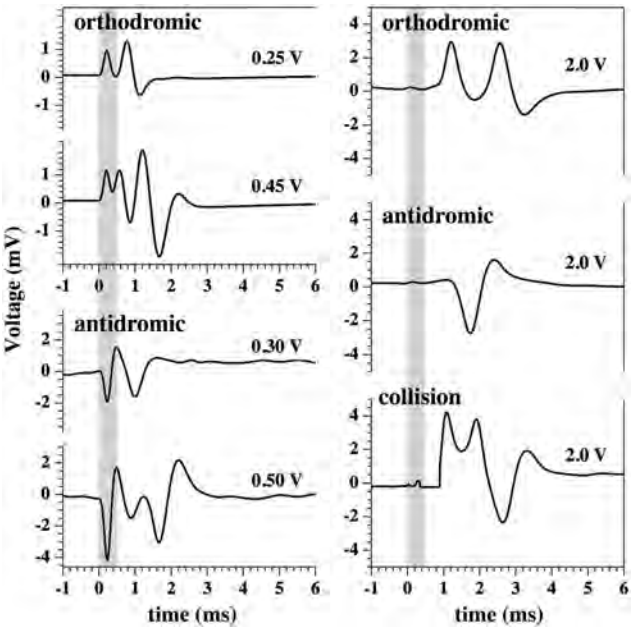

FIG. 8. Simultaneous stimulation of both MGF and LGF in an earthworm. Left, top: Single and double stimulation in the orthodromic direction only. Left, bottom: Single and double stimulation in the antidromic direction only. Right: Collision experiment with stimulation of both the MGF and LGF in the orthodromic direction. In the antidromic direction, only the MGF is stimulated. One can recognize that the antidromic signal is still present in the recording after collision. The grey-shaded regions mark the stimulation artifact. The left and right panels were from different axons.

stimulated in the antidromic direction, it was unavoidable that it had collided with one of the two action potentials in the orthodromic direction. This demonstrates that the antidromic pulse did not annihilate upon collision.

From Figs. 6–8 and the data in Table I, we conclude that action potentials in the giant axons pass through each other without significant distortion.

2. Experiments on giant axons from the abdominal part of the ventral cord of a lobster

In contrast to the earthworm, the ventral cord of a lobster possesses two median and two lateral giant axons (Fig. 3). The median axon is not segmented as in the ventral cord of the earthworm. It has been described in the literature that in the abdominal part of the ventral cord, the first (i.e., at the lowest stimulus) and largest electrical signals correspond to the LGFs [22]. The MGF pulse (which displays a slower velocity than the LGF) appears as a next electrical signal after an increase in stimulus voltage. The small fibers in the ventral cord generate small signals and require high stimulation voltage. Figure 9 (left) shows that an increasing number of giant axons is stimulated after an increase in voltage. Figure 9 (right) shows an experiment with one major orthodromic signal (top) and two antidromic signals

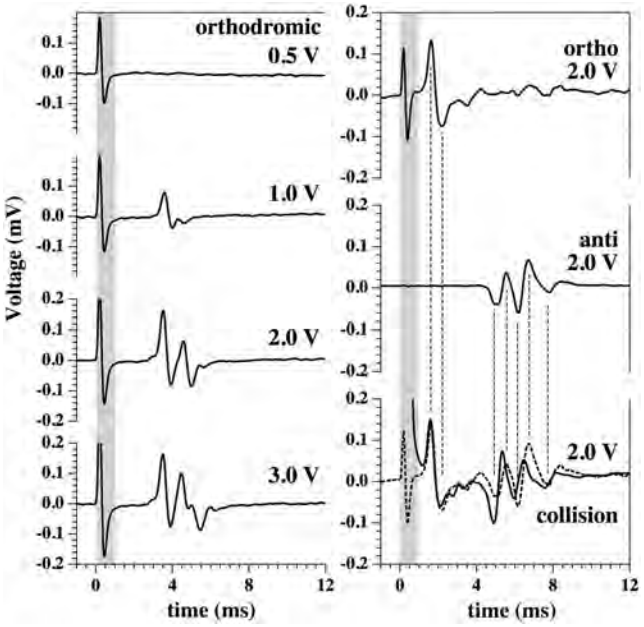

FIG. 9. Left: Action potentials after stimulation in the orthodromic direction show the successive generation of action potentials in the giant axons when increasing the stimulation voltage. Right: The collision experiment in the abdominal part of the ventral cord of a lobster at a stimulation voltage of 2 V. Top: Stimulation in the orthodromic direction only. Center: Stimulation in the antidromic direction only. Bottom: Collision experiment (solid line) compared with the sum of the top (orthodromic) and the center (antidromic) traces (dashed line). The two traces are virtually superimposable.

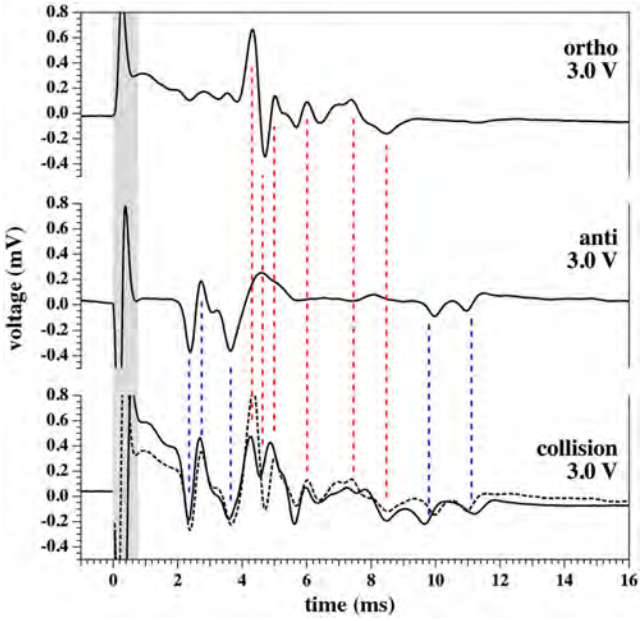

FIG. 10. Same as in Fig. 9 (right) but with higher stimulation voltage (3 V, different preparation). More axons are stimulated, and all giant fibers are active. The bottom trace shows the collision experiment (solid line) compared with the sum of the top (orthodromic) and the center (antidromic) traces. Again, the two traces are virtually superimposable, indicating that no annihilation of any of the signals took place.

(center). Figure 9 (bottom right) shows the collision experiment. The dashed line is the sum of the orthodromic and antidromic pulses from the single-side stimulation experiments. It can be seen that the summed individual signals are nearly identical to the signal in the collision experiment. It is most likely that the three signals in this experiment correspond to the lateral giant fibers of the ventral cord. Thus, one can conclude that pulses in one of the lateral fibers have passed through each other and did not annihilate. However, one cannot fully exclude the possibility that different neurons were stimulated in the two directions, e.g., one signal in the LGF in one direction and two signals in the MGFs in the other direction. Under such conditions, pulses would actually never collide. For this reason, we repeated the experiment in the ventral cord of a different preparation at higher stimulation voltage (Fig. 10). Now, more action potentials are excited in both the orthodromic and antidromic directions (at least four in each direction). The antidromic signal displays some signals with slow velocity that probably correspond to the MGF fibers. Thus, all giant fibers are stimulated. The bottom trace in Fig. 10 shows the collision experiment. It shows that all signals in the collision experiment are conserved compared to the summed signals of orthodromic and antidromic stimulation. None of the signals was annihilated upon collision. We take this as convincing evidence that annihilation upon collision is not observed in the abdominal part of the ventral cord of a lobster. This experiment was reproduced in eleven different preparations. Additionally, we repeated these experiments in other nerves from lobsters, including nerves from the legs and the connectives close to the lobster brain. In total, the above experiments were confirmed in 30 different nerve bundles from the walking legs, 16 preparations of the thorax ventral cord, and 12 samples from lobster connectives. Those results will be reported independently.

IV. DISCUSSION

We investigated the collision of action potentials in giant axons of the earthworm both experimentally and theoretically. Orthodromic and antidromic pulses were stimulated at both ends of the isolated axon. We showed, in at least 30 independent nerve preparations, that colliding action potentials pass through each other without significant perturbation. In less than 15% of the preparations, we found annihilation of pulses. In all of these cases, penetration could be reestablished by slight changes in the position of the axon on the electrodes. We believe that these cases reflect effects related to the extreme ends of the axon. We confirmed these findings in preparations from the ventral

cord of a lobster. When exciting all giant axons at large stimulation voltage at both ends of the nerve, all signals in the orthodromic and antidromic directions were maintained after collision without major perturbation. No evidence for pulse annihilation was found. In nonlinear hydrodynamics simulations, we further studied the penetration of pulses using the soliton theory [11,14]. As expected, this theory indicates that solitary pulses pass through each other with the production of minor amounts of small amplitude noise. This is consistent with our experimental finding. However, it is seemingly in conflict with expectations based on electrophysiological models such as the Hodgkin-Huxley model [1], where a refractory period is expected to lead to pulse annihilation.

Indeed, it is widely believed that action potentials do annihilate upon collision. However, pulse annihilation is not well documented in the experimental literature. The most relevant report by Tasaki from 1949 [3] discussed annihilation in myelinated nerve fibers in the Sartorius muscle of a toad. Tasaki reported pulse annihilation in this preparation. The analysis of the results involved saltatory conduction between the nodes of Ranvier in the myelinated nerve. To our knowledge, Tasaki's experiments were never reproduced. In 1982, Tasaki and Iwasa reported the mechanical response of colliding pulses in squid axons [36]. They found a slight modification of the mechanical pulse at the site of the collision, but pulse annihilation was not examined. We have not succeeded in finding further original publications on pulse annihilation, and it is not certain that the common notion of the existence of pulse annihilation is well rooted in experiment. However, within the context of the Hodgkin-Huxley model, it seems natural to expect pulse annihilation on theoretical grounds. The refractory period is a brief period after stimulation of an action potential during which the nerve is not excitable. It has been found in many nerves. Talo and Lagerspetz [37] reported refractory periods of 1.2–1.5 ms around room temperature, both for median lateral fiber and for lateral giant fiber of earthworms. Kladt *et al.* [27] reported refractory periods of 0.7–2.8 ms in intact earthworms. These numbers are comparable to those found by us ($\approx$2 ms, data are not shown). Thus, empirically short refractory periods exist in earthworms and many other nerves. As our experiments show, the existence of a refractory period does not automatically imply the annihilation of colliding action potentials. It seems plausible to postulate that two colliding pulses annihilate because they are expected to enter into unexcitable regions of the neuron immediately after their collision. In the context of the HH model, the existence of refractory periods is a consequence of relaxation processes in channel proteins after firing. The original model considers only sodium and potassium channels. However, neurons from other sources may contain many different Na and K channels, as well as many other channel proteins, such as calcium channels. Thus, one cannot easily generalize the properties of a particular neuron such as the squid axon for which the HH model was designed. Since there exists no general theory for the voltage-dependent and temporal behavior of channel proteins, the properties of such proteins are typically parametrized from experiment. The model by Bostock and collaborators for the myelinated axons in humans contains 66 parameters describing five different channels that display different concentrations in different regions of the nerve [32]. The Fitzhugh-Nagumo model [38–40] is a simplification of the Hodgkin-Huxley model. It has been shown that this model (using only sodium and potassium channels) possesses parameter regimes in which pulses can penetrate [41]. Thus, it seems that the Hodgkin-Huxley model does not necessarily exclude the possibility of penetrating pulses. Interestingly, Tasaki dismissed the idea that the refractory period is responsible for pulse annihilation in his original publication from 1949 [3]. He rather believed that during pulse collision, the currents inside and outside of the nerve add up to zero such that the condition for regenerating the pulse is not met during collision.

The experiment by Tasaki [3] on toad nerves indicates that there may be examples for pulse annihilation (even though reproducing this experiment would be helpful). However, we can falsify the general belief that annihilation must always occur because of the presence of a refractory period. Here, we have demonstrated penetration of pulses in myelinated (earthworm) and nonmyelinated (lobster) giant axons.

The notion of penetrating pulses is not consistent with the Hodgkin-Huxley model if there is a refractory period (such as earthworm axons). It is, however, in agreement with the assumption of the existence of mechanical pulses in nerves. Mechanical dislocations in various nerves have been experimentally confirmed in squid axons, and nerves from crab and garfish [9,10,36,42–47]. Thus, it is clear that action potentials possess a mechanical component.

To simulate colliding pulses, we applied the soliton theory that considers the nerve pulse as an electromechanical compressional pulse. It makes use of the hydrodynamic theory of sound propagation in the presence of nonlinear materials and dispersion. The nonlinearity in the elastic constants is generated by a phase transition in the lipid chains that influences the elastic properties of the membrane. The soliton theory has the following features: It describes an adiabatic pulse in a membrane cylinder (the axon) in which, by necessity, no heat is dissipated. Thus, the temperature of a nerve would be the same before and after the pulse [11]. This has, in fact, been observed in numerous experiments [4,5,7]. During the pulse, a change in both nerve area and thickness is predicted. This has been confirmed in early experiments that find both a contraction of the neuron and a slight dislocation of the membrane by about 1 nm (see, e.g., Refs. [9,10]). In contrast, the Hodgkin-Huxley model is of a dissipative nature and

should result in measurable changes in heat that are not found in experiments. Furthermore, since neither mechanical dislocations or temperature changes are explicitly contained in the Hodgkin formalism, it cannot be used to describe them. It is interesting to note that the soliton theory also contains a feature comparable to a refractory period [48]. It is the consequence of mass conservation. The action potential in the soliton theory consists of a region of higher area density of the neuronal membrane. To obey mass conservation, each pulse must be accompanied by a dilated region that prevents pulses from being arbitrarily close. However, the existence of such a feature does not prevent colliding pulses from penetrating nearly without dissipation.

The earthworm axon consists of many single neurons connected by gap junctions, and one may not consider it as representative for single axons of other species. We note, however, that the action potential in the earthworm is larger than the dimension of the individual neurons in the axon. Thus, the pulse is a property of the axon as a whole and not of the individual neurons. Furthermore, we provided evidence for the giant axons of the ventral cord of a lobster that suggests that the observation of undistorted penetration of action potentials is more generic.

ACKNOWLEDGMENTS

We thank to Professor Andrew D. Jackson from the Niels Bohr International Academy for useful discussions and for a critical reading of the manuscript. This work was supported by the Villum Foundation (VKR 022130).

[1] A. L. Hodgkin and A. F. Huxley, *A Quantitative Description of Membrane Current and Its Application to Conduction and Excitation in Nerve*, J. Physiol. **117**, 500 (1952).

[2] A. L. Hodgkin, *The Conduction of the Nervous Impulse* (Liverpool University Press, Liverpool, England, 1964).

[3] I. Tasaki, *Collision of Two Nerve Impulses in the Nerve Fiber*, Biochim. Biophys. Acta **3**, 494 (1949).

[4] B. C. Abbott, A. V. Hill, and J. V. Howarth, *The Positive and Negative Heat Production Associated with a Nerve Impulse*, Proc. R. Soc. B **148**, 149 (1958).

[5] J. V. Howarth, R. D. Keynes, and J. M. Ritchie, *The Origin of the Initial Heat Associated with a Single Impulse in Mammalian Non-myelinated Nerve Fibres*, J. Physiol. **194**, 745 (1968).

[6] J. Howarth, *Heat Production in Non-myelinated Nerves*, Phil. Trans. R. Soc. A **270**, 425 (1975).

[7] J. M. Ritchie and R. D. Keynes, *The Production and Absorption of Heat Associated with Electrical Activity in Nerve and Electric Organ*, Q. Rev. Biophys. **18**, 451 (1985).

[8] In addition to the initial heat that is in phase with the voltage changes, there is a slow metabolic release of heat that is uncorrelated with the action potential [4].

[9] K. Iwasa and I. Tasaki, *Mechanical Changes in Squid Giant-Axons Associated with Production of Action Potentials*, Biochem. Biophys. Res. Commun. **95**, 1328 (1980).

[10] K. Iwasa, I. Tasaki, and R. C. Gibbons, *Swelling of Nerve Fibres Associated with Action Potentials*, Science **210**, 338 (1980).

[11] T. Heimburg and A. D. Jackson, *On Soliton Propagation in Biomembranes and Nerves*, Proc. Natl. Acad. Sci. U.S.A. **102**, 9790 (2005).

[12] T. Heimburg and A. D. Jackson, *On the Action Potential as a Propagating Density Pulse and the Role of Anesthetics*, Biophys. Rev. Lett. **02**, 57 (2007).

[13] S. S. L. Andersen, A. D. Jackson, and T. Heimburg, *Towards a Thermodynamic Theory of Nerve Pulse Propagation*, Prog. Neurobiol. **88**, 104 (2009).

[14] B. Lautrup, R. Appali, A. D. Jackson, and T. Heimburg, *The Stability of Solitons in Biomembranes and Nerves*, Eur. Phys. J. E **34**, 57 (2011).

[15] E. R. Kandel, J. H. Schwartz, and T. M. Jessell, *Principles of Neural Science*, 4th ed., (McGraw-Hill, New York, 2000).

[16] D. Pinault, *Backpropagation of Action Potentials Generated at Ectopic Axonal Loci: Hypothesis that Axon Terminals Integrate Local Environmental Signals*, Brain Res. **21**, 42 (1995).

[17] J. H. Fuller and J. D. Schlag, *Determination of Antidromic Excitation by the Collision Test: Problems of Interpretation*, Brain Res. **112**, 283 (1976).

[18] J. Kimura, *Collision Technique. Physiologic Block of Nerve Impulses in Studies of Motor Nerve Conduction Velocity*, Neurology **26**, 680 (1976).

[19] B. Murray and P. Shizgal, *Evidence Implicating Both Slow-and Fast-Conducting Fibers in the Rewarding Effect of Medial Forebrain Bundle Stimulation*, Behavioural Brain Research **63**, 47 (1994).

[20] P. J. Mill, *Recent Developments in Earthworm Neurobiology*, Comp. Biochem. Physiol. **73A**, 641 (1982).

[21] J. Gunther, *Neuronal Syncytia in the Giant Fibres of Earthworms*, J. Neurocytol. **4**, 55 (1975).

[22] C. K. Govind and F. Lang, *Growth of Lobster Giant Axons: Correlation between Conduction Velocity and Axon Diameter*, J. Comp. Neurol. **170**, 421 (1976).

[23] C. D. Drewes and R. A. Pax, *Neuromuscular Physiology of the Longitudinal Muscle of the Earthworm, Lumbricus Terrestris. I. Effects of Different Physiological Salines*, J. Exp. Biol. **60**, 445 (1974).

[24] P. D. Evans, E. A. Kravitz, B. R. Talamo, and B. G. Wallace, *The Association of Octopamine with Specific Neurones Along Lobster Nerve Trunks*, J. Physiol. **262**, 51 (1976).

[25] http://cdn.adinstruments.com/adi-web/manuals/PowerLab_Teaching_Series_OG.pdf.

[26] R. E. Coggeshall, *A Fine Structural Analysis of the Ventral Nerve Cord and Associated Sheath of Lumbricus terrestris L*, J. Comp. Neurol. **125**, 393 (1965).

[27] N. Kladt, U. Hanslik, and H.-G. Heinzel, *Teaching Basic Neurophysiology Using Intact Earthworms*, J. Undergrad. Neurosci. Educ. **9**, A20 (2010).

[28] K. Y. H. Lagerspetz and A. Talo, *Temperature Acclimation of the Functional Parameters of the Giant Nerve Fibres in Lumbricus terrestris L. I. Conduction Velocity and the Duration of the Rising and Falling Phase of Action Potential*, J. Exp. Biol. **47**, 471 (1967).

[29] G. E. Johnson, *Giant Nerve Fibers in Crustaceans with Special Reference to Cambarus and Palaemonetes*, J. Comp. Neurol. **36**, 323 (1924).
[30] D. K. Hartline and D. R. Colman, *Rapid Conduction and the Evolution of Giant Axons and Myelinated Fibers*, Curr. Biol. **17**, R29 (2007).
[31] T. Heimburg, *The Capacitance and Electromechanical Coupling of Lipid Membranes Close to Transitions. The Effect of Electrostriction*, Biophys. J. **103**, 918 (2012).
[32] J. Howells, L. Trevillion, H. Bostock, and D. Burke, *The Voltage Dependence of I_h in Human Myelinated Axons*, J. Physiol. **590**, 1625 (2012).
[33] C. Y. Kao, *Basis for After-Discharge in the Median Giant Axon of the Earthworm*, Science **123**, 803 (1956).
[34] C. Y. Kao and H. Grundfest, *Postsynaptic Electrogenesis in Septate Giant Axons. I. Earthworm Median Giant Axon*, J. Neurophysiol. **20**, 553 (1957).
[35] Note that this is an experiment on a different axon, as in the left-hand panels. The shapes of the pulses and the respective stimulation voltages are different.
[36] I. Tasaki and K. H. Iwasa, *Rapid Pressure Changes and Surface Displacements in the Squid Axon Associated with Production of Action Potentials*, Jpn. J. Physiol. **32**, 69 (1982).
[37] A. Talo and K. Y. H. Lagerspetz, *Temperature Acclimation of the Functional Parameters of the Giant Nerve Fibres in Lumbricus terrestris L. II. The Refractory Period*, J. Exp. Biol. **47**, 481 (1967).
[38] R. FitzHugh, *Mathematical Models of Threshold Phenomena in the Nerve Membrane*, Bull. Math. Biophys. **17**, 257 (1955).
[39] R. FitzHugh, *Impulses and Physiological States in Theoretical Models of Nerve Membrane*, Biophys. J. **1**, 445 (1961).
[40] J. Nagumo, S. Arimoto, and S. Yoshizawa, *An Active Pulse Transmission Line Simulating Nerve Axon*, Proc. IRE **50**, 2061 (1962).
[41] O. V. Aslanidi and O. A. Mornev, *Can Colliding Nerve Pulses Be Reflected?*, JETP Lett. **65**, 579 (1997).
[42] I. Tasaki, K. Iwasa, and R. C. Gibbons, *Mechanical Changes in Crab Nerve Fibers During Action Potentials*, Jpn. J. Physiol. **30**, 897 (1980).
[43] I. Tasaki and P. M. Byrne, *Tetanic Contraction of the Crab Nerve Evoked by Repetitive Stimulation*, Biochem. Biophys. Res. Commun. **106**, 1435 (1982).
[44] I. Tasaki and K. Iwasa, *Further Studies of Rapid Mechanical Changes in Squid Giant Axon Associated with Action Potential Production*, Jpn. J. Physiol. **32**, 505 (1982).
[45] I. Tasaki and K. H. Iwasa, *Further Studies of Rapid Mechanical Changes in Squid Giant Axon Associated with Action Potential Production*, Jpn. J. Physiol. **32**, 505 (1982).
[46] I. Tasaki, K. Kusano, and M. Byrne, *Rapid Mechanical and Thermal Changes in the Garfish Olfactory Nerve Associated with a Propagated Impulse*, Biophys. J. **55**, 1033 (1989).
[47] I. Tasaki and M. Byrne, *Volume Expansion of Nonmyelinated Nerve Fibers During Impulse Conduction*, Biophys. J. **57**, 633 (1990).
[48] E. Villagran Vargas, A. Ludu, R. Hustert, P. Gumrich, A. D. Jackson, and T. Heimburg,, *Periodic Solutions and Refractory Periods in the Soliton Theory for Nerves and the Locust Femoral Nerve*, Biophys. Chem. **153**, 159 (2011).

Journal of Physics: Conference Series **558** (2014) 012018 doi:10.1088/1742-6596/558/1/012018

Electromechanical properties of biomembranes and nerves

T Heimburg*, A Blicher, L D Mosgaard and K Zecchi
The Niels Bohr Institute, University of Copenhagen, 2100 Copenhagen Ø, Denmark
E-mail: theimbu@nbi.dk

Abstract. Lipid membranes are insulators and capacitors, which can be charged by an external electric field. This phenomenon plays an important role in the field of electrophysiology, for instance when describing nerve pulse conduction. Membranes are also made of polar molecules meaning that they contain molecules with permanent electrical dipole moments. Therefore, the properties of membranes are subject to changes in trans-membrane voltage. Vice versa, mechanical forces on membranes lead to changes in the membrane potential. Associated effects are flexoelectricity, piezoelectricity, and electrostriction.

Lipid membranes can melt from an ordered to a disordered state. Due to the change of membrane dimensions associated with lipid membrane melting, electrical properties are linked to the melting transition. Melting of the membrane can induce changes in trans-membrane potential, and application of voltage can lead to a shift of the melting transition. Further, close to transitions membranes are very susceptible to piezoelectric phenomena.

We discuss these phenomena in relation with the occurrence of lipid ion channels. Close to melting transitions, lipid membranes display step-wise ion conduction events, which are indistinguishable from protein ion channels. These channels display a voltage-dependent open probability. One finds asymmetric current-voltage relations of the pure membrane very similar to those found for various protein channels. This asymmetry falsely has been considered a criterion to distinguish lipid channels from protein channels. However, we show that the asymmetry can arise from the electromechanical properties of the lipid membrane itself.

Finally, we discuss electromechanical behavior in connection with the electromechanical theory of nerve pulse transduction. It has been found experimentally that nerve pulses are related to changes in nerve thickness. Thus, during the nerve pulse a solitary mechanical pulse travels along the nerve. Due to electromechanical coupling it is unavoidable that this pulse generates a trans-membrane voltage. In the past, we have proposed that this electromechanical pulse is the origin of the action potential in nerves.

1. Introduction

Biological membranes are thin quasi-twodimensional layers mainly consisting of proteins and lipids. While research mostly focusses on the properties of individual macromolecules, e.g., on ion channel proteins or ion pumps, the total membrane possesses macroscopic cooperative features such as melting transitions and curvature fluctuations that cannot be understood on the molecular level. These properties are expressed in susceptibilities such as heat capacity, lateral compressibility, bending elasticity or capacitive susceptibility. Lipid membranes can melt from a solid to a liquid phase. In these transitions, the order of the lipids changes. Thus, the melting is associated to both, enthalpy and entropy changes. Such transitions can also be found in biological membranes under physiological conditions. As an example, a heat


Content from this work may be used under the terms of the Creative Commons Attribution 3.0 licence. Any further distribution of this work must maintain attribution to the author(s) and the title of the work, journal citation and DOI.
Published under licence by IOP Publishing Ltd

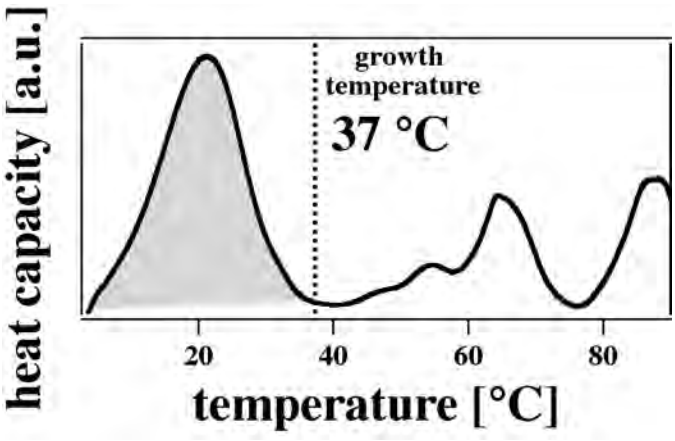

Figure 1. Heat capacity profile of E. *coli* membranes. The grey-shaded region below growth temperature represents the membrane melting transition. The peaks above growth temperature show protein unfolding. From [5].

capacity profile of E. *coli* membranes is shown in figure 1. In the melting transition, the spatial dimensions of the membrane change. For instance, upon melting the synthetic lipid dipalmitoyl phosphatidylcholine (DPPC) increases its area by about 24% and reduces its thickness by 16%. The heat absorbed in the transition is about 35 kJ/mol.

Membranes are very thin. They possess a thickness of about 5nm in their solid state. The core of the membrane is composed of hydrocarbon chains. Therefore, the membrane interior can be considered an insulator. Consequently, the biomembrane has the properties of a capacitor. Typically, the capacitance of a membrane is of the order of 1 $\mu F/cm^2$. In biological cells, the membrane is exposed to voltage differences of the order of 100 mV. Thus, the biological membrane is charged under physiological conditions.

The dimensional changes in the melting transitions have a number of consequences. Among those are [1]:

- both hydrostatic and lateral pressure changes influence the phase state of the membrane and are intrinsically coupled to heat absorption or release.
- hydrostatic and lateral pressure changes voltage across the membrane, and the charge on the membrane capacitor can change. Thus, the membrane is piezoelectric.
- voltage changes can induce membrane melting.

These features are important for various properties of biological membranes. For instance, it was shown that biomembranes slightly above a melting transition can support electromechanical solitons that resemble nerve pulses [2]. Further, in the transition one finds density fluctuations that result in the spontaneous formation of pores in the membrane [3]. These pores display open-close characteristics very similar to those reported for protein ion channels [4].

The thermodynamics of biological membranes putatively explains many properties of excitatory cells on the level of macroscopic physics rather than on the level of molecular biology. This review will introduce into some of these phenomena.

2. Membrane capacitors

The capacitance, C_m, of a planar membrane is given by

$$C_m = \varepsilon\varepsilon_0 \frac{A}{D} \,, \tag{1}$$

where ε_0 is the vacuum permittivity, ε is the dielectric constant, A is the membrane area and D is the membrane thickness. The charge, q, on a capacitor is given by

$$q = C_m \cdot V_m \,, \tag{2}$$

where V_m is the transmembrane voltage. Since in the transition the area changes by about 24%

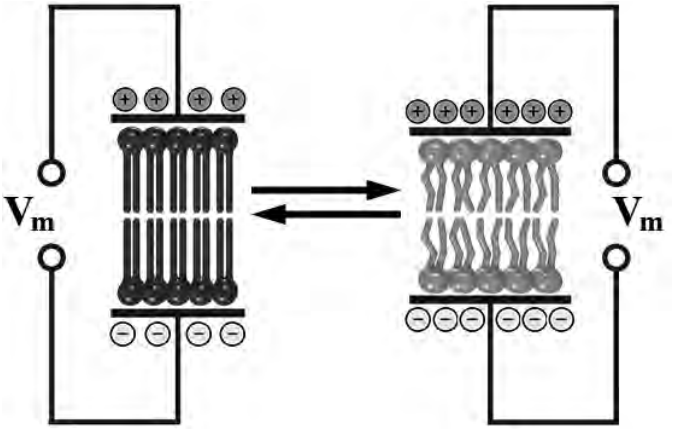

Figure 2. During the melting transition of a membrane both its area and thickness changes. This implies that the capacitance of the membrane varies as a function of phase state. It is higher in the liquid state.

and the thickness by -16%, one finds an increase in capacitance upon melting from a solid to a liquid membrane phaseof approximately 50%.

2.1. Capacitive susceptibility

The capacitance solely depends on the dimensions of the membrane, if $\varepsilon = constant$. However, the opposite charges on the two plates of a capacitor attract each other and generate a force on the membrane. This effect is called 'electrostriction'. If the voltage across a membrane increases, the forces on the membrane also increases. Therefore the capacitance changes as well. For a symmetric membrane, the capacitance always increases upon increasing the voltage. This effect can be taken into account by considering the capacitive susceptibility, $\hat{C}_m$:

$$\hat{C}_m = \frac{dq}{dV_m} = C_m + V_m \frac{\partial C_m}{\partial V_m} \,, \tag{3}$$

where the charge, q, is given by equation (2). The second term in this equation could be considered an excess capacitance. It assumes a maximum in the melting transition (see figure 3).

3. Fluctuations

Due to the fluctuation-dissipation theorem, all response functions (susceptibilities) are related to the mean square fluctuations of extensive variables. For instance, the heat capacity, $c_p = (\partial H/\partial T)_p$, is given by

$$c_p = \frac{\langle H^2 \rangle - \langle H \rangle^2}{kT^2} \,, \tag{4}$$

while the isothermal volume compressibility, $\kappa_T^V = -(\partial V/\partial p)_T$, is related to volume fluctuations

$$\kappa_T^V = \frac{\langle V^2 \rangle - \langle V \rangle^2}{kT} \,, \tag{5}$$

and the capacitive susceptibility is given by

$$\hat{C}_m = \frac{\langle q^2 \rangle - \langle q \rangle^2}{kT} \,. \tag{6}$$

Similarly, fluctuations in area are related to the isothermal area compressibility and fluctuations in curvature to the bending elasticity. The heat capacity assumes a maximum in the melting

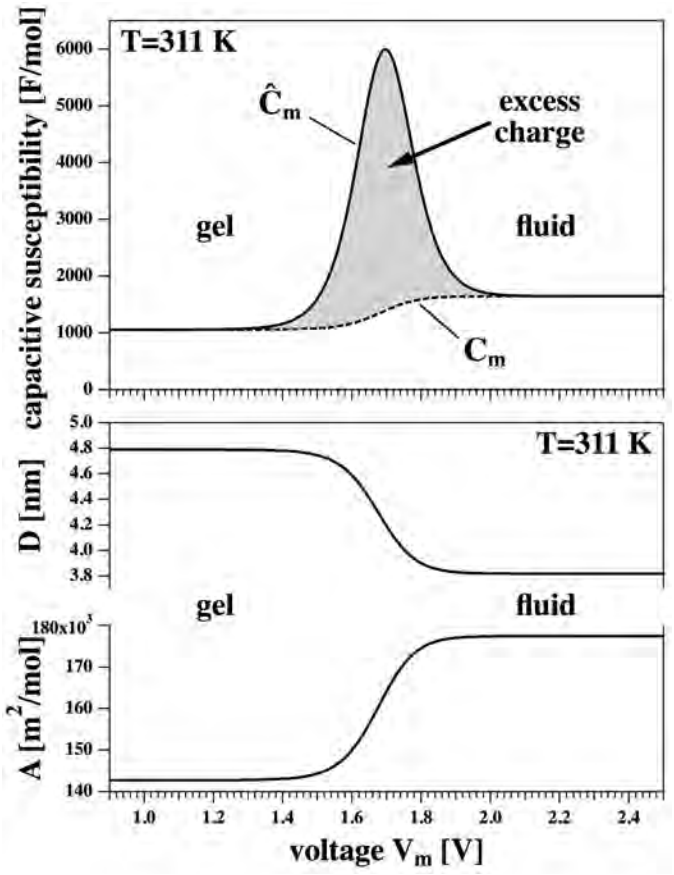

Figure 3. Increase in voltage reduces thickness and increases area. As a consequence, membranes can be moved through their melting transition by voltage changes. The capacitive susceptibility, $\hat{C}_m$, reaches a maximum at the melting temperature. The voltage-induced transition is associated to an excess charge. From [1].

transition and thus the fluctuations are at maximum. Similarly, compressibility, bending elasticity and capacitive susceptibility all assume maxima in the transition regime.

It has been shown that in melting transitions, excess volume changes are proportional to excess enthalpy changes, i.e., $\Delta V(T) = \gamma_V \Delta H(T)$. Here, γ_V is a material constant. This implies that excess volume and enthalpy fluctuations are also proportional functions. A consequence is that excess heat capacity and isothermal volume compressibility are proportional functions of temperature, pressure, etc. I.e.,

$$\Delta c_p \propto \Delta \kappa_T^V \tag{7}$$

Similarly one can directly or indirectly conclude from experiment that the excess heat capacity is proportional to other response functions of lipid membranes close to transitions [6, 7, 1], f.e.,

$$\begin{aligned} \Delta c_p &\propto \Delta \kappa_T^A \quad \text{(area compressibility)} \\ \Delta c_p &\propto \Delta \kappa_B \quad \text{(bending elasticity)} \\ \Delta c_p &\propto \Delta \hat{C}_m \quad \text{(capacitive susceptibility)} \end{aligned} \tag{8}$$

These relations are not based on first principles and should be taken as empirical correlations found to be true for membranes. The proportionality constants depend on the dimensions of the solid and liquid membrane. The heat capacity is easy to measure in a calorimeter. The other response functions can readily be calculated from the calorimetric experiment.

4. The nervous impulse

The nerve pulse consists of a propagating voltage pulse with typical velocities of 1-100 m/s that last about 1 ms. It follows that the typical dimension of a nerve pulse is about 1 mm to 10 cm.

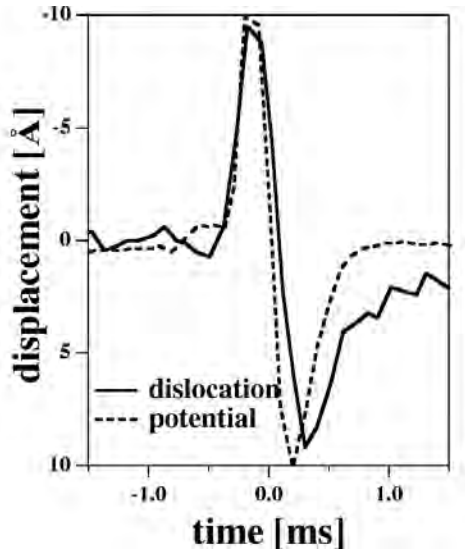

Figure 4. Thickness change of a squid axon during the action potential as a function of time (solid line). The dashed line represents the voltage change. The two functions are within error proportional. Adapted from [8].

Thus, it is of macroscopic dimension. In the biological literature, the nerve pulse is considered a purely electrical phenomenon involving capacitors (the membrane), resistors (ion channel proteins) and electrical currents (ion flows). However, during the nerve pulse one also finds changes in nerve dimensions (thickness and length [8, 9], see figure 4) and in temperature [10]. Thus, the nerve pulse should be considered a thermodynamic or hydrodynamic phenomenon. Below, we show that the nerve pulse can be seen as a localized density pulse related to the propagation of sound.

4.1. Sound velocity

The above relations (equation (8)) help to determine other membrane properties that are related to the response functions. The lateral sound velocity, c, in membranes is defined as

$$c^2 = \left(\frac{\partial \rho^A}{\partial p}\right)_S = \frac{1}{\kappa_S^A \rho^A} \tag{9}$$

Thus, it depends both on the lateral density and on the adiabatic compressibility, κ_S^A. The adiabatic compressibility is a function of frequency because it depends on the translocation of heat from the membrane to the membrane environment. The smaller the frequency, the larger is the aqueous volume that contributes as a heat reservoir and the larger is the adiabatic compressibility [11]. In the limit of zero frequency on obtains the isothermal limit and the adiabatic compressibility, κ_S^A is equal to the isothermal compressibility, κ_T^A. The frequency dependence of the sound velocity is called 'dispersion'. The sound velocity in membranes is generally higher at higher frequencies

Using the above thermodynamic relations between heat capacity and compressibility, on can calculate the low frequency sound velocity as a function of temperature (or as a function of density). Since the compressibility displays a maximum in the melting transition, the lateral sound velocity displays a minimum (shown in figure 5, left. From [2]). In this figure, small density corresponds to the liquid membrane phase while high density corresponds to the solid membrane phase. The membrane in the liquid phase is thus a spring with interesting spring properties: upon compression of the liquid phase the spring first becomes softer (in the transition) and then becomes stiffer (in the solid phase).

The lateral density of the membrane shall be given by $\rho^A = \rho_0^A + \Delta\rho^A$, where ρ_0^A is the density of the liquid membrane. The sound velocity is a non-linear function of the lateral density change,

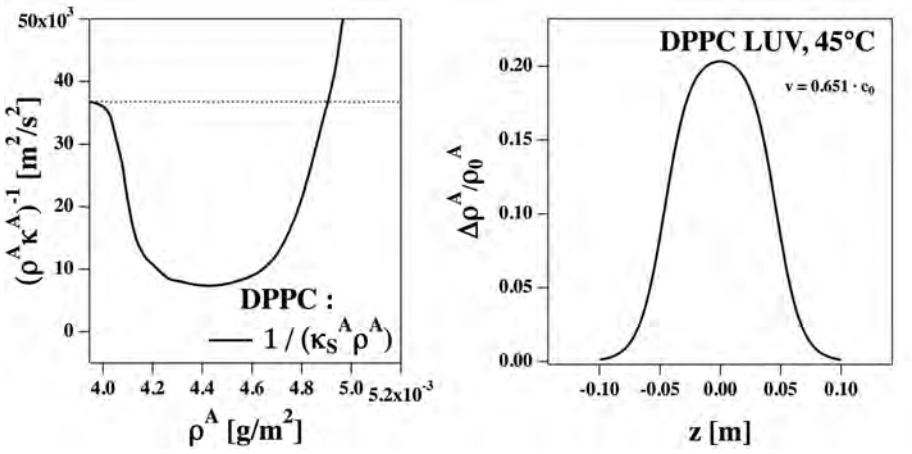

Figure 5. Left: The sound velocity in a lipid membrane close to a transition is a function of density [2]. Small density corresponds to a liquid membrane whereas high density corresponds to a solid membrane. The pronounced minimum is found in the chain melting regime. It is caused by the maximum of area fluctuations in the membrane at the transition. Right: Density soliton in a membrane cylinder using the sound velocity profile shown in the left hand panel [2]

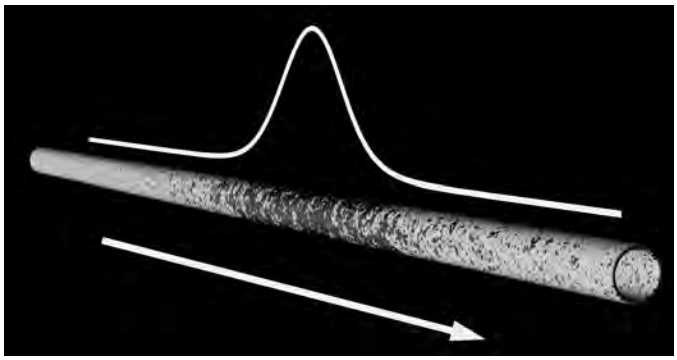

Figure 6. Schematic representation of a density soliton in a cylindrical membrane. The pulse consists of a traveling solid segment (dark shade) traveling in a liquid membrane environment.

$\Delta\rho^A$, which can be Taylor-expanded into

$$c^2 = c_0^2 + p\Delta\rho^A + q(\Delta\rho^A)^2 + ... \tag{10}$$

4.2. Solitons in nerve axons

The non-linearity of the sound velocity and the presence of dispersion give rise to the possibility of soliton propagation. Below, we show as a quasi-one-dimensional example a long cylindrical membrane comparable to the axon of a nerve. The wave equation for one-dimensional sound propagation is given by [12]

$$\frac{\partial^2}{\partial t^2}\Delta\rho = \frac{\partial}{\partial x}\left(c^2\frac{\partial}{\partial x}\Delta\rho\right) \ . \tag{11}$$

By inserting equation (10) into this equation, we obtain

$$\frac{\partial^2}{\partial t^2}\Delta\rho = \frac{\partial}{\partial x}\left((c_0^2 + p\Delta\rho + q\rho^2 + ...)\frac{\partial}{\partial x}\Delta\rho\right) - h\frac{\partial^4}{\partial x^4}\Delta\rho \tag{12}$$

The second term is an ad hoc dispersion term that describes the frequency dependence of the elastic constants. Its introduction into the wave equation is justified in [2]. When inserting the

parameters p and q obtained from fitting equation (10) to the experimental sound velocity profile, one finds that the above equation possesses solitary solution, i.e., localized density pulses that travel along the membrane cylinder without dissipation and without changing shape. A typical solution of equation (12) is shown in figure 5 (right). The pulse possesses a maximum amplitude and a minimum velocity when increasing the overall energy of the pulse. The maximum amplitude corresponds to the density change between liquid and solid membrane phase. Thus, the solitary pulse consists of a solid region traveling in a liquid membrane environment. This is schematically shown in figure 6.

The soliton described above shares many similarities with the nervous impulse:

- It displays a velocity similar to those of myelinated nerves.
- It is associated to transient changes in membrane thickness.
- It is associated to a reversible release and re-uptake of heat.

However, the physical principles underlying soliton propagation are very different from the mechanisms considered for nerve pulse propagation in the field of electrophysiology.

5. Ion channels

The textbook description for nerve pulse conduction is the Hodgkin-Huxley model [13]. It suggests that the nerve pulse is generated by ion currents through channel proteins. These currents charge the membrane capacitor. According to the model, channel proteins conduct ions in a voltage-dependent manner. Thus, they are considered being "voltage-gated". Combined with cable theory, this generates the possibility of propagating electrical pulses called 'action potentials'. The opening and closing of channels can be experimentally observed in electrical recordings [14]. To the contrary, in the soliton theory described above no ion channel proteins are required.

It is an interesting fact that membranes in the complete absence of proteins can form voltage-gated pores that display properties indistinguishable from protein channels [15, 4]. An example is given in figure 7 where one can see an increase in channel open-likelihood upon increase in voltage. These ion channel events result from area fluctuations in the membrane, as described by equation (8). In the melting transition, the fluctuations are large and the membrane permeability displays a maximum. Every change in a thermodynamic variable that potentially changes the membrane state can alter the permeability of the membrane [16, 3].

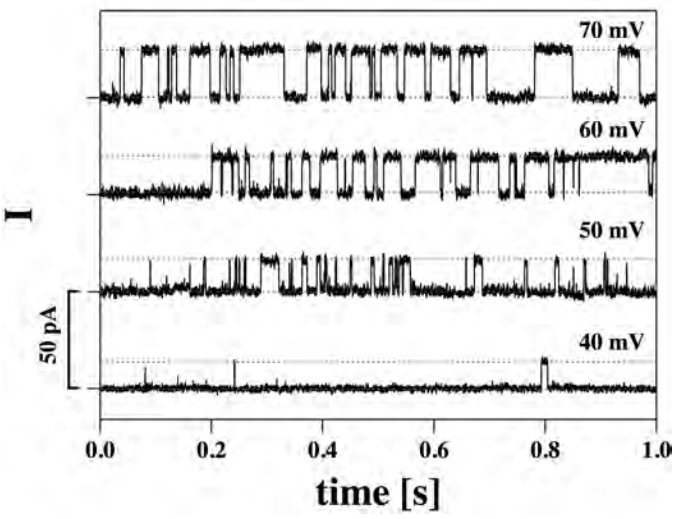

Figure 7. Quantized current events through a synthetic lipid membrane. One finds channel-like events in the complete absence of proteins. The open likelihood of of pore displays a pronounced voltage dependence. [4].

Due to the increase in channel open-probability shown in figure 7, the current-voltage relation is not linear. In particular, if the membrane displays a net polarization, V_0, in the absence of an external field, the current-voltage relation may be asymmetric and different for positive and negative voltages. A spontaneous membrane polarization could originate from an asymmetric distribution of lipids on the two sides of the membrane, or from membrane curvature. The latter effect is called 'flexoelectricity'. Its investigation was pioneered by A. G. Petrov [17]. Flexoelectricity is caused by the different dipole density on the two monolayers in curved membranes. Membrane curvature could possibly originate from slight pressure difference on the two sides of the membrane due to suction on the recording pipette. An example for an asymmetric non-linear current-voltage relation is shown in figure 8.

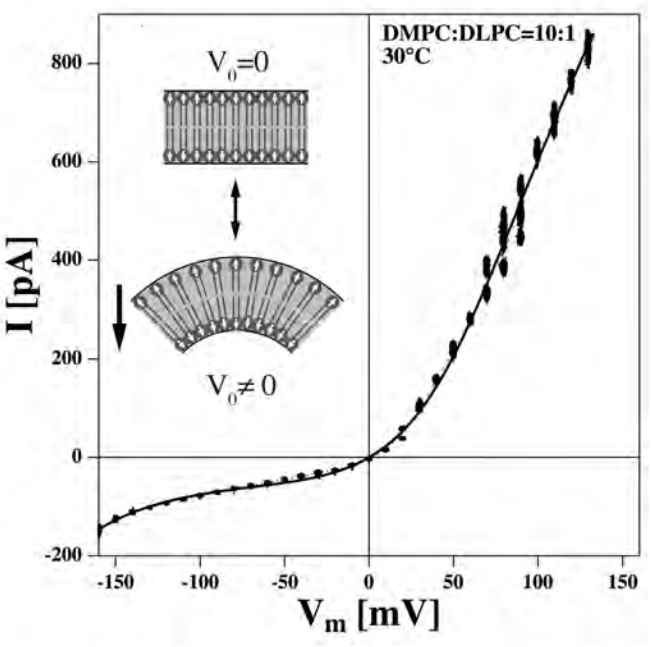

Figure 8. The current-voltage relation of the permeability of a synthetic lipid membrane is not generally symmetric even though the composition of the membrane itself is symmetric [4]. This could be caused by a permanent polarization of the membrane due to flexoelectricity [17, 18] - see insert.

In the absence of spontaneous polarization V_0 of the membrane, the electrostatic force, $\mathcal{F}$, exerted on a planar membrane by external voltage is given by

$$\mathcal{F} = \frac{1}{2}\frac{C_m V_m^2}{D} \tag{13}$$

where C_m is the membrane capacitance, V_m is the transmembrane voltage and D is the membrane thickness [1]. This force potentially reduces the thickness of the membrane [19]. The electrical work performed on the membrane by a change in thickness from D_1 to D_2 is

$$W_{el} = \int_{D_1}^{D_2} \mathcal{F} dD \equiv \alpha V_m^2 \tag{14}$$

where α is a constant. In the presence of a spontaneous polarization associated to a transmembrane voltage V_0, the electrical work instead assumes the form $W_{el} = \alpha(V_m - V_0)^2$. Since electrostatic work leads to membrane thinning, it is generally assumed that the work necessary to form a pore is proportional to the work necessary to reduce membrane thickness membrane [20, 21].

Therefore, the free energy for pore formation is given by

$$\Delta G = \Delta G_0 + \alpha(V_m - V_0)^2 \ , \tag{15}$$

where ΔG_0 is a constant.

The probability, $P_{open}(V_m)$, of finding an open pore in the membrane at a fixed voltage is given by

$$P_{open}(V_m) = \frac{K(V_m)}{1 + K(V_m)} \quad ; \quad K(V_m) = \exp\left(-\frac{\Delta G}{kT}\right) , \tag{16}$$

where $K(V_m)$ is the voltage-dependent equilibrium constant between open and closed states of a single pore.

The current-voltage relation for the lipid membrane is proportional to the likelihood of finding an open channel for a given voltage:

$$I_m = \gamma_p \cdot P_{open} \cdot V_m \tag{17}$$

where γ_p is the conductance of a single pore (or N identical pores). Eqs. 15-17 contain the theoretical description for the I-V curves of lipid channels. The solid line in figure 8 is a fit using the above description. It fits the experimental data nearly perfectly. Thus, a description based on the concept of forces induced by charging the membrane capacitor is very well able to describe experimental data of membrane permeability.

6. Summary

In this review, we summarized the evidence for electromechanical behavior of the biological membrane. The membrane can be seen as a capacitor with a spontaneous polarization. Due to forces on the capacitor, changes in transmembrane voltage can change the physical state of the membrane. E.g., it can induce membrane melting or freezing. Vice versa, lateral pressure changes in the membrane can alter the voltage on a membrane. Thus, the membrane displays piezoelectric features.

In a melting transition, the membrane displays a non-linear response to lateral pressure changes. This fact leads to the possibility of propagating density solitons in cylindrical membranes that share many similarities with the action potential in nerves. For instance, thickness and temperature changes in the nerve membrane are correctly described by the soliton approach. Further, the presence of melting transitions enhances the probability of area fluctuations in the membrane. These fluctuations lead to ion-channel-like events that are practically indistinguishable from protein ion channels. These protein channels are believed to be responsible for the nerve pulse in traditional theories. However, an electromechanical approach towards the physics of biological membranes intrinsically contains all these phenomena using the language of thermodynamics.

References

[1] Heimburg T 2012 *Biophys. J.* **103** 918–929
[2] Heimburg T and Jackson A D 2005 *Proc. Natl. Acad. Sci. USA* **102** 9790–9795
[3] Mosgaard L D and Heimburg T 2013 *Acc. Chem. Res.* **46** 2966–2976
[4] Blicher A and Heimburg T 2013 *PloS ONE* **8** e65707
[5] Heimburg T 2007 *Thermal biophysics of membranes* (Berlin, Germany: Wiley VCH)
[6] Heimburg T 1998 *Biochim. Biophys. Acta* **1415** 147–162
[7] Ebel H, Grabitz P and Heimburg T 2001 *J. Phys. Chem. B* **105** 7353–7360
[8] Iwasa K and Tasaki I 1980 *Biochem. Biophys. Research Comm.* **95** 1328–1331
[9] Iwasa K, Tasaki I and Gibbons R C 1980 *Science* **210** 338–339
[10] Ritchie J M and Keynes R D 1985 *Quart. Rev. Biophys.* **18** 451–476
[11] Mosgaard L D, Jackson A D and Heimburg T 2013 *J. Chem. Phys.* **139** 125101
[12] Sommerfeld A 1992 *Mechanik der deformierbaren Medien* (*Vorlesungen über theoretische Physik* vol 2) (Harri Deutsch)
[13] Hodgkin A L and Huxley A F 1952 *J. Physiol. London* **117** 500–544

[14] Hille B 1992 *Ionic channels of excitable membranes* (Cambridge: Cambridge University Press)
[15] Laub K R, Witschas K, Blicher A, Madsen S B, Lückhoff A and Heimburg T 2012 *Biochim. Biophys. Acta* **1818** 1–12
[16] Heimburg T 2010 *Biophys. Chem.* **150** 2–22
[17] Petrov A G 1999 *The lyotropic state of matter. Molecular physics and living matter physics.* (Amsterdam: Gordon and Breach Science Publishers)
[18] Petrov A G 2001 *Biochim. Biophys. Acta* **1561** 1–25
[19] White S H and Thompson T E 1973 *Biochim. Biophys. Acta* **323** 7–22
[20] Winterhalter M and Helfrich W 1987 *Phys. Rev. A* **36** 5874–5876
[21] Glaser R W, Leikin S L, Chernomordik L V, Pastushenko V F and Sokirko A I 1988 *Biochim. Biophys. Acta* **940** 275–287

arXiv:1411.6883v1 [physics.bio-ph] 25 Nov 2014

Electrical properties of polar membranes

Lars D. Mosgaard†, Karis A.Zecchi†, Thomas Heimburg*

Niels Bohr Institute, University of Copenhagen, Blegdamsvej 17, 2100 Copenhagen Ø, Denmark

ABSTRACT Biological membranes are capacitors that can be charged by applying a field across the membrane. The charges on the capacitor exert a force on the membrane that leads to electrostriction, i.e. a thinning of the membrane. Since the force is quadratic in voltage, negative and positive voltage have an identical influence on the physics of symmetric membranes. However, this is not the case for a membrane with an asymmetry leading to a permanent electric polarization. Positive and negative voltages of identical magnitude lead to different properties. Such an asymmetry can originate from a lipid composition that is different on the two monolayers of the membrane, or from membrane curvature. The latter effect is called 'flexoelectricity'. As a consequence of permanent polarization, the membrane capacitor is discharged at a voltage different from zero. This leads to interesting electrical phenomena such as outward or inward rectification of membrane permeability.
Here, we introduce a generalized theoretical framework, that treats capacitance, polarization, flexoelectricity and piezoelectricity in the same language.

*corresponding author, theimbu@nbi.dk. †LDM and KAZ contributed equally to this work.

Keywords: membranes, polarization, electrostriction, flexoelectricity, capacitance, capacitive susceptibility, dielectric constant

Introduction

Many signaling processes in biology involve electrical phenomena. These processes are related to the movement of ions and the orientation of polar molecules. Biological molecules typically contain charged groups that are at the origin of electrical fields and dipole moments. Furthermore, membranes and macromolecules are surrounded by electrolytes containing charged ions. At physiological ionic strength, the Debye length of electrostatic interactions in the aqueous medium is about 1 nm. It is caused by the shielding of charges by ions. However, in the hydrophobic cores of membranes and proteins, the dielectric constant is small, and no ions that could shield electrostatic interactions are present. Thus, the length scale of electrostatic interactions is significantly larger. Generally, under physiological conditions the range of the electric fields is similar to the size of biological macromolecules. In this publication we will focus on the electrostatics of membranes that determines capacitance, polarization, piezoelectricity and flexoelectricity.

There exist large concentration differences of ions across the membranes of biological cells. For instance, the concentration of potassium is about 400 mM inside and only 20 mM outside of a squid axon. If the membrane is selective for potassium, this results in a Nernst potential across the biological membrane. The combination of the Nernst potentials of different ions yields a resting potential, which for biological cells is in the range of ± 100 mV. The central core of a membrane is mostly made of hydrophobic non-conductive material. Thus, the biomembrane is considered a capacitor, e.g., in the Hodgkin-Huxley model for the nervous impulse (1). During the nerve pulse, currents are thought to flow across ion channel proteins that transiently charge or discharge the membrane capacitor. Within this model, the membrane is assumed to be a homogeneous planar capacitor with constant dimensions. The capacitance can be calculated from the relation

$$C_m = \varepsilon \cdot \frac{A}{d} \tag{1}$$

where ε is the dielectric constant, A is the membrane area and d is the membrane thickness.

Let us assume that the membrane is surrounded by a conducting electrolyte solution. In the presence of an applied voltage, the charged capacitor consists of one plate with positive charges and one plate with negative charges at distance d. The field inside the capacitor can be determined using the superposition of the fields of the two plates (illustrated in Fig. 1). The field inside a charged capacitor is different from zero, while it is zero outside of the capacitor. If no field is applied, the capacitor is not charged.

The charges on a capacitor generate mechanical forces on the two membrane layers (2). These forces can change the dimensions of the capacitor such that both the area and the thickness of the membrane change (see fig. 2). As a result, the capacitance is not generally a constant (2). The capacitance increases upon charging the membrane by an applied field because the membrane thickness decreases and the area increases. This effect is known as electrostriction. Close to phase transitions in the membrane (in which the compressibility of the membrane is large (3)), the membrane should be considered as a nonlinear capacitor. A small change in voltage can result in large changes in thickness and capacitance. The coupling between the membrane voltage and its dimensions renders the membrane piezoelectric, i.e., mechanical changes in the membrane can create a membrane potential and vice versa.

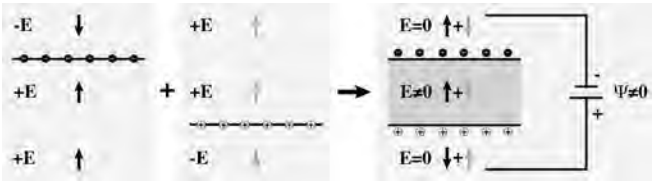

Figure 1: Illustration of capacitive effects. The field inside a charged capacitor can be obtained by the superposition of the fields of a positively and a negatively charged plate at distance d. The charged capacitor displays an internal field different from zero, while the field is zero outside of the capacitor.

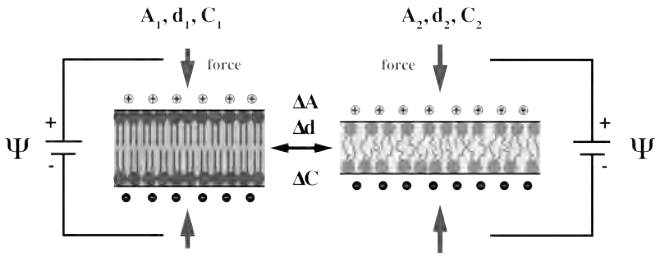

Figure 2: Illustration of the electrostriction effect upon charging the membrane capacitor. The potential difference, Ψ, results in a force on the membrane that leads to a compression of the membrane to a state with larger area, A, and lower thickness, d.

On average, about 80% of the lipids are zwitterionic. Zwitterionic lipids possess permanent electrical dipole moments. Examples of such lipids are phosphatidylcholines and phosphatidylethanolamines. About 10% of biological lipids carry a net negative charge, including phosphatidylinositol and phosphatidylserine. It is known that biomembranes often display asymmetric distributions of lipids such that charged lipids are mostly found in the inner leaflet of the bilayer (4). Biomembranes also contain integral and peripheral proteins with asymmetric distribution (or orientation) between inside and outside, which carry both positive and negative charges. Due to such compositional asymmetries, a spontaneous electrical dipole moment of the membrane can be generated in the absence of an externally applied field. A redistribution or reorientation of polar

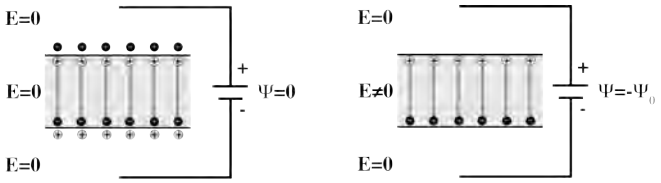

Figure 3: Illustration of polarization by chemical asymmetry. Left: If the membrane contains permanent electrical dipoles, it is charged even if the applied potential is zero. Both, the fields inside and outside of the capacitor are zero. Right: In order to discharge the capacitor, a potential of $\Psi = -\Psi_0$ has to be applied.

molecules in an external field resembles the charging of a capacitor. If the membrane possesses a spontaneous polarization, the membrane capacitor in equilibrium can be charged even in the absence of an external field (illustrated in Fig. 3). In order to discharge this capacitor, a potential of $\Psi = -\Psi_0$ has to applied. We call Ψ_0 the spontaneous membrane potential, or the offset potential. In a theoretical treatment one has to be very careful to correctly account for both capacitive and polarization effects.

The polarization effects described above rely on an asymmetric distribution of charges or dipoles on the two sides of a membrane. Interestingly, even a chemically symmetric lipid membrane made of zwitterionic (uncharged) lipid may be polarized. The individual monolayers of zwitterionic lipids display trans-layer voltages on the order of 300 mV (5, 6). Any

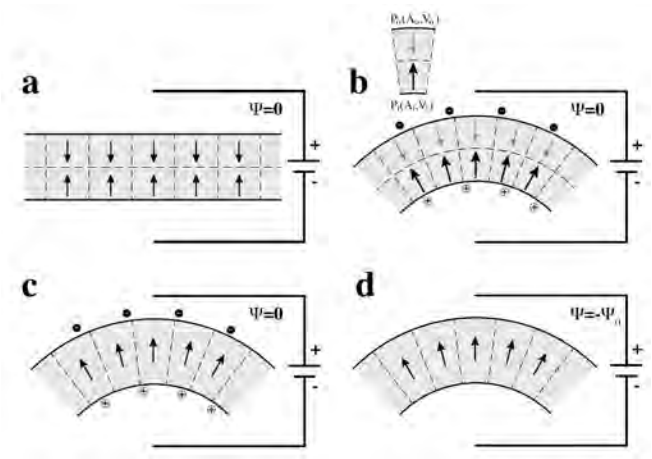

Figure 4: Illustration of polarization by curvature. a. The two monolayers of the symmetric membrane display opposite polarization. b. upon bending (flexing) the membrane, the polarization in the two layers changes. c. effective polarization of the membrane. d: In order to discharge the capacitor, a potential of $\Psi = -\Psi_0$ has to be applied.

geometric deformation that breaks the symmetry between the two monolayers of a membrane results in a net polarization if these distortions alter the relative dipole orientation on the two layers. In particular, curvature induces different lateral pressure on the two sides of a membrane. Thereby, curvature can induce polarization in the absence of an applied field. This consideration was introduced by Meyer in 1969 (7) for liquid crystals. It was applied to curved lipid bilayers by Petrov in 1975 (8). He called this effect 'flexoelectricity'. Upon bending (or flexing) the membrane, both area, A, and volume, V, of the opposing monolayers change in opposite directions. If the polarization is a function of area and volume the polarization of the outer monolayer is given by $P_o \equiv P_o(A_o, V_o)$ and that of the inner monolayer is given by $P_i \equiv P_i(A_i, V_i)$, respectively. Therefore, curvature can induce a net polarization across the membrane. This is illustrated in Fig. 4. This polarization is counteracted by opposing charges adsorbing to the membranes (Fig. 4b and 4c). In order to discharge the membrane, a potential $\Psi = -\Psi_0$ has to be applied. As in the case of chemical asymmetry, at zero applied field, the field inside the capacitor is zero. The cases of a chemically asymmetric planar membrane and a chemically symmetric curved membrane are conceptually similar.

Charged capacitors, polarization, flexoelectricity and piezoelectricity all involve the spatial separation of charges. Thus, they all represent aspects of the same electrostatic phenomena. However, in the literature they are often treated as different things and they are described by a different language. In this communication we formulate a general thermodynamical description of the electrostatics of lipid membranes, which represents a generalization of a study on the capacitance of membranes previously published by our group (2). It will be used to generalize the effect of an externally applied electric field on the lipid melting transition. We will introduce the thermo-

dynamics of a polarized lipid membrane in an electric field, which then results in a generalization of electrostriction effects on lipid membranes. 1

Theory

When the molecules of dielectric materials are placed in an external electric field, they orient themselves to the free energy. In capacitors, net macroscopic dipoles are induced in the dielectric medium and tend to counteract the applied field. As a response to an applied electric field, mechanical changes can be observed, e.g., in piezoelectric crystals. To deal with these effects, authors like Frank treated the electrostatic effects within a thermodynamical framework (9). He considered the electrical work performed on a fluid during any infinitesimal and reversible change, $dW_{el} = Ed(vD)$. This type of consideration leads to expressing the electric displacement, D, in a volume, v, as an extensive variable with the electric field, E, as its conjugated intensive variable. Vector notation has been dropped assuming planar geometry.

When we consider a membrane capacitor, its hydrophobic core separates the two capacitor plates and acts both as a compressible and dielectric material. Choosing hydrostatic pressure (p), lateral pressure (π), temperature (T) and applied electric field (E) as intensive variables, we can write the differential of the Gibbs free energy as

$$\mathrm{d}G = -S\mathrm{d}T + v\mathrm{d}p + A\mathrm{d}\pi - (vD)\mathrm{d}E + ... \qquad (2)$$

where the conjugated extensive variables are S (entropy), v (volume), A (area) and vD (electric displacement). The electrical contribution to the free energy due to an applied electric field comes from the final term, which we will refer to as the electrical free energy, G^{el}.

The electric displacement is related to the total polarization, P_{tot} by

$$D = \varepsilon_0 E + P_{tot}. \qquad (3)$$

where ε_0 is the vacuum permittivity. Most materials have zero polarization at zero electric field, and polarization is only induced by an external field. For a linear dielectric material the induced polarization is $P_{\text{ind}} = \varepsilon_0 \chi_{el} E$, where χ_{el} is the electric susceptibility. We are interested in extending our considerations to a dielectric material which can display spontaneous polarization, P_0, in the absence of an applied field such that

$$P_{tot} = \varepsilon_0 \chi_{el} E + P_0. \qquad (4)$$

The spontaneous polarization, P_0, can originate from asymmetric lipid bilayers, e.g., from curvature (flexoelectricity) or from different composition of the two monolayers. The electric displacement takes the form

$$D = \varepsilon(E + E_0), \qquad (5)$$

where ε is the dielectric constant, $\varepsilon = \varepsilon_0(1 + \chi_{el})$ and $E_0 \equiv P_0/\varepsilon$ is the electric field related to the spontaneous polarization, P_0, at $E = 0$.

Using eq. (5), we can determine the the electrical free energy:

$$\begin{aligned} G^{el} &= -\int_0^E (vD)\mathrm{d}E' = -\varepsilon v \left(\frac{E^2}{2} + E_0 E\right) \\ &= -\frac{\varepsilon}{2} v \left((E + E_0)^2 - E_0^2\right) , \end{aligned} \qquad (6)$$

where we have assumed the volume of the lipid membrane to be constant. Assuming that the dielectric properties of the medium are homogeneous across a membrane with thickness d, we can define $Ed = \Psi$ where Ψ represents the applied electric potential difference. This leads to

$$G^{el} = -\frac{\varepsilon}{2}\frac{A}{d}\left((\Psi + \Psi_0)^2 - \Psi_0^2\right) , \qquad (7)$$

where Ψ_0 is the offset potential related to E_0 ($E_0 d = \Psi_0$). The pre-factor contains the capacitance of a planar capacitor ($C_m = \varepsilon A/d$). Thus, the electric free energy is given by

$$G^{el} = -\frac{1}{2} C_m \left((\Psi + \Psi_0)^2 - \Psi_0^2\right). \qquad (8)$$

At $\Psi = 0$ the electrical contribution to the free energy is zero.

Electrostriction

The charges on a capacitor attract each other. These attractive forces can change the dimensions of the membrane and thereby change the capacitance. If $\Psi_0 = 0$, the electric contribution to the free energy according to eq. (8) is $G^{el} = -\frac{1}{2} C_m \Psi^2$. For $A \approx$ const. and $\Psi =$ const., the force $\mathcal{F}$ acting on the layers is

$$\mathcal{F} = \frac{\partial G^{el}}{\partial d} = -\frac{1}{2}\left(\frac{\partial C_m}{\partial d}\right)\Psi^2 = \frac{1}{2}\frac{C_m \Psi^2}{d} . \qquad (9)$$

This is the force acting on a planar capacitor given in the literature (e.g., (2)). If there exists a constant offset potential Ψ_0, we find instead (eq. (8))

$$\mathcal{F} = \frac{1}{2}\frac{C_m}{d}\left((\Psi + \Psi_0)^2 - \Psi_0^2\right) . \qquad (10)$$

Thus, one expects that the force on a membrane is a quadratic function of voltage which displays an offset voltage when the membrane is polarized. This force can reduce the membrane thickness and thereby increase the capacitance of a membrane. Note, however, that for $(\Psi + \Psi_0)^2 - \Psi_0^2 < 0$, the force $\mathcal{F}$ is negative. As a consequence, capacitance will be decreased.

Let us assume a membrane with constant area and small thickness change, $\Delta d << d$. Then the change in capacitance, ΔC_m, caused by a change of thickness, Δd, is given by

$$\Delta C_m = -\varepsilon \frac{A}{d^2} \Delta d \qquad (11)$$

Thus, the change in capacitance is proportional to the change in thickness. If the thickness is a linear function of the force ($\mathcal{F} \propto \Delta d$), one finds that the capacitance is proportional to the force $\mathcal{F}$. Therefore, it is a quadratic function of voltage with an offset of Ψ_0,

$$\Delta C_m \propto \left((\Psi + \Psi_0)^2 - \Psi_0^2\right) \ . \qquad (12)$$

The magnitude of the change in capacitance depends on the elastic constants of the membrane.

Relation (12) was studied by various authors. Using black lipid membranes, Alvarez and Latorre (10) found a quadratic dependence of the capacitance on voltage (Fig. 5). In a symmetric membrane made of the zwitterionic (uncharged) lipid phosphatidylethanolamine (PE), the offset potential Ψ_0 in a 1 M KCl buffer was found to be zero. In an asymmetric membrane with one monolayer made of PE and the other made of the charged lipid phosphatidylserine (PS), a polarization is induced. In a 1 M KCl buffer, the offset potential is $\Psi_0 = 47$ mV, while it is $\Psi_0 = 116$ mV in a 0.1 M KCl buffer. It is obvious from Fig. 5 that within experimental error the shape of the capacitance profile is unaffected by the nature of the membrane. Only the offset potential is influenced by composition and ionic strength. This suggests that the offset potential has an ionic strength dependence. In this publication, we do not explore the theoretical background of this experimental fact.

In a range of $\pm 300mV$ around the minimum capacitance, the change in capacitance, ΔC_m, is of the order of < 1.5 pF, while the absolute capacitance, $C_{m,0}$, at $\Psi = 0$ is approximately 300 pF (10). Thus, the change in capacitance caused by voltage is very small compared to the absolute magnitude of the capacitance.

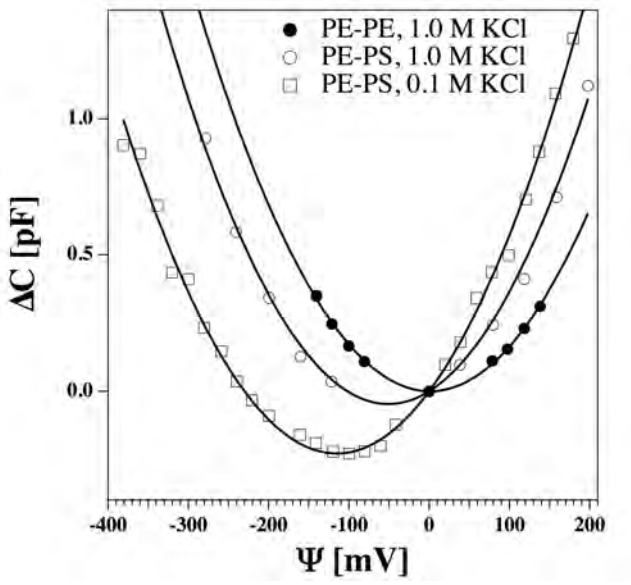

Figure 5: The change in capacitance as a function of potential in a black lipid membrane. Solid circles: Symmetric membrane in 1 M KCl. Both monolayers are made from zwitterionic bacterial phosphatidyl ethanolamine (PE). Open circles: Asymmetric membrane in 1 M KCl. One monolayer is consists of bacterial PE, while the other monolayer consist of the charged bovine brain phosphatidylserine (PS). Open squares: Same as open circle, but with smaller salt concentration (0.1 M KCl). The absolute capacitance, $C_{m,0}$ at $\Psi = 0$ V is approximately 300 pF. Raw data adapted from (10).

Influence of the potential on the capacitance close to a melting transition

As discussed above, the influence of voltage on the capacitance is small in the gel and in the fluid phase because membranes are not very compressible in their pure phases. However, close to the phase transition between gel and fluid, membranes become very compressible. In this transition, the thickness of the membrane, d, decreases by about 16% and the area, A, increases by about 24% (3) for the lipid dipalmitoyl phosphatidylcholine (DPPC). Therefore, the capacitance of the fluid membrane is about 1.5 time higher than the capacitance of the gel phase (2). According to eq. (8), the Gibbs free energy difference caused by an external electric field can be written as

$$\Delta G^{el} = G^{el}_{fluid} - G^{el}_{gel} = -\frac{\Delta C_m}{2}\left((\Psi + \Psi_0)^2 - \Psi_0^2\right) \ , \qquad (13)$$

where ΔC_m is the difference between the capacitance of gel and fluid phase. Here, we assumed that both the offset potential Ψ_0 and the dielectric constant ε do not change with the state. We have confirmed the latter in experiments on the dielectric constant in the melting transition of oleic acid using a parallel plate capacitor (data not shown). We found that the changes of the dielectric constant caused by the melting of oleic acid ($T_m \approx 17°$C) are very small.

It has been shown experimentally that in the vicinity of the lipid melting transition changes of various extensive variables are proportionally related (3, 11, 12). For instance, changes in enthalpy are proportional to changes in area, in volume and we assume that a similar relation holds for changes in thickness.

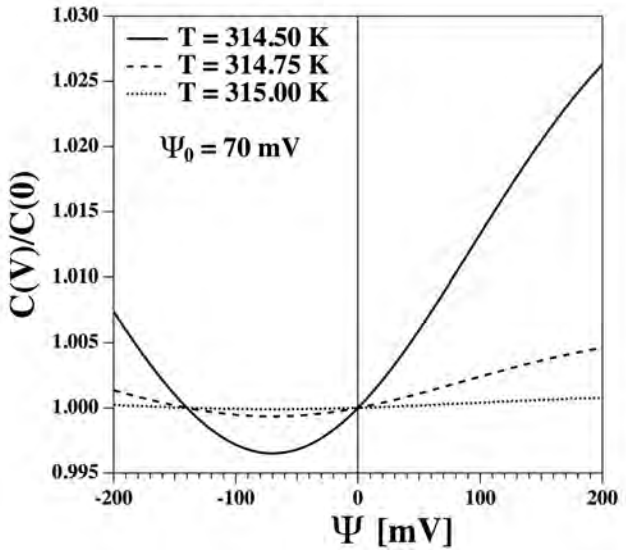

Figure 6: The relative change in capacitance of a lipid membrane as a function of applied voltage at three different temperatures above the melting temperature. Parameters are for LUV of DPPC, where $\Delta C \approx 656$ J/(mol·V^2) and Ψ_0 was chosen to be 70 mV.

Further, close to transitions the elastic constants are closely related to the heat capacity. For instance, the temperature-dependent change of the isothermal compressibility is proportional to heat capacity changes. Thus, membranes are more compressible close to transitions, and it is to be expected that the effect of potential changes on membrane capacitance is enhanced. This will be calculated in the following.

We assume that the lipid melting transition is described by a two-state transition governed by a van't Hoff law, so that the equilibrium constant between the gel and the fluid state of the membrane can be written as (2, 13)

$$K(T,\Psi) = \exp\left(-n\frac{\Delta G}{RT}\right) \tag{14}$$

where n is the cooperative unit size which describes the number of lipids that change state cooperatively (for LUVs of DPPC we used $n = 170$ (14)). The free energy difference between gel and fluid membranes is given by

$$\Delta G = (\Delta H_0 - T\Delta S_0) + \Delta G^{el}\,, \tag{15}$$

where $\Delta H_0 = 35$ kJ/mol and $\Delta S_0 = 111.4$ J/mol K (for DPPC). From the equilibrium constant we can calculate the fluid fraction, the average fraction of the lipids that are in the fluid state,

$$f_f(T,\Psi) = \frac{K(T,\Psi)}{1+K(T,\Psi)}. \tag{16}$$

For DPPC LUV, the thickness in the gel and fluid state is given by $d_g = 4.79$ nm and $d_f = 3.92$ nm , respectively. The area per lipid is $A_g = 0.474$ nm^2 and $A_f = 0.629$ nm^2 (3). We assume a dielectric constant of $\varepsilon = 4 \cdot \varepsilon_0$ independent of the state of the membrane. The area is described by $A(T,\Psi) = A_g + f_f \cdot \Delta A$, and the membrane thickness by $d(T,\Psi) = d_g - f_f \cdot \Delta d$, respectively. The temperature and voltage-dependent capacitance, $C = \varepsilon A(T,\Psi)/d(T,\Psi)$ is shown in fig. 6. For small variations in the potential, the change in capacitance is a quadratic function of voltage. For large potentials, one finds the capacitance of the fluid phase which is assumed being constant. One can recognize that the sensitivity of the capacitance to voltage changes close to the transition is much larger than that of the pure phases (Fig. 5). It is also a sensitive function of the temperature. Fig. 6 shows $C_m(\Psi)$ for three different temperatures above the melting temperature of DPPC at 314.15 °C. At $T = 314.5$ K, the change in capacitance at $\Psi - \Psi_0 = 300$ mV is approximately 3% compared to the about 0.5% experimentally measured in the absence of a transition (Fig. 5). Due to the presence of a melting transition, the curve profile in Fig. 6 is only a quadratic function of potential close to $\Psi = -\Psi_0$.

The dependence of the melting temperature on the applied potential

The total free energy difference between gel and fluid phase, ΔG, consists of an enthalpic and an entropic contribution,

$$\Delta G = \Delta H_0 - T\Delta S_0 + \Delta G^{el}\,, \tag{17}$$

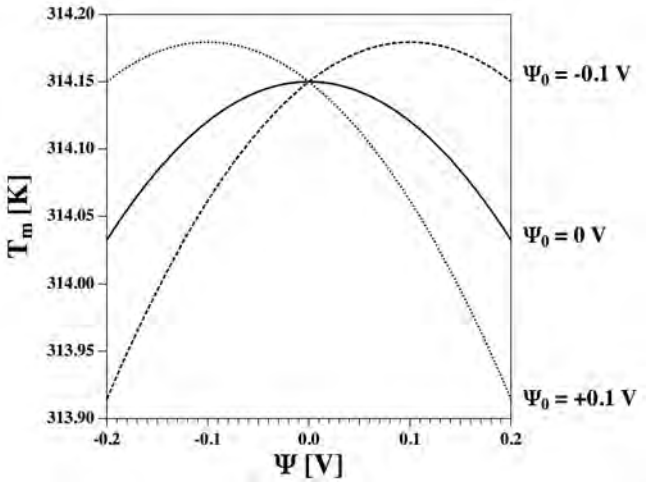

Figure 7: The lipid melting temperature as a function of applied potential with three different offset potentials, Ψ_0=0.1 V, Ψ_0=0V, and Ψ_0=-0.1 V. The parameters are taken from LUV of DPPC, where $\Delta C \approx 656\ J/(mol \cdot V^2)$ for $\varepsilon = 4 \cdot \varepsilon_0$.

At the melting temperature, T_m, the Gibbs free energy difference ΔG is zero, so that

$$\begin{aligned} T_m &= T_{m,0}\left(1 + \frac{\Delta G^{el}}{\Delta S_0}\right) \\ &= T_{m,0}\left(1 - \frac{1}{2}\frac{\Delta C_m}{\Delta S_0}\left((\Psi+\Psi_0)^2 - \Psi_0^2\right)\right), \end{aligned} \tag{18}$$

where $T_{m,0} = \Delta H_0/\Delta S_0$ is the melting temperature in the absence of an external field (for DPPC: $\Delta H_0 = 35$ kJ/mol, $T_{m,0} = 314.15$ K and $\Delta S_0 = 111.4$ J/mol· K (3)). This result describes the effect of electrostriction on the lipid melting transition in the presence of spontaneous polarization. It is a generalization of the electrostriction effect described by Heimburg (2) who treated this phenomenon in the absence of polarization effects. Fig. 7 shows the dependence of T_m on an applied voltage for three different offset potentials, Ψ_0. It can be seen that in the presence of an applied filed, the spontaneous polarization and its sign influences that melting temperature.

Generalization for $\Psi_0 \neq$ const

The orientation of lipid dipoles can change upon lipid melting. It seems to be obvious from lipid monolayer experiments that the polarization of liquid expanded and solid condensed layers is different. We assume the same to be true for bilayers. Let us assume that the net offset potentials originating from membrane polarization in the gel and the fluid phase are given by Ψ_0^g and Ψ_0^f, respectively. The free energy is now given by

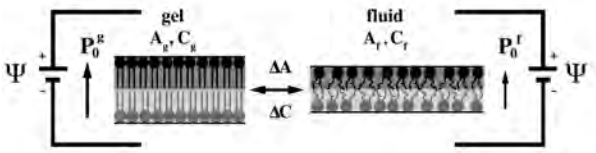

Figure 8: A polar membrane with different lipid composition on the top and bottom monolayer undergoing a melting transition from gel to fluid. The gel state possesses an area A_g and a capacitance C_g, while the fluid state displays A_f and C_f. The net offset potentials caused by membrane polarization are Ψ_0^g and Ψ_0^f, respectively. The differences in area and capacitance between the two states are given by ΔA and ΔC.

$$\begin{aligned}\Delta G^{el} &= -\frac{C_f}{2}\left((\Psi+\Psi_{0,f})^2-\Psi_{0,f}^2\right)\\ &\quad -\frac{C_g}{2}\left((\Psi+\Psi_{0,g})^2-\Psi_{0,g}^2\right)\\ &= -\frac{\Delta C}{2}((\Psi+\Psi_{0,g})^2-\Psi_{0,g}^2)\\ &\quad -C_f\Psi(\Psi_{0,f}-\Psi_{0,g}) \qquad (19)\end{aligned}$$

This can be inserted in eq. (17) to obtain the change in melting temperature due to an applied field.

The dielectric susceptibility

In (2) we defined a capacitive susceptibility, $\hat{C}=(\partial q/\partial V)=C+V(\partial C/\partial V)$. This susceptibility has a maximum at the melting temperature, which is a consequence of the fact that the capacitance of gel and fluid lipid phases differ. By analogy, we now introduce a dielectric susceptibility, $\hat{\varepsilon}=(\partial D/\partial E)$, which is given by:

$$\hat{\varepsilon}\equiv\left(\frac{\partial D}{\partial E}\right)=\left(\frac{\partial(\varepsilon E+P_0)}{\partial E}\right)=\varepsilon+E\left(\frac{\partial\varepsilon}{\partial E}\right)+\left(\frac{\partial P_0}{\partial E}\right) \qquad (20)$$

Thermodynamic susceptibilities are linked to fluctuation relations. For instance, in (2) we showed that the capacitive susceptibility is given by $\hat{C}=(\langle q^2\rangle-\langle q\rangle^2)/kT$, i.e., it is proportional to the fluctuations in charge. This fluctuation relation is valid as long as the distribution of states is described by Boltzmann statistics and the area and thickness are kept constant. Analogously, for constant volume, v, the dielectric susceptibility, $\hat{\varepsilon}$, is given by

$$\hat{\varepsilon}=v\frac{\langle D^2\rangle-\langle D\rangle^2}{kT}\,. \qquad (21)$$

Since this is a positive definite form, $\hat{\varepsilon}$ is always larger than zero. The mean displacement, $\langle D\rangle$, always increases with an increase in the electric field, E. If either ε or the permanent polarization P_0 are different in the gel and the fluid state of a membrane, one can induce a transition. In this transition, the dielectric susceptibility displays an extremum.

Capacitive susceptibility, piezoelectricity and flexoelectricity

As mentioned above, the polarization of a membrane can change by compressing, stretching or bending the membrane. The corresponding electrostatic phenomena are called electrostriction, piezoelectricity and flexoelectricity. In the past, some simple relations were derived by A. G. Petrov (15). For instance, piezoelectricity was described as the area-dependence of polarization. Correspondingly, flexoelectricity was described as the curvature-dependence of the polarization assuming that polarization is zero in the planar state of the membrane. However, upon changing the membrane area, its capacitance also changes. Thus, in the presence of a field not only the polarization but also the charge on the capacitor can change. In the case of membrane curvature, the polarization may be different from zero in the planar state. Further, if there exists an applied potential, the capacitance of the membrane plays a role. In the following, we derive general equations for electrostriction, piezoelectricity and flexoelectricity. We will find that some relations previously derived by Petrov are special cases of our more general description.

The charge on a capacitor

The dependence of the charge on a capacitor on potential, Ψ, surface area, A, and curvature, c is given by

$$dq=\left(\frac{\partial q}{\partial\Psi}\right)_{A,c}d\Psi+\left(\frac{\partial q}{\partial A}\right)_{\Psi,c}dA+\left(\frac{\partial q}{\partial c}\right)_{\Psi,A}dc\,. \qquad (22)$$

Here, we assume that Ψ, A and c are variables that can be controlled in the experiment. The charge on a capacitor is given by

$$q=A\cdot D=A(\varepsilon E+P_0)=\varepsilon\frac{A}{d}(\Psi+\Psi_0)=C_m(\Psi+\Psi_0)\,. \qquad (23)$$

Thus, the change of the charge on a capacitor as a function of potential, lateral pressure, and curvature is given by:

$$\begin{aligned}dq &= \left[(\Psi+\Psi_0)\left(\frac{\partial C_m}{\partial\Psi}\right)_{A,c}+C_m+C_m\left(\frac{\partial\Psi_0}{\partial\Psi}\right)_{A,c}\right]d\Psi\\ &\quad +\left[(\Psi+\Psi_0)\left(\frac{\partial C_m}{\partial A}\right)_{\Psi,c}+C_m\left(\frac{\partial\Psi_0}{\partial A}\right)_{\Psi,c}\right]dA\\ &\quad +\left[(\Psi+\Psi_0)\left(\frac{\partial C_m}{\partial c}\right)_{\Psi,A}+C_m\left(\frac{\partial\Psi_0}{\partial c}\right)_{\Psi,A}\right]dc \qquad (24)\end{aligned}$$

or in abbreviated form as

$$\begin{aligned}dq &\equiv [(\Psi+\Psi_0)\alpha_{A,c}+C_m+C_m\beta_{A,c}]\,d\Psi\\ &\quad +[(\Psi+\Psi_0)\alpha_{\Psi,c}+C_m\beta_{\Psi,c}]\,dA\\ &\quad +[(\Psi+\Psi_0)\alpha_{\Psi,A}+C_m\beta_{\Psi,A}]\,dc \qquad (25)\end{aligned}$$

The first term describes the change of charge on a capacitor allowing for the possibility that both capacitance and polarization can depend on voltage. The second term describes piezoelectricity, i.e., the change of charge by changing area, taking

into account the area dependence of both capacitance and polarization. The last term describes flexoelectricity, which relates to the change of charge caused by changes in curvature. Here, both dependence of capacitance and polarization on curvature are considered.

One could write similar equations, if the lateral pressure, π, were controlled instead of the area, A.

Capacitive susceptibility

The capacitive susceptibility is given by $\hat{C}_m = \partial q/\partial\Psi$. It was discussed in detail in (2). In contrast to the capacitance, it can have a maximum in a melting transition. If lateral pressure and curvature are constant, we find from eq. (26) that

$$\hat{C}_m = \left(\frac{\partial q}{\partial \Psi}\right)_{A,c} = (\Psi + \Psi_0)\alpha_{A,c} + C_m + C_m\beta_{A,c} \quad (26)$$

If the spontaneous polarization is zero at all voltages, this reduces to

$$\hat{C}_m = C_m + \Psi\left(\frac{\partial C_m}{\partial \Psi}\right)_{A,c} \quad (27)$$

which is the relation given by Heimburg (2012).

Piezoelectricity

Let us assume that in eq. (25) Ψ and c are constant. We then obtain

$$dq = [(\Psi + \Psi_0)\alpha_{\Psi,c} + C_m\beta_{\Psi,c}]\, dA\ . \quad (28)$$

This effect is the 'piezoelectric effect'. It corresponds to the charging of a capacitor by changing the surface area of the membrane. At $\Psi = 0$, we obtain for a small change in area, ΔA,

$$\Delta q \approx (\Psi_0\alpha_{\Psi,c} + C_m\beta_{\Psi,c})\,\Delta A\ . \quad (29)$$

If $\Psi_0(\Delta A = 0)$ is zero, the capacitor is uncharged for $\Psi = 0$. Then the charge on the capacitor after a change in area of ΔA is given by

$$q(\Delta A) = C_m\beta_{\Psi,c}\Delta A \qquad \text{or} \qquad \Psi_0(\Delta A) = \beta_{\Psi,c}\Delta A\ . \quad (30)$$

A similar relation was given by Petrov and Usherwood (19).

Inverse piezoelectric effect: The elastic free energy density of membrane compression is given by $g = \frac{1}{2}K_T^A(\Delta A/A_0)^2$, where K_T^A is the lateral compression modulus and A_0 is the equilibrium area prior to compression. In the presence of an applied potential, the free energy is given by

$$g = \frac{1}{2}K_T^A\left(\frac{\Delta A}{A_0}\right)^2 - \frac{1}{2}\frac{C_m}{A_0}\left((\Psi + \Psi_0)^2 - \Psi_0^2\right) \quad (31)$$

In order to obtain the free energy, G, this has to be integrated over the surface area of the lipid membrane. At constant compression modulus, K_T^A, and constant potential Ψ, the area change ΔA equilibrates such that

$$\begin{aligned}\frac{\partial g}{\partial A} &= K_T^A\frac{\Delta A}{A_0^2} - \frac{C_m}{A_0}\left(\frac{\partial \Psi_0}{\partial A}\right)_{\Psi,c}\Psi \quad (32)\\ &\quad -\frac{1}{2A_0}\left(\frac{\partial C_m}{\partial A}\right)_{\Psi,c}\left((\Psi + \Psi_0)^2 - \Psi_0^2\right) = 0\end{aligned}$$

Therefore,

$$\Delta A(\Psi) = A_0\left[\frac{C_m\beta_{\Psi,c}}{K_T^A}\Psi + \frac{\alpha_{\Psi,c}}{K_T^A}\left((\Psi + \Psi_0)^2 - \Psi_0^2\right)\right]\ . \quad (33)$$

Here, the first linear term is due to the area dependence of the membrane polarization, while the second quadratic term originates from the area dependence of the capacitance.

Flexoelectricity

Let us assume that in eq. (25) Ψ and π are constant. Then we find

$$dq = [(\Psi + \Psi_0)\alpha_{\Psi,A} + C_m\beta_{\Psi,A}]\, dc\ . \quad (34)$$

This is the (direct) 'flexoelectric effect'. It describes the charging of a capacitor by curvature. If we further assume that the capacitance does not depend on curvature and that the coefficient $\beta_{\Psi,A}$ is constant, we obtain

$$q(c) = C_m\,(\Psi + \Psi_0(0)) + C_m\beta_{\Psi,A}c\ , \quad (35)$$

where $C_m\,(\Psi + \Psi_0(0))$ is the membrane charge at $c = 0$. If the applied potential, Ψ, is zero and the polarization in the absence of curvature is also assumed being zero, we obtain

$$q(c) = C_m\beta_{\Psi,A}c \qquad \text{or} \qquad \Psi_0(c) = \beta_{\Psi,A}c\ . \quad (36)$$

Thus, the offset potential Ψ_0 is proportional to the curvature. This relation is a special case of the flexoelectric effect described in eq. (34). It was previously discussed by Petrov (15). He introduced a flexoelectric coefficient, f, which is given by $f \equiv \varepsilon\cdot\beta_{\Psi,A}$. Petrov found experimentally that $f = 10^{-18}$ [C], or $\beta_{\Psi,A} = 2.82\cdot 10^{-8}$ [m] for $\varepsilon = 4\varepsilon_0$, respectively.

Inverse flexoelectric effect: In the absence of a spontaneous curvature, the elastic free energy density of bending is given by $g = \frac{1}{2}K_Bc^2$, where K_B is the bending modulus. In the presence of an applied potential and assuming that C_m does not depend on curvature, the free energy density is given by

$$g = \frac{1}{2}K_Bc^2 - \frac{1}{2}\frac{C_m}{A}\left((\Psi + \Psi_0)^2 - \Psi_0^2\right) \quad (37)$$

In order to obtain the free energy, G, this has to be integrated over the surface area of the lipid membrane. At constant potential Ψ, the curvature c equilibrates such that

$$\frac{\partial g}{\partial c} = K_Bc - \frac{C_m}{A}\left(\frac{\partial \Psi_0}{\partial c}\right)_{\Psi,A}\Psi = K_Bc - \frac{C_m}{A}\beta_{\Psi,A}\Psi = 0 \quad (38)$$

Therefore,

$$c(\Psi) = \frac{C_m}{A}\frac{\beta_{\Psi,A}}{K_B}\Psi = \frac{\varepsilon}{d}\frac{\beta_{\Psi,A}}{K_B}\Psi \quad (39)$$

This effect is called the 'inverse flexoelectric effect'. It describes how curvature is induced by an applied potential. It depends on the bending modulus. In melting transitions, the curvature-induction by voltage is enhanced because K_B approaches a minimum (3). This implies that in the presence of an applied field, the curvature of a membrane changes upon changing the temperature - in particular close to transitions.

Both, the investigation of flexoelectric and inverse flexoelectric effects have been pioneered by Petrov (15). In Petrov's nomenclature, eq. (39) assumes the form $c(\Psi) = (f/d\cdot K_B)\Psi$.

Discussion

In this publication, we have provided a general thermodynamic treatment of polarization effects on the properties of lipid membranes. When applied to a membrane in an electrolyte, these electric effects can all be related to the charging (or discharging) of capacitors by either potential, curvature or area (or lateral pressure) changes. The latter two effects can lead to an offset potential or a spontaneous polarization. This is important because biological membranes are known to be polar and changes in voltage are generally considered to be central to the understanding of the functioning of cells. We show that a permanent or spontaneous polarization of a membrane influences the properties of a membrane capacitor such that it is discharged at a voltage different from zero. We relate this voltage to an "offset potential". The existence of this potential has the consequence that membrane properties even of chemically symmetric membranes are controlled differently for positive and negative voltages. We derived equations for the piezoelectric and inverse piezoelectric effect. The first considers the change in the offset potential when changing the membrane area. The second considers the change in membrane area by an applied field, which depends on the elastic modulus of the membrane. Finally, we derived general relations for the flexoelectric and the inverse flexoelectric effect. The flexoelectric effect is the change in the offset potential by changing curvature. The inverse flexoelectric effect is the change in curvature induced by an applied potential. We showed that in some simple limiting cases, our derivations lead to relations identical to those of Petrov (15). Petrov pioneered the field of membrane flexoelectricity (e.g., (8, 15–21)).

An electric field applied across a lipid membrane generates a force normal to the membrane surface due to the charging of the membrane capacitor. The resulting reduction in membrane thickness is called electrostriction (2). For fixed membrane dimensions, the electrostrictive force is a quadratic function of voltage. Due to membrane thinning induced by the forces, one finds an increase in membrane capacitance. This has been demonstrated for symmetric black lipid membranes made from phosphatidylethanolamines (Fig. 5, (10). However, for an asymmetric membrane made of charged lipids on one side and zwitterionic lipids on the other side (thus displaying polarity) the minimum capacitance is found at a voltage different from zero (Fig. 5, (10)). This indicates that a permanent electric polarization of the membrane influences the capacitive properties of a membrane. This has also been found in biological preparations. Human embryonic kidney cells display an offset potential of -51 mV (22). This indicates that the capacitance in electrophysiological models such as the Hodgkin-Huxley model (1) is incorrectly used because offset potentials are not considered. However, it is very likely that the offset potentials are closely related to the resting potentials of membranes. It should also be noted that the capacitance is typically dependent on the voltage. This effect has also not been considered in classical electrophysiology models. We treat that here in terms of a 'capacitive susceptibility' (eq. (26), cf. (2)).

Electrostrictive forces also influence melting transitions of lipid membranes. Since the fluid state of the membrane displays a smaller thickness than the gel phase, an electrostrictive force will shift the state of the membrane towards the fluid state. Heimburg (2) calculated a decrease of the melting temperature, T_m, which is a quadratic function of voltage. Since the membrane was considered being symmetric, the largest T_m is found at $\Psi = 0$. Here, we showed that a membrane which displays a spontaneous polarization in the absence of an applied electric field possesses an offset potential, Ψ_0, in the free energy (eq. (13)). The respective equation contains the term $((\Psi + \Psi_0)^2 - \Psi_0^2) = \Psi^2 + 2\Psi\Psi_0$, which is approximately linear for $\Psi \ll \Psi_0$ (eq. (8). In fact, Antonov and collaborators found a linear dependence of the melting temperature on voltage (23). This indicates that the membranes studied by Antonov and collaborators (23) were polar.

Antonov's experiment determined the voltage-dependence of the melting temperature by measuring the permeability changes in the transition. It is well known that membranes display maximum conductance in lipid phase transitions (24, 25). Furthermore, it has been found that membranes can form pores that appear as quantized conduction event upon the application of potential difference across the membrane (25–29). The likelihood to form a pore is thought to be proportional to the square of the applied electric potential (30, 31). This is based on the assumption that an increase in voltage thins the membrane and eventually leads to an electric breakdown linked to pore formation. Laub et al. (32) found that the current-voltage (I-V) relation for a chemically symmetric phosphatidylcholine membrane patch formed on the tip of a glass pipette was a non-linear function of voltage which was not symmetric around $\Psi = 0$, but rather outward rectified. Blicher et al. (14) proposed that a voltage offset can explain the outward-rectification. They proposed that the free energy difference between an open and a closed pore, ΔG_p, can be expressed by

$$\Delta G_p = \Delta G_{p,0} + \alpha(V - V_0)^2 \,, \tag{40}$$

where $\Delta G_{p,0}$ and α are coefficients and V_0 is a voltage offset. This equation has the same analytic form as used here for the electrostatic free energy ($G = -(C_m/2)((\Psi + \Psi_0)^2 - \Psi_0^2)$). Assuming that the equilibrium constant between an open and a closed form of a membrane pore is given by $K_p = \exp(-\Delta G_p/kT)$ and the likelihood of finding an open pore is given by $P_{open} = K_p/(1 + K_p)$, Blicher and collaborators concluded that the I-V relation could be expressed as

$$I = \gamma_p P_{open} V \tag{41}$$

This relation perfectly fitted the experimental current-voltage data. Thus, inward and outward rectified I-V profiles can be found in pure lipid membranes in the complete absence of proteins. They find their origin in the polarization of the membrane.

Here, we investigated two possible mechanisms that can give rise to spontaneous polarization in the absence of an applied field, which both break the symmetry of the membrane. The first (flexoelectricity) acts by allowing the membrane to be curved (thus introducing a curvature, c) and a difference of the lateral tension within the two monolayers. The second mechanism acts by assuming a chemically or physically asymmetric lipid composition on the two leaflets. An example for a physically asymmetric membrane is a situation where one monolayer is in a fluid state while the other monolayer is in a gel

state. Chemical asymmetry assumes a different lipid composition on the two sides of the membrane. The magnitude of the resulting offset, Ψ_0, is strongly influenced by experimental conditions such as the lipid composition, salt concentration, pH, or the presence of divalent ions. Permanent polarization of the lipids can not only lead to an electrical offset but also to an enhanced dielectric constant. For biological membranes, polarization asymmetries can originate from any constituting element of the membrane including integral membrane proteins. We can also speculate that other membrane adhesive molecules with large dipoles can be used to create an asymmetric membrane, e.g., soluble proteins or lipid-associated molecules such as long-chain sugars. Depending on the nature of the asymmetry, the system can display piezoelectric properties.

The offset potential can have interesting consequences for capacitive currents. The charge on a capacitor is given by $q = C_m(\Psi + \Psi_0)$. Therefore, for constant Ψ_0 the capacitive current is given by

$$I_c(t) = \frac{dq}{dt} = C_m \frac{d\Psi}{dt} + (\Psi + \Psi_0) \frac{dC_m}{dt} \qquad (42)$$

For a positive change in potential, the first term in eq. (42) is positive and leads to a positive current. If the change in voltage happens instantaneously, the corresponding current peak is very short. The second term describes the temporal change in capacitance induced by the voltage change. It depends on the relaxation time of the membrane capacitance, which close to transitions can range from milliseconds to seconds. Thus, it can be distinguished from the first term. Let us consider the situation shown in Fig. 6 ($\Psi_0 = 70$ mV, T=314.5 K) with a membrane capacitance of ≈ 1 μF/cm^2. Here, a jump from $\Psi = -70$ mV to $\Psi = -10$ mV yields a positive change in capacitance of $\Delta C_m = 2.6$ nF/cm^2. If the offset potential were $\Psi_0 = -70$ mV instead, the same jump would change the capacitance by $\Delta C_m = -7.8$ nF/cm^2. Therefore, the second term in eq. (42) is positive in the first situation but negative in the second situation. For this reason, depending on the offset potential and holding potential, the capacitive current associated to the second term in eq. (42) can go along the applied field or against the applied field. Similarly, for a jump in potential of +60 mV, the capacitive current would depend on the holding potential before the jump. For $\Psi_0 = 70$ mV, the change in capacitance is $\Delta C_m = -2.6$ nF/cm^2 for a jump from -130 mV to -70 mV. It is $\Delta C_m = +8.9$ nF/cm^2 for a jump from $+70$ mV to $+130$ mV. The typical time-scale of processes in biomembranes is a few milliseconds to a few ten milliseconds. It can be different for different voltages. Thus, slow currents on this time-scale against an applied field can originate from voltage-induced changes in lipid membrane capacitance. If the offset-potential also depends on voltage, this situation is more complicated.

Flexoelectric and piezoelectric phenomena have also be considered to be at the origin of an electromechanical mechanism for nerve pulse propagation (33). In 2005, Heimburg and Jackson proposed that the action potential in nerves consists of an electromechanical soliton. The nerve pulse is considered as a propagating local compression of the membrane with a larger area density. According to the piezoelectric effect treated here (eq. (28), a change in membrane area can lead to the charging of the membrane capacitor. Alternatively, due to the inverse piezoelectric effect a change in the applied membrane potential can induce area changes (eq. (33) and thus induce a density pulse. The inverse piezoelectric effect is very dependent on the lateral compressibility of a membrane. Thus, is is largely enhanced in the melting transition where the compressibility is high. Further, these effects will largely depend on membrane polarization.

Finally, it should be mentioned that some of the polarization effects on artificial membranes are not very pronounced because changes in polarization due to changes in area are not very large. For instance, a voltage change of 200 mV changes the transition temperature by only 0.12 K. However, the absolute magnitude of the effect largely depends on offset polarizations. These could be influenced by lipid-membrane-associated molecules (such as proteins) with large dipole moments.

Conclusion

Here, we provided a unified thermodynamic framework for capacitive changes, piezoelectricity and flexoelectricity. It treats all of these effects in terms of the electric field, E, and the electric displacement, D. We show that a spontaneous membrane polarization leads to offset potentials that form the origin for a number of interesting membrane phenomena, including voltage-dependent changes in capacitance, voltage-induced curvature, rectified current-voltage relations for membrane conductance, and capacitive currents against the applied field.

Author Contributions: LDM, KAZ and TH developed the theory, made the calculations, designed and wrote the article together.

Acknowledgments: We thank to Prof. Andrew D. Jackson from the Niels Bohr International Academy for useful discussions and for a critical reading of the manuscript. This work was supported by the Villum foundation (VKR 022130).

References

1. Hodgkin, A. L., and A. F. Huxley. 1952. A quantitative description of membrane current and its application to conduction and excitation in nerve. J. Physiol. London 117:500–544.

2. Heimburg, T. 2012. The capacitance and electromechanical coupling of lipid membranes close to transitions. the effect of electrostriction. Biophys. J. 103:918–929.

3. Heimburg, T. 1998. Mechanical aspects of membrane thermodynamics. Estimation of the mechanical properties of lipid membranes close to the chain melting transition from calorimetry. Biochim. Biophys. Acta 1415:147–162.

4. Rothman, J. E., and J. Lenard. 1977. Membrane asymmetry. Science 195:743–753.

5. Vogel, V., and D. Möbius. 1988. Local surface potentials and electric dipole moments of lipid monolayers: contributions of the water/lipid and the lipid/air interfaces. J. Coll. Interf. Sci. 126:408–420.

6. Brockman, H. 1994. Dipole potential of lipid membranes. Chem. Phys. Lipids 73:57–79.

7. Meyer, R. B. 1969. Piezoelectric effects in liquid crystals. Phys. Rev. Lett. 22:918–921.

8. Petrov, A. G., 1975. Flexoelectic model for active transport. In Physical and chemical basis of information transfer, Plenum Press, New York, 111–125.

9. Frank, H. S. 1955. Thermodynamics of a fluid substance in the electrostatic field. J. Chem. Phys. 23:2023–2032.

10. Alvarez, O., and R. Latorre. 1978. Voltage-dependent capacitance in lipid bilayers made from monolayers. Biophys. J. 21:1–17.

11. Ebel, H., P. Grabitz, and T. Heimburg. 2001. Enthalpy and volume changes in lipid membranes. i. the proportionality of heat and volume changes in the lipid melting transition and its implication for the elastic constants. J. Phys. Chem. B 105:7353–7360.

12. Schrader, W., H. Ebel, P. Grabitz, E. Hanke, T. Heimburg, M. Hoeckel, M. Kahle, F. Wente, and U. Kaatze. 2002. Compressibility of lipid mixtures studied by calorimetry and ultrasonic velocity measurements. J. Phys. Chem. B 106:6581–6586.

13. Græsbøll, K., H. Sasse-Middelhoff, and T. Heimburg. 2014. The thermodynamics of general and local anesthesia. Biophys. J. 106:2143–2156.

14. Blicher, A., and T. Heimburg. 2013. Voltage-gated lipid ion channels. PloS ONE 8:e65707.

15. Petrov, A. G., 1999. The lyotropic state of matter. Molecular physics and living matter physics. Gordon and Breach Science Publishers, Amsterdam.

16. Petrov, A. G. 1984. Flexoelectricity of lyotropics and biomembranes. Nuovo Cimento D 3:174–192.

17. Petrov, A. G., and V. S. Solokov. 1986. Curvature-electric effect in black lipid membranes. Eur. Biophys. J. 139–155.

18. Petrov, A. G., and V. S. Solokov. 1989. Curvature-electric effects in artificial and natural membranes studied using patch-clamp techniques. Eur. Biophys. J. 17:139–155.

19. Petrov, A. G., and P. N. R. Usherwood. 1994. Mechanosensitivity of cell membranes. Eur. Biophys. J. 23:1–19.

20. Petrov, A. G. 2001. Flexoelectricity of model and living membranes. Biochim. Biophys. Acta 1561:1–25.

21. Petrov, A. G., and F. Sachs. 2002. Flexoelectricity and elasticity of asymmetric biomembranes. Phys. Rev. E 65:021905–1–021905–5.

22. Farrell, B., C. Do Shope, and W. E. Brownell. 2006. Voltage-dependent capacitance of human embryonic kidney cells. Phys. Rev. E 73:041930–1–041930–17.

23. Antonov, V. F., E. Y. Smirnova, and E. V. Shevchenko. 1990. Electric field increases the phase transition temperature in the bilayer membrane of phosphatidic acid. Chem. Phys. Lipids 52:251–257.

24. Papahadjopoulos, D., K. Jacobson, S. Nir, and T. Isac. 1973. Phase transitions in phospholipid vesicles. fluorescence polarization and permeability measurements concerning the effect of temperature and cholesterol. Biochim. Biophys. Acta 311:330–340.

25. Blicher, A., K. Wodzinska, M. Fidorra, M. Winterhalter, and T. Heimburg. 2009. The temperature dependence of lipid membrane permeability, its quantized nature, and the influence of anesthetics. Biophys. J. 96:4581–4591.

26. Antonov, V. F., V. V. Petrov, A. A. Molnar, D. A. Predvoditelev, and A. S. Ivanov. 1980. The appearance of single-ion channels in unmodified lipid bilayer membranes at the phase transition temperature. Nature 283:585–586.

27. Kaufmann, K., and I. Silman. 1983. The induction by protons of ion channels through lipid bilayer membranes. Biophys. Chem. 18:89–99.

28. Heimburg, T. 2010. Lipid ion channels. Biophys. Chem. 150:2–22.

29. Mosgaard, L. D., and T. Heimburg. 2013. Lipid ion channels and the role of proteins. Acc. Chem. Res. 46:2966–2976.

30. Winterhalter, M., and W. Helfrich. 1987. Effect of voltage on pores in membranes. Phys. Rev. A 36:5874–5876.

31. Glaser, R. W., S. L. Leikin, L. V. Chernomordik, V. F. Pastushenko, and A. I. Sokirko. 1988. Reversible breakdown of lipid bilayers: Formation and evolution of pores. Biochim. Biophys. Acta 940:275–287.

32. Laub, K. R., K. Witschas, A. Blicher, S. B. Madsen, A. Lückhoff, and T. Heimburg. 2012. Comparing ion conductance recordings of synthetic lipid bilayers with cell membranes containing trp channels. Biochim. Biophys. Acta 1818:1–12.

33. Heimburg, T., and A. D. Jackson. 2005. On soliton propagation in biomembranes and nerves. Proc. Natl. Acad. Sci. USA 102:9790–9795.